ABSTRACT

Title of Document: PROBING THE 3D STRUCTURE AND FUNCTION OF A CATION/H^+ EXCHANGER IN PLANT REPRODUCTION.

Daniel D. Czerny

Doctor of Philosophy, 2015

Directed By: Professor Heven Sze

Department of Cell Biology & Molecular Genetics

Maintaining intracellular pH and K^+ homeostasis are necessary for a cell to divide, grow, and communicate with other cell types. How a cell responds to stimuli and subsequently regulates intracellular pH and K^+ content are largely unknown. Ion transporters, including cation/H^+ exchangers are one potential determinant of intracellular pH and K^+ content. A novel family of CHX transporters, predicted to exchange a cation for a H^+, is found in all land plants, though their functions in the plant and the mode of transport are mostly unknown.

What is the mode of transport of *Arabidopsis thaliana* CHX17? Model structures of the CHX17 transmembrane domain were built from two crystallized bacterial Na^+/H^+ antiporters. Based on protein architecture and homology, residues were selected for mutagenesis and CHX17 activity was tested in yeast. Thr170 and Lys383 in the discontinuous α-helices of transmembrane 4 and 11, and Asp201 and Lys355 in the

middle of transmembranes 5 and 10 are necessary for CHX17 activity. Results suggest these are core residues that participate in cation binding and/or catalysis. Glu111 near the cytosolic surface of CHX17 was necessary for activity, suggesting CHX17 could be regulated by cytosolic pH. Thus the protein fold and mode of transport of *Arabidopsis* CHX17 resemble a K^+/H^+ exchanger.

What roles do K^+/H^+ exchangers play in plant reproduction? *chx17/18/19* mutant plants showed a 56%-77% reduction in seed set though the biological basis was unknown. Reciprocal crosses showed reduced seed set was primarily caused by defects in the male gametophyte. Mutant *chx17/18/19* pollen grains developed normally and pollen tubes grew and reached most ovules. However, half the ovules receiving a mutant pollen tube failed to develop. Wild-type pistils that received *chx17/18/19* pollen showed unfertilized ovules, ovules with single fertilizations, and some embryos that developed similarly to wild-type. Thus, some triple mutant pollen showed failure to complete fertilization. When fertilization was successful, embryos from self-fertilized *chx17/18/19* pods showed delays in development. Our findings suggest maintenance of pH and K^+ homeostasis in endomembrane compartments by CHX17 and its homologs could regulate membrane trafficking events necessary for pollen tube growth, male gamete fusion, and embryo development.

PROBING THE 3D STRUCTURE AND FUNCTION OF A CATION/H^+ EXCHANGER IN PLANT REPRODUCTION.

By

Daniel D. Czerny

Dissertation submitted to the Faculty of the Graduate School of the
University of Maryland, College Park, in partial fulfillment
of the requirements for the degree of
Doctor of Philosophy
2015

Advisory Committee:
Professor Heven Sze, Chair/Advisor
Professor Caren Chang
Associate Professor Vincent Lee
Professor Zhongchi Liu
Associate Professor Jianhua Zhu

© Copyright by

Daniel D. Czerny

2015

DEDICATION

This document is dedicated to my parents.

ACKNOWLEDGEMENTS

It is my great honor to acknowledge the tireless work of my advisor Dr. Heven Sze. She has taught me many things over the past years. She has taught me how to design experiments that together prove (or disprove) a hypothesis, how to present data from those experiments in a clear manner, and how to describe everything in a clear, concise manner. I have also learned how to give seminars on a variety of scientific topics that have logic and flow. When I started working in Dr. Sze's lab, I could do none of these things very effectively. So, I need to thank her for the many hours she has spent teaching me how to be a scientist.

It is also my honor to acknowledge my co-workers Dr. Senthilkumar Padmanaban and Dr. Salil Chanroj for their assistance, guidance, and input in this research. Both my project and this document would be of far less quality without them.

I also thank my thesis examining committee members Dr. Caren Chang, Dr. Vincent Lee, Dr. Zhongchi Liu, and Dr. Jianhua Zhu for the constructive input. I also need to thank everyone who works on the ground floor of the Bioscience Research Building for their help. I would lastly like to acknowledge other members of the Sze Lab for the help in ways large and small. They include Dr. Robert Su, Dr. Yongxian Lu, Dr. Xiyan Li, Kara Levin, Zoya Riaz, Warren Zhang, and Tim Barry.

Table of Contents

LIST OF TABLES vii

LIST OF FIGURES viii

LIST OF ABBREVIATIONS x

Chapter I: POTASSIUM/PROTON EXCHANGERS: WHAT ARE THEIR MODES OF ACTION AND ROLES IN THE PLANT? 1

A. *CHX* GENES HAVE DIVERSIFIED AS PLANTS ADAPTED TO LIFE ON LAND. 2

A.1. Evolution of land plants. 2

A.2. Evolution of sexual reproduction in mosses, ferns, and gymnosperms. 5

A.3. Sexual reproduction in angiosperms. 8

A.4. Genomic changes that facilitated plants colonizing dry land. 18

A.5. What are CHX transporters? 25

A.6. What are the cellular functions of *CHX* genes? 31

A.7. What is the mode of transport? Homology modeling can provide insights into the mode of CHX17 transport. 41

A.8. What are the biological functions of CHX transporters? Analysis of *chx* mutants indicates roles in signal transduction and development. 46

B. STATEMENT OF THE PROBLEM AND RESEARCH AIMS. 48

AIM 1. DETERMINE THE IN PLANTA FUNCTION OF *CHX17*, *18*, OR *19* IN SEED SET. 48

AIM 2. TEST THE MODE OF TRANSPORT FOR CHX17. 48

SIGNIFICANCE 49

Chapter II: CHX TRANSPORTERS INVOLVED IN pH AND K^+ HOMEOSTASIS OF THE ENDOMEMBRANE SYSTEM ARE CRITICAL FOR MALE FERTILITY AND EMBRYO DEVELOPMENT 50

A. ABSTRACT 51

B. INTRODUCTION 52

C. MATERIALS AND METHODS 56

C.1. Plants 56

C.2. Mutants and Genotyping plants 56

C.3. Segregation analysis 57

C.4 Analysis of *chx17/18/19* mutant plants 57

D. RESULTS 60

D.1. TRIPLE MUTANT *CHX17/18/19* PLANTS SHOW REDUCED SEED SET AND SHORTER SEED PODS. 60

D.2. Male fertility is compromised in pollen carrying *chx17/18/19*. 63

D.3. Development of *chx17/18/19* pollen grain is similar to wild-type..... 71
D.4. Pollen tube grow and target ovules in vivo..... 71
D.5. *chx17/18/19* pods contain unfertilized ovules and single fertilization events. . 76
D.6. Delayed embryo development of self-fertilized triple mutants 80
E. DISCUSSION..... 83
E.1. Male transmission defect and failed fertilization. 83
E.2. Female contribution to seed development..... 85
E.3. Working model: Roles of three related *CHX* genes in reproduction..... 87

Chapter III: MODELING AND MUTAGENESIS REVEAL THE ACTIVE CORE AND A UNIVERSAL STRESS PROTEIN-LIKE DOMAIN IN THE PLANT CATION/PROTON EXCHANGER CHX17. 89

A. ABSTRACT..... 90
B. INTRODUCTION..... 91
B.1. CHX transporters in plants..... 91
B.2. What are the roles of *CHX17*, *18*, and *19* in the plant?..... 93
B.3. What is the evidence for CHX transporters functioning as cation/H^+ exchangers?..... 93
B.4. *E. coli* NhaA and *T. thermophilus* NapA are CPA2 transporters with solved crystal structures. 94
B.5. What approach was used? What are the novel findings?..... 96
C. MATERIAL AND METHODS..... 97
C.1. Generating a 3D model structure of CHX17..... 97
C.2. Yeast and bacterium..... 97
C.3. CHX17 point mutation constructs..... 98
C.4. Transformation of yeast and bacterium..... 99
C.5. Testing CHX17 activity in yeast 101
C.6. GFP-tagged CHX17 proteins 102
D. RESULTS 105
D.1. Modeling the 3D structure of CHX17..... 105
D.2. AtCHX17 TM domain has a protein fold similar to *T. thermophilus* NapA and to *E. coli* NhaA. 108
D.3. 3D model-guided approach to select critical residues 111
D.4. Testing CHX17 residues by expression in yeast..... 114
D.5. CHX17 carrying D201A or K355A mutation was active when expressed in E. coli..... 120
D.6. Mutated CHX17 proteins are expressed in yeast. Activity of wild-type or mutated AtCHX17 is unaffected by a GFP tag at the C-tail..... 122

D.7. CHX17-GFP proteins are intact and localized to endomembranes. 122
D.8. Modeling the hydrophilic C-tail revealed similarity to a universal stress protein (USP)-like domain. 125
E. DISCUSSION 129
E.1. Relating secondary transport to protein structure. 129
E.2. Transport core at TM4-5 and TM11-12 130
E.3. Distinctions between CPA2 versus CPA1: a pH sensor? 135
E.4. Two conformational states of CHX. 136
E.5. USP-like domain at the C-tail: a regulatory domain? 139
F. CONCLUSION 144

Chapter IV: CONCLUSIONS AND FUTURE DIRECTIONS 145

A. CONCLUSIONS 146
B. FUTURE DIRECTIONS 151
B.1. Do mutant *chx17/18/19* sperm cells respond to secreted EC1 peptides from the egg cell? 151
B.2. What is the 3D structure of CHX17-TM (residues 1-440)? Could additional site-directed mutagenesis of CHX17 provide new information on pH regulation or structural rearrangements during the transport cycle? 153
B.3. What are functions of the CHX17 hydrophilic C-tail? Does the CHX17 C-tail interact with other proteins that have potential roles in stress tolerance? 155

Chapter V. APPENDICES 157

A. SUPPLEMENTAL INFORMATION FOR CHAPTER II 160
A.1. Tables of materials for Chapter II 160
A.2. Supplemental Results for Chapter II 162
B. SUPPLEMENTAL INFORMATION FOR CHAPTER III 172
B.1. Tables of materials for Chapter III 172
B.2. Supplemental Results for Chapter III 182

REFERENCES 195

LIST OF TABLES

Chapter II

II-1. Reciprocal crosses show male fertility is compromised in the triple *chx17/18/19* mutant. 68

II-2. Only one of three *CHX* genes is sufficient to restore male fertility. Thus, *CHX18* or *CHX19* play overlapping roles in male and female fertility. 70

Chapter III

III-1. Selected conserved and non-conserved residues in cation/protein antiporters from prokaryotes and eukaryotes. 113

III-2. Summary of residues critical for AtCHX17 activity. 143

LIST OF FIGURES

Chapter I

I-1. Key innovations that facilitated plant adaptation to life on dry land. 4

I-2. Modifications in the alternation of generations facilitated plants adapting to dry land. 7

I-3. A series of innovations evolved to facilitate adaptations of plants to dry land. 11

I-4. The growth and navigation of a pollen tube delivers two sperm cells to the ovule for double fertilization. 13

I-5. Seed development in the model plant *Arabidopsis*. 17

I-6. The number of *CHX* genes has increased as plants colonized dry land. 19

I-7. The CPA1 and CPA2 transporter subfamilies likely evolved from different bacterial transporters. 22

I-8. CHX transporters have diversified from early plants to flowering plants. 24

I-9. Expression of *Arabidopsis CHX* genes in pollen and sperm. 27

I-10. Promoter activity of diverse *CHX* genes in various plant tissues. 30

I-11. Organelles of the secretory and endocytic pathways have distinct luminal pHs. 33

I-12. Model of transporters that influence luminal pH homeostasis. 36

I-13. The crystal structure of *T. thermophilus* NapA shows the active state of a Na^+/H^+ antiporter. 44

Chapter II

II-1. Triple *chx17/18/19* mutant plants showed reduced seed set. 62

II-2. Gene structures of *Arabidopsis CHX17*, *CHX18*, and *CHX19* and verification of genotypes. 65

II-3. *chx17/18/19* pollen grain development is similar to wild-type. 72

II-4.	Time-course of ovule development in wild-type pistils pollinated with WT or *chx17/18/19* pollen.	73
II-5.	Mutant pollen tubes reached many ovules though half remain undeveloped.	75
II-6.	Decreased male fertility of *chx17/18/19* mutant pollen produces pods with unfertilized ovules, embryo only, as well as developing seeds.	78
II-7.	Pods of self-pollinated triple *chx17/18/19* mutants contained unfertilized ovules, single fertilizations and developing embryos.	79
II-8.	Delayed embryo development in developing seeds of self-pollinated *chx17/18/19* mutant.	82

Chapter III

III-1.	Protein domains and transmembrane segments of AtCHX17-TM.	107
III-2.	3D structure models of CHX17-TM.	109
III-3.	Residues critical for CHX17 activity in yeast.	117
III-4.	Mutations in critical residues failed to inactivate AtCHX17 expressed in *E. coli*.	121
III-5.	Mutated and wild-type CHX17 protein tagged with GFP are expressed in yeast.	124
III-6.	Model 3D structure of AtCHX17 C-tail has a universal stress protein-like domain.	127
III-7.	Residues in the active core of AtCHX17 and mechanism of exchanger.	134
III-8.	Two conformational states of CHX17 that allow alternating access of the cation binding site to both sides of the membrane.	137
III-9.	The predicted transport cycle of CHX17.	140

LIST OF ABBREVIATIONS

Amp	Ampicillin
At	*Arabidopsis thaliana*
cDNA	Complementary DNA
CHX	Cation/H^+ Exchanger
CHX17-TM	CHX17 transmembrane domain
CPA	Cation/Proton Antiporter
CPY	Carboxypeptidase Y
CYT	Cytosolic
DAP	Days after pollination
DAPI	4',6-diamidino-2-phenylindole
DIC	Differential Interference Contrast
EcNhaA	*E. coli* NhaA Na^+/H^+ antiporter
ER	Endoplasmic reticulum
EXT	Extracellular
F1	The first filial generation
gDNA	genomic DNA
GFP	Green fluorescent protein
HygB	Hygromycin B
KEA	K^+ Efflux Antiporter
LB	Luria-Bertani
NHE	Na^+/H^+ Exchanger

NHX	Na$^+$/H$^+$ Exchanger
PCR	Polymerase Chain Reaction
PM	Plasma membrane
PT	Pollen tube
PVC	Prevacuolar compartment
RFP	Red fluorescent protein
RLK	Receptor-like kinase
SEM	Standard error of the mean
T-DNA	Transfer-DNA
TGN	*Trans*-Golgi network
TM	Transmembrane
TtNapA	*T. thermophilus* NapA Na$^+$/H$^+$ antiporter
URA	Uracil
USP	Universal stress protein
WT	Wild-type
YNB	Yeast nitrogen base
YPAD	Yeast extract peptone adenine dextrose
YTMK	Yeast extract tryptone mannitol potassium (K$^+$)

Chapter I: POTASSIUM/PROTON EXCHANGERS: WHAT ARE THEIR MODES OF ACTION AND ROLES IN THE PLANT?

A. CHX genes have diversified as plants adapted to life on land.

A.1. Evolution of land plants.

Flowering plants have diversified on dry land largely due to innovative adaptations. For instance, early land plants, similar to the moss *Physcomitrella patens*, developed pores at the gametophyte surface. These pores are surrounded by primitive guard cells, which probably serve to regulate the aperture to balance water loss and CO_2 uptake for photosynthesis (Peterson et al., 2010). Subsequently, primitive vascular tissues first appeared in plants that include the club moss *Selaginella* (Fig. I-1**)**. The development of xylem and phloem has allowed land plants to increase in size by having efficient means for transporting water and nutrients (Sieburth and Deyholos, 2006).

To overcome the lack of an aqueous environment essential for flagellated male gametes to reach the egg, flowering land plants developed several reproductive innovations. The male gametophyte that carries two sperm cells has been reduced to a two or three-celled pollen grain that can survive desiccation as it is transported by wind or insects to the pistil. The female gametophyte is the seven-celled embryo sac embedded within the pistil (McCormick, 2004; Sundaresan and Alandete-Saez, 2010). Once a pollen grain reaches a compatible stigma, the grain hydrates, germinates, and extends a single-celled tube that burrows into the ovary and navigates through the extracellular matrix (ECM) to an available embryo sac (Takeuchi and Higashiyama, 2011). Upon entering the embryo sac, the tube ruptures at the tip to extrude two immotile sperm cells so they are in close proximity to the egg cell and central cell. Successful double fertilization will result in an embryo and endosperm, which will lead to the development of a mature seed (Berger et al., 2006). This remarkable process has been challenging to study due to the minute sizes

Fig. I-1. Key innovations that facilitated plant adaptation to life on dry land.

Innovations that facilitate adaptation to dry land are indicated by black boxes on the right-hand diagonal line. Most of the adaptations for life on land arose once during the history of plants. Genome sequences of algae, lower land plants, gymnosperms, and angiosperms have enhanced our understanding of plant evolution by identifying genes involved in facilitating survival on dry land. (Fig. from S. Freeman, 2007. *Biological Science*, 3rd Ed. Benjamin Cummings. San Francisco, CA.)

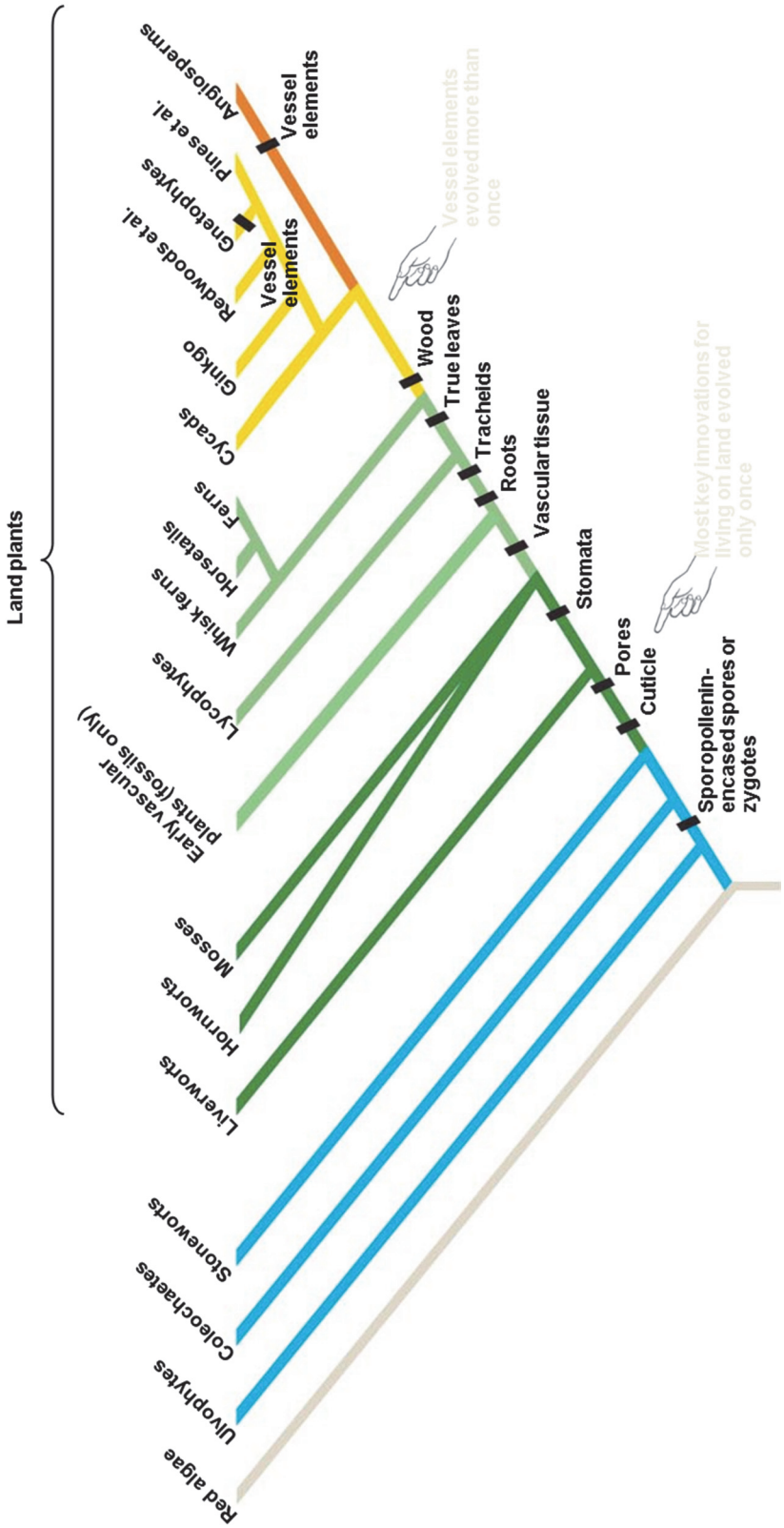
Land plants
Angiosperms
Pines et al.
Gnetophytes
Redwoods et al.
Ginkgo
Cycads
Ferns
Horsetails
Whisk ferns
Lycophytes
Early vascular plants (fossils only)
Mosses
Hornworts
Liverworts
Stoneworts
Coleochaetes
Ulvophytes
Red algae
Vessel elements
Vessel elements
Vessel elements evolved more than once
Wood
True leaves
Tracheids
Roots
Vascular tissue
Stomata
Pores
Cuticle
Sporopollenin-encased spores or zygotes
Most key innovations for living on land evolved only once

and the inaccessibility of the reproductive tissues. Thus, the molecular, biochemical, and cellular bases of each step are largely unknown.

A.2. Evolution of sexual reproduction in mosses, ferns, and gymnosperms.

Seed plants have become the largest class of land plants due to a number of innovations that allowed these plants to reproduce in dry environments. In *P. patens*, the female oogonia reside within an archegonium, and motile male antherozoids require an aqueous path to reach the archegonium in order to fertilize the oogonia This reproduction method is common to nonvascular and seedless vascular plants (Fig. I-2A, B).

As plants colonized dry land, a series of innovative adaptations allowed plants to thrive in an environment with limited water. Development of both a cuticle layer and stomata were crucial for regulating water loss (Freeman, 2008). Arguably, the most crucial adaptation for success on dry land was in reproduction. Both gymnosperms and angiosperms reproduce using a male gametophyte that extends a pollen tube into the female gametophyte to fertilize the gametes to produce a seed.

Gymnosperms characteristically lack a structure to enclose developing seeds. In these plants, mature pollen grains are dispersed primarily by wind, and for successful reproduction, the grains must land on a megaspore in the vicinity of the micropyle. The pollen tube grows into the megaspore to fertilize one of the two egg cells. The unfertilized egg cell is degraded (Freeman, 2008). During this process, pollen tube growth is slow relative to angiosperms. Gymnosperm pollen tubes grow *in vivo* at rates between 1 and 10 μm per hour (Williams, 2008).

Fig. I-2: Modifications in the alternation of generations facilitated plants adapting to dry land.

(A) Nonvascular plants, such as mosses, have a life cycle dominated by the haploid gametophyte stage. Mitosis produces haploid gametes in the gametangia. Fertilization occurs within the female archegonium, forming the diploid sporophyte. The sporophyte forms on the gametophyte because the gametophyte supplies nutrition to the sporophyte. Spores are formed by meiosis in the sporophyte, and the spores germinate to produce the next gametophyte generation. **(B)** In ferns, the diploid sporophyte stage became dominant in the life cycle. Ferns produce haploid spores that develop into a small mature gametophyte. In ferns, sperm and eggs are produced on separate gametophytes. The sperm swim to the egg, and fertilization produces a diploid sporophyte that grows to many times the size of the gametophyte. Unlike in mosses, the mature sporophyte does not rely on the gametophyte for nutrition. (Fig. from Freeman 2008. *Biological Science*. Pearson, 3rd ed. New York City.)

(a) Mosses: Gametophyte is large and long lived; sporophyte depends on gametophyte for nutrition.

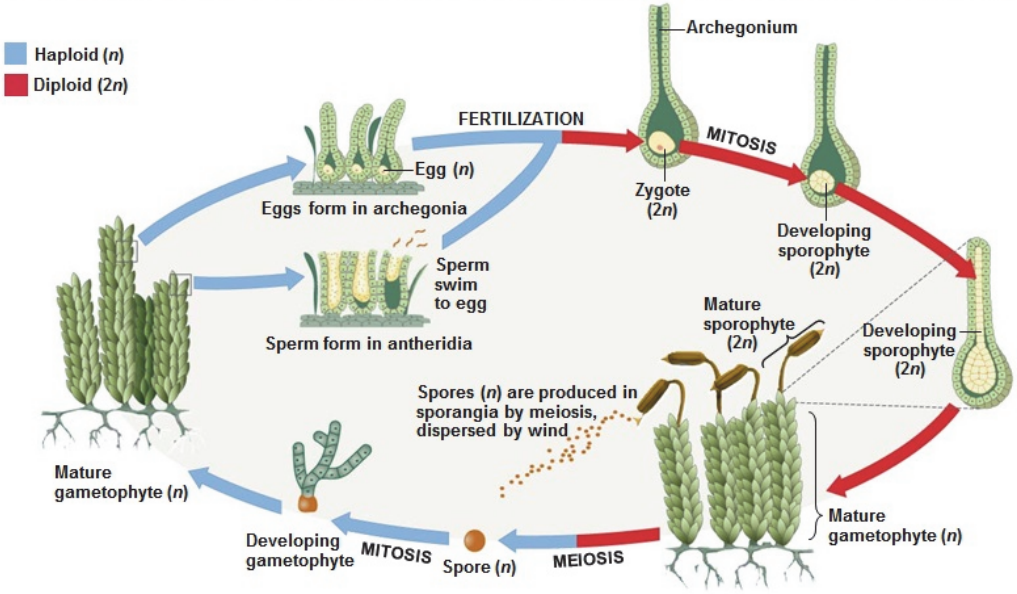

(b) Ferns: Sporophyte is large and long lived but, when young, depends on gametophyte for nutrition.

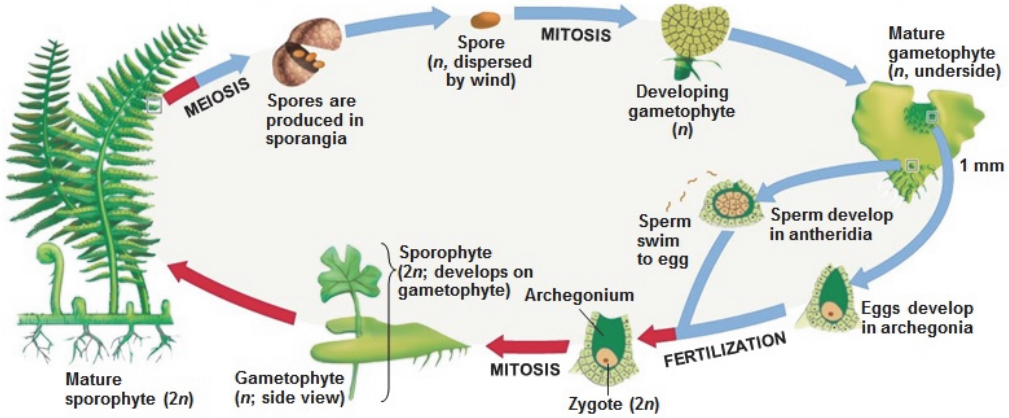

In vitro growth rates for gymnosperm pollen are <1 to 20 µm per hour (Williams, 2008). In contrast, *Arabidopsis* pollen tubes grow *in vitro* at approximately 60 µm per hour (Boavida and McCormick, 2007).

In conifers, including spruce and Douglas fir trees, a possible reason for slow pollen tube growth could be that mature pollen grains do not contain fully-developed male gametes. In addition, the lack of callose plugs and pectin in gymnosperm pollen tubes could contribute to slower growth relative to angiosperm pollen tubes (Fernando,et al., 2005). The evolution of pollen tubes allowed reproduction without water. However, a slow growth rate and an unprotected female gametophyte both limited the utility of this innovation for gymnosperms. Many of the cellular and molecular mechanisms of gymnosperm pollen tube growth remain unknown.

A.3. Sexual reproduction in angiosperms.

The female gametophyte in angiosperms is enclosed within the pistil tissue of the flower. The pollen tube must successfully navigate through the stigma, style, and transmitting tract to arrive at an unfertilized ovule and deliver two sperm cells. In order to do this, the pollen tube communicates with the female cells through gradients of signaling molecules (Dresselhaus and Franklin-Tong, 2013). Once a pollen tube arrives at an embryo sac, the tube ruptures to release two sperm cells. One sperm fuses with the egg cell to produce the embryo, and the second sperm fuses with the diploid central cell to produce the triploid endosperm (Hamamura, et al., 2011). Key evolutionary traits necessary for the success of plants on dry land evolved only once. The adaptations listed

in Fig. I-3 are central to plant life on dry land. Among these traits, double fertilization (Fig. I-4) is an intricate process that requires precise communication between the male and female gametes.

A.3a The embryo sac is the angiosperm female gametophyte.

The embryo sac consists of seven cells: an egg cell, a central cell, two synergids, and three antipodal cells (Yadegari and Drews, 2004). Each embryo sac can attract a single pollen tube; however, both how the PT is attracted and how PT attraction is attenuated were initially unknown. The embryo sac was hypothesized to secrete attractant molecules to guide pollen tubes into the micropyle for double fertilization. The origin of one type of signaling molecule was discovered in *Torenia fournieri*, which has an embryo sac that protrudes outside the micropyle. Laser ablation of one *T. fournieri* synergid reduced pollen tube attraction, and ablation of both synergids completely blocked pollen tube attraction, which indicated the synergids are a source of attractant molecules (Higashiyama, et al., 2001). These *Torenia* attractants were identified as small secreted cysteine-rich defensin-like peptides, termed LUREs, and showed the capability *in vitro* to attract pollen tubes (Okuda, et al., 2009). Are LUREs universal PT attractants, or are LUREs specific for one species?

A. thaliana LURE1 proteins formed a species-specific cluster among defensin-like proteins, which indicates the possibility for species-specific attraction of pollen tubes into an embryo sac. Interestingly, expression of one member of the *AtLURE1* family in a *T. fournieri* embryo sac allowed attraction of *A. thaliana* pollen tubes into the *Torenia* embryo sac (Takeuchi and Higashiyama, 2012). These experiments indicate genes encoding small secreted cysteine-rich peptides have evolved rapidly to mediate species-

Fig. I-3: **A series of innovations evolved to facilitate adaptation of plants to dry land.**

The phylogenetic tree shows the series of evolutionary innovations necessary for plants to colonize dry land. All land plants have a common Charophyte ancestor, and the evolution of vascular tissue, seeds, and flowers have allowed the diversification of land plants and their adaptation to different land environments. Seeds and flowers arose only once during plant evolution, making seed plants and flowering plants both monophyletic. (Fig. from Freeman 2008. *Biological Science*. Pearson, 3rd ed. New York City.)

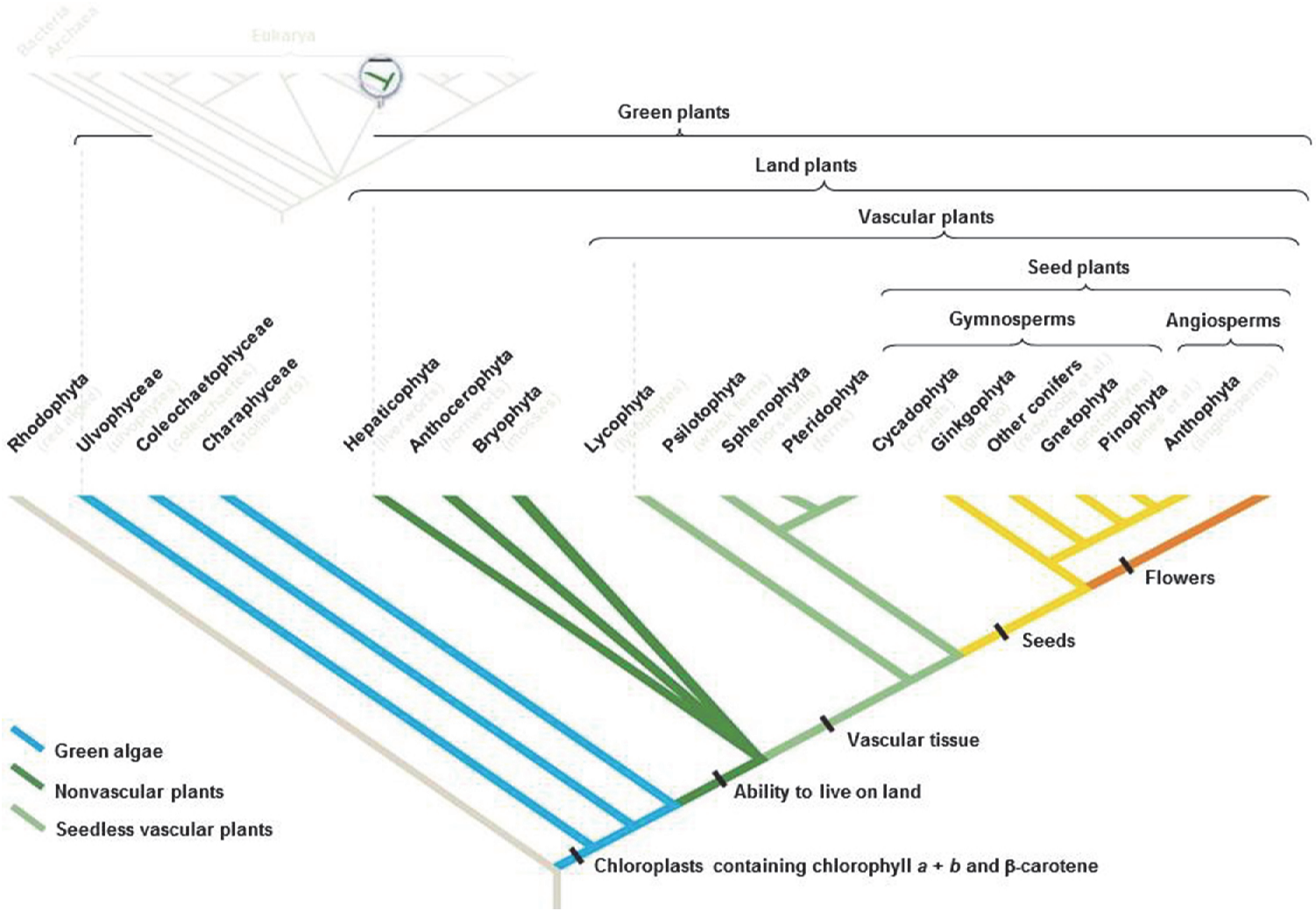
Green plants
Land plants
Vascular plants
Seed plants
Gymnosperms
Angiosperms
Rhodophyta
Ulvophyceae
Coleochaetophyceae
Charaphyceae
Hepaticophyta
Anthocerophyta
Bryophyta
Lycophyta
Psilotophyta
Sphenophyta
Pteridophyta
Cycadophyta
Ginkgophyta
Other conifers
Gnetophyta
Pinophyta
Anthophyta
Flowers
Seeds
Vascular tissue
Ability to live on land
Chloroplasts containing chlorophyll a + b and β-carotene
Green algae
Nonvascular plants
Seedless vascular plants

Fig. I-4: **The growth and navigation of a pollen tube delivers two sperm cells to the ovule for double fertilization.**

Panels (A) and (B) show the 6 steps in angiosperm reproduction. **(A)** The desiccated pollen grain lands on the stigma cells of a receptive flower. The grain is hydrated on the stigma and extends a tube through the pistil. The tube grows through the pistil by obtaining nutrients from the extracellular matrix and integrating gradients of guidance cues from unfertilized embryo sacs. **(B)** The pollen tube delivers two sperm cells into the embryo sac. The tube enters through the micropyle and grows towards a synergid cell. The pollen tube tip will burst and release the 2 sperm cells. **(C)** In double fertilization, one sperm cell fuses with the egg cell to generate the embryo, and the second sperm cell fuses with the diploid central cell to generate the triploid endosperm. (Figs. **A** and **B** from Taiz, et al. *Plant Physiology* 6th ed. Sinauer 2014. Fig. **C** from Hamamura, et al. (2012) *Curr. Opin. Plant Biol*. **15**:70-77.)

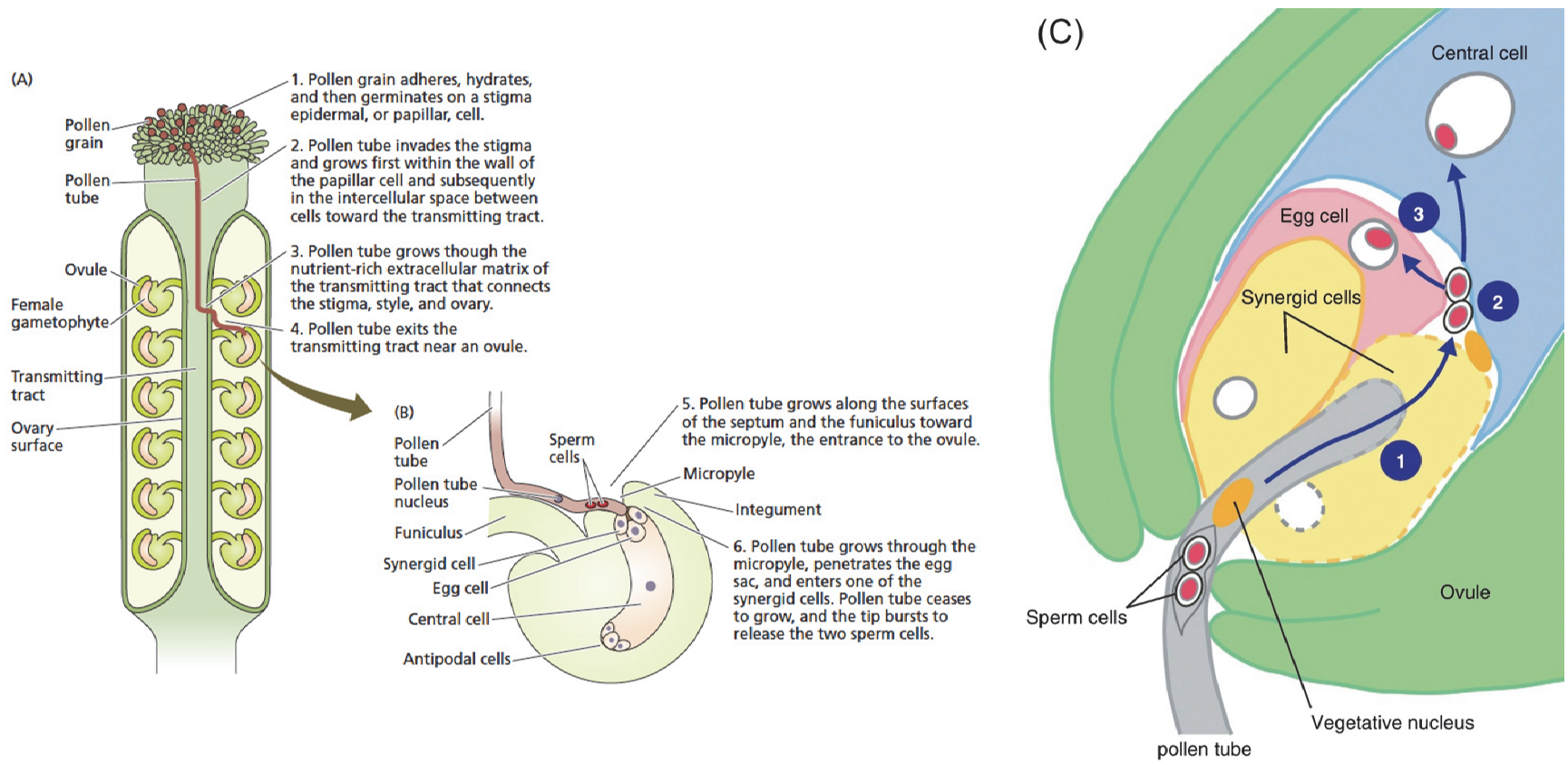
(A)
Pollen grain
Pollen tube
Ovule
Female gametophyte
Transmitting tract
Ovary surface
1. Pollen grain adheres, hydrates, and then germinates on a stigma epidermal, or papillar, cell.
2. Pollen tube invades the stigma and grows first within the wall of the papillar cell and subsequently in the intercellular space between cells toward the transmitting tract.
3. Pollen tube grows though the nutrient-rich extracellular matrix of the transmitting tract that connects the stigma, style, and ovary.
4. Pollen tube exits the transmitting tract near an ovule.
(B)
Pollen tube
Pollen tube nucleus
Funiculus
Synergid cell
Egg cell
Central cell
Antipodal cells
Sperm cells
5. Pollen tube grows along the surfaces of the septum and the funiculus toward the micropyle, the entrance to the ovule.
Micropyle
Integument
6. Pollen tube grows through the micropyle, penetrates the egg sac, and enters one of the synergid cells. Pollen tube ceases to grow, and the tip bursts to release the two sperm cells.
(C)
Central cell
Egg cell
Synergid cells
Sperm cells
Ovule
Vegetative nucleus
pollen tube
1
2
3

specific fertilization events, but species-specific LURE peptide receptors remain unknown.

Successful delivery of sperm cells into the embryo sac is also under species-specific controls. The *FERONIA* (*FER*) gene, which encodes a receptor-like kinase (RLK), was identified from analysis of mutant plants with reduced seed set (Huck, et al., 2003). In the embryo sac, *FER* is expressed in the synergid cells, and FER protein localizes to the PM. When a WT pollen tube enters a *fer* mutant ovule, tube growth does not cease, and tip burst does not occur, which results in unfertilized ovules displaying excessive PT growth (Escobar-Restrepo, et al., 2007). Amino acid analysis of the extracellular domain of FER, which is postulated to function in ligand binding, showed the greatest degree of sequence divergence among *Arabidopsis* species (Escobar-Restrepo, et al., 2007). This suggests rapid evolution of *FER*, which would block fertilization by related species to facilitate reproductive success of a single species.

The *A. thaliana* egg cell was shown to secrete small peptides upon perception of sperm cells released into the embryo sac. A small gene family of five *Egg Cell-1* (*EC1*) genes was specifically expressed in the egg cell of unfertilized ovules (Sprunck, et al., 2012). EC1 peptides tagged with GFP, from a family of five highly-similar genes, accumulate inside the egg cell of an unfertilized embryo sac. When sperm cells are released from the pollen tube, EC1-GFP peptides are secreted from the egg cell. Wild-type *Arabidopsis* sperm cells respond to these secreted peptides by redistributing the fusogen protein HAP2(GCS1) from endomembranes to the plasma membrane (Sprunck, et al., 2012). Specific cross-talk between gametes is important for reproductive success of the plant by blocking unfavorable fertilization by a related species.

A.3b. The pollen tube is the angiosperm male gametophyte.

The pollen tube delivers the two immotile sperm cells, as shown in Fig. I-4. To accomplish this, the pollen tube interacts with multiple cell types in the pistil and integrates multiple guidance signals to locate an unfertilized embryo sac (Beale and Johnson, 2013). The first step occurs when the desiccated pollen grain lands on a compatible stigma. The pollen grain will adhere to the papillar cells of the stigma and become hydrated. The tube will emerge from the grain and penetrate the female tissues to locate an unfertilized embryo sac embedded within the pistil (Edlund, et al., 2004). Recognition of compatible pollen grains on the stigma is an important first step in angiosperm reproduction.

Once the pollen tube has entered the pistil, the tube grows by tip-directed growth through the ECM of the style and transmitting tract. Polar tip-directed growth is controlled by exocytosis of membrane vesicles at the tube tip as well as tip-directed gradients of Ca^{2+} and H^{+} (Cheung and Wu, 2008). As the pollen tube grows through the pistil, the tube must sense and respond to a multitude of guidance cues. Once the pollen tube arrives at an unfertilized embryo sac, tip growth must cease. Subsequently, the pollen tube tip ruptures to release the sperm cells. This process has been shown to involve RLKs expressed in the pollen tube. In the pollen tube, the *ANXUR1/2* RLKs, which are pollen-specific *FERONIA* homologs, are likely involved in maintaining integrity of the pollen tube tip until the tube penetrates the micropyle because *anx1/2* mutant tubes burst prematurely *in vitro* (Boisson-Dernier, et al., 2009). Once a PT penetrates an ovule, a signaling pathway involving synergid-localized *FER* could down-

regulate *ANX1/2*, leading to PT burst. This communication between the gametophytes could have evolved rapidly to facilitate species-specific fertilization.

A.3.c Double fertilization and seed development

Analysis of double fertilization using fluorescent markers has permitted an in-depth characterization of gamete functions and events inside the embryo sac (Berger, 2011). Using confocal imaging of fluorescent-tagged proteins, sperm cells pause for approximately 7.5 minutes before initiating plasma membrane fusion with the female gametes, all of which occurs within 20 minutes of the sperm being released from the pollen tube (Fig. I-4). This pause suggests signaling events between the gametes are necessary for fusion of their plasma and nuclear membranes. Identification of mutants defective in gamete interactions would provide clues to how the gametes communicate with each other. The *hap2(gcs1)* mutant was originally discovered in *Arabidopsis* plants with reduced seed set (von Besser, et al., 2006). The HAP2(GCS1) protein was later shown to be conserved in *Chlamydomonas*, where it facilitated cell membrane fusion (Liu, et al., 2008). In *A. thaliana*, *hap2(gcs1)* sperm cannot fuse with either female gamete (Mori, et al., 2006).

Development of the embryo and endosperm is coordinated. Proper seed development requires nourishing the embryo with nutrients from the endosperm. *Arabidopsis* embryo development progresses through a series of defined stages (Fig. I-5). Initially, the zygote is divided asymmetrically into a small apical cell and a larger basal suspensor cell. The apical cell undergoes a series of defined cell divisions as it matures through the globular, heart, and torpedo stages. These divisions pattern the embryo and specify the cotyledons, shoot apical meristem, and roots (Lau, et al., 2012). As the

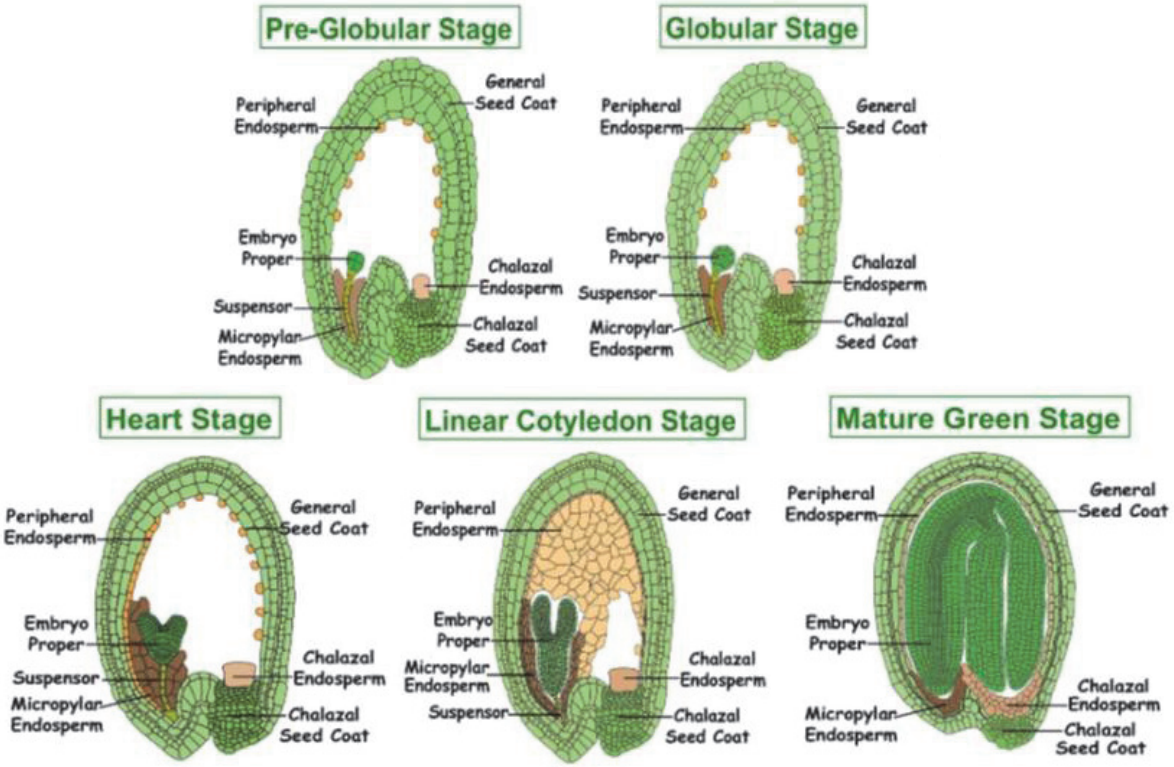

Fig. I-5: **Seed development in the model plant *Arabidopsis*.**

After successful double fertilization, the embryo and endosperm develop synchronously. The embryo is divided into the embryo proper, which will give rise to the entire seedling, and the suspensor, which is hypothesized to move nutrients from the endosperm to the embryo proper. The endosperm is separated into 3 types: micropylar, peripheral, and chalazal. As the embryo matures and enlarges, it uses the stored nutrients from the endosperm. When the embryo has completely matured, it occupies almost the entire volume of the seed, and the endosperm has been reduced to small peripheral cell layers. (Fig. from Le, et al. (2010) *Proc. Nat. Acad. Sci. USA*. **107**:8063-8070.)

embryo matures and increases in size, it grows to occupy the space once filled by the endosperm (Fig. I-5). The mature cotyledon stage embryo can survive desiccation inside a seed and grow into a seedling under the proper environmental conditions.

A.4. Genomic changes that facilitated plants colonizing dry land.

A.4a. Genomes of plants.

Availability of the complete genome sequences of plants shed light on genes that diversified for survival and successful reproduction on land. As plants evolved from algae to early land plants (Timme and Delwiche, 2010) and then to gymnosperms and angiosperms, the plants became larger and more complex. For instance, plants developed vascular tissues which permitted long-distance water and nutrient flow (Quatrano et al., 2007). The ability to maintain cellular homeostasis under changing environmental conditions became more important. As plants evolved and colonized dry land, genes encoding transporters, cell wall remodeling proteins, and signaling components including protein kinases and transcription factors diversified (Cuming et al., 2007; Popper et al., 2011). Some cation transporters, such as the Na^+/H^+ exchanger (NHX) family, have been conserved from algae to flowering plants and have not significantly increased in number (Chanroj et al., 2012). This indicates their functions are largely conserved whether in a unicellular alga or in a multicellular plant. Other cation transporters, such as the cation/H^+ exchanger (CHX) family, have diversified (Fig. I-6). Why would plants need additional genes encoding these transporters?

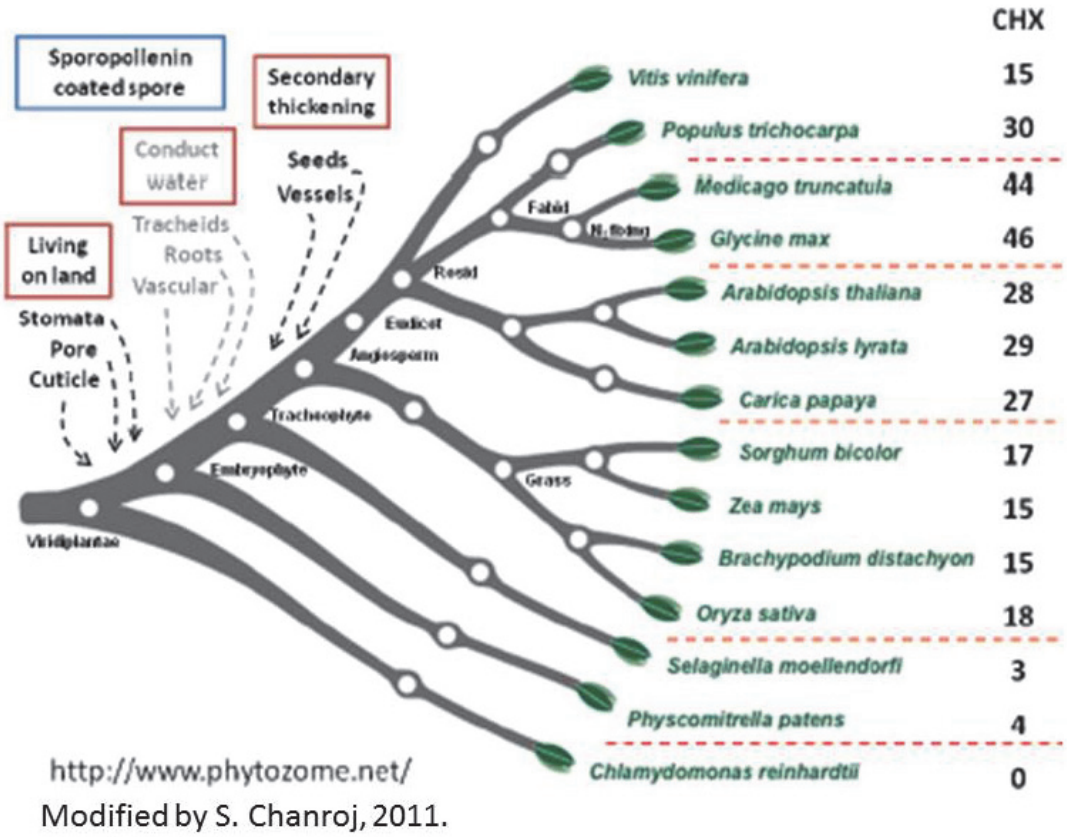

Fig. I-6. The number of *CHX* genes has increased as plants colonized dry land.

The unicellular alga *Chlamydomonas* lacks *CHX*–like genes. Early land plants contain a limited number of *CHX* genes. Representative monocots possess 15-18 *CHX* genes, and eudicots often have 27 or more *CHX* genes. The increase in *CHX* genes from early land plants to eudicots suggests *CHX* genes have increased in number to facilitate plants adapting to dry land. (Fig. from Chanroj, 2011. Plant-specific K^+ transporters with distinct properties and their emerging roles in endomembrane trafficking. Ph.D. Thesis, Univ. of Maryland.)

A.4b. Genes encoding cation/H^+ antiporters in flowering plants.

In plants, genes encoding cation/proton antiporters (CPAs) are classified into two subfamilies: CPA1, consisting of the NHX transporters, and CPA2, consisting of CHX transporters and K^+ efflux antiporters (KEA) (Fig. I-7). (Maser et al., 2001; Chanroj et al., 2012). Plant NHX transporters are well-characterized and classified into 3 subtypes according to phylogeny. The three subtypes intriguingly correspond to their subcellular locations in vacuolar, endosomal, and plasma membrane groups. Vacuolar and endosomal NHX transporters have functions including cell size regulation, cell expansion, and vesicle trafficking, which implicate NHX transporters in cation and pH homeostasis (Bassil et al., 2012). In addition, plasma membrane NHX7/SOS1 functions in salt tolerance by facilitating long-distance Na^+ transport as shown by promoter-GUS expression in root vasculature and increased Na^+ accumulation in mutant plants under salt stress (Shi et al., 2002). In contrast to the NHX transporters, relatively little information is known about the CPA2 subfamily, including CHX transporters.

A.4c. Diversification of CHX genes.

From analyzing protein sequences, the number of *CHX* genes has increased from algae to land plants (Chanroj et al., 2012). The filamentous green alga *Spirogyra pratensis* has one or two *CHX* genes. The early land plants *Selaginella* and *Physcomitrella* have 3 and 4 *CHX* genes, respectively (Fig. I-6). The *CHX* genes from *Spirogyra*, *Selaginella*, and *Physcomitrella* are most similar to *Arabidopsis CHX20* (Fig. I-8) (Chanroj et al., 2012). Representative monocots, including *O. sativa* and *Z. mays*, have between 15 and 18 *CHX* genes. Dicot genomes, including *M. truncatula* (45), *P. trichocarpa* (30), and *A. thaliana* (28), often contain higher numbers of *CHX* genes

Fig. I-7. The CPA1 and CPA2 transporter subfamilies likely evolved from different bacterial transporters.

A phylogenetic tree built from protein sequences shows three distinct evolutionary branches in the CPA (cation proton antiporter) superfamily. The CPA1 subfamily of NHX transporters likely arose from an ancestral gene of *E. coli* NhaP. In the CPA2 subfamily, KEA transporters likely arose from an ancestral gene of *E. coli* KefC, and CHX transporters likely arose from an ancestral gene of *E. coli* NhaA. (Fig. taken from Chanroj et al., 2012. *Frontiers Plant Sci*. 3:25.)

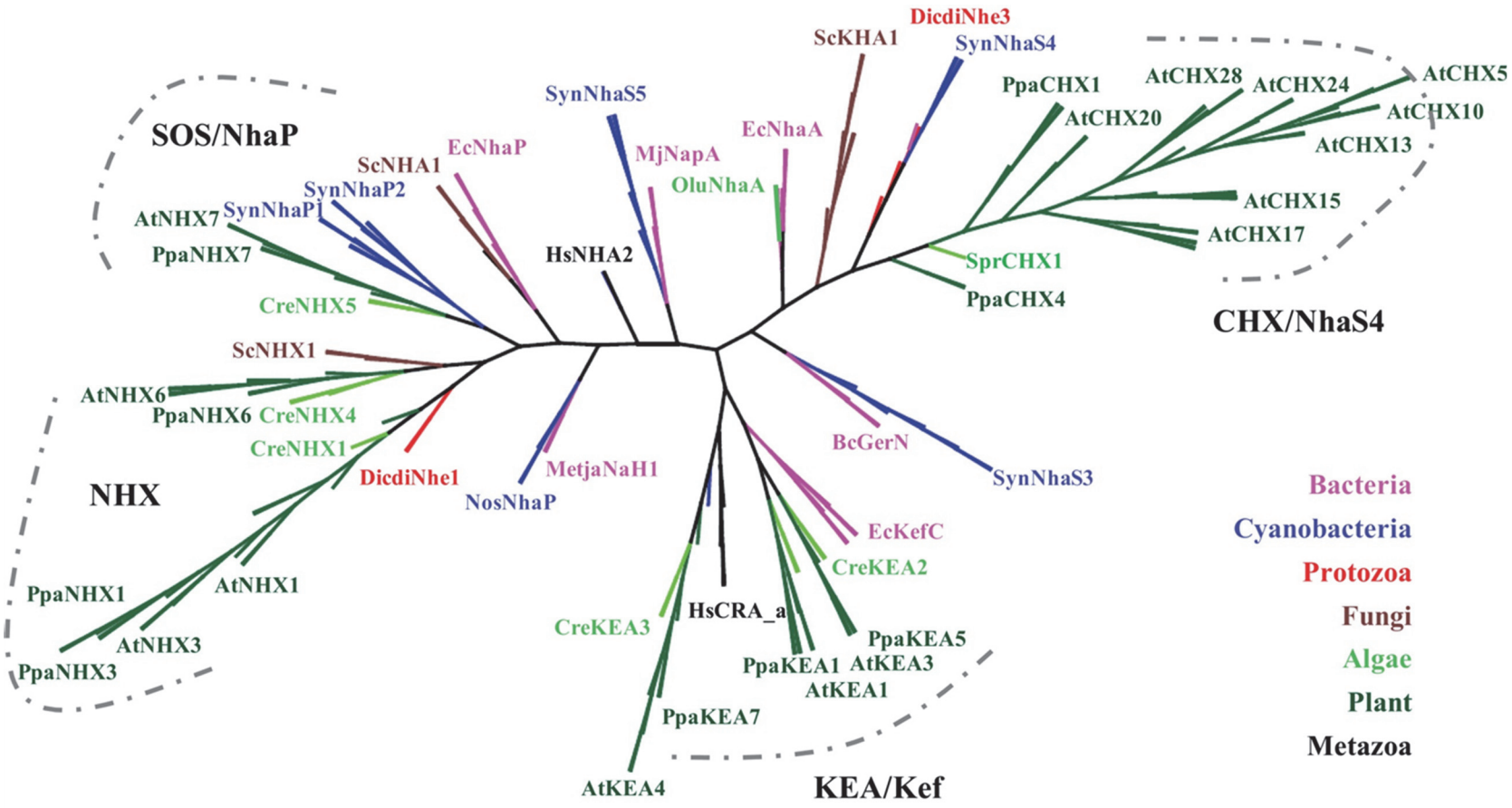
SOS/NhaP
NHX
KEA/Kef
CHX/NhaS4
AtNHX7
SynNhaP1
SynNhaP2
ScNHA1
EcNhaP
PpaNHX7
CreNHX5
ScNHX1
AtNHX6
PpaNHX6
CreNHX4
CreNHX1
DicdiNhe1
NosNhaP
MetjaNaH1
PpaNHX1
AtNHX1
AtNHX3
PpaNHX3
HsNHA2
SynNhaS5
MjNapA
OluNhaA
EcNhaA
ScKHA1
DicdiNhe3
SynNhaS4
PpaCHX1
AtCHX20
AtCHX28
AtCHX24
AtCHX5
AtCHX10
AtCHX13
AtCHX15
AtCHX17
SprCHX1
PpaCHX4
BcGerN
SynNhaS3
EcKefC
CreKEA2
HsCRA_a
CreKEA3
PpaKEA5
PpaKEA1
AtKEA3
AtKEA1
PpaKEA7
AtKEA4
Bacteria
Cyanobacteria
Protozoa
Fungi
Algae
Plant
Metazoa

Fig. I-8. CHX transporters have diversified from early plants to flowering plants.

A) Subclades of plant CHX proteins. Early land plants, indicated by green lines on the phylogenetic tree, contain *CHX* proteins that are most similar to *Arabidopsis* CHX20 (subclade IVa). Rice (*O. sativa*) *CHX* genes, indicated by blue lines on the tree, are most similar to a specific subset of *Arabidopsis CHX*. Rice and other monocots lack *CHX* homologs for *Arabidopsis* genes including *CHX13*, *CHX21*, and *CHX23*. (Fig. taken from Chanroj, et al. (2012) *Frontiers Plant Sci*. 3:25.) Abbreviations are Spra = *Spirogyra pratensis*, Ppa = *Physcomitrella patens*, Smo = *Selaginella moellendorffii*, and Synel = *Synechocystis elongatus*. **B)** Model of the deduced CHX protein. There are about 12 transmembrane spans at the N-terminus, and a hydrophilic tail at the C-terminus. In this model, the N and C termini face the cytosol.

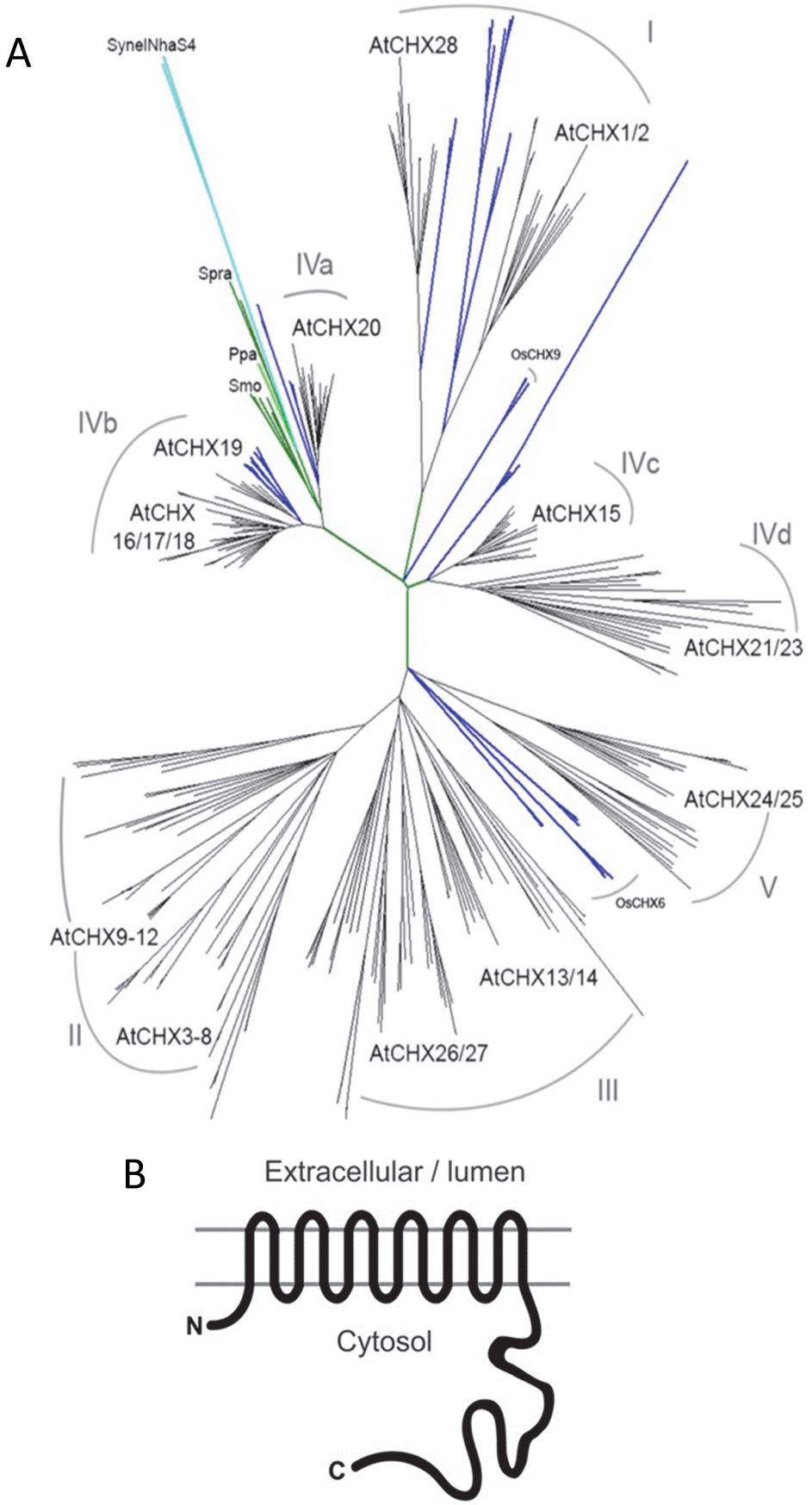
A
SynelNhaS4
AtCHX28
I
AtCHX1/2
Spra
IVa
AtCHX20
Ppa
Smo
OsCHX9
IVb
AtCHX19
IVc
AtCHX
16/17/18
AtCHX15
IVd
AtCHX21/23
AtCHX24/25
V
OsCHX6
AtCHX9-12
AtCHX13/14
II
AtCHX3-8
AtCHX26/27
III
B
Extracellular / lumen
N
Cytosol
C

(Fig.I- 2) (Chanroj et al., 2012). Since the number of CHX genes has increased sharply in land plants, these results suggest a hypothesis that CHX genes diversified to facilitate plants adapting to life on land.

A.5. What are CHX transporters?

A.5a. CHX genes are predicted cation/H^+ exchangers and half are expressed in pollen.

Among the nearly 1,000 *Arabidopsis thaliana* genes encoding membrane transporters, the family of 28 predicted CHX transporters is rare or absent in metazoan genomes (Arabidopsis Genome Initiative, 2000; Bock et al., 2006). CHX transporters have an N-terminal transmembrane domain consisting of 10-12 transmembrane spans and a C-terminal hydrophilic domain of unknown function (Fig. I-8B) (Sze et al., 2004). Reverse transcription PCR analysis of *CHX* genes showed they are expressed in pollen, vegetative tissues (root and leaf), or both (Sze et al., 2004). Surprisingly, 18 out of 28 *A. thaliana CHX* genes are expressed in the male gametophyte, which suggests roles in pollen development, germination, and tube growth (Sze et al., 2004) and perhaps in fertilization. Together, transcriptome studies of developing pollen grains and pollen tubes have shown multiple groups of *CHX* genes share overlapping expression patterns (Honys and Twell, 2003; Qin et al., 2009). For example, *CHX04*, *CHX09*, *CHX21*, and *CHX26* are not expressed in the pollen grain, but their expression increases sharply in germinating pollen and pollen tubes (Fig. I-9). These results suggest *CHX* genes support crucial functions at different stages in the male gametophyte. *Arabidopsis CHX* genes are also expressed in leaves and roots, which suggest *CHX* genes could perform functions that are not pollen-specific.

Fig. I-9. Expression of *Arabidopsis CHX* genes in pollen and sperm.

Results taken from the Pollen Transcriptome Navigator (pollen.umd.edu) that summarizes published datasets (Honys and Twell, 2004; Qin et al., 2009). **A)** *CHX* genes induced in *in vivo* grown pollen tubes. Genes including *CHX09* and *CHX21* are not expressed in the pollen grain, but are induced in both pollen tubes grown *in vitro* and in a semi-*in vivo* assay. **B)** Downregulation of some *CHX* genes in pollen tubes. Genes including *CHX14* and *CHX27* are expressed in tricellular and mature pollen grains, but are down-regulated after pollen tube emergence. **C)** *CHX* genes expressed in pollen grain and in tubes. Genes including *CHX02* and *CHX15* are initially expressed in tricellular pollen and remain expressed at a similar level after pollen tube emergence. **D)** *CHX18* expression in sperm cells. Of the related *CHX16-20* genes, *CHX19* is highly expressed in pollen grains and pollen tubes. Only *CHX18* is expressed in sperm cells, but not in tube cells (Borges et al., 2008).

Abbreviation on X-axis is defined as follows. **MS** is microspore, **BC** is bicellular pollen, **TC** is tricellular pollen, and **MP** is mature pollen. (Data of Honys & Twell, 2004)

pol refers to dry pollen, **0.5h** and **4 h** refer to pollen tubes germinated *in vitro* for 30 min and 4 h, respectively; **SIV PT** refers to pollen tubes germinated in the semi-in vivo assay, data of Qin, et al., 2009), **sperm** refers to transcriptome data of sperm cells (Borges et al 2008).

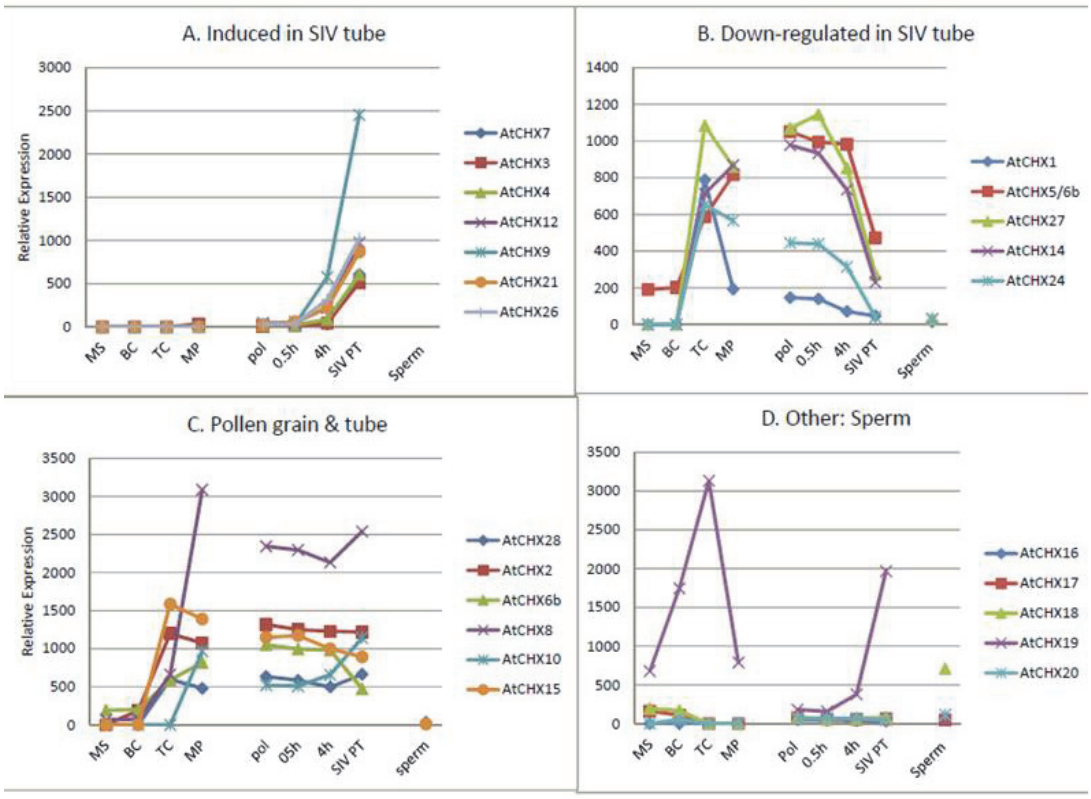
A. Induced in SIV tube
Relative Expression
3000
2500
2000
1500
1000
500
0
MS
BC
TC
MP
pol
0.5h
4h
SIV PT
Sperm
AtCHX7
AtCHX3
AtCHX4
AtCHX12
AtCHX9
AtCHX21
AtCHX26
B. Down-regulated in SIV tube
1400
1200
1000
800
600
400
200
0
AtCHX1
AtCHX5/6b
AtCHX27
AtCHX14
AtCHX24
C. Pollen grain & tube
3500
AtCHX28
AtCHX2
AtCHX6b
AtCHX8
AtCHX10
AtCHX15
D. Other: Sperm
AtCHX16
AtCHX17
AtCHX18
AtCHX19
AtCHX20

A.5b. CHX genes expressed in roots and leaves.

Using Northern blots, *CHX17* expression was shown to be induced in seedlings by external stresses including high NaCl, K^+ starvation, and acidic pH. In addition, *CHX17* was implicated in root K^+ homeostasis, as *chx17* mutants accumulate less K^+ than WT under low K^+ conditions. This phenotype could arise from *CHX17* expression in the epidermis and cortex of the mature zone of the root (Cellier et al., 2004). Subsequently, *CHX17* expression was shown in seeds, mature roots, and stipules *in vivo* using a pCHX17:YFP construct (Fig. I-10A, C). In roots, pCHX17:YFP signal intensity increased by approximately 175-300 fold under low K^+ stress (Chanroj et al., 2013). Since *chx17* roots are similar to WT, this suggests *CHX17* does not function in bulk K^+ uptake, and *CHX17* could instead function in redistributing K^+ into membrane compartments.

Analysis of the guard cell transcriptome using the ATH1 GeneChip showed *CHX20* was the only *CHX* gene expressed in guard cells (Padmanaban et al., 2007). To test *CHX20* expression *in vivo*, pCHX20:GUS activity was assayed. GUS activity was observed specifically in guard cells from cotyledons, sepals, anthers, and rosette leaves (Fig. I-10F). A low level of GUS activity was also observed in root cap cells (Padmanaban et al., 2007). The presence of *CHX20* in guard cells suggests an essential role for *CHX20* in stomata function.

Fig. I-10. Promoter activity of diverse *CHX* genes in various plant tissues.

CHX transporters are expressed in both the vegetative (roots and shoots) and reproductive tissues of *Arabidopsis thaliana*.

A) *pCHX17::YFP* expression in developing seeds (Chanroj et al., 2013).

B) *pLat52::GUS* in Wt and mutant *CHX21/23* pollen (Lu et al., 2011).

C) *pCHX17::YFP* expression in roots (Chanroj et al., 2013).

D) *pCHX13::GUS* in pollen tubes (Sze et al., 2004).

E) *pCHX23::GUS* in pollen grains (Sze et al., 2004).

F) *pCHX20::GUS* in guard cells (Padmanaban et al., 2007).

The phenotypes of *chx* mutant plants indicate CHX transporters function in critical processes such as stomata movement, pollen tube guidance, and seed development. (Plant cartoon from Taiz, L. and E. Zeiger, 2002. *Plant Physiology*. 3rd Ed. Sinauer. Sunderland, MA). Figure designed by D. Czerny.

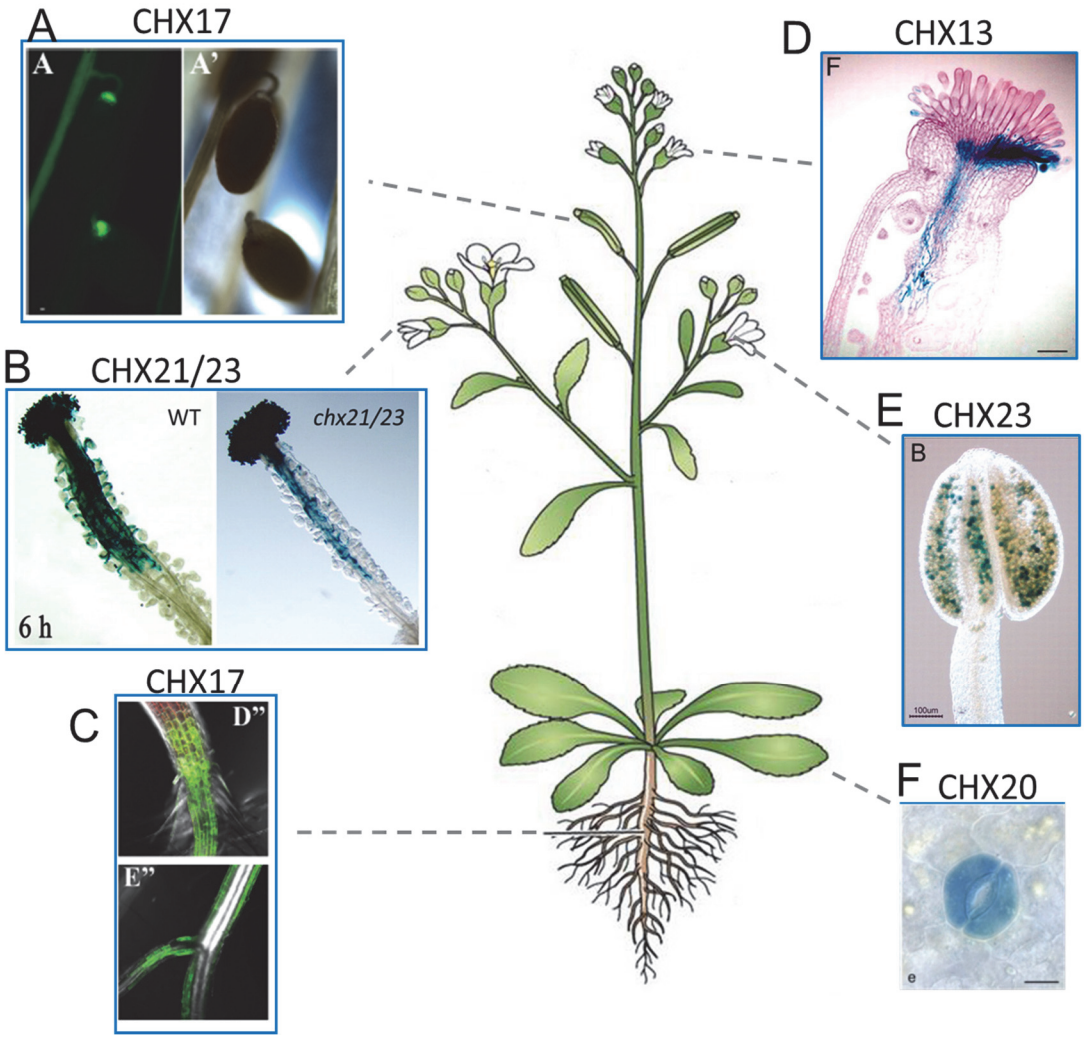
A
CHX17
A
A'
B
CHX21/23
WT
chx21/23
6 h
C
CHX17
D"
E"
D
CHX13
F
E
CHX23
B
F
CHX20
e

A.6. What are the cellular functions of *CHX* genes?

A.6a. pH homeostasis.

In eukaryotic cells, the pH of the cytosol and each subcellular compartment is maintained, though the mechanisms of cellular pH homeostasis are not completely understood. In animal cells, cytosolic pH is approximately neutral, and luminal pH in the compartments fluctuates from pH 7.2 in the ER lumen, to pH 6.0 in the TGN, to pH 6.3 in early endosomes, and finally to pH 4.7 in the lysosome (Casey et al., 2010). In plant cells, *in vivo* endoluminal pH was recently determined by using genetically-encoded fluorescent pH sensors. In tobacco epidermal cells or *Arabidopsis* roots, the pH of the secretory pathway compartments acidified from the ER to the TGN, became alkaline through endosomes and the PVC before becoming acidified in the vacuole (Fig.. I-11A) (Martiniere et al., 2013). Alternatively, in *Arabidopsis* protoplasts, pH-sensitive GFP constructs targeted to compartments in the secretory and endocytic pathways showed a gradual acidification from the ER to the vacuole (Fig. I-11B) (Shen et al., 2013). However, the luminal pH in the MVB/PVC is debatable, as pH values of 6.2 and 7.1 were obtained using two different pH-sensitive GFP probes targeted to the PVC (Martiniere et al., 2013; Shen et al., 2013). In animal cells, the distribution and activities of Na^+/H^+ exchangers (NHEs) were shown to influence cellular pH levels (Orlowski and Grinstein, 2007). NHE1 in the slime mold *Dictyostelium discoideum* functions in alkalinizing cytosolic pH for chemotaxis (Patel and Barber, 2005). Much less information is known about plant transporters that modulate intracellular pH.

Fig. I-11. Organelles of the secretory and endocytic pathways have distinct luminal pHs.

A) The steady state luminal pH values of the secretory and endocytic compartments in *Arabidopsis* roots and tobacco epidermal cells. The pH was measured using the genetically encoded fluorescent pH sensor pHluorin targeted to individual compartments by fusions with compartment resident proteins, e.g., vacuolar sorting receptor 2 (VSR2) for the PVC. Using this method, luminal pH in the ER was near neutral, and the pH gradually becomes more acidic, reaching 6.1 in TGN. Endosome luminal pH was more alkaline, reaching pH 7.1 in late endosomes, and was pH 6.0 in the vacuole. Results were similar for both roots and epidermal cells. (Fig. taken from Martiniere et al., (2013) *Plant Cell*. 25:4028.) **B)** Organelle luminal pH in *Arabidopsis* protoplasts. pH was measured using two modified pH-sensitive GFP proteins fused to sorting signals for each compartment (e.g., the HDEL peptide for the ER). Luminal pH in the nucleus and ER was approximately neutral, and the pH acidified from the *cis*-Golgi, through the TGN, and PVC, which has a pH of 6.2. The pH of the vacuole is 5.2. (Fig. taken from Shen et al., (2013) *Mol. Plant*. 6:1419.) Overall, both methods show a gradual acidification of luminal pH by 1.5-2 units. However, varying luminal pH values were reported for the late endosome.

In a plant cell, how does a compartment maintain a homeostatic pH? A simple working model is given here. The H^+-pumping ATPases on the PM (PM-ATPase) or on

A

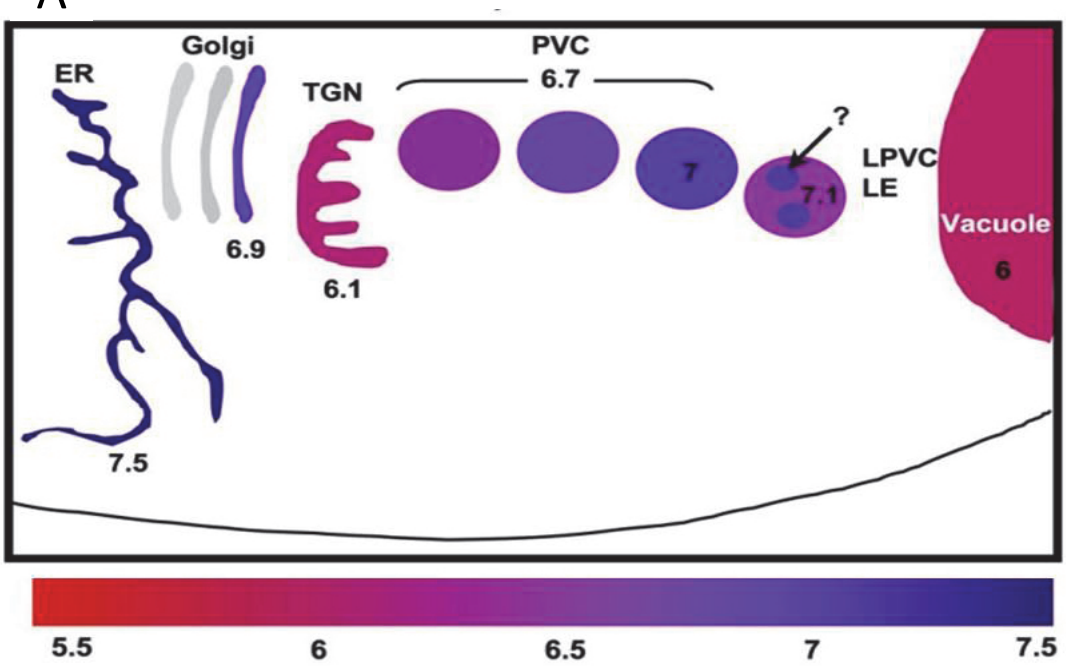
ER
Golgi
TGN
PVC
6.7
?
LPVC
LE
Vacuole
6
7
7.1
6.9
6.1
7.5
5.5
6
6.5
7
7.5

B

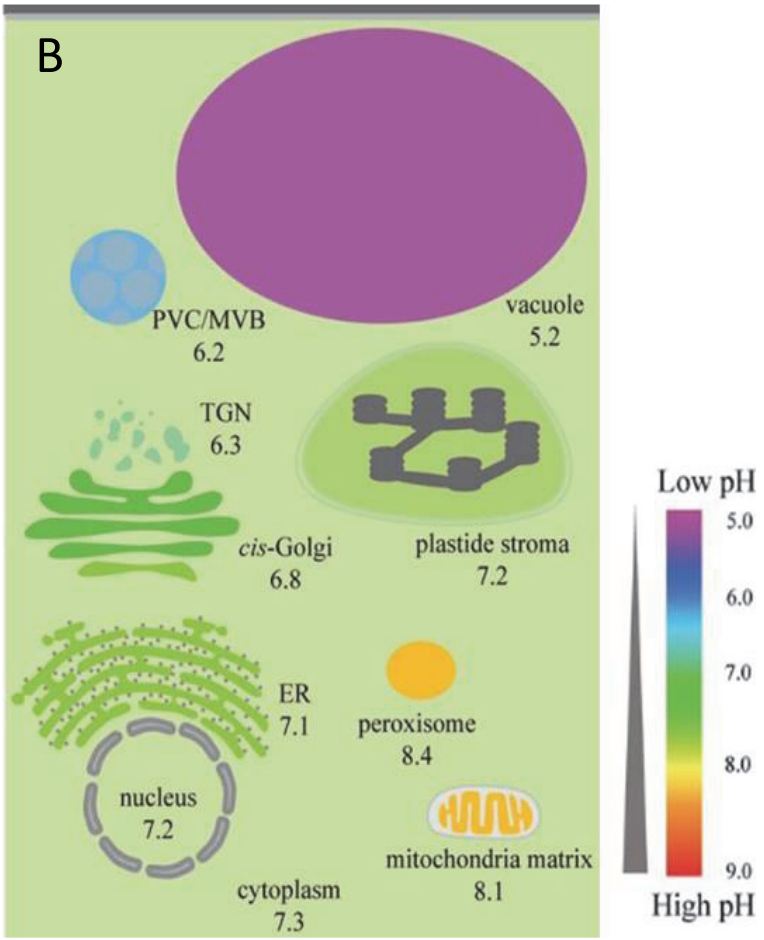
PVC/MVB
6.2
vacuole
5.2
TGN
6.3
cis-Golgi
6.8
plastide stroma
7.2
ER
7.1
peroxisome
8.4
nucleus
7.2
mitochondria matrix
8.1
cytoplasm
7.3
Low pH
5.0
6.0
7.0
8.0
9.0
High pH

the vacuole and organelles (V-ATPase) are the primary active transporters in the plant (Sze, 1985). These are electrogenic H^+ pumps that use energy from ATP hydrolysis to move H^+ from the cytosol into the extracellular space or the lumen of a compartment. For the V-ATPase, H^+ translocation generates an electrical potential (inside positive) across a compartment membrane (Fig. I-12A). Subsequent net anion influx into the compartment could dissipate the electrical potential, allowing bulk H^+ flow. Thus, the compartment lumen would become acidified, and a pH gradient would be generated (Fig. I-12B). Movement of H^+ down the concentration gradient into the cytosol could alkalinize the compartment and acidify a local cytosolic region. Such movement could be accomplished by secondary active transporters which use the energy from the H^+ gradient to move Na^+, K^+, or Ca^{2+} against their concentration gradients (Fig. I-12C).

Heterologous expression of *CHX* genes in yeast mutants defective in multiple cation transporters has provided clues to the functions of *Arabidopsis* CHX transporters. Yeast cation transport mutants transformed with an empty vector are sensitive to alkaline external pH. Expression of *CHX17* in the LMB11 (*ena1-4Δ*, *nha1Δ*, *kha1Δ*) yeast mutant rescued the alkaline pH sensitivity, indicating *CHX17* could somehow regulate pH homeostasis similar to the endogenous KHA1 transporter. KHA1 is a yeast homolog of CHX transporters (Maresova and Sychrova, 2006; Chanroj et al., 2012). The yeast mutant KTA40-2 (*ena1-4Δ*, *nha1Δ*, *kha1Δ, nhx1Δ*) harboring an empty vector grows poorly at pH 7.5, but grows robustly at acidic pH. Expression of *CHX20* in KTA40-2 yeast rescues the alkaline-sensitive phenotype only in the presence of limiting (3 mM or less) K^+ (Padmanaban et al., 2007).

Fig. I-12. Model of transporters that influence luminal pH homeostasis.

A) In plants, the V-ATPase (blue) and the V-PPase (orange) are distributed among the intracellular compartments, including the vacuole. These electrogenic transporters move H^+ into the compartment lumen. Movement of positive-charged H^+ generates an electrical potential across the membrane (positive inside) with little change in lumen pH.

B) To balance the movement of H^+, anion transporters, e.g. the NO_3^- transporter ClCa (purple), move anions into the compartment lumen. Subsequently, bulk H^+ entry acidifies the lumen, and an acid-inside pH gradient is formed across the membrane.

C) To modulate the luminal pH, secondary-active cation/H^+ exchangers, e.g. CHX (green), use energy from the H^+ gradient to bring K^+ or Na^+ into the lumen against their concentration gradients. The luminal pH becomes less acidic. The combined activities of these three classes of transporters modulate pH homeostasis in cellular compartments. This mechanism functions in all membrane compartments, but using different transporters, to modulate the luminal pH. Figure designed by D. Czerny.

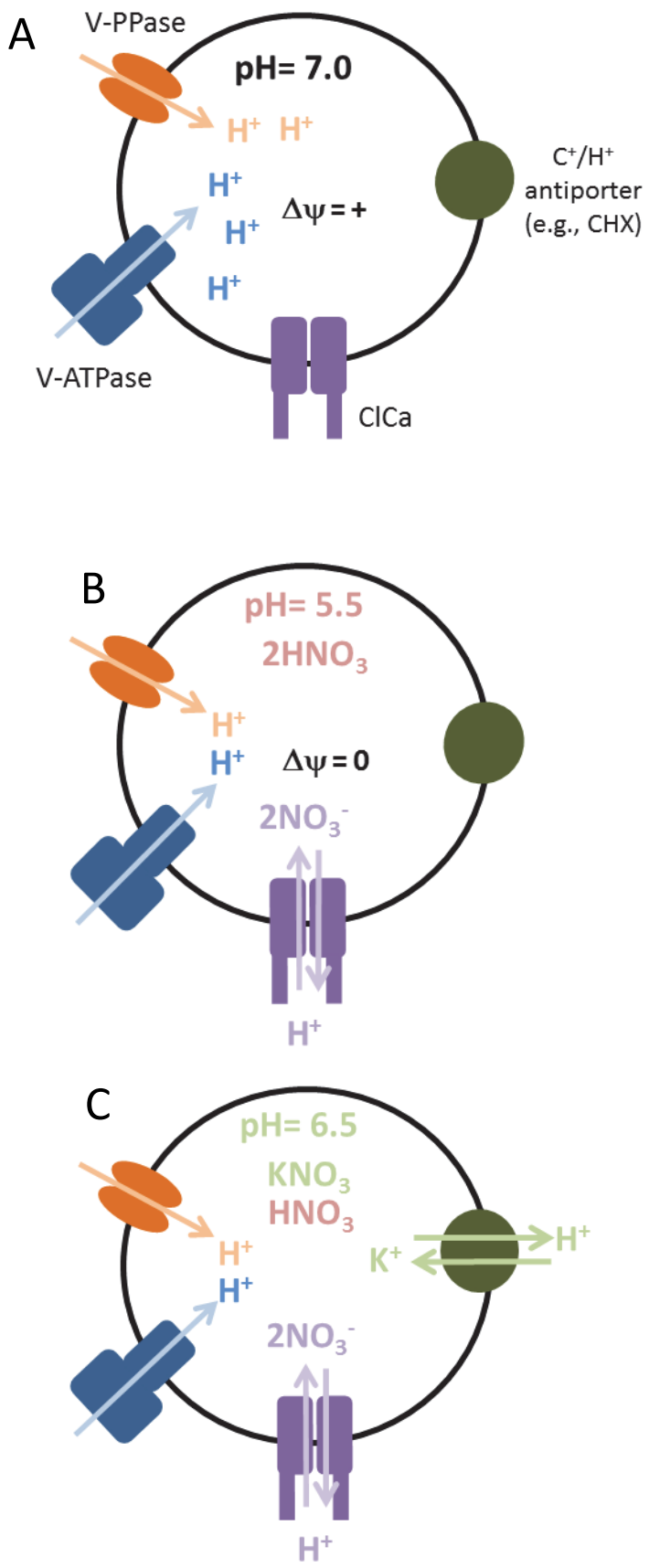
A
V-PPase
pH= 7.0
H+ H+
H+
H+
H+
Δψ = +
C+/H+
antiporter
(e.g., CHX)
V-ATPase
ClCa
B
pH= 5.5
2HNO3
H+
H+
Δψ = 0
2NO3-
H+
C
pH= 6.5
KNO3
HNO3
H+
H+
K+
H+
2NO3-
H+

In addition, expression of *CHX16-20* also rescues the alkaline-sensitive phenotype in the presence of 0.6 mM K^+ (Chanroj et al., 2011). These results show CHX transporters somehow influence intracellular pH when yeast encounters an alkaline environment. However, the mechanism by which CHX transporters confer tolerance to alkaline pH remains unknown.

A.6b. K^+ homeostasis

Functional studies in yeast suggest that CHX transporters could have roles in acquisition or redistribution of K^+ within yeast cells. To test if expression of CHX transporters facilitates K^+ uptake in yeast, the LMM04 *(trk1,2Δ*, *tok1Δ*) K^+ uptake-deficient yeast mutant was transformed with *CHX15-20*. In the presence of limiting K^+ (8 mM), CHX transporters showed different abilities to rescue yeast growth. Only *CHX17, 18* or *19* conferred strong yeast tolerance to pH 7.5 at 8 mM K^+. In contrast, *CHX16* partially rescued yeast growth between pH 4.3 and 7.5. When K^+ was replete (58 mM), only *CHX16, 19,* or *20* could rescue yeast growth at pH 4.3 (Chanroj et al., 2011). These results show individual CHX transporters are functionally diverse, and can mediate K^+ uptake under varying external pH and K^+ concentrations. The results suggest CHX16 to CHX20 have roles in regulating K^+ homeostasis.

To test the alkali cation specificity for CHX transporters, *CHX17* and *CHX20* were expressed in the *E. coli* mutant LB2003, which lacks 3 major K^+ uptake mechanisms. An advantage of using a prokaryotic expression system is any heterologous protein will be inserted into the PM, and substrate movement mediated by transporters can be directly measured across the PM (Uozumi, 2001). Using the K^+ analog $^{86}Rb^+$ in competition experiments with cold cations, CHX17 and CHX20 both showed substrate

preference for K^+ over Na^+ when expressed in *E. coli* (Chanroj et al., 2011). This result shows CHX17 and CHX20 both transport K^+, which is necessary for understanding how these transporters affect pH and cation homeostasis in the cytosol and in the lumen of an endomembrane compartment.

A.6c. Role in protein sorting and membrane trafficking

Cellular growth, signaling and development depend on the proper synthesis and sorting of proteins and other cargo to the right destination at the appropriate time. The yeast mutant KTA40-2 lacks several cation transporters and secretes the vacuolar enzyme carboxypeptidase Y (CPY) to the external medium. Expression of *CHX17* reduced the amount of extracellular CPY under alkaline, but not acidic, external pH (Chanroj et al., 2011). This result is consistent with *CHX17* being functional at pH 7.5 in yeast as assayed by alkaline pH tolerance. Additionally, *CHX17* can be implicated in protein sorting pathways through its effect on CPY trafficking. *CHX17* activity in yeast is sufficient to redirect vesicle trafficking to reduce the secretion of vacuolar CPY by potentially reestablishing pathways for CPY protein sorting to the vacuole.

Another line of evidence for CHX17 affecting membrane trafficking and sorting pathways was shown by yeast resistance to hygromycin B (HygB). HygB is a cationic antibiotic that, upon endocytosis, can bind to ribosomes to inhibit translation (Brodersen et al., 2000). Yeast cation transport mutants transformed with an empty vector are sensitive to HygB. Among the related CHX16-20 transporters, only CHX17-19 were able to confer yeast tolerance to 100 µg/ml HygB, similar to the yeast KHA1 transporter (Chanroj et al., 2011). Since only the highly-related CHX17-19 could confer HygB tolerance, this result indicates possible differences in membrane localization and pH-

dependent activity for CHX transporters. A hypothesis for yeast tolerance to HygB is that KHA1 and CHX17-19 restore endosome luminal pH in the cation transport mutants similar to WT levels. These transporters could move H^+ into the cytosol, which could modulate luminal pH in order to efficiently move cargoes, including HygB, to the vacuole. Acidification of endosomes by CHX17-19 could enhance HygB trafficking to the vacuole for degradation, thus conferring tolerance.

A.6d. Diversity of CHX and NHX transporters

In addition to CHX transporters, plant genomes contain another subfamily of cation/H^+ exchangers, known as AtNHX1-8 in *A. thaliana*. A fundamental question is: how do CHX transporters differ in function from NHX transporters? Valuable insights are emerging from heterologous expression in yeast. CHX17 and its yeast homolog KHA1 could both confer alkaline pH tolerance. *S. cerevisiae* NHX1 (ScNHX1) could confer slight tolerance to alkaline pH, but *Arabidopsis* NHX1 and NHX2 could not confer alkaline pH tolerance. Using the same concentration of HygB, ScNHX1 could provide yeast tolerance to HygB, whereas CHX17 could not provide tolerance (Chanroj et al., 2011). These assays show CPA1 and CPA2 transporters have distinct functions when expressed in yeast. CPA1 members confer strong tolerance to HygB, but CPA2 members can support yeast growth at alkaline pH. Molecular structure and function analysis of CHX transporters could provide evidence for functional differences from NHX transporters, but this awaits further experimentation.

A.6e. Protein localization in the plant

To understand the cellular roles of CHX transporters, their localizations were tested using fluorescent protein fusions. Mesophyll protoplasts were used to test

localization of CHX17-19. CHX17 tagged with a fluorescent protein colocalized with the RFP-syntaxin 21 (PVC) and GFP-ARA7 (endosome) markers, which indicates a PVC localization. Using CHX17-RFP as a PVC marker, CHX18-GFP and CHX19-GFP both colocalized with CHX17-RFP to provide evidence for shared localization at the PVC (Chanroj et al., 2011). These data were corroborated by testing localization of GFP fusions in stable transgenic plants. Under the 35S promoter, CHX16, 17, 18, or 19 tagged with GFP colocalized at the cell periphery and at intracellular puncta. Colocalization of the CHX16, 17, 18, and 19-GFP signal with the PM marker PIP2-RFP and distribution of CHX17-GFP signal in Hechtian strands after sucrose plasmolysis indicated these transporters localize to the plasma membrane (Chanroj et al., 2013). To identify the intracellular puncta labeled by CHX-GFP, transgenic plants were treated with the drug wortmannin, which blocks vesicle trafficking out of endosomes and the PVC (Robinson et al., 2008). After wortmannin treatment, the CHX17-GFP signal changed from puncta to ring-like structures. This change in labeling pattern is consistent with wortmannin causing PVC expansion (Chanroj et al., 2013). Since CHX16, 17, 18, or 19 localize to dynamic membrane compartments in the plant, these transporters could influence vesicle trafficking to the vacuole and among endosomes.

CHX transporters were also localized to the ER membrane. In protoplasts, CHX20-RFP fluorescence colocalized with the ER lumen marker GFP-HDEL to indicate CHX20 is found on ER membranes (Chanroj et al., 2011). In addition, to test the subcellular distribution of CHX23, the pLat52:CHX23-RFP construct and a collection of fluorescent markers were transiently expressed in tobacco pollen by particle bombardment. The pattern of CHX23-RFP signal was similar to the ER membrane

markers SIP2.1-GFP and GFP-HDEL. These results were supported by analyzing pCHX23:CHX23-GFP signal in transgenic *Arabidopsis* pollen. Thus, CHX23 is associated with the ER membrane (Lu et al., 2011). At least 2 CHX transporters are localized to the ER membrane, and one possible function for these transporters could be to control the pH of microdomains of ER lumen to facilitate folding of proteins into the ER membrane. In summary, CHX transporters are found on dynamic membranes (ER, PVC, and PM) involved in the secretory and endocytic pathways. This localization suggests CHX transporters could regulate luminal pH in compartments to influence either the vesicle trafficking machinery or activities of protein cargo trafficked among those compartments.

A.7. What is the mode of transport? Homology modeling can provide insights into the mode of CHX17 transport.

The mode of CHX transport has not yet been directly demonstrated. BLAST sequence comparisons of *Arabidopsis* CHX proteins with other eukaryotic and prokaryotic sequences predicted the *Arabidopsis* proteins were similar to $K^+(Na^+)/H^+$ exchangers. Phylogenetic analysis indicated that CHX proteins in higher plants most likely originated from an ancestral gene the of *E. coli* $Na^+(Li^+)/H^+$ antiporter EcNhaA (Fig. I-7) (Chanroj et al., 2012). Thus, EcNhaA can serve as a model to study the mode(s) of transport for CHX transporters. EcNhaA is the primary $Na^+(Li^+)/H^+$ antiporter in *E. coli* and functions in maintaining cytosolic pH near neutral when the bacterium encounters an alkaline environment. EcNhaA activity increases sharply between pH 6.5 and 8.5, reaching a maximum at pH 8.5 (Taglicht et al., 1991b). In addition, the crystal structure of EcNhaA was solved at pH 4 in 2005 (Hunte et al., 2005).

This structure shows the 12 TM helices of EcNhaA can be divided into two inverted repeats of 5 TM helices each. In contrast to CHX transporters, EcNhaA lacks a hydrophilic C-terminal domain. When EcNhaA is folded in the *E. coli* plasma membrane, the last two TM helices in each inverted repeat- 4 and 5, 11 and 12- form the transport core. TM spans 4 and 11 consist of discontinuous α-helices with intersecting unstructured extended chains in the middle of each TM span. These segments are in close proximity and form the binding site for Na^+(Li^+) and H^+ ions (Boudker and Verdon, 2010). Recently, the NapA Na^+/H^+ antiporter from *T. thermophilus* was crystalized as a dimer at pH 7.8, at which the transporter is active. In contrast to EcNhaA, TtNapA contains 13 TM spans, although the transport core of TtNapA contains discontinuous α-helices in TM spans 4 and 11, similar to EcNhaA (Fig. I-13A) (Lee et al., 2013). As in the EcNhaA transport core, TtNapA contains two conserved Asp residues on TM span 5 and a Lys residue on TM 10 in close proximity to the intersecting discontinuous α-helices (Fig. I-13B, C) (Furrer et al., 2007; Lee et al., 2013). From analysis of the EcNhaA and TtNapA crystal structures, insights into cation transporter structure-function relationships can be applied to test the mode of transport of plant CHX transporters.

It is now possible to build a three-dimensional model using a known crystal structure of a related transporter (Kelley and Sternberg, 2009). Protein alignments can help find conserved residues shared among a protein of interest and related proteins (Edgar, 2004). This homology model-guided approach was used to characterize the *H. sapiens* CPA2 transporter HsNHA2 based on the EcNhaA crystal structure. From protein alignments and the HsNHA2 model structure, HsNHA2 amino acids that are both conserved with EcNhaA and possess charged sidechains were identified within the

discontinuous helices in HsNHA2 TM spans 4 and 11. Site-directed mutagenesis of HsNHA2 confirmed these residues were important for transport function using expression in a cation transporter-deficient yeast mutant and testing for growth over a range of pH values or concentrations of NaCl and LiCl. Wild-type HsNHA2 could confer tolerance to LiCl and NaCl, but yeast expressing HsNHA2 point mutants at critical residues were sensitive (Schushan et al., 2010). Analysis of HsNHA2 based on a model structure showed residues conserved with EcNhaA are required for transporter activity in addition to novel HsNHA2 residues that have roles in transporter function.

Fig. I-13. The crystal structure of *T. thermophilus* NapA shows the active state of a Na^+/H^+ antiporter.

A) The crystal structure of the TtNapA Na^+/H^+ antiporter (PDB: 4BWZ) at pH 7.8. The 13 TM spans are colored from blue (TM-1) to red (TM12). **B)** Model showing the mechanism of the TtNapA antiporter using a schematic representation of the outward-facing crystal structure and an inward-facing homology model. Na^+ and H^+ ions sequentially bind to the transport core containing the conserved Asp157 residue. When Asp157 is facing outward, two H^+ bind within the transport core, which triggers a conformational change. This conformational change exposes Asp157 to the cytosol, which causes the H^+ to dissociate and one Na^+ ion to bind to the transport core. Na^+ binding causes another conformational change in TtNapA, returning the dimer to the outward-facing conformation. (Fig. from Lee, et al. (2013) *Nature*. 501:573.) **C)** Model showing the mechanism of the EcNhaA Na^+/H^+ antiporter. The protonation states of Asp163 and Asp164 control the transport cycle of EcNhaA. When Asp163 is deprotonated, Asp164 is accessible to the cytosol. Asp164 releases a H^+ to the cytosol and binds a Na^+ from the cytosol. Na^+ binding allows Asp163 to bind a H^+ from the periplasm, which causes a conformational change that exposes Asp163 to the cytosol and Asp164 to the periplasm. Asp164 exchanges the Na^+ for a periplasmic H^+, and Asp163 releases the H^+ to the cytosol. Deprotonation of Asp163 completes the cycle, and Asp164 again faces the cytosol. (Fig. from from Arkin, et al. (2007) *Science*. 317:799.) Figure designed by D. Czerny.

A

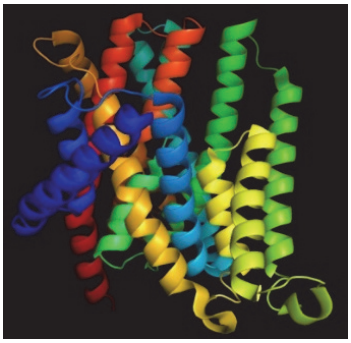

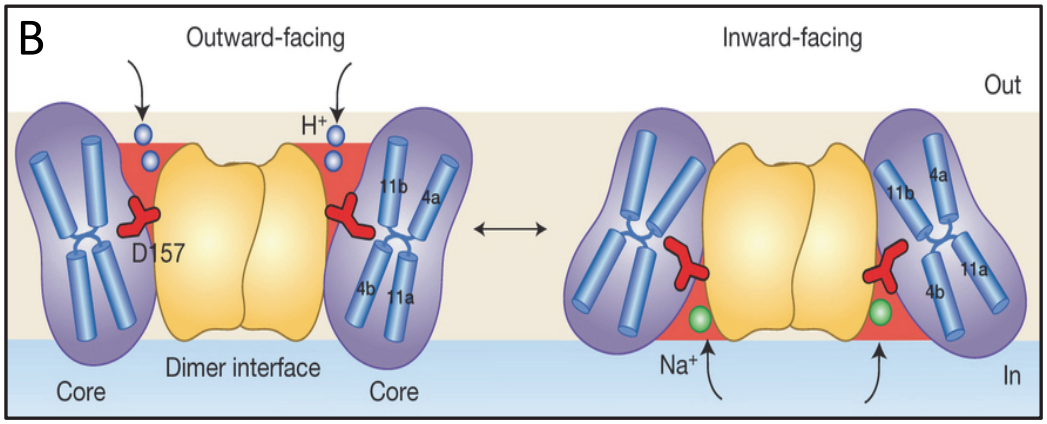
B
Outward-facing
Inward-facing
Out
H+
D157
11b
4a
4b
11a
Dimer interface
Core
Core
Na+
In

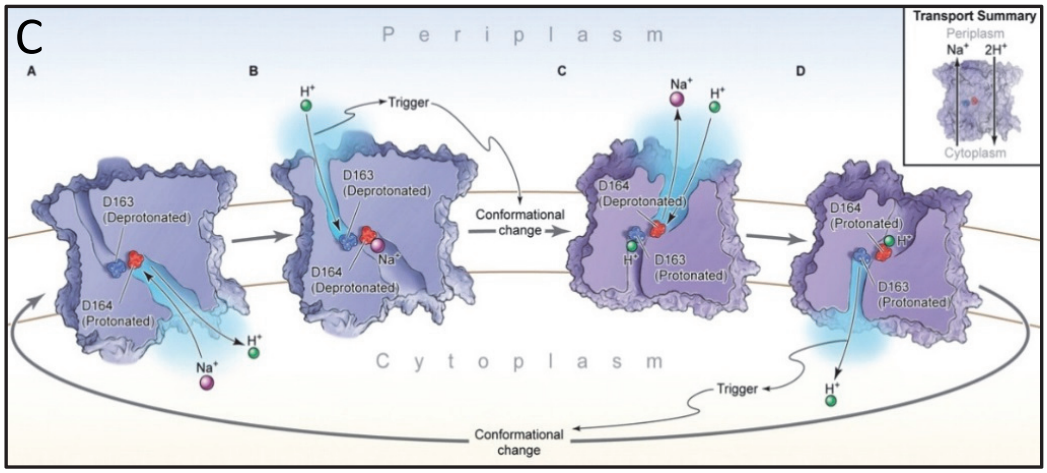
C
Periplasm
A
B
C
D
Transport Summary
Periplasm
Na+
2H+
Cytoplasm
Trigger
D163 (Deprotonated)
D164 (Protonated)
D164 (Deprotonated)
Conformational change
D164 (Protonated)
Cytoplasm
Conformational change

A.8. What are the biological functions of CHX transporters? Analysis of *chx* mutants indicates roles in signal transduction and development.

A.8a. Guard cell movement: CHX20

Analysis of *chx* mutants has shown potential functions for *CHX* genes in regulating pH and K^+ homeostasis. *CHX20* is the only *Arabidopsis* CHX transporter expressed in guard cells, and *chx20* mutants show impaired light-induced stomatal opening (Padmanaban et al., 2007). Using the membrane-permeable dye Acridine Orange, vacuolar acidification was shown to accompany stomatal closure (Bak et al., 2013). In yeast, *CHX20* expression acidifies the cytosolic pH and alkalinizes the vacuolar pH as measured by a pH-sensitive GFP (Chanroj et al., 2011). Thus, CHX20 could influence pH and K^+ homeostasis in guard cells by possibly either loading K^+ into endomembrane compartments to increase turgor or alkalinizing the vacuole to open stomata.

A.8b. Pollen tube targeting: CHX21/23

A double *chx* mutant has phenotypes indicating roles in pollen function. *CHX21* and *CHX23* are functionally-redundant genes expressed in pollen (Fig. I-10E). *chx21/23* mutant pollen tubes grow through the transmitting tract similar to wild-type tubes. However, *chx21/23* tubes rarely target ovules to complete double fertilization, resulting in only a single seed in *chx21/23* seed pods (Lu et al., 2011). By staining for pLat52:GUS activity, WT tubes could grow through the ovary and target ovules, which was indicated by blue coloring after tube burst within ovules. With *chx21/23* pollen tubes, growth along the transmitting tract was similar to WT, but *chx21/23* tubes did not grow along the funiculus towards the ovules, as seen by lack of blue staining in ovules

(Fig. I-10B) (Lu et al., 2011). This result shows *CHX21/23* function in pollen tube guidance by targeting tube growth from the transmitting tract onto the funiculus and into the ovule. *CHX21/23* possibly function in regulating vesicle trafficking to the tube tip to reorient growth towards the ovules by either perceiving female guidance cues or mediating the tube's response to those cues.

A.8c. K^+ uptake at PM: CHX13

CHX13 encodes a PM-localized transporter expressed in roots, flowers, siliques, and pollen tubes (Fig. I-10D). *CHX13* is upregulated in roots under low K^+ conditions similarly to *CHX17*, and, as shown in yeast, CHX13 mediates high-affinity K^+ uptake. In addition, *chx13* plants show reduced growth and leaf chlorosis when germinated on low K^+ medium at varying pH (Zhao et al., 2008). These results show CHX13 functions in K^+ uptake into the cell rather than K^+ homeostasis in compartments, which is distinct from the suggested functions of other characterized CHX transporters. Taken together, *CHX* genes are expressed in pollen, leaf, and root and have different capabilities to regulate cellular K^+ content. However, these genes share a similar proposed function in maintaining pH and K^+ homeostasis.

A.8d. Reproduction and seed set: CHX16/17/18/19

chx17 single mutant plants do not have a detectable phenotype, so higher-order mutants of the related genes *CHX16/17/18/19* were generated. However, double *chx17/18* and *chx17/19* mutants also did not display a phenotype, thus triple and quadruple mutants were generated. Interestingly, homozygous *chx17/18/19* and *chx16/17/18/19* plants were recovered significantly below the expected ratio from self-fertilized parents heterozygous for one gene. From analyzing mature seed pods,

chx17/18/19 and *chx16/17/18/19* plants showed 56%-77% reduced seed set relative to wild-type (Chanroj et al., 2013). This result shows *CHX16/17/18/19* are necessary for full seed set, but how these genes function in reproduction and/or seed development remains obscure.

B. Statement of the problem and research aims.

Eighteen of the 28 *Arabidopsis CHX* genes are expressed in pollen; however, their in planta functions are for the most part unknown. The first goal of this research is to understand the biological basis for the reduced seed set observed in *chx17/18/19* plants. The second goal is to understand the mode of transport of CHX17 using 3D model structure-guided mutagenesis to identify core residues involved in CHX17 catalysis.

Aim 1. Determine the *in planta* function of *CHX17, 18,* or *19* in seed set.

We use single, double and triple mutant plants to test what step of sexual reproduction is compromised. We show that *CHX17*, *18*, and *19* share overlapping roles in male fertility. Together with previous studies, these findings suggest that modulation of pH and K^+ homeostasis by *CHX17, 18* or *19* transporters are critical for successful fertilization and seed development.

Aim 2. Test the mode of transport for CHX17.

Though annotated as a cation/H^+ exchanger, there is no direct evidence for its mode of transport. The mode of CHX17 transport was tested by 3D model structure-guided mutagenesis followed by functional assays in yeast. Two model structures of the CHX17 transport domain were built based on templates of TtNapA and EcNhaA crystal structures. This is the first study to identify several key residues that form the transport

core in a plant CPA2 transporter. Thus, this study shows CHX17 shares striking similarities to known cation/H^+ exchangers. Furthermore, 3D modeling reveals a conserved tandem universal stress protein domain at the carboxylic terminus of plant CHX transporters.

Significance

Using *A. thaliana* CHX17 as a model, this research provides the first evidence that its mode of transport resembles a K^+/H^+ exchanger. *chx17/18/19* mutant plants show reduced seed set relative to WT, possibly due to male gametophyte defects that compromise fertilization. The genes in the embryo sac also facilitate embryo development possibly through endosperm function. Taken together, this research has shown K^+/H^+ exchange by CHX transporters is necessary for proper male gametophyte function and embryo development.

Chapter II: CHX TRANSPORTERS INVOLVED IN pH AND K+ HOMEOSTASIS OF THE ENDOMEMBRANE SYSTEM ARE CRITICAL FOR MALE FERTILITY AND EMBRYO DEVELOPMENT

A. ABSTRACT

Several predicted cation/H^+ exchangers (AtCHX17, CHX18 and CHX19) localize to the prevacuolar compartment and the plasma membrane in plants, have roles in K^+ and pH homeostasis, and affect protein sorting in yeast. However, the roles of these three related *CHX* genes in the plant are not known. A triple homozygous mutant, *chx17/18/19,* was recovered at a reduced frequency, due to a 67% reduction in seed set relative to wild-type and double mutants. Reciprocal crossing of the *chx17/18/19* mutant with wild-type indicated that the defect was largely due to the male gametophyte, and partially due to female gametophyte. *chx17/18/19* pollen grains developed similar to wild-type, and mutant pollen tubes grew and targeted ovules. Although aniline blue-stained pollen tubes reached many ovules, about half of the ovules remained undeveloped, suggesting a failure to complete fertilization. Pods from wild-type pistils pollinated with triple mutant pollen contained a mixture of unfertilized ovules, single-fertilized ovules, and developing seeds. Single fertilization events were recognized as globular embryo only or endosperm only; whereas double fertilization produced an embryo and an endosperm. From transcriptome analysis, *CHX* expression in the pollen tube and sperm cells suggested that altered pH and K^+ homeostasis of the pollen tube, sperm, or both can partially compromise male fertility. When fertilization is successful, self-pollinated triple mutants produced embryos delayed in development. It is possible the female gametophyte influences embryo development and seed set due to *CHX18* expression in the micropylar endosperm. Our results highlight the critical roles of pH and cation homeostasis and membrane trafficking on male fertility, successful double fertilization, and embryo development.

B. INTRODUCTION

Early land plants, such as mosses and ferns, reproduce using motile male gametes that can swim through an aqueous medium to the female gametes. However, in flowering plants, sperm cells find the egg cell and the central cell nucleus in the absence of an aqueous environment due to the evolution of reproductive innovations. The two sperm cells are protected inside a tiny male gametophyte, the pollen grain, which can withstand desiccation as it is transported over long distances by wind or pollinators. When a pollen grain lands on a receptive stigma, it hydrates, germinates, and extends a pollen tube inside the pistil tissues that surround and protect the female gametophyte. Inside the pistil, there is continuous communication between male and female cells as the tube navigates to an available embryo sac. Once inside the embryo sac, the tube ruptures to release the two sperm cells. One sperm fuses with the egg cell nucleus and the other with the central cell nucleus to complete double fertilization (Dresselhaus and Franklin-Tong, 2013). Subsequent development of the embryo and the endosperm produces a seed that tolerates desiccation and harsh environments to remain viable for long periods. Although the major steps of reproduction have been known for decades, the molecular and cellular bases of pollen-pistil interactions that culminate in successful double fertilization are poorly understood.

Comparison of genomes has revealed a striking diversification of one transporter family (CHX cation/H^+ exchangers) in monocot and eudicot plants relative to early land plants. The cation/proton antiporter (CPA) superfamily is conserved across phyla and classified into two major groups. The CPA1 family is found in prokaryotes and all eukaryotes, and members include mammalian NHE and plant NHX transporters, both of

which are Na$^+$/H$^+$ exchangers (Brett et al., 2005; Chanroj et al., 2012). CPA2 transporters are predominantly conserved in bacteria, archaea, fungi, and plants, but not in metazoans (Chanroj et al., 2012). The plant CHX family belongs to the CPA2 family. Genomes of early land plants, like club moss and moss, contain 3-4 copies of *CHX* genes (Mottaleb et al., 2013), but genomes of flowering plants, like rice and *Arabidopsis*, predict 17 and 28 members, respectively. This observation is not unusual, as many gene families expanded in flowering plants (Lehti-Shiu et al., 2009). It is surprising that most of the 28 *CHX* genes in *A. thaliana* are expressed in pollen (Sze et al., 2004). Their functions in pollen are mostly unknown. Perhaps the diversification of CHX transporters in monocots and dicots was related to reproductive success on land (Chanroj et al., 2012), and ability to survive environmental stress.

A few functional studies on *CHX* genes would support these ideas. First, two *CHX* genes, *CHX21 and CHX23*, were shown to be necessary for pollen tube targeting to ovules. Double mutant *chx21/23* pollen can germinate and extend a tube in the transmitting tract, but tubes fail to turn at the funiculus and thus do not reach the micropyle. This result indicates that wild-type *CHX21/23* could function in either pollen tube perception of female guidance cues or in signal transduction to mediate a change in growth direction (Lu et al., 2011). Another gene, *CHX20*, is the only member of the CHX family to be expressed in guard cells. The stomatal apertures in three *chx20* mutants were reduced by 35% relative to WT {Padmanaban, 2007, Participation of endomembrane cation/H+ exchanger AtCHX20 in osmoregulation of guard cells}. However, the role of *CHX20* is distinct from that of *NHX1/2*, because *nhx1/nhx2* mutants prevent vacuole enlargement and show perturbed vacuolar morphology (Andres et al.,

2014). As CHX20 was localized to reticulate membranes resembling ER, we postulate a role in osmoregulation due to membrane trafficking and remodeling needed to increase vacuolar volume and PM area (Padmanaban et al., 2007). Thus, not only are some CHX transporters critical in pollen tube navigation in flowering plants, but also CHX20 alone is important for mediating the opening of leaf pores for gas exchange and subsequent vegetative success on land.

So far, the best-characterized member of the family is *CHX17* from *Arabidopsis thaliana*. CHX17, CHX18 and CHX19 share similar membrane localization on the PVC and PM in plant cells. These proteins also share similar activities in yeast mutants (Chanroj et al., 2011; Chanroj et al., 2013). CHX17, 18 and 19 are thought have roles in pH homeostasis, as their expression in an alkaline-sensitive yeast strain conferred tolerance to growth at pH 7.5. Two lines of evidence suggest CHX17 mediated K^+ transport. First, CHX17 expression in an *E. coli* strain deficient in K^+ uptake pathways restored growth on low K^+ medium and mediated $^{86}Rb^+$ uptake. Second, *CHX17* as well as *CHX18* and *CHX19* restored growth of yeast lacking K^+ uptake transporters on low K^+ medium (Chanroj et al., 2011). These results in yeast are in general consistent with their role as K^+/H^+ antiporters localized to endomembranes, but the mode of transport at the PM is less clear. Whether CHX17 moves K^+ via a channel, uniporter, or symporter mode has yet to be established (Chanroj et al., 2011; Mottaleb et al., 2013). Although *CHX17*, *CHX18*, and *CHX19* confer tolerance to the aminoglycoside antibiotic HygB, *CHX16* or *CHX20* are unable to confer resistance to the drug in a yeast strain lacking several cation transporters (Chanroj et al., 2011). Thus, multiple CHX members show diversity based on their distinct biochemical properties and perhaps differential membrane localization.

Although the four related genes *CHX16, CHX17, CHX18, and CHX19* were functionally similar in a heterologous system, their biological roles *in planta* remained unknown. Vegetative growth under various stress conditions using single, double, or triple *chx* mutants was not distinguishable from WT plants (Chanroj, 2011). When generating a quadruple mutant, the recovery of homozygous *chx16/17/18/19* mutants was less than expected. Further analysis showed significant reduction in seed set relative to WT (Chanroj et al., 2013). Here, we show that *CHX17, 18*, and *19* are important for male and female fertility. Even though triple mutant *chx17/18/19* pollen tubes grow somewhat slowly, they do target and enter ovules. However, many targeted ovules fail to develop into seeds and appear unfertilized. A fraction of ovules within each pod are fertilized and develop, though embryo development is retarded when a triple mutant pistil is pollinated by triple mutant pollen. These results suggest that *CHX17*, *CHX18*, and *CHX19* play roles critical for successful fertilization and for subsequent embryo development. Our findings underscore the critical roles of K^+ and pH homeostasis on dynamic endomembranes for male gametophyte function, fertilization and seed development.

C. MATERIALS AND METHODS

C.1. Plants

Arabidopsis thaliana, ecotype Columbia-0, was grown in Miracle-Gro® potting mix supplemented with 5% Perlite. Seeds were stratified at 4°C for 3 days. Plants were grown in chambers under long day conditions (16-hour photoperiod) at 150 µE m^{-2} s^{-1} illumination, 21°C, and 60% relative humidity. Plants were watered once every 5 days. *Arabidopsis* mutants used in this study are listed in Tables II-S1 to S3.

C.2. Mutants and Genotyping plants

Genomic DNA was isolated from leaves of 4 to 5-week-old plants (Edwards et al., 1991). One or two rosette leaves per plant were placed in 450 µl of Edward buffer (200 mM Tris, pH 7.5, 250 mM NaCl, 25 mM EDTA, 0.5% SDS). Leaves were homogenized using a plastic pestle and automatic drill. Samples were vortexed for 5 seconds and centrifuged at 13000 rpm for 5 min in a benchtop microcentrifuge (Eppendorf 5415C). Supernatant (300 µl) was transferred to a fresh tube and mixed with 300 µl isopropanol by inversion. After incubating for 2 min, samples were centrifuged at 13000 rpm for 5 min (Eppendorf 5415C). The supernatant was removed, and pellets were washed twice with 500 µl of 70% ethanol. Samples were air-dried for 15-20 min. Pellets were resuspended in 100 µl of sterile water.

Genotypes for WT Columbia-0 and *chx* mutants were determined by PCR using either 2 gene-specific primers or one gene-specific primer and a T-DNA border primer (Table II-S4). *Taq* DNA polymerase (NEB M0273L) was used to amplify DNA in a three-step PCR program for 40 cycles. Each cycle was denaturation: 95°C for 30 s,

annealing: 55°C for 30 s, and elongation: 68°C for 60 s. PCR products were run on a 1% agarose gel and visualized on a Bio-Rad Gel-Doc system using ethidium bromide fluorescence.

C.3. Segregation analysis

Reciprocal crosses were performed to test transmission of a *chx18* or *chx19* T-DNA mutant allele through the pollen or the embryo sac. To test male transmission, pollen from a parent carrying a heterozygous gene was used to pollinate a pistil carrying the WT gene. Parental plants were genotyped (C.2) for the presence of WT genomic sequence or T-DNA insertions in the *CHX17*, *CHX18*, and *CHX19* genes (Fig. II-S1). Stage 12 flower buds (Smyth et al., 1990) were emasculated, and pistils were pollinated 2 days later, using anthers from stage 13 or 13L flowers (Sanders et al., 2000). Seeds developed on the plant for seven days. Plants were left to dry, and seed pods were collected. F1 seeds were planted, and genomic DNA was collected from leaves of 4-5-week-old plants for genotype analyses.

C.4 Analysis of *chx17/18/19* mutant plants

a. *Measuring pod size and seed set*

For testing WT, double *chx* mutants, and *chx17/18/19* plants, seed pods were collected from the primary bolts of 9-week-old plants. Pods were collected starting from the fourth pod below the inflorescence, and photographed (Nikon Coolpix 995). Pod length was measured in ImageJ (NIH). A minimum of 10 plants per line were analyzed. Four pods of average length per plant were split open and examined under a stereomicroscope (Nikon SMZ1000), to score seed set per pod.

b. ***DAPI staining of nucleus***

To test pollen development, WT and *chx17/18/19* pollen grains from opened flowers at stage 13 (Smyth et al., 1990) were stained with DAPI. DAPI (4',6-diamidino-2-phenylindole) was prepared in a detergent solution containing 0.1 M sodium phosphate pH 7, 1 mM EDTA, 0.1% Triton X-100, and 0.4 µg/ml DAPI. Pollen from 1-3 flowers was dabbed onto a microscope slide, and 30 µl of DAPI-detergent solution was added. Slides were incubated in the dark for 15 min before viewing on a fluorescence microscope (Nikon E600) with a UV filter (maximum excitation wavelength at 360 nm and emission at 410 nm). A minimum of 100 grains per line were examined.

c. ***Aniline Blue staining of pollen tubes*** **in vivo**

To visualize pollen tube growth *in vivo*, WT and *chx17/18/19* pistils were stained with Aniline Blue which labels PT callose (Mori et al., 2006). Self-fertilized WT and *chx17/18/19* pistils were analyzed at stages 15 and 16, which corresponds to 2-3 DAP (Smyth et al., 1990). Pistils were fixed under vacuum in 75% ethanol/25% acetic acid for 2 h at room temperature. Pistils were incubated in 75%, 50%, 30% ethanol, and deionized water for 10 minutes each. Pistils were incubated in 8M NaOH overnight, and washed once with deionized water. Pistils were incubated for 2 h in 0.1% decolorized Aniline Blue (Fisher Scientific A-967) in 100 mM K_2HPO_4, at pH 10. Each pistil was placed on a glass slide and gentle pressure was applied to two sides of the cover slip to split the ovary wall and expose ovules and transmitting tract. Images were recorded using a Nikon E600 fluorescence microscope with a UV filter (maximum excitation wavelength at 360 nm and emission at 410 nm). Several frames of a single pistil were

captured with a 10x objective lens, and a composite image was arranged in Photoshop CS2 (Adobe). Tubes arriving at each ovule were examined using the 20x objective lens.

d. ***Visualizing embryo development. Chloral hydrate clearing and Nomarski microscopy***

To examine the cellular basis for reduced seed set in *chx17/18/19* plants, ovules from self- or manually-pollinated pods were analyzed. Seed pods at varying developmental stages on the primary bolt were collected and fixed in 90% ethanol/10% acetic acid overnight at room temperature. Pods were washed two times in 90% ethanol for 30 min per wash and then cleared in a solution of chloral hydrate/glycerol/water (8:1:2) (Berleth and Jurgens, 1993). Each pod was then opened and all ovules were removed. Ovules or developing seeds were mounted in the chloral hydrate solution and examined with DIC microscopy (Nikon E600).

D. RESULTS

Higher-order *chx* mutant plants were tested, as single and double T-DNA insertion mutants among *chx17, chx18*, and *chx19* showed no detectable vegetative phenotype. Although pods of the quadruple mutant of *chx16/17/18/19* showed 50-70% reduced seeds (Chanroj et al., 2013), we noticed that plants with triple mutant combinations that included a null in *chx16* showed little to no change in seed set relative to WT. Thus a triple mutant combination with T-DNA insertions in 3 genes- *CHX17*, *CHX18*, and *CHX19*- was examined.

D.1. Triple mutant *chx17/18/19* plants show reduced seed set and shorter seed pods.

Vegetative growth of *chx17/18/19* plants (or triple mutant) was similar to WT (Fig. II-1A-i). In addition, flower development from stage 9 through stage 15, (approximately 6 DAP), was also similar between WT and *chx17/18/19* (Fig. II-S1). However, seed pods of *chx17/18/19* plants were shorter than WT (Fig. II-1A-ii). Triple mutant seed pod length varied from 8.8 to 10.3 mm, compared to 13.0 mm in WT (Fig. II-1B). When seed pods were cleared of pigments, we observed a random pattern of gaps along the *chx17/18/19* pods instead of two continuous rows of seeds as in WT pods (Fig. II-1A-iii and II-1A-iv). Progeny from three separate *chx17/18/19* plants showed, on average, 11-21 seeds per pod, compared to 48 seeds per pod in WT (Fig. II-1C). Homozygous double mutant *chx17chx/18* or *chx17chx/19* plants showed seed set and pod length similar to WT (Fig. II-1B, II-1C, and II-S2A). These results show loss of function of 3 *CHX* genes, *chx17/18/19,* is sufficient to cause reduced seed set.

Fig. II-1. Triple *chx17/18/19* mutant plants showed reduced seed set.

A) Plants and seed pods. **(i)** Wild-type (WT) Columbia-0 and *chx17/18/19* plants have similar vegetative and reproductive growth. **(ii)** *chx17/18/19* seed pods were shorter than those of WT. **(iii)** *chx17/18/19* pods contained reduced seeds. Pigments of pods were cleared with ethanol. Scale bar = 1.0 mm. **(iv)** Developing seeds viewed in split pods. *chx17/18/19* pods contained a mixture of aborted and developing seeds. At least 44 seed pods per genotype were analyzed. Scale bar = 0.5 mm. **B)** Pod lengths of *chx17/18/19* mutant are 21 to 29% shorter than pods of WT or double mutants *chx17/18* or *chx17/19*. Results show mean, and bars represent SEM. (n = 234 to 610 pods) **C)** Seed number per pod was reduced 56-77% in *chx17/18/19* mutant relative to WT or the *chx17/18* and *chx17/19* double mutants. Four siliques of average length were split open per plant to count seeds. Results show mean, and bars represent SEM. (n = 44 to 126 pods). (D. Czerny grew the plants, analyzed the phenotype, generated the micrographs, and assembled the figure.)

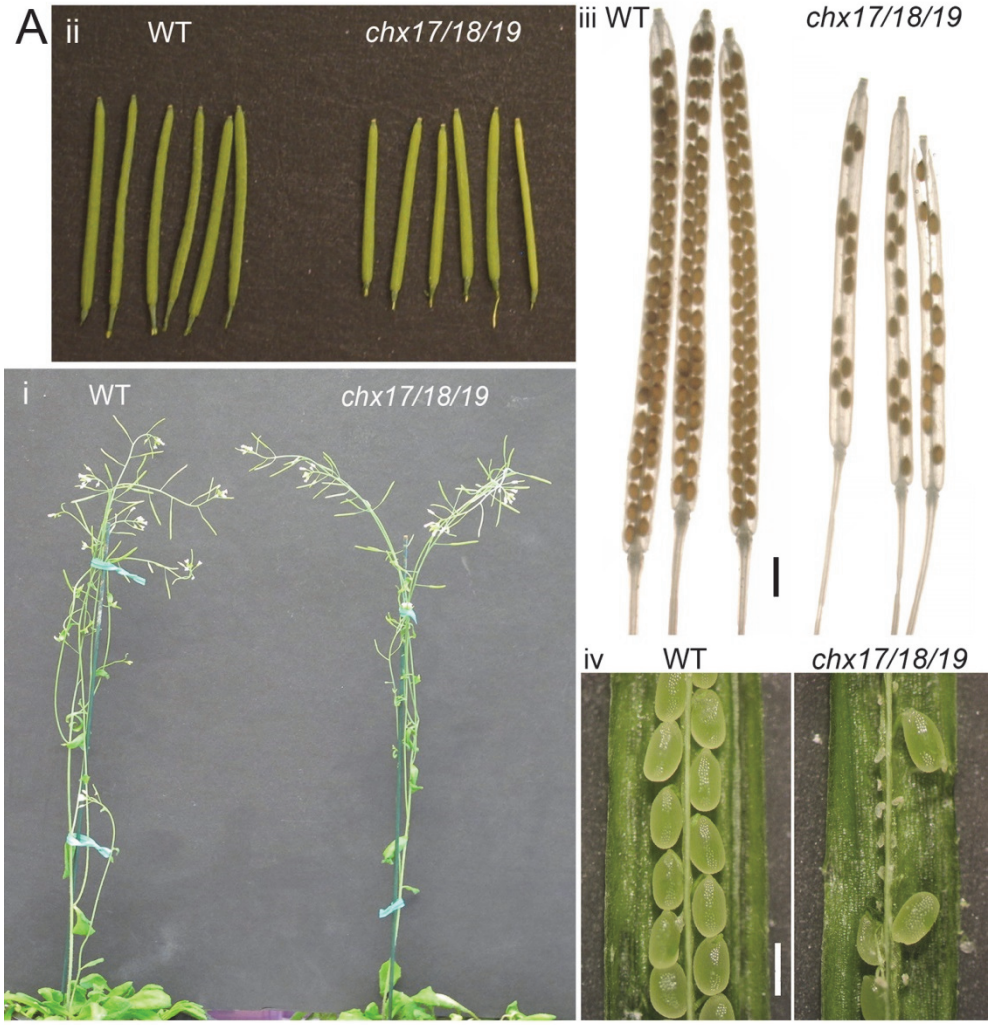
A
ii
WT
chx17/18/19
iii WT
chx17/18/19
i
WT
chx17/18/19
iv
WT
chx17/18/19

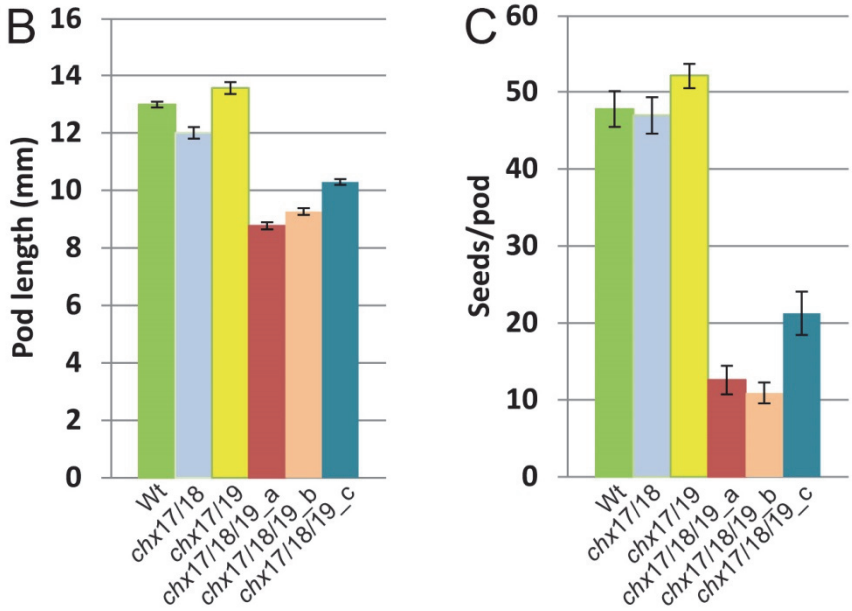
B
Pod length (mm)
0
2
4
6
8
10
12
14
16
Wt
chx17/18
chx17/19
chx17/18/19_a
chx17/18/19_b
chx17/18/19_c
C
Seeds/pod
0
10
20
30
40
50
60
Wt
chx17/18
chx17/19
chx17/18/19_a
chx17/18/19_b
chx17/18/19_c

D.2. Male fertility is compromised in pollen carrying *chx17/18/19*.

We tested whether the reduction in seed set was due to defects in the male gametophyte, in the female gametophyte, or in both. As double mutants behaved like WT, we first tested segregation of a heterozygous *CHX18*$^{+/-}$ or *CHX19*$^{+/-}$ gene in a double mutant background by reciprocal crossing (Fig. II-2A). For example, pollen from a double *chx17*$^{-/-}$*19*$^{-/-}$ mutant plant carrying a heterozygous *CHX18*$^{+/-}$ gene was placed onto a pistil of a double *chx* mutant carrying a wild type *CHX18*$^{+/+}$. Transmission efficiencies of *chx18-1* and *chx19-2* mutant alleles were tested by PCR genotyping of F1 progeny. Parents were genotyped for mutant or WT alleles of *CHX17*, *CHX18*, and *CHX19* by PCR prior to crossing (Fig. II-2B). The F1 progeny was tested for homozygous WT *CHX18*$^{+/+}$ or heterozygous *CHX18*$^{+/-}$. PCR-amplified products of 1 kb or 0.5 kb were used to distinguish either the WT or mutant allele, respectively (Fig. II-2C). If a *CHX* gene has minimal or no effect on male fertility, then the number of progeny containing homozygous wild-type *CHX18*$^{+/+}$ would be approximately equal to progeny carrying heterozygous *CHX18*$^{+/-}$.

To test the function of the male gametophyte, pollen from a double *chx* mutant plant carrying a heterozygous *CHX18*$^{+/-}$ was transferred to a WT pistil. Table II-1 shows that only 10% (instead of 50%) of the progeny were triple heterozygotes, indicating fertility of triple *chx* mutant pollen was severely reduced(Table II-1-a) ($X^2 > 6.64$). In contrast, 90% of the progeny was homozygous for WT *CHX18*, indicating successful fertilization by the double mutant *chx17/19* mutant pollen. In the reciprocal cross, female transmission of the triple *chx* mutant was 38% instead of 50%, showing partial compromised function in the *chx17/18/19* embryo sac. Thus, one functional *CHX* out of

Fig. II-2. Gene structures of *Arabidopsis CHX17*, *CHX18*, and *CHX19* and verification of genotypes. A) Gene structure of *CHX17, CHX18* and CHX*19* and location of T-DNA insertions. Exons and introns are shown as boxes and lines, respectively. Bold arrows indicate right and left border primers (RP and LP) used to amplify wild-type *CHX* sequence. Arrows refer to T-DNA left border primer (LBb1 or LBb1.3) used to detect the T-DNA insertion. Number 1 refers to first base of start codon ATG, and the number at the end of the gene structure refers to the third base of the stop codon. Base # above the triangle denotes position of T-DNA insertion. *chx17-4*, *chx18-1*, and *chx19-2* correspond to SALK_033417, SALK_001563, and SALK_100047, respectively. Primer sequences are shown in Table II-S1. **B)** Genotype of male (*chx17*$^{-/-}$ *chx18*$^{+/-}$ *chx19*$^{-/-}$) and female (*chx17*$^{-/-}$ *chx18*$^{+/+}$ *chx19*$^{-/-}$) parents used in a reciprocal cross was verified. Genomic DNA from parents was tested for homozygous or heterozygous *CHX17*, *CHX18*, or *CHX19* genes by PCR. Lane 'a' shows fragments amplified with LP and RP primer pairs, and lane 'b' shows fragments amplified using the T-DNA primer with either LP or RP primers. The WT allele produces a PCR-amplified product of ~1 kb., whereas mutant alleles give a PCR product of approximately 0.5 kb. **C)** The number of F1 progeny heterozygous for *CHX18* was less than expected. Lanes 1-7 show a sample of F1 plants that were genotyped. Lanes labeled '18LP-18RP primer pair' or '18LP-LBb1' show a PCR-amplified DNA fragment if genomic DNA had a copy of the wild-type *CHX18* or a T-DNA-inserted *chx18,* respectively. Lane 'S' is 100 bp DNA size standard. Lanes WT or 'Mut' contained gDNA isolated from wild-type or the triple *chx17/18/19* mutant. D. Czerny and K. Levin conducted experiments. D. Czerny and K. Levin assembled figure.

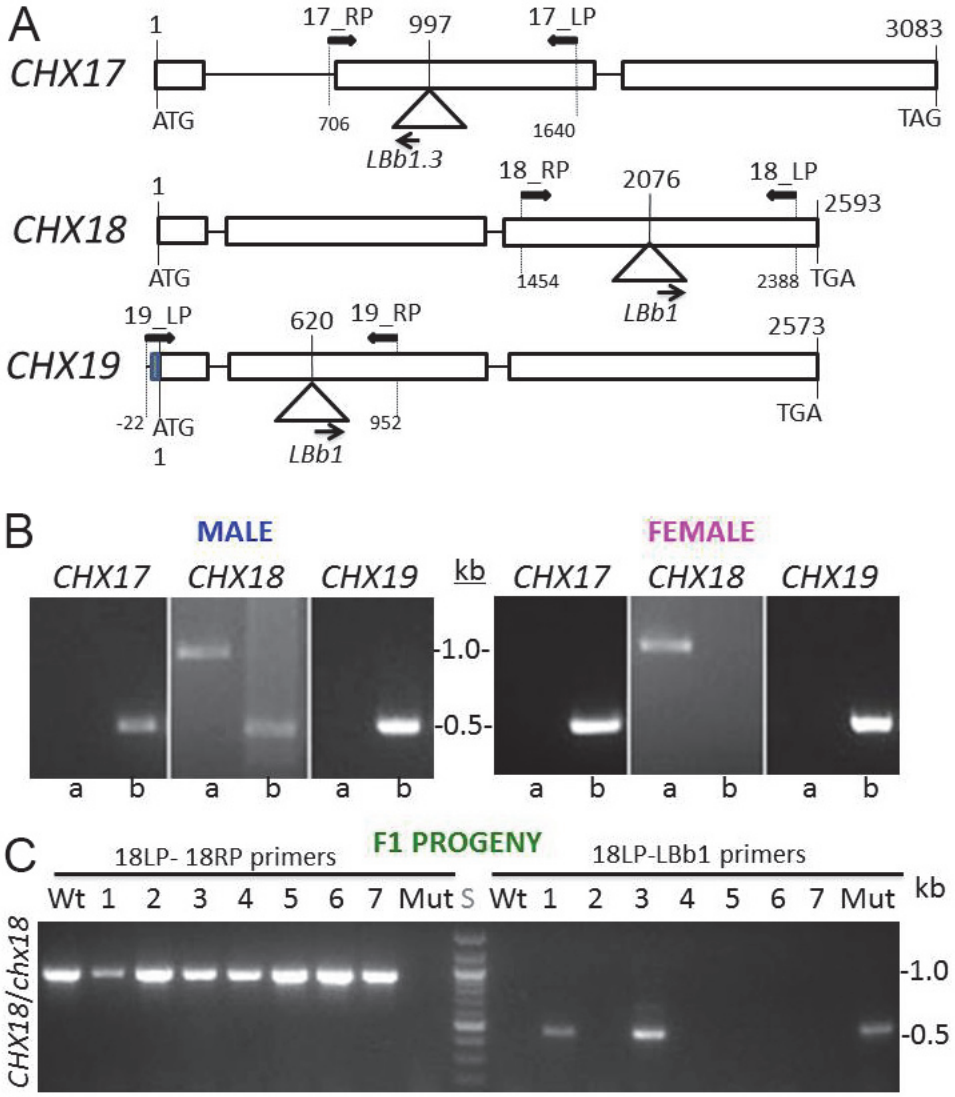
A
CHX17
1
17_RP
997
17_LP
3083
ATG
706
1640
TAG
LBb1.3
CHX18
1
18_RP
2076
18_LP
2593
ATG
1454
2388
TGA
LBb1
CHX19
19_LP
620
19_RP
2573
-22
ATG
1
952
TGA
LBb1
B
MALE
FEMALE
CHX17
CHX18
CHX19
kb
CHX17
CHX18
CHX19
-1.0-
-0.5-
a
b
C
F1 PROGENY
18LP- 18RP primers
18LP-LBb1 primers
Wt 1 2 3 4 5 6 7 Mut S Wt 1 2 3 4 5 6 7 Mut
kb
CHX18/chx18
-1.0
-0.5

3 *CHX* genes can restore fertility in both gametophytes, but fertility in the triple *chx* mutant pollen is compromised to a greater extent than that of the triple *chx* mutant embryo sac.

In order to test if other single *CHX* genes can similarly restore fertility, pollen from *chx17/19* or *chx17/18* double mutants heterozygous for either *CHX18*$^{+/-}$ or *CHX19*$^{+/-}$ was used to pollinate double mutant *chx17/19* or *chx17/18* pistils with a single WT *CHX*. Transmission of the mutant *chx18-1* allele through the pollen was 5% instead of 50%, (Table II-2-a) ($X^2 > 6.64$). Similarly, transmission of the *chx19-2* allele through the pollen was only 3% of the F1 progeny (Table II-2-c). In addition, the transmission of the *chx18-1* allele through the female was below the expected frequency, showing an average of 30% transmission instead of 50% (Table II-2-b) ($X^2 > 6.64$). Transmission of the *chx19-2* allele through the embryo sac was 25% instead of 50% (Table II-2-d). Taken together, these results indicate that one functional *CHX18* or *CHX19* is sufficient to restore WT-like function in both the male and female gametophytes. Moreover, both crossing experiments show the *chx17/18/19* male gametophyte is compromised to a greater extent than the *chx17/18/19* female gametophyte. We thus focused on the effects of *CHX17*, *CHX18*, and *CHX19* on male fertility.

Table II-1: Reciprocal crosses show male and female fertility are both compromised in the triple *chx17/18/19* mutant.

Pollen grains from a double mutant *chx17*$^{-/-}$*chx19*$^{-/-}$ parent heterozygous for *CHX18*$^{+/-}$ were used to pollinate a WT stigma (a). WT pollen grains were used to pollinate a double mutant pistil heterozygous for *CHX18*$^{+/-}$ (b). F1 seeds from these crosses were planted and leaves were collected for DNA extraction and genotyping. The observed (Obs) segregation of F1 progeny are shown below as number of individuals recovered or percent (%). Exp. refers to expected ratio. Number of F1 plants tested was 112-115. thrgrsdv sfTer.\The results are significantly different from the expected ratio when $X^2 >$ 6.64 at a *p* value of 0.01 (df = 1). D. Czerny conducted the experiments and analyzed the results with assistance from K. Levin.

	Female: Egg or Central cell			Male: Pollen or Sperm			F1 progeny			Expect	Obs (%)	X^2
		CHX			CHX			CHX				
	17	18	19	17	18	19	17	18	19			
a	+	+	+	-	+	-	+/-	+/+	+/-	1	101 (90)	72.3
	+	+	+	-	-	-	+/-	+/-	+/-	1	11 (10)	
b	-	+	-	+	+	+	+/-	+/+	+/-	1	72 (62)	7.3
	-	-	-	+	+	+	+/-	+/-	+/-	1	43 (38)	

A X^2 value above 6.64 (p 0.01 = 6.64) indicates the observed results are significantly different from the expected segregation ratio (Exp

Table II-2. A wild-type copy of either *CHX18* or *CHX19* alone is sufficient to restore both male and female fertility. Thus, these two genes have overlapping roles in male and female fertility.

Pollen grains from a double mutant *chx17*$^{-/-}$*chx19*$^{-/-}$ parent heterozygous for *CHX18*$^{+/-}$ were manually transferred to a double mutant pistil carrying WT *CHX18*$^{+/+}$ (a). Reciprocal crosses were also conducted (b). Similar reciprocal crosses were performed with double mutant *chx17*$^{-/-}$*chx18*$^{-/-}$ heterozygous for *CHX19*$^{+/-}$ (c, d) and the double mutant alone. Seeds from these crosses were planted and leaves were collected for DNA extraction and genotyping. The observed (Obs) segregation of F1 progeny are shown below as number of individuals recovered or percent (%). Total F1 plants tested ranged from 65 to 139. Transmission Efficiency % = (# of plants receiving mutant allele/ # of plants receiving WT allele) X 100, as published previously (Boisson-Dernier et al., 2009). The results are significantly different from the expected ratio when $X^2 > 6.64$ at a *p* value of 0.01 (df = 1). D. Czerny conducted the experiments and analyzed the results with assistance from K. Levin.

	Female: Egg or Central cell			Male: Pollen or Sperm			F1 progeny			Expect	Obs (%)	Trans Eff (%)	X^2
		CHX			CHX			CHX					
	17	18	19	17	18	19	17	18	19				
a	-	+	-	-	+	-	-/-	+/+	-/-	1	62 (95)	4.8	53.6
	-	+	-	-	-	-	-/-	+/-	-/-	1	3 (5)		
b	-	+	-	-	+	-	-/-	+/+	-/-	1	98 (70)	42	23.4
	-	-	-	-	+	-	-/-	+/-	-/-	1	41 (30)		
c	-	-	+	-	-	+	-/-	-/-	+/+	1	92 (97)	3	83.4
	-	-	+	-	-	-	-/-	-/-	+/-	1	3 (3)		
d	-	-	+	-	-	+	-/-	-/-	+/+	1	69 (75)	33	23
	-	-	-	-	-	+	-/-	-/-	+/-	1	23 (25)		

A X^2 value above 6.64 (p 0.01 = 6.64) indicates the observed results are significantly different from the expected segregation ratio (Expect).

D.3. Development of *chx17/18/19* pollen grain is similar to wild-type.

The basis of reduced male fertility was tested by observing pollen grain development. Mature pollen grains were collected from stage 13 or 14 flowers (Smyth et al., 1990) and incubated with DAPI (4',6-diamidino-2-phenylindole) to stain double-stranded DNA. The number of nuclei was counted using fluorescence microscopy (Fig. II-3A). Mature *chx17/18/19* pollen grains contained 3 nuclei, similar to mature grains from WT plants (Fig. II-3B). These results indicate loss of 3 *CHX* genes did not visibly perturb the development of the pollen grain.

D.4. Pollen tube grow and target ovules *in vivo*.

D.4a. Manual pollination.

To test pollen fertility and tube growth, pollen from the *chx17/18/19* mutant or a WT plant was manually transferred to a WT pistil. In general, seed set is reduced to 25% when pistils were pollinated by mutant pollen, in contrast to >97% seeds per pod when WT pollen was supplied to a WT or triple mutant pistil (Fig. II-6B). Pollen tube growth in the pistil was examined up to 3-4 DAP using aniline blue. Aniline blue stains callose abundant in pollen tubes, and also callose in vascular tissues of the funiculus, which is clearly visible in unpollinated pistils. One DAP, WT pollen tubes are visible at the distal end of the pistil (Fig. II-4). Furthermore, most ovules had received a pollen tube as observed at higher magnification (not shown). In pistils pollinated with *chx17/18/19* mutant pollen, many tubes are visible along the length of the pistil at 1 DAP, though fewer tubes were visible at the distal end, suggesting pollen germination or tube growth in the *chx17/18/19* mutant is retarded relative to WT.

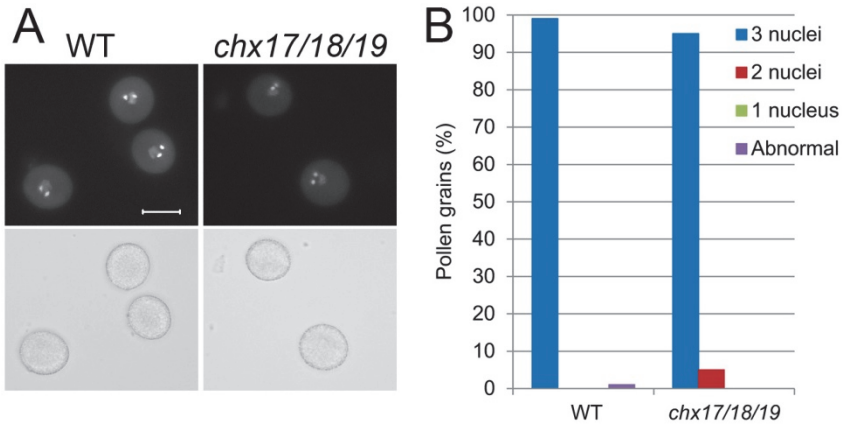

Fig. II-3. ***chx17/18/19* pollen grain development is similar to wild-type. A)** Representative images of DAPI-stained pollen grains observed by UV fluorescence (top) or bright-field (bottom) microscopy. Scale bar = 10 µm. **B)** Nearly all WT and *chx17/18/19* pollen grains contained 3 nuclei as visualized by DAPI staining. Total grains scored were 108 and 200 from WT and *chx17/18/19*, respectively. D. Czerny conducted the experiments. K. Levin assisted in data collection.

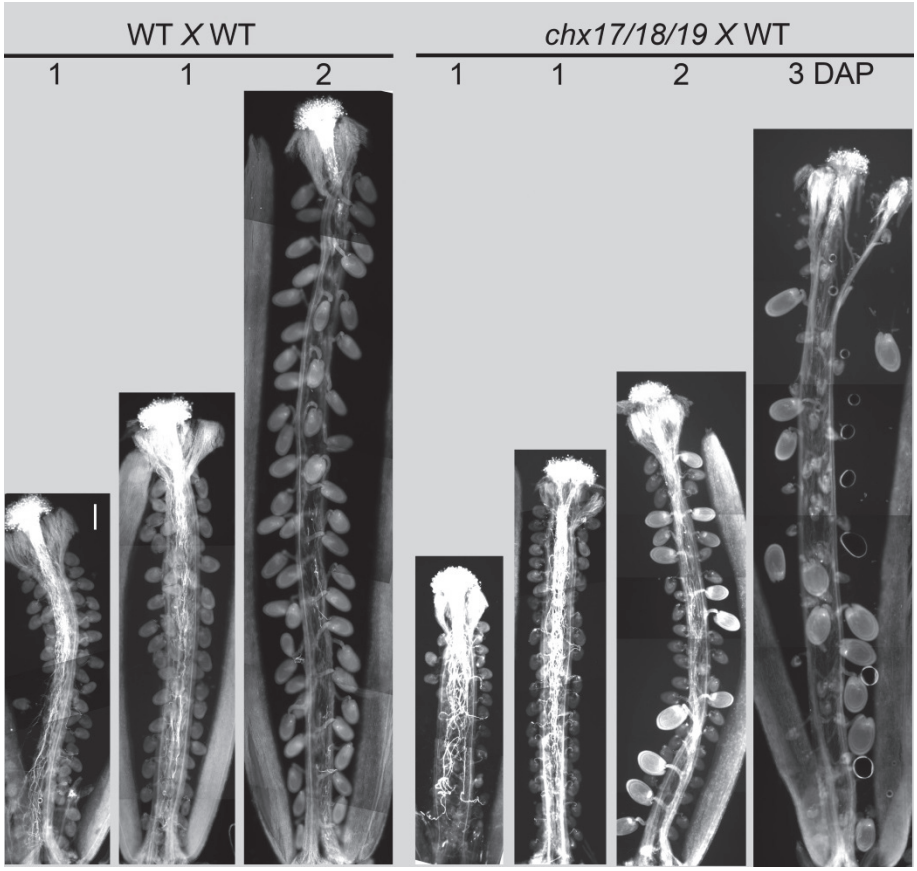

Fig. II-4. **Time-course of ovule development in wild-type pistils pollinated with WT or *chx17/18/19* pollen**. WT pistils were manually pollinated with pollen from WT or triple *chx17/18/19* flowers. Pods were fixed at 0 to 3 DAP. Siliques were stained with aniline blue, split open and observed by fluorescence microscopy. Scale bar = 200 µm. D. Czerny crossed plants and prepared samples for microscopy. R. Su analyzed pollen tube growth in the pistil and collected images.

By 2 DAP, some ovules have increased in size, but a significant number of ovules (50% or more) remain small and are referred to here as 'undeveloped ovules'. At 3 DAP, developing ovules/seeds were much larger; however, the 'undeveloped ovules' from WT pistils given triple mutant pollen had begun to shrivel (Fig. II-4). We observed that a fraction of ovules may not have received a tube, as at least half of those with a visible pollen tube failed to develop (Supp. Fig. II-S4). In contrast, pistils pollinated with WT pollen show nearly all ovules (97%) have increased in size by 2 DAP (Fig. II-4). Thus, *chx17/18/19* mutant pollen grains germinate, extend tubes, and are able to target ovules, though both tube number and tube length are slightly reduced relative to WT. Mutant pollen tubes germinated *in vitro* were 50% shorter and less abundant than WT tubes (Fig. II-S3), though excess pollen grains *in vivo* ensured that many tubes reached ovules.

D.4b. Self-pollination.

Similar results were observed in pods from self-pollinated triple mutants compared to those from manual pollination of WT pistils with triple mutant pollen. In pods of self-pollinated WT plants, fluorescent pollen tubes are visible outside each developing ovule/seed (not shown). Mutant *chx17/18/19* pollen tubes also grew through the female transmitting tissues to the distal end of the pod as evident from observing developing seeds along the length of the ovary (Fig. II-5A). Though triple mutant tubes did reach the distal end, many small undeveloped ovules were seen along the entire length of the pod, suggesting that PTs did not reach all ovules (Fig. II-5A). However on closer examination, pollen tubes had entered at least half of the undeveloped ovules whether the pistils were WT or the triple mutant (Fig. II-5B and II-5C). These results

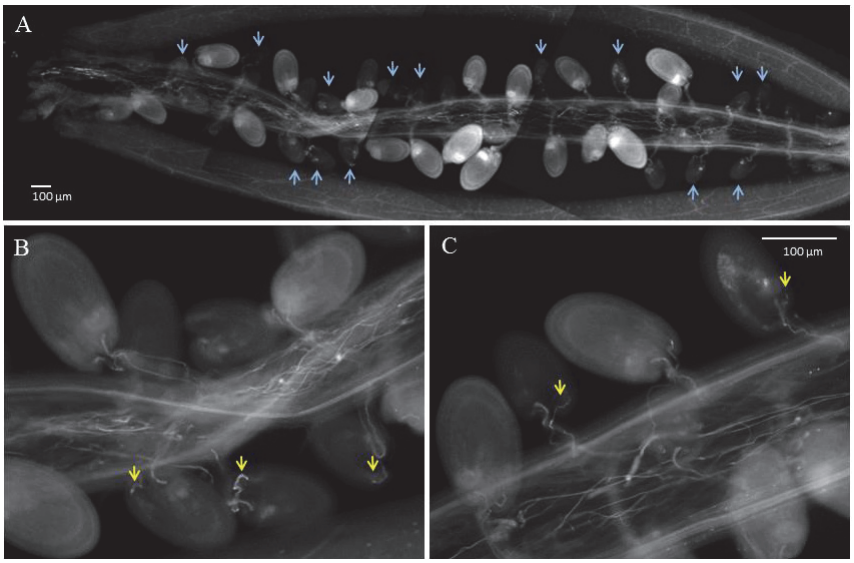

Fig. II-5. Mutant pollen tubes reached many ovules though half remain undeveloped.

Ovules were examined after self-pollination of *chx17/18/19* mutant flowers. **A)** Developing seeds are larger than undeveloped ovules within a pod at 4 DAP. Arrows point to undeveloped ovules with a visible pollen tube at this focal plane. **B-C)** Magnified panels of same pod show aniline blue-stained tubes have entered ovules that either develop or remain undeveloped. Vascular strand is visible at the chalazal end of each ovule. The images in A were viewed with a 10x objective lens, while B and C used a 20x objective lens. Scale bars = 100 µm. D. Czerny crossed plants and prepared samples for microscopy. R. Su generated the micrographs.

indicated *in vivo* pollen tube growth and guidance of triple mutant PTs were not defective, though the number of pollen tubes reaching ovules appears to be reduced. Instead, results suggest that even when *chx17/18/19* tubes reach ovules, there is failure to complete fertilization.

D.5. *chx17/18/19* pods contain unfertilized ovules and single fertilization events.

To visualize embryogenesis and endosperm development, pods from manual pollination of WT pistils with *chx17/18/19* pollen and from self-pollinated *chx17/18/19* flowers were collected, treated with chloral hydrate, and every ovule per pod was examined by DIC microscopy (Berleth and Jurgens, 1993). Pods from WT pistils pollinated with *chx17/18/19* pollen contained 3 types of ovules: i) unfertilized ovules; ii) single-fertilized ovules containing either embryo only or endosperm only; and iii) normal seeds that contain both developing embryo and endosperm (Fig. II-6A). Pods from control WT plants yielded nearly all normal seeds, which is similar to pods obtained from triple mutant pistils pollinated by WT pollen (Fig. II-6B). These results are consistent with the reciprocal crossing study where male fertility is severely compromised by loss of *CHX17*, *18*, and *19* functions in the male gametophyte.

Pods of self-pollinated triple mutants consisted of i) 33% unfertilized ovules; ii) 11% single-fertilized ovules; and iii) 55% normal developing seeds (Fig. II-7F). The central nucleus or egg cell is visible in unfertilized ovules (Fig. II-7B). Single fertilizations, though less frequent, are consistently observed, mostly as globular embryo only (Fig. II-7C). The embryos fail to develop beyond the globular stage, which has between 16 and 100 cells (Capron et al., 2009). We also noticed developing endosperm

Fig. II-6. Decreased male fertility of *chx17/18/19* mutant pollen produces pods with unfertilized ovules, embryo only, as well as developing seeds. WT pistils received WT or *chx17/18/19* mutant pollen. **A)** Pods were examined by DIC microscopy at 5 DAP. *(a)* WT control: 99% show a heart stage embryo when a WT pistil received WT pollen; *(b)* embryos at heart to late heart stage (98%) formed when a *chx17/18/19* mutant pistil received WT pollen. Pods from a WT pistil that received *chx17/18/19* pollen showed *(c1)* 63.0% unfertilized ovules *(c2)* 7.0% early globular embryo only, and *(c3)* 30.0% embryos at heart stage. Representative images are shown. Scale bar in (a) is 100 µm. **B)** Relative distribution of unfertilized (Unfert) ovule, embryo (Emb) only, or endosperm (Endo) only is shown as a table **A)** and bar graph **B)**. Average number of developing seeds per pod for each treatment obtained from at least 10-14 pods examined per treatment. D. Czerny crossed plants and prepared samples for microscopy. S. Padmanaban analyzed images.

A

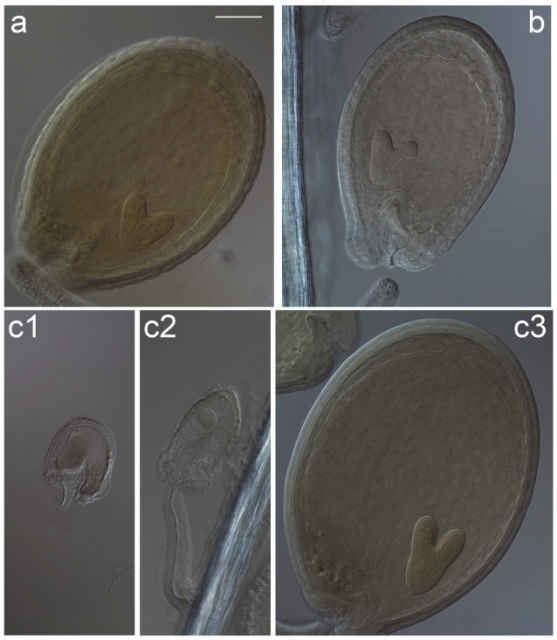

B

Pollen x pistil	Developing embryo	Unfertilized ovule	Embryo only	Endosperm only
WT x WT	45.4	0.6	0.0	0.0
WT x *chx17/18/19*	40.5	1.0	0.0	0.0
chx17/18/19 x WT	11.3	23.9	2.6	0.2

C

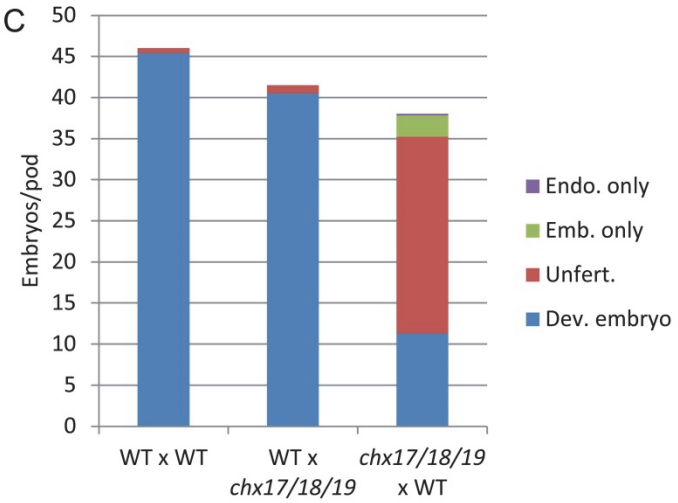

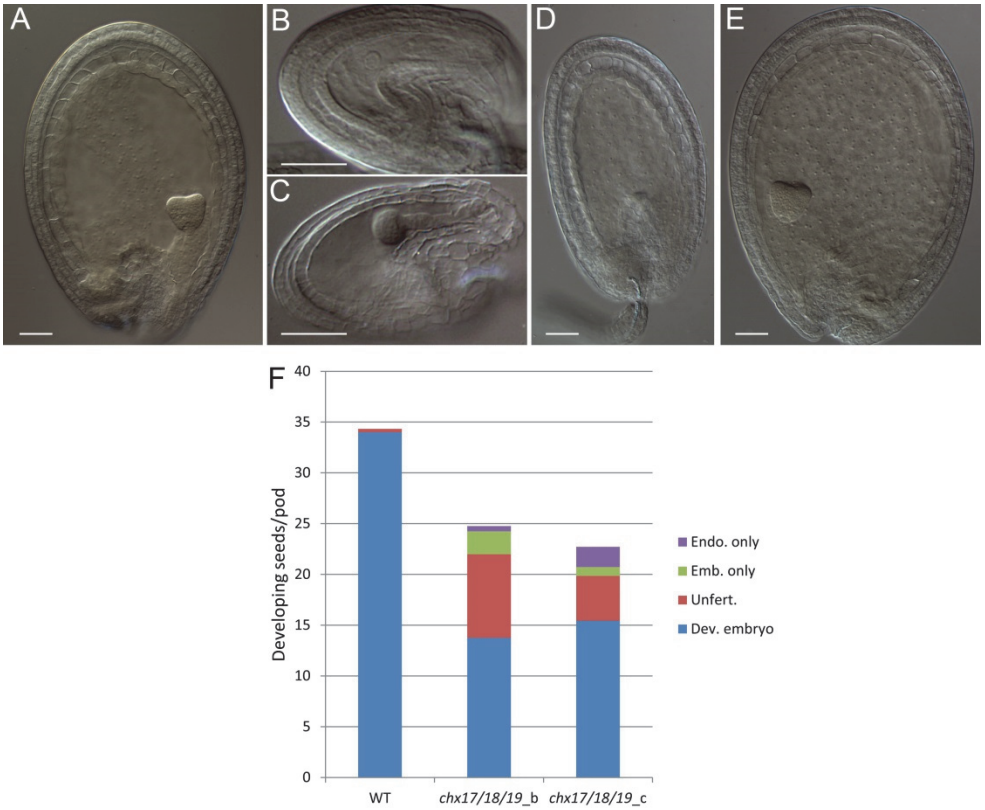

Fig. II-7. Pods of self-pollinated *chx17/18/19* mutants contained unfertilized ovules, single fertilizations, and developing embryos. A) Control: Developing embryo and endosperm about 3 days after a WT pistil was self-pollinated with WT pollen. **B-E)** Differential development of ovules in pods about 3 days after a triple mutant pistil was self-pollinated. **B)** Unfertilized; **C)** Embryo only; **D)** Endosperm only and **E)** Developing embryo. Scale bar in each panel is 50 µm. **F)** Bar graph shows distribution of ovule development per pod in two *chx17/18/19* mutants. Pods of triple mutant 'b' and 'c' showed 32-44% seed abortion with 11-12% being single fertilization events. D. Czerny crossed plants and prepared samples for microscopy. S. Padmanaban observed samples and analyzed images.

without any visible embryo (Fig II-7D). These results suggest a single fertilization event had occurred. Unlike embryo only, endosperm only ovules varied in size, and reached at least twice the length of the original ovule (Fig. II-7D). About half of the ovules developed normally, judging by the development of an embryo and an endosperm, similar to WT development (Fig. II-7E).

D.6. Delayed embryo development of self-fertilized triple mutants

In WT pods, most embryos within one pod developed at near similar rates and reached the late heart stage by 4 or 5 DAP (Fig. II-8A). Similarly, reciprocal crosses using one WT parent with a *chx17/18/19* parent produced heterozygous embryos that developed at a rate comparable to homozygous WT embryos. Some embryos (80-90%) produced from mutant pollen and wild-type pistil also developed to the late heart stage by 4-5 DAP (Fig. II-8G). However, seeds within a single pod from self-ed triple mutant plants showed a range of developmental stages (Fig. II-8B- to II-8E). When some embryos had reached the late torpedo stage, other embryos were at the globular stage, early to late heart, as well as early torpedo stages (Fig. II-8G and II-8H). Thus, homozygous mutant embryos showed a delay in their development. Results would suggest that *CHX* genes from either the male or the female gametophyte can contribute to embryo and seed development.

Fig. II-8. Delayed embryo development in developing seeds of self-pollinated *chx17/18/19* mutant. Six DAP, pods were fixed and cleared with chloral hydrate as above. **A)** WT embryos are mostly at the torpedo stage. **B-F)** Mutant ovules at various developmental stages obtained from a single pod include **B)** globular, **C)** early heart, **D)** late heart, **E)** early torpedo, and **F)** torpedo. Scale bar in A = 100 µm. **G)** Development of embryos within a pod is relatively constant in WT pistils pollinated with *chx17/18/19* mutant pollen. The graph shows the distribution of embryo stages from pods of control WT x WT, WT pistil x *chx17/18/19* pollen or *chx17/18/19* pistil x WT pollen. **H)** Embryo development of self-pollinated triple mutants is delayed. WT and the *chx17/18/19* mutant were self-pollinated and pods were examined by DIC microscopy to determine the stage of embryo development. Results are average of 10 pods per treatment. D. Czerny crossed plants and prepared samples for microscopy. S. Padmanaban examined ovules and collected images.

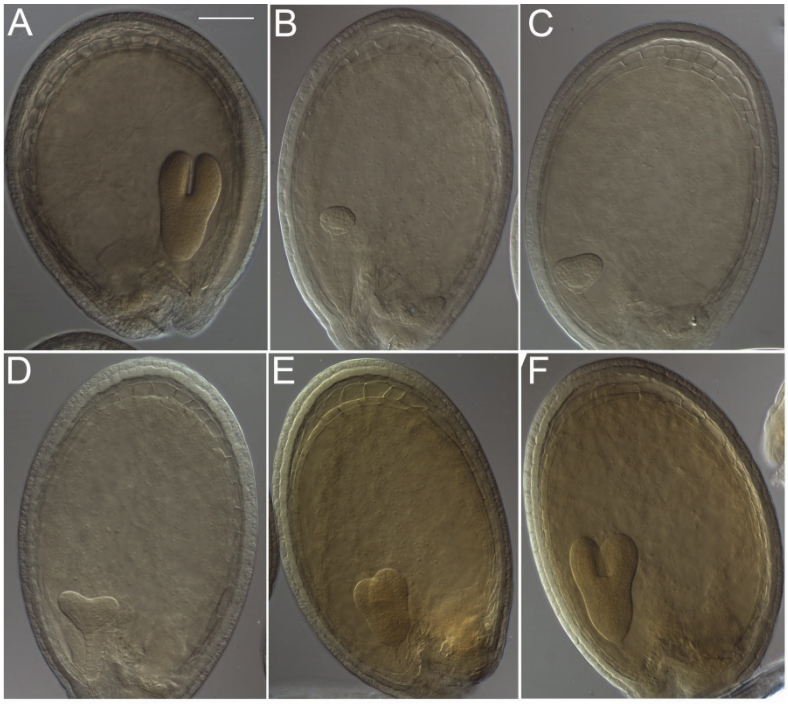
A
B
C
D
E
F

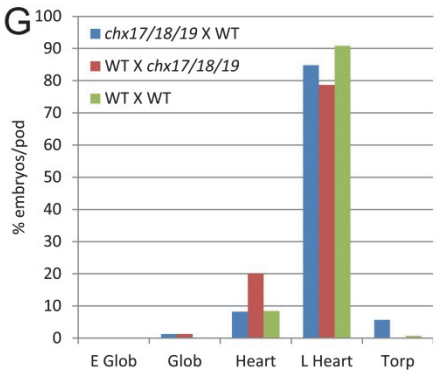
G
chx17/18/19 X WT
WT X chx17/18/19
WT X WT
% embryos/pod
100
90
80
70
60
50
40
30
20
10
0
E Glob
Glob
Heart
L Heart
Torp

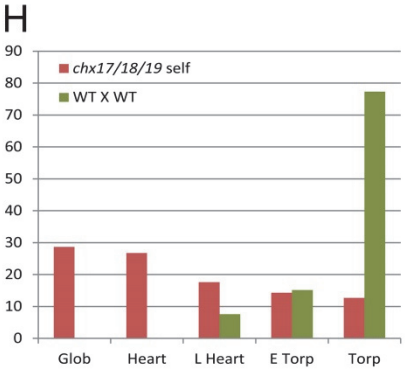
H
chx17/18/19 self
WT X WT
90
80
70
60
50
40
30
20
10
0
Glob
Heart
L Heart
E Torp
Torp

E. DISCUSSION

In spite of advances in CHX17 activity by using yeast, the physiological roles of *CHX17*, *18* or *19* in plants remain unknown. Previously, we reported that a mutant with loss of 4 genes, *CHX16, 17, 18* and *19* produced less seeds per pod (Chanroj et al., 2013). We verified that the triple *chx17/18/19* mutant showed a similar reduction in seed set. However, the double *chx17chx18* or *chx17chx19* mutants were similar to WT. The *chx18/19* double mutant was not available. Thus *CHX16* contributes a relatively minor role. Here we show that three genes, *CHX17*, *CHX18*, and *CHX19*, play overlapping roles in pollen tube vigor and sperm robustness, as the *chx17/18/19* triple mutant showed impaired fertilization.

E.1. Male transmission defect and failed fertilization.

First, reciprocal crossing demonstrated the *chx17/18/19* mutant had a major defect in male fertility. Pollen grain development in triple mutants was unchanged compared to WT grains, indicating the CHX17, 18 or 19 transporters did not influence microsporogenesis or male gametogenesis. *In vitro* pollen germination and tube growth were reduced about 50% in the triple mutant relative to WT. However, this slowed growth did not deter mutant tubes from reaching the distal end of the ovary. In fact, aniline blue staining demonstrated that mutant pollen tubes targeted and entered most ovules. Developed ovules occurred in a random pattern along the ovary and were also found at the distal end, suggesting that tube growth and guidance were not impaired in *chx17/18/19* pollen.

Even though mutant pollen tubes grew and targeted many ovules, about 50% of the targeted ovules remained undeveloped. In WT pollen, both sperm cells are released

simultaneously during tube rupture. One sperm fuses with the egg cell to form a zygote that develops into the embryo. The second sperm unites with the central cell nucleus. Subsequent nuclear division and cellularization produce the endosperm. However, mutant pollen sometimes produced single fertilization events. First, some ovules develop only a globular embryo with no detectable endosperm tissue. Second, some ovules enlarge in size due to proliferation of the endosperm nuclei, with no visible embryo. Either of these examples will lead to abortion and failed seed development, as embryogenesis and endosperm development are coordinated to produce a viable seed (Berger, 2003). The presence of single fertilization events would suggest that reduced seed set is not solely due to failure in pollen tube rupture. Instead, one of the two sperms failed to complete fertilization. Although we consider the possibility for some failure in tube burst, the presence of unfertilized egg cells or central cell nuclei in ovules that have received a *chx17/18/19* tube would suggest that fertilization was compromised.

CHX18 is the major CHX member expressed in sperm cells according to a transcriptomic study (Borges et al., 2008). Partial success in fertilization by triple mutant sperm could be due to *CHX20* expression, which occurs at a low level in sperm cells. Although CHX20 also mediates cation and pH homeostasis in yeast (Padmanaban et al., 2007), it differs from CHX17, CHX18 or CHX19 in its membrane localization and its activity. CHX20 is unable to confer yeast tolerance to HygB (Chanroj et al., 2011).

Interestingly, several other mutants with defects in fertilization share similar phenotypes with the *chx17/18/19* triple mutant. For instance, mutations in sperm cell-expressed genes, such as *HAP2(GCS1)*, cause a male transmission defect due to impaired PT guidance and fertilization (von Besser et al., 2006). HAP2(GCS1) is a

transmembrane protein that was localized to the perinuclear region or the ER (Sprunck et al., 2012). A homologous protein in *Chlamydomonas* is needed for cell-cell attachment prior to cell fusion, suggesting that the plant HAP2(GCS1) might act as a fusogen for gamete recognition, attachment, and fusion (Liu et al., 2008). A mutation in another PM-localized protein in sperm cells, GEX2, also reduced seed set in *gex2-1* mutants. Semi-*in vivo* assays using *gex2-1* PTs carrying RFP-labeled sperm cells showed that sperm fusion with the egg and central cell nuclei were reduced (Mori et al., 2014). Mutant sperm cells failed to attach to the egg cell PM, indicating GEX2 functions in gamete interaction leading to gamete fusion. Self-fertilized homozygous *gex2-1* mutants produced 30% developed seeds, suggesting additional proteins function in gamete attachment and can partially compensate for loss of GEX2 {Mori, 2014, Gamete Attachment Requires GEX2 for Successful Fertilization in Arabidopsis}. Based on the proposed roles of CHX17 and its closest homologs in endomembrane pH and cation homeostasis necessary for cargo sorting, it is tempting to propose that CHX18 plays a role in the proper sorting and delivery of GEX2 and/or HAP2(GCS1) to the sperm cell PM to promote gamete attachment and fusion.

E.2. Female contribution to seed development

Reciprocal crosses of a triple *chx* mutant pistil with WT pollen resulted in a significant decrease in recovery of heterozygous progeny,. However, this decrease in recovery was less severe than that observed using *chx17/18/19* pollen in the reciprocal experiment. Thus, *CHX17*, *CHX18*, or *CHX19* also contribute to female gametophyte function, although the basis for this remains unclear. Transcriptome studies show that *CHX18* is expressed in the central, synergid, and egg cells (Schmid et al., 2012).

Although defects were not visible in seed development, the vigor of heterozygous seeds produced from the above cross could be slightly compromised, possibly during seed germination.

We found that only self-pollinated *chx17/18/19* mutant seed pods showed ovules with delays in embryo development when fertilization was successful (Fig. II-8H). Such a delay was not observed in reciprocal crosses of mutant pollen or pistil with WT pistil or pollen (Fig. II-8G). We offer two explanations: i) the *chx17/18/19* female gametophyte is impaired in sperm attraction, so the time of fertilization in ovules varies widely; and ii) time of fertilization is similar, though embryo development depends on factors from the endosperm. Results from WT pollen applied to a mutant pistil did not show delayed embryo development. So, we favor the second possibility for the following reasons. First, we showed before that *CHX17* is highly expressed at the anterior end of the developing seed (Chanroj et al., 2013). This is supported by transcriptome analysis which shows *CHX17* and *CHX18* are expressed in the micropylar endosperm of the early embryo (Le et al., 2010). Second, RNA-seq analysis showed that both *CHX17* and *CHX18* are expressed in the central cell (Schmid et al., 2012). Union of a sperm cell with a central cell nucleus and subsequent proliferation produces the micropylar endosperm that surrounds the embryo. A recent study demonstrated that cysteine-rich ESF1 peptides accumulated in the central cell and in the micropylar endosperm. Furthermore, purified ESF1 peptides have a role in early development of the embryo {Costa, 2014, Central Cell-Derived Peptides Regulate Early Embryo Patterning in Flowering Plants}. These results suggest that the endosperm surrounding the embryo plays a critical role in producing peptide cues that affect the development of the suspensor and preglobular

embryo. It is possible that CHX17 and CHX18 could play crucial roles in sorting and secreting peptides from the micropylar endosperm to the target cells.

E.3. Working model: Roles of three related *CHX* genes in reproduction

It is intriguing that expression of only one of three related *CHX* genes, in either the male or female gametophyte, is sufficient to restore full seed set when these genes show differential expression in the WT plant. *CHX17* is expressed highly in root and leaf tissues (Sze et al., 2004; Chanroj et al., 2013) and transcript is not detected in mature pollen grains or in pollen tubes (Honys and Twell, 2004; Bock et al., 2006; Qin et al., 2009). *CHX18* transcript is detected in vegetative tissues and sperm cells (Borges et al., 2008). However, *CHX18* expression was low or absent in pollen grains and pollen tubes. *CHX19* is expressed during male gametogenesis and also in pollen tubes germinated on a stigma (Qin et al., 2009). Our results suggest that loss of 2 *CHX* genes in this subclade could induce thethird functional gene to be expressed in additional cell types to restore WT-like seed development. This idea is partly supported by increased transcript levels of *CHX18* and *CHX19* in single *chx17-4* mutants. In addition, *CHX18* or *CHX19* transcript levels increased in *chx17/19* or *chx17/18* double mutants, respectively (Chanroj et al., 2013). The functional studies here further support the ability of related genes to compensate for loss of homologous genes expressed in specific, yet different, cell types.

We propose a model for how loss of either *CHX17*, *18* or *19* might produce the phenotypes we observed. These three proteins share nearly identical activities in functional studies. Expression of *CHX17*, *18*, or *19* conferred alkaline pH tolerance in a yeast mutant sensitive to growth at pH 7.5, which suggests *CHX* genes have a role in pH homeostasis. *CHX17* expression supports growth of K^+ uptake mutants in yeast and *E.*

coli, suggesting a role in K^+ transport and K^+ homeostasis. In addition, CHX17 confers tolerance to HygB, and HygB tolerance is related to the proper sorting of HygB cargo in dynamic endomembranes leading to detoxification and cell proliferation. We showed that *CHX17* expression could reduce secretion of the vacuolar CPY enzyme. As CHX17 has been localized to the PVC and PM in plant cells (Chanroj et al., 2013), these results suggest that proper regulation of endomembrane luminal pH and cation levels play an important role in protein and cargo sorting (Chanroj et al., 2011). Thus, *chx17/18/19* pollen could have reduced tube growth when membrane trafficking in the tip is perturbed. Triple mutant sperm cells may be incompetent to complete fertilization due to inability to sort either the attachment protein GEX2 or the fusogen HAP2(GCS1) to the PM. The role of CHX transporters in the female gametophyte is significant but smaller than in the male gametophyte. Female cells secrete cues to attract pollen tubes and sperm cells for fertilization, which could implicate CHX transporters in female gametophyte function (Sprunck et al., 2012). These ideas will need to be tested and revised. Our study highlights CHX transporters as modulators of intracellular pH and ion gradients that influence membrane trafficking and cargo sorting events that are critical for plant reproductive success.

Chapter III: MODELING AND MUTAGENESIS REVEAL THE ACTIVE CORE AND A UNIVERSAL STRESS PROTEIN-LIKE DOMAIN IN THE PLANT CATION/PROTON EXCHANGER CHX17.

A. ABSTRACT

Proliferation of a novel family of predicted cation/H^+ exchangers (CHX) suggests roles in vegetative and reproductive innovations of land plants. However, molecular evidence for the transport mechanism of any plant cation/proton antiporter type 2 (CPA2) member is lacking. We used a model structure-guided mutagenesis approach to identify residues involved in catalysis or regulation of *Arabidopsis thaliana* CHX17. A model of the transmembrane (TM) domain built using Phyre2 showed a protein fold that matched the bacterial Na^+/H^+ antiporters EcNhaA and TtNapA with high confidence. The CHX17 model has 12-13 transmembrane (TM) spans with a characteristic cross-over of TM4 and TM11 in the middle of the membrane. An aspartate (Asp) residue in TM5 is conserved in cation/H^+ antiporters, but residues in the unwound regions of TM4 and TM11 are less conserved. Based on the model structure, residues were mutated and CHX17 activity was tested in a yeast mutant as growth on a conditional medium. We show that Asn200 and Asp201 in TM5, and Lys355 in TM10 are critical for activity. Asp201 can be replaced by Glu, though Lys355 was not replaceable by Arg. The residues Thr170 and Lys383 in the flexible unwound regions of TM4 and TM11, respectively, are important for activity. Thus, CHX17 resembles a cation/H^+ exchanger with a catalytic central core at TM4-5 and TM11 where four critical residues are in close proximity. Glu111 at the rim of TM2 is located far from the active site. The E111C mutation inhibited CHX17 activity, suggesting a role as a pH sensor. Point mutations and truncations of the hydrophilic C-tail had no effect on activity, raising the possibility the hydrophilic domain is not directly altering transport activity. 3D modeling of the hydrophilic tail reveals a

universal stress protein-like domain which may be involved in protein-protein interactions and signaling in response to stress cues.

B. INTRODUCTION

B.1. CHX transporters in plants

Genomes of all flowering plants encode a novel family of predicted cation/H^+ exchangers (CHX) that are generally absent in metazoan genomes. *Arabidopsis thaliana CHX* genes are expressed in vegetative and reproductive tissues, with over half of the *CHX* genes expressed in pollen (Sze et al., 2004). Phylogenetic analysis of CHX proteins has shown the number of *CHX* genes has increased from 3-4 in early land plants to over 40 in eudicots. CHX proteins from early land plants are similar to *A. thaliana* CHX20, suggesting *CHX20* and the related *CHX16-19* genes are founding members of this family. The proliferation of *CHX* genes suggests they could function in adaptation to life on dry land through potential roles in vegetative survival, reproductive innovations, or both (Chanroj et al., 2012). However, l direct evidence for the transport function of *A. thaliana* CHX transporters is lacking.

To understand the molecular functions of CHX transporters, we have functionally expressed *CHX* genes in single-celled hosts. Expression of *CHX* genes in yeast mutants lacking multiple cation transporters has provided evidence for possible cellular functions of *Arabidopsis* CHX transporters. The yeast mutant KTA40-2, which lacks multiple cation transport systems, is sensitive to alkaline external pH (Maresova and Sychrova, 2005). Expression of *CHX16* to *CHX20* in the KTA40-2 mutant conferred tolerance to pH 7.5 (Chanroj et al., 2011). This finding suggests that CHX transporters mediate

cation/H^+ exchange to maintain pH homeostasis in subcellular compartments and the cytosol. In all eukaryotic cells, control of intracellular pH homeostasis by a variety of transporters is necessary for essential functions such as cell proliferation, secretion, and endocytosis (Casey et al., 2010).

The yeast mutant KTA40-2 is also sensitive to the drug hygromycin B (HygB), a phenotype related to proper membrane trafficking and cargo sorting (Chanroj et al., 2011). HygB is an antibiotic that binds to the small ribosomal subunit to inhibit translation (Brodersen et al., 2000). KTA40-2 yeast transformed with *CHX17*, *18*, or *19* could grow on medium containing 100 µg/ml HygB. However, KTA40-2 yeast transformed with either *CHX16* or *CHX20* were sensitive to the drug (Chanroj et al., 2011). Together, these results suggest functional diversity among CHX proteins, possibly related to different subcellular localizations, pH-dependent activities, or modes of transport.

To test the cations transported by CHX17 and CHX20, these proteins were expressed in the LB2003 *E. coli* mutant that lacks three K^+ uptake mechanisms. In a bacterial host, a CHX protein would be localized on the PM, which would facilitate measurement of cation uptake into the cell (Uozumi, 2001). The *E. coli* mutant alone is unable to proliferate on medium with 2-4 mM K^+. Expression of either *CHX17* or *CHX20* restored growth of the bacteria cultured in low K^+-containing medium. LB2003 *E. coli* cells also took up radioactive $^{86}Rb^+$, a K^+ analog. In competition experiments with non-radiolabeled cations, K^+ competed and inhibited $^{86}Rb^+$ uptake at a lower concentration relative to Na^+ (Chanroj et al., 2011). Thus, CHX17 and CHX20 both

appear to transport cations with a preference for K^+. However, the mode of K^+ transport was unclear.

B.2. What are the roles of *CHX17*, *18*, and *19* in the plant?

What are potential functions of K^+ transporters in *A. thaliana*? CHX17, 18, and 19 show similar membrane localization in plant cells and similar activities in yeast, suggesting they might perform overlapping functions (Chanroj et al., 2011). CHX17, 18 or 19 fused to a fluorescent protein localized to prevacuolar compartments (PVC) and the plasma membrane (PM) of transgenic plants (Chanroj et al., 2013). Mutants defective in one or two of these genes did not display any obvious phenotype, but a triple *chx17/18/19* mutant showed reduced seed set relative to WT (Chanroj et al., 2013). How loss of function mutations in *CHX17*, *18*, and *19* perturb seed set is unclear. It is possible that these CHX transporters share a common role in pH and K^+ homeostasis necessary for male gametophyte function and successful reproduction.

B.3. What is the evidence for CHX transporters functioning as cation/H^+ exchangers?

To gain insight into *CHX* gene function, their evolutionary history was studied using phylogenetic trees. The CPA superfamily was divided into two families. The CPA1 family consists of plant Na$^+$/H$^+$ exchangers (NHX), and the CPA2 family consists of plant CHX transporters and K$^+$ efflux antiporters (KEA) (Brett et al., 2005). CPA2 transporters are abundant in genomes of bacteria, algae, fungi, and plants, but are rare in metazoan genomes (Chanroj et al., 2012). The numbers of *NHX* and *KEA* genes have not significantly increased during plant evolution, but *CHX* genes have proliferated and

diversified specifically in flowering land plants. In addition, genes encoding CPA transporters evolved from distinct ancestral bacterial genes, with CPA1 transporters arising from an NhaP-like transporter, KEA transporters arising from a KefC-like transporter, and CHX transporters arising from an NhaA-like transporter (Chanroj et al., 2012). Therefore, CHX transporters in flowering plants likely originated from an ancestor of the *E. coli* Na^+/H^+ antiporter NhaA.

B.4. *E. coli* NhaA and *T. thermophilus* NapA are CPA2 transporters with solved crystal structures.

E. coli NhaA (EcNhaA) is a model cation/H^+ antiporter with extensive genetic, biochemical, and structural data available (Padan, 2008). The primary cellular function of EcNhaA is supporting growth at alkaline pH in the presence of Na^+ or Li^+. EcNhaA is electrogenic: 2 H^+ are imported into the cell as 1 Na^+ is exported (Arkin et al., 2007). EcNhaA is active from pH 6.5-8.5, and its transport activity increases to a maximum level at pH 8.5 (Taglicht et al., 1991a). The pH-dependent increase in EcNhaA activity suggests the presence of a pH sensor domain in the protein that could modulate transport activity in response to pH. Accordingly, mutagenesis of EcNhaA identified amino acids clustered at the cytoplasmic face of the protein that function in the pH response (Krulwich et al., 2011). For example, Glu78 has a role in the pH-dependence of EcNhaA activity. Point mutations of Glu78 shifted the pH profile of the transporter toward alkaline pH, toward acidic pH, or removed pH-dependent activity (Herz et al., 2010).

The crystal structure of EcNhaA at pH 4 was solved in 2005. The structure shows 12 α-helical TM spans. The folding of the TM spans in the membrane forms two funnels; one open to the cytosol and another to the periplasm are separated by a barrier in the

middle of the membrane (Hunte et al., 2005). Mutagenesis in EcNhaA has identified residues that are necessary for $Na^+(Li^+)/H^+$ antiport. Negatively-charged acidic residues could function in cation binding and transport. In EcNhaA, point mutations of conserved Asp163 and Asp164 to Asn abolished $Na^+(Li^+)/H^+$ antiport activity and caused alkaline pH sensitivity in the *E.coli* host (Inoue et al., 1995). In addition, the crystal structure and mutagenesis studies suggested TM spans 4, 5, 11, and 12 form the transport core (Hunte et al., 2005).

Recently, the *Thermus thermophilus* Na^+/H^+ antiporter NapA (TtNapA) was crystalized at 3Å resolution (Lee et al., 2013). TtNapA was crystallized as a dimer at pH 7.8, where the transporter is active. The structure shows 13 TM spans in each monomer with discontinuous helices in TM4 and TM11 crossing over each other. Similar to the EcNhaA fold, the TM4-TM11 assembly in TtNapA is predicted to contain the cation binding site (Lee et al., 2013). TtNapA was originally identified from the *T. thermophilus* genome as a translated open reading frame belonging to the CPA2 family. Despite a low percent sequence identity (21%) with EcNhaA, TtNapA contains amino acid residues within its TM domain that are conserved with EcNhaA. TtNapA residues Asp156, Asp157, and Lys305 were mutated to alanine, and the point mutations were expressed in a cation antiport-deficient *E. coli* mutant. In the presence of elevated NaCl or LiCl, *E. coli* expressing the D156A and D157A point mutations grew very poorly. TtNapA with a K305A mutation conferred slight NaCl or LiCl tolerance to the bacteria (Furrer et al., 2007). Together, the crystal structures and mutagenesis analysis of these two prokaryote transporters could serve as prototypes to guide the molecular functional studies of plant CPA2 transporters, such as *A. thaliana* CHX17.

B.5. What approach was used? What are the novel findings?

Here, we used a model structure-guided mutagenesis approach to identify residues that participate in activity in *A. thaliana* CHX17. Analysis of models built from the *E. coli* NhaA or *T. thermophilus* NapA templates suggested key residues for mutagenesis. The working hypothesis was if these CHX17 residues were important for K^+ transport activity or for sensing pH, then a single residue mutation would inhibit CHX17 activity. Activity was tested as yeast growth after expression of a mutated *CHX17* in a yeast mutant sensitive to hygromycin B. Our results revealed conserved and previously unrecognized residues located within a four-helix bundle of TM4-5 and TM11-12, and these results support a model that CHX17 behaves like a cation/H^+ exchanger with a potential pH sensor. Furthermore, secondary structure and 3D modeling strongly suggest a tandem universal stress protein-like domain at the hydrophilic C-tail.

C. MATERIAL AND METHODS.

C.1. Generating a 3D model structure of CHX17

To guide site-directed mutagenesis, a 3D model of the CHX17 transmembrane domain was generated with the protein homology/analogy recognition engine (Phyre2) (Kelley and Sternberg, 2009). The Phyre2 server has a library of known protein structures (PDB and SCOP), and each protein query is constructed to a profile. This 'fold library' also stores the known and predicted secondary structures of proteins. When the sequence of CHX17-TM (residues 1-440) is entered as query, a profile is constructed after psi-BLAST to collect sequence homologs. The secondary structure of CHX17-TM is also predicted based on three prediction programs, and a final consensus prediction is given. The profile and secondary structure of CHX17-TM is then compared in a profile-profile alignment to proteins in the fold library. The top 10 highest scoring alignments are used to construct full 3D models of the query. Two 3D models for CHX17-TM were obtained. One corresponds to the template *T. thermophilus* NapA (PDB code 4BWZ) (Lee et al., 2013), and another to the template *E. coli* NhaA (PDB code 1ZCD) (Hunte et al., 2005). To identify conserved amino acid residues among CHX17 and related cation/H^+ exchangers, amino acid sequence alignments were generated using the MUSCLE program (Edgar, 2004; Tamura et al., 2011).

C.2. Yeast and bacterium

The yeast mutant strain KTA40-2 (*ena1-4Δ*, *nha1Δ*, *kha1Δ, nhx1Δ*) was grown in YPAD medium prior to transformation. *Escherichia coli* mutant strain LB2003 (*trkAΔ, kup1Δ, kdpABCDEΔ*) was maintained in YTMK medium. *E. coli* strains DH5α (Life

Technologies 18265-017) and TOP10 (Life Technologies C4040) were maintained in low-salt LB medium.

C.3. CHX17 point mutation constructs

C.3a. Point mutation constructs

Single-residue point mutations were generated using the Quik Change II site-directed mutagenesis kit according to the manufacturer's instructions (Agilent Genomics 200521). The selected amino acids included E111, T170, N200, D201, H284, E311, K355, T382, K383, C458A, C562A, and C607A. Two complementary oligonucleotides containing the desired base change, flanked by unmodified nucleotide sequence, were synthesized (Table III-S1). The two primers were used to amplify CHX17 cDNA in the pDONR221 Gateway vector, termed pECHX17 (Life Technologies 12536-017). Initial denaturation conducted at 95°C for 30 s was followed by 12-18 cycles at 95°C 30 s and 55°C at 1 min, and then 68°C at 1 minute/kb of plasmid length. One µl of Dpn I restriction enzyme (10 U/µl) was added directly to each amplification reaction, mixed thoroughly, and incubated at 37°C for 1 h to digest the parental supercoiled dsDNA. One µl of the Dpn I-treated DNA was transferred from each control and sample reaction to separate aliquots of the competent XL10-Gold *E. coli* cells. The transformation reactions were gently mixed and incubated on ice for 30 min. The reactions were transferred to 42°C water bath for 45 s and then on ice for 2 min. NZY+ broth (0.5 ml) was added to each tube and incubated at 37°C for 1 h with shaking at 225–250 rpm. An aliquot of 100 ul per transformation was plated on agar plates containing 100 µg/ml ampicillin. After incubation at 37°C for 16 h, transformants were selected. Plasmids were isolated and sequenced to confirm the desired mutation. WT or mutated CHX17 cDNA was

recombined into the destination vector pYES-DEST52 (Life Technologies 12286-019). Plasmids were transformed into NEB10β *E. coli* (New England Biolabs C3019H) and amplified. Yeast strain KTA40-2 was transformed to test for growth tolerance to HygB.

b. CHX17 hydrophilic C-tail truncation constructs

To generate truncations in the hydrophilic C-tail of CHX17, cDNA sequences truncating different lengths of the hydrophilic C-tail were amplified by PCR using iProof polymerase (Bio-Rad 172-5331) with appropriate primers (Table III-S3) and the WT CHX17 cDNA in the pPAB404 plasmid as template (Chanroj et al., 2011). The PCR products were recombined into the pDONR221 Gateway plasmid (Life Technologies 12536-017) using Gateway BP Clonase II enzyme mix (Life Technologies 11789-020). Plasmids were transformed into NEB10β *E. coli* (New England Biolabs C3019H), and plasmids were recovered as above using alkaline lysis. DNA sequencing to check the CHX17 truncation sequences was performed as above (Genewiz). C-tail truncation sequences were recombined into pYES-DEST52 (Life Technologies 12286-019) using Gateway LR Clonase II enzyme mix (Life Technologies 11791-020), and plasmids were recovered as above.

C.4. Transformation of yeast and bacterium

C.4a. Yeast transformation

The yeast mutant strain KTA40-2 (*ena1-4Δ*, *nha1Δ*, *kha1Δ, nhx1Δ*) was transformed according to Gietz and Schiestl (Gietz and Schiestl, 2007). To prepare cells for transformation, yeast were grown in YPAD medium (1.0% yeast extract, 2.0% peptone, 0.01% adenine, and 2.0% glucose) plus 50 mM KCl overnight prior to transformation. A 10 ml YPAD overnight culture was diluted with 10 ml YPAD plus 50

mM KCl and incubated for 4-6 hours to reach mid-log phase. The yeast culture was pelleted at 2500 x g for 10 min in a Sorvall RC5C with an SS-34 rotor. The culture was washed with 10 ml sterile water and resuspended to A_{600} of between 2 and 2.5 by using 4 ml of FCC solution (5% v/v glycerol, 10% v/v DMSO). Cells were aliquoted and stored at -80°C for transformation.

For transformation, 12.5 µl of yeast cells were incubated with 65 µl of 50% PEG3350, 10 µl of 1.0 M lithium acetate, 5 µl of salmon sperm DNA, and 1 µg of plasmid DNA. Transformation volumes were increased to 100 µl using sterile water. The transformation mixture was incubated in a 42°C water bath for 90 min and pelleted at 5000 rpm for 1 min in a benchtop microcentrifuge (Eppendorf 5415C). Yeast pellets were resuspended in 200 µl of sterile water, and 120 µl was plated on YNB(A) selection plates containing 100 mM KCl and lacking uracil for selection. Plates were incubated at 30°C for 2 d before 8-12 colonies were subcultured onto YNB(A) selection plates. Plasmids containing CHX17 point mutations or C-tail truncations were transformed into KTA40-2 yeast as above. Wild-type CHX17 and empty vector pYES-c1 (Padmanaban et al., 2007) were also transformed into KTA40-2 yeast as controls.

b. E. coli transformation

Transformation of *E. coli* strains DH5α (Life Technologies 18265-017) and TOP10 (Life Technologies C4040) were performed as described in Maeder et al. (Maeder et al., 2009). Briefly, *E. coli* cells were mixed with at least 200 ng of plasmid DNA on ice and incubated on ice for 5 min. Transformation was by heat-shock at 42°C for 2 min. Cells were incubated on ice for 2 min. Low-salt LB medium was added to cells, and cultures were incubated in a 37°C shaker for 1 hr. Cultures were spread on solid low-salt

LB plates for selection using appropriate antibiotics (100 µg/ml Ampicillin, 30 µg/ml Chloramphenicol, or 50 µg/ml Kanamycin). Plates were incubated at 37°C overnight to recover bacteria colonies.

C.5. Testing CHX17 activity in yeast

The yeast mutant KTA40-2 was transformed (Gietz and Schiestl, 2007) with WT or mutated CHX17 constructs, and positive transformants were selected on YNB(A), pH 6.0 supplemented with 50 mM KCl, amino acids, and 2% glucose. Eight to twelve independent transformants were subcultured. For testing CHX17 point mutations, six independent transformants per construct were inoculated into 1.0 ml of YNB(A) at pH 6.0 minus uracil and supplemented with 50 mM KCl and 2% glucose. Cultures were incubated for 24 h in a 30°C shaker. The 1 ml cultures were poured into 1 ml YNB(A) at pH 6.0 minus uracil and supplemented with 50 mM KCl and 2% glucose plus 4 ml YNB(A) at pH 6.0 without uracil, KCl, and glucose. These 6 ml cultures were incubated for 16 h in a 30°C shaker. Cells were normalized to A_{600} of 0.2 using K^+-free YNB(A) at pH 6.0. Ten-fold serial dilutions were performed in K^+-free YNB(A) at pH 6.0. Five µl of each serial dilution was spotted on solid YNB(A) plates minus uracil and containing 2% galactose, to induce gene expression, plus varying concentrations of Hygromycin B (EMD Millipore 400052). For testing CHX17-GFP constructs, test media contained 2% glucose, as the plasmid contained a constitutive promoter. For testing CHX17 C-tail truncation constructs, yeast cells were normalized to 0.4 A_{600} prior to serial dilutions.

To test growth on liquid culture, yeast transformants were inoculated into 2.0 ml of YNB(A) at pH 6.0 minus uracil and supplemented with 50 mM KCl and 2% glucose. Cultures were incubated in a 30°C shaker overnight. Cultures were pelleted at 3700 x g

for 10 min in a tabletop Beckman X-15R centrifuge with an SX4750 rotor. Pellets were suspended in 8.0 ml of YNB(A) at pH 6.0 plus 2% galactose without KCl and uracil. Yeast cultures usually at A_{600} between 1.1 and 1.3 were normalized to 0.1 . Test culture medium was 6.0 ml YNB(A) at pH 6.0 plus 2% galactose without KCl and uracil, with or without hygromycin B at 0, 25, 50, 75, or 100 µg/ml. Cultures were incubated in a 30°C shaker and 600 µl of culture was removed at 0, 10, 22, 26, 31, 45, or 55 h to measure absorbance at 600 nm. The OD at late log phase (20-30 h) was averaged.

C.6. GFP-tagged CHX17 proteins

C.6a. Construction of CHX17-GFP clones.

To make CHX17-GFP fusion constructs, WT or mutated CHX17 cDNA in the entry vector (pECHX17) was recombined using LR Clonase into pGWFDR196 Gateway-compatible vector to give an in-frame fusion of enhanced GFP at the C-terminus of CHX17. This vector was constructed with the yeast constitutive PMA1 promoter in the Gateway vector pGWF2 (Li et al., 2008). Constructs shown in Table III-S2 included wild type pDX17-GFP-pGWFDR196, and CHX17 mutated at E111C, T170A, N200D, D201A, D201E, D201N, H284A, K355A, K355Q, K355R, K383A, C458A, C562A and C607A. Insertion of the cassette by homologous recombination was verified by PCR with a set of CHX17 gene-specific primers. The yeast mutant KTA40-2 was transformed with above constructs and selected on YNB(A) agar plates without uracil for selection. From each transformation, six colonies were selected and analyzed by fluorescence microscopy, and CHX17-GFP activity was tested for HygB tolerance.

C.6b. Imaging GFP-tagged CHX17 in yeast

Aliquots of yeast strains grown to mid-logarithmic phase in YNB medium lacking URA were analyzed in 10-well glass-bottom microscope slides. Cells were examined by fluorescence and brightfield microscopy with a Nikon E600 microscope using an oil-immersed objective at 100X magnification. Using a SPOT imaging software (Diagnostic Instruments), images for GFP fluorescence and DIC were taken.

C.6c. Protein extraction, separation and immuno-detection

To detect CHX17-GFP protein, total proteins from yeast cultures were isolated, gel-separated and immunostained with anti GFP antibodies. Briefly, yeast was grown in 5 ml YNB medium overnight to OD_{600} of 1.0. Cells were pelleted and washed once with water. The pellet was suspended in 1.0 ml of 2M lithium acetate and incubated at room temperature for 5 min. Cells were pelleted and suspended in 500 µl of water. Freshly-made 1.85 M NaOH/7.4% (v/v) β-ME was added (85µl) and mixed by vortexing. After incubating on ice for 10 min, 40 µl of 100% (w/v) TCA was added and mixed to precipitate proteins on ice for 10 min. Proteins were collected 13,000 rpm for 10 min at 4°C using a microfuge. The pellet was washed with 500 µl of cold (-20°C) acetone and air-dried for 15 min on ice. The pellet was suspended in 500 µl of SDS phosphate saline buffer (pH 7.4). A 50 µl of sample was mixed with 50µl of 2x SDS-PAGE gel loading dye. After heating at 70°C for 15 min, the sample was spun at 13k rpm for 5 min at room temperature. The supernatant (80 µl) with total protein (50-80 µg) is loaded onto a large 7.5% acrylamide gel and run at 4 mAmp for 16 h. One gel was stained for protein with Coomassie Blue, and another was used for immunoblotting.

After protein separation, the gel was incubated in transfer buffer (25 mM Tris, 192 mM glycine, 15% (v/v) methanol) for 2-5 min. Proteins from gel was transferred to Immobilon-PVDF membrane (Bio-Rad 162-0177) at 100 V for 1 hr. The positions of the wells were marked on the membrane before transfer to blocking buffer (5% non-fat milk in 1.0 M glycine, 1% w/v BSA). The membrane was incubated for 1 hr at room temperature with gentle agitation on a rocking platform (Hoefer Scientific). The membrane was washed 3 times for 5 min each with buffer (1X PBS with 0.1% Tween-20). The membrane was incubated with antibody incubation buffer containing polyclonal rabbit anti-GFP-IgG (1:3000, Abcam ab290) with gentle agitation for 1 hr at room temperature. The membrane was washed 3 times with buffer. The blot was incubated with goat anti-rabbit IgG HRP-conjugated secondary antibody (1:3000, Sigma Aldrich A6154) for 1 hr with gentle agitation. The membrane was washed with buffer at least 3-4 times, 5 min each. The blot was incubated with SuperSignal HRP substrate (Pierce 34080) for 1 min. The blot was exposed to X-ray film (Thermo Scientific 34090) for 30 s up to 10 min before developing (Kodak X-OMAT 5000RA).

D. RESULTS

D.1. Modeling the 3D structure of CHX17

CHX17 from *A. thaliana* is an 820 amino acid protein comprised of an N-terminal transmembrane (TM) domain (430 residues) and a C-terminal hydrophilic tail (of 390 residues) (Sze et al., 2004). Analysis of conserved protein domains shows that the N-terminal TM domain of the CHX17 protein is similar to a KefB-type K^+ transport system or a Pfam domain seen in Na^+/H^+ antiporters. The hydrophilic C-terminal tail has weak homology to an adenine nucleotide alpha-hydrolase (AANH) superfamily (Fig. III-1A).

The number of TM spans in plant CHX17 and related CPA2 transporters is still uncertain. Based on TM prediction programs, there are 10-13 TM spans, with a consensus of 12 TM (Schwacke et al., 2003). The blue lines in Fig. III-1B show residues predicted to form the 12 TM spans according to TMHMM 2.0 (Krogh et al 2001). Homology modeling of CHX17 with the crystal structure of EcNhaA also revealed 12 α-helices that span the membrane (Fig. III-1B, green line) though the placement of 2 TM spans differed from that of TMHMM2.0. Oddly, the model of CHX17 according to the crystal structure of TtNapA predicted 13 TM spans (Fig. III-1B, orange line). An extra TM could change the location of the N terminus from the cytosolic to the extracellular or lumen side, assuming a model in which the C-tail plays a regulatory role in the cytosol. For simplicity and consistency, we have adopted the TM number according to TtNapA. The first TM span in EcNhaA or AtCHX17 is referred to as TM-1 (minus 1), and the following TM observed in CHX17 and in TtNapA, but not in EcNhaA, is given TM1. TM spans from 2-12 in CHX17 are numbered as in EcNhaA or TtNapA (Fig. III-1B).

Fig. III-1. Protein domains and transmembrane segments of AtCHX17-TM.

A) The AtCHX17 protein has an N-terminal transmembrane (TM) domain and a C-terminal hydrophilic tail. The TM domain has similarity to a Na^+/H^+ exchanger, or a Kef-type K^+ transport system from residues 37-423. The C-tail has homology to an adenine nucleotide alpha-hydrolase (AANH).

B) Transmembrane segments. TM regions predicted by TMHMM2.0 (blue lines), or alignment with *E. coli* NhaA (red). Transmembrane α-helices predicted from secondary structure and 3D models using EcNhaA (green) and TtNapA (orange) as templates. Dots infer discontinuous regions within α-helices TM4 and TM11.

C) Conserved residues and residues predicted in the discontinuous helices of AtCHX17 and AtNHX1 are shown with TtNapA and EcNhaA (see legend for Table III-1).

D. Czerny designed and revised the figure. T. Barry assisted with generating panel C.

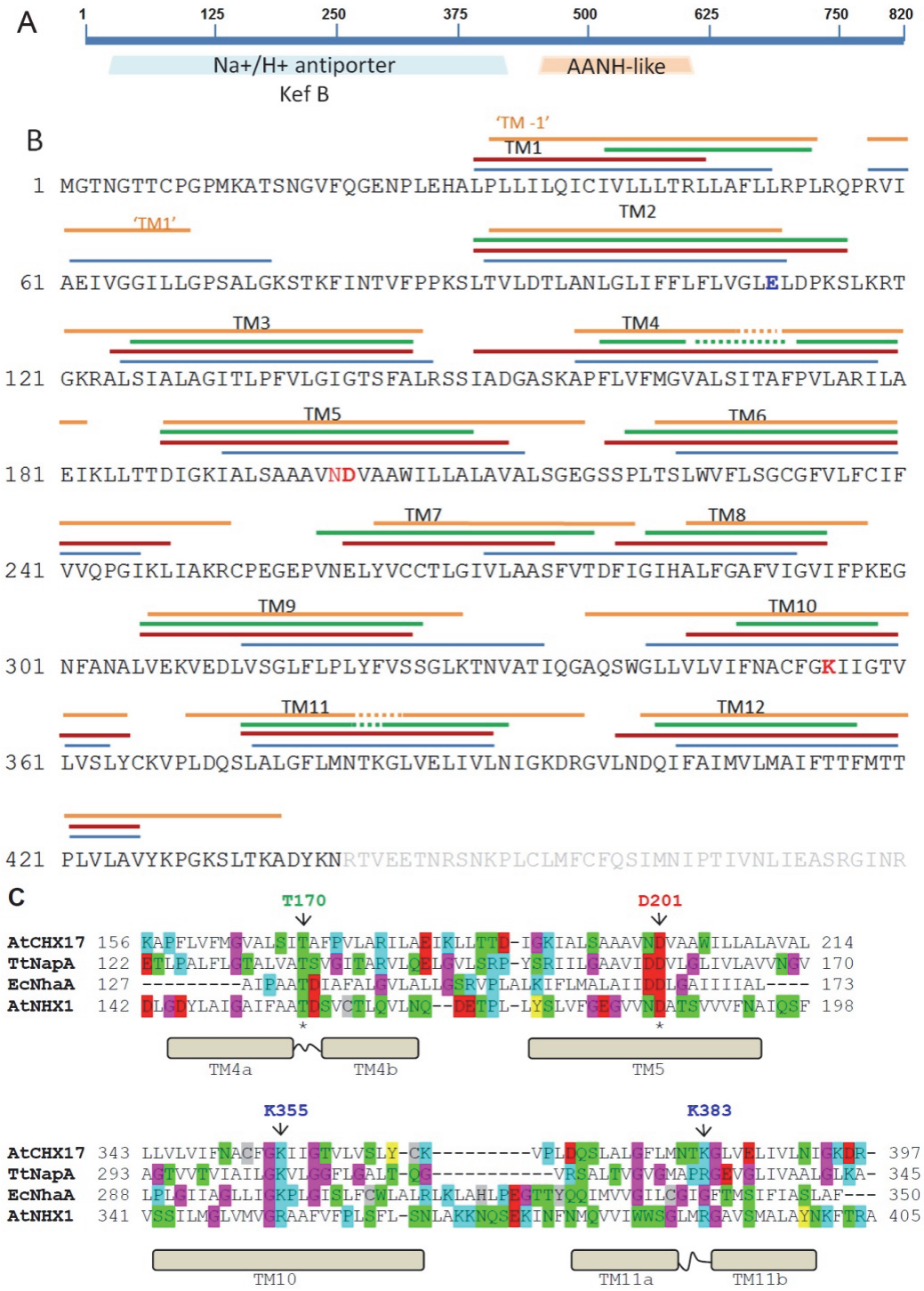
A
1
125
250
375
500
625
750
820
Na+/H+ antiporter
Kef B
AANH-like
B
'TM -1'
TM1
1 MGTNGTTCPGPMKATSNGVFQGENPLEHALPLLILQICIVLLLTRLLAFLLRPLRQPRVI
'TM1'
TM2
61 AEIVGGILLGPSALGKSTKFINTVFPPKSLTVLDTLANLGLIFFLFLVGLELDPKSLKRT
TM3
TM4
121 GKRALSIALAGITLPFVLGIGTSFALRSSIADGASKAPFLVFMGVALSITAFPVLARILA
TM5
TM6
181 EIKLLTTDIGKIALSAAAVNDVAAWILLALAVALSGEGSSPLTSLWVFLSGCGFVLFCIF
TM7
TM8
241 VVQPGIKLIAKRCPEGEPVNELYVCCTLGIVLAASFVTDFIGIHALFGAFVIGVIFPKEG
TM9
TM10
301 NFANALVEKVEDLVSGLFLPLYFVSSGLKTNVATIQGAQSWGLLVLVIFNACFGKIIGTV
TM11
TM12
361 LVSLYCKVPLDQSLALGFLMNTKGLVELIVLNIGKDRGVLNDQIFAIMVLMAIFTTFMTT
421 PLVLAVYKPGKSLTKADYKNRTVEETNRSNKPLCLMFCFQSIMNIPTIVNLIEASRGINR
C
T170
D201
AtCHX17 156 KAPFLVFMGVALSITAFPVLARILAEIKLLTTD-IGKIALSAAAVNDVAAWILLALAVAL 214
TtNapA 122 ETLPALFLGTALVATSVGITARVLQELGVLSRP-YSRIILGAAVIDDVLGLIVLAVVNGV 170
EcNhaA 127 ---------AIPAATDIAFALGVLALLGSRVPLALKIFLMALAIIDDLGAIIIIAL---- 173
AtNHX1 142 LLGDYLAIGAIFAATDSVCTLQVLNQ--DETPL-LYSLVFGEGVVNDATSVVVFNAIQSF 198
TM4a
TM4b
TM5
K355
K383
AtCHX17 343 LLVLVIFNACFGKIIGTVLVSLY-CK---------VPLLQSLALGFLMNTKGLVELIVLNIGKDR- 397
TtNapA 293 AGTVVTVIAILGKVLGGFLGALT-QG-----------VRSALTVGVGMAPRGEVGLIVAALGLKA- 345
EcNhaA 288 LPLGIIAGLLIGKPLGISLFCWLALRLKLAHLPEGTTYQQIMVVGILCGIGFTMSIFIASLAF--- 350
AtNHX1 341 VSSILMGLVMVGRAAFVFPLSFL-SNLAKKNQSEKINFNMQVVIWWSGLMRGAVSMALAYNKFTRA 405
TM10
TM11a
TM11b

D.2. AtCHX17 TM domain has a protein fold similar to *T. thermophilus* NapA and to *E. coli* NhaA.

Using the CHX17-TM sequence (1-440) as the query, Phyre2 (Kelley & Steinberg 2009) yielded two model structures based on crystal structures of bacterial Na^+/H^+ antiporters. One was based on the structure of *Thermus thermophilus,* an archaebacterium, NapA, and another from *E. coli* NhaA (Fig.III-2 A-B). The CHX17-TM region shared 26% and 16% identity with TtNapA (394 residues) and EcNhaA (388 residues), respectively. CHX17 residues 31-436 or 92% aligned with TtNapA (Fig. III-S1B-C). The probability that CHX17-TM is homologous with TtNapA is given a confidence of 100% (Fig. S1A). Even though the sequence identity is low, a confidence level of 90% or higher indicates CHX17 shares a similar protein fold to TtNapA and to EcNhaA. Thus, both 3D models are useful, though some differences exist (Fig. III-1B). An extra TM span in CHX17 model from TtNapA is seen at the N terminus.

The CHX17-TM domain consists of two inverted repeats at TM1-5 and TM8-12 connected by TM spans 6 and 7. This is better visualized in the linear 2D topology model in Fig. III-2C. The 3D model shows the discontinuous regions in the middle of TM4 and TM11 α-helices intersect (Fig. III-1C and Fig. III-2A-B). The active core is predicted to be in TM4-5 and TM11-12 (Fig. III-2), based on studies of crystallized secondary active transporters (Forrest et al., 2011). The core is defined as a region in the center of the protein with residues critical for transport or binding. Apart from a conserved Asp in TM5, additional residues in the core of plant CPA2 are untested and unknown, so we used CHX17 as a prototype to select residues with potential function.

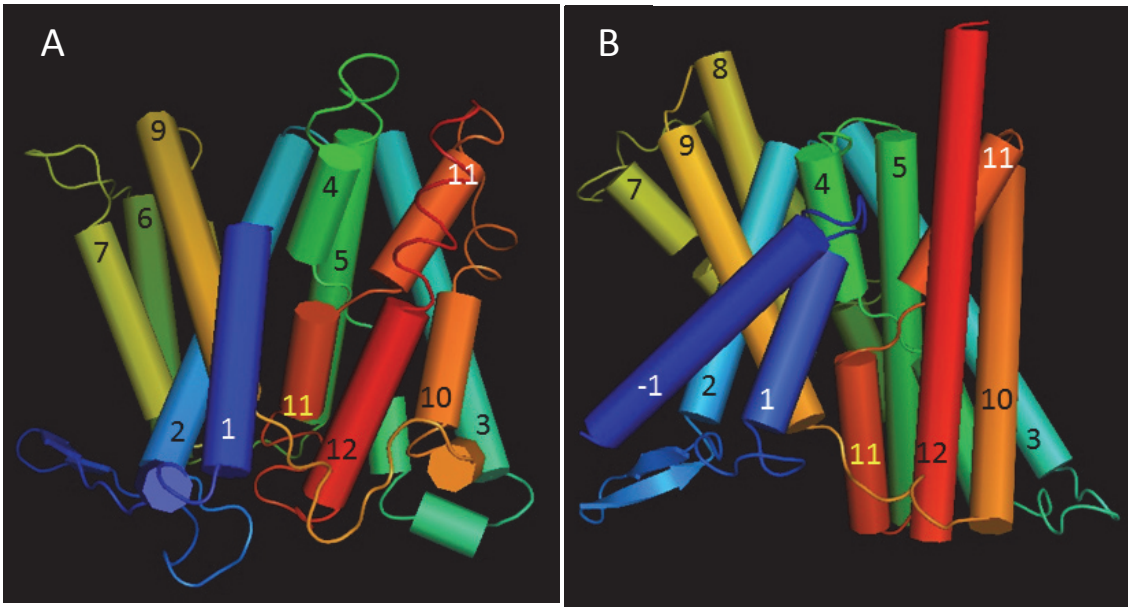

Figure III-2. 3D structure models of CHX17-TM.

Amino acids 1-440 in AtCHX17 were used to construct the models using the Phyre2 server. **A)** Model based on *E. coli* NhaA (PDB 1ZCD)**.** The model shows 12 TM hows 12 TM CD) tCHX17 we**B)** Model based on *T. thermophilus* NapA (PDB 4BWZ). The extra TM seen at the N terminus in this model is labeled as -1. Both models show TM spans 4 and 11 contain discontinuous α-helices which cross over in the middle of the membrane.

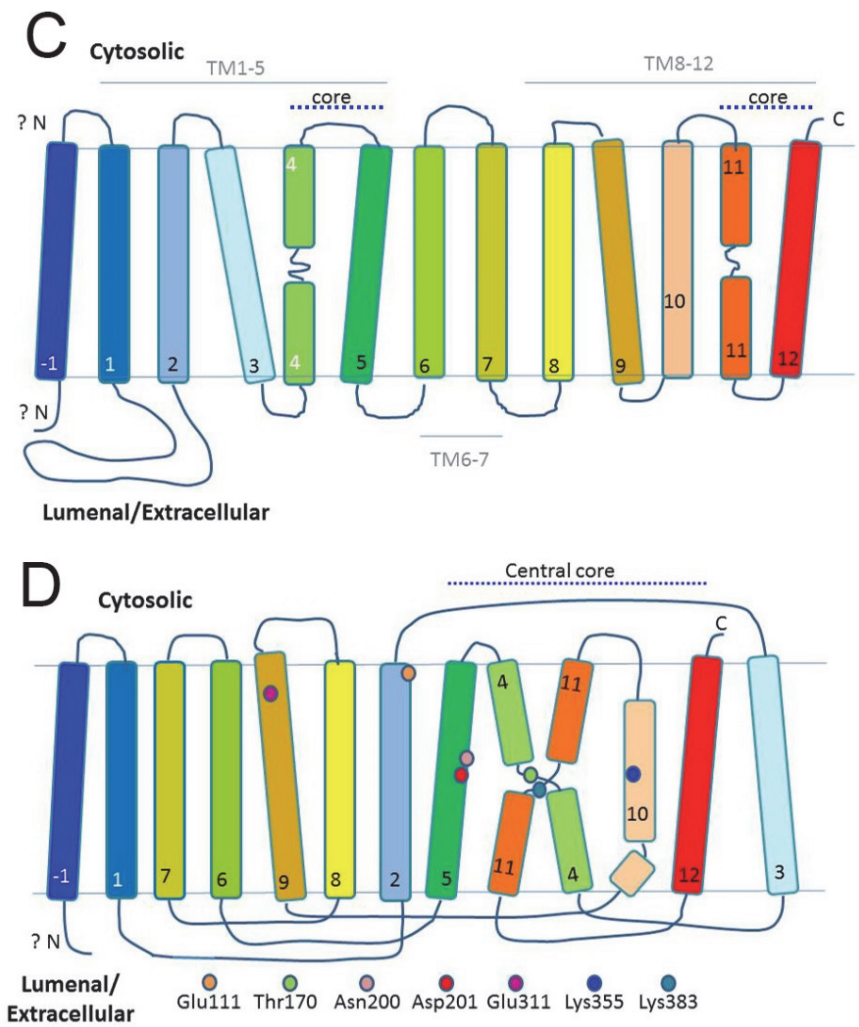

Fig. III-2. C) Unfolded AtCHX17 protein shows two inverted repeats at TM1-5 and TM8-12. Each inverted repeat contains a V-motif, an arm and half of a predicted core. The C-terminus of the TM domain is modeled to face the cytosol, though location of N terminus is uncertain. **D)** The folded protein according to the 3D models in either A or B show four helices at the core. TM 4-5 and TM11-12 are predicted to form the central transport core. Several residues (circles) were selected for site-directed mutagenesis.

D.3. 3D model-guided approach to select critical residues

Multiple protein alignments highlighted a few candidate residues that are conserved among CPA2 and CPA1 members (Fig. III-S2; Table III-1). CHX17-D201 (Asp201) in the middle of TM5 is strictly conserved as seen D164 in EcNha1 or D157 in TtNapA, D721 in AtKEA2, D279 in human NHA2 or D185 in AtNHX1 (member of the CPA1 family) (Inoue et al., 1995; Schushan et al., 2010). However, two tandem Asp (as in EcNhaA D163-D164) at this location are only seen in prokaryotes and also in HsNHA2, but not in AtCHX17 or AtNHX1, which has a 'ND' instead (Table III-1). AtKEA1 or AtKEA2 have 'QD' in the middle of TM5, thus a basic residue precedes the invariant Asp in TM5 of many CPA2 transporters. A highly conserved basic residue is located in TM10 as R353 (Arg) in AtNHX1 or R432 in HsNHA2; however, in bacteria and plant CPA2, the basic residue is a Lys. Lys355 in TM10 of AtCHX17 is conserved solely as Lys in the entire AtCHX family, which is also seen in AtKEA2 as K878 (Table III-1).

The 3D model highlighted for the first time the proximity of TM4 and TM11 to the conserved D201 in CHX17-TM (Fig. III-2) and the presence of unwound residues in the middle of the TM4 and TM11 α-helices. As the unwound regions are thought to participate in cation binding and transport in EcNhaA (Screpanti and Hunte, 2007), residues within this region in CHX17 (see Table III-1, TM11-dis) were selected for mutagenesis.

Table III-1. Selected conserved and non-conserved residues in cation/proton antiporters from prokaryotes and eukaryotes. Multiple CPA transporters were first aligned using MUSCLE to identify conserved residues with EcNhaA or TtNapA. Then the known secondary and 3D structures of EcNhaA or TtNapA were compared with the predicted secondary structure and 3D model of AtCHX17 to find residues that superimpose. This method allowed prediction of residues in the discontinuous helices of TM4 and TM11 in other CPAs. Protein residue numbers correspond to AtCHX17 (At4g23700), EcNhaA (BAB96592), SynNhaS4 (NP_440311), TtNapA (Q72IM4) (Furrer et al., 2007), AtKEA1 (At1g01790); AtKEA2 (O65272.2; At4g00630.2) (Aranda-Sicilia et al., 2012); HsNha2 (NP_849155.2) (Schushan et al., 2010), AtNHX1 (At5g27150), and PeNHX3 (ACU01854) (Wang et al., 2014). * indicates mutated residue that caused a decrease in growth or in EcNhaA activity. TM indicates transmembrane location of residue; 'dis' refers to discontinuous helix; and 'mid' denotes middle. (see Fig. III-S2 for amino acid sequence alignment.)

D. Czerny made protein alignments and built the table.

TM	AtCHX17	EcNhaA	SynNhaS4	TtNapA	ScKHA1	AtKEA1	AtKEA2	HsNHA2	AtNHX1	PeNHX3
TM2	E 111	E78	E88	E74	E104	E657	E637	G 191	Q97	Q100
TM4	I169	A131	I148	A125	V168	L709	L689	A243	A154	A158
TM4-dis	T170	T132*	T149	T126*	T169	S710	S690	V 244*	T156*	T159
TM4-dis	A171	D133*	A150	S127*	A170	S711	S691	S245*	D157	D160
TM4	F172	I134	F151	V128	F171	T712	T692	P246	S158	S161
TM5-mid	N200	D163	D179	D156	N199	Q740	Q720	D 278	N184	N187
TM5-mid	D201	D164	D180	D157	D200	D741	D721	D 279	D185	D188
TM8	H284	H225	D262	A236	H285	S831	S811	H 356	S271	S274
TM9	E311	E252	E289	E258	E312	E853	E833	E 386	T298	T301
TM10-mid	K355	K300	K333	K305	K356	K898	K878	R 432	R353	R356
TM11-dis	T382	I337*	T360	P330*	C383	P925	P905*	P459*	M389*	M392*
TM11-dis	K383	G338*	R361	R331*	K384	G926	G906*	K 460*	R390*	R393*
TM11-dis	G384		G362	G332	G385	G927	G907	A461	G391	G394

D.4. Testing CHX17 residues by expression in yeast

D.4a. Asp201 and K355 are critical for CHX17 activity

We tested WT or mutated CHX17 activity in a yeast (*S. cerevisiae*) mutant that lacks several cation exchangers and pumps. The mutant KTA40-2 lacks PM-localized Na^+-ATPases (*ena1-4Δ*), a PM-localized Na^+/H^+ exchanger (*nha1Δ*), a vacuolar Na^+/H^+ exchanger (*nhx1Δ*), and an endosomal K^+/H^+ exchanger (*kha1Δ*) and is sensitive to the drug Hygromycin B (HygB) (Maresova and Sychrova, 2005). We showed previously that CHX17 expression in KTA40-2 yeast conferred resistance to 100 µg/ml HygB (Chanroj et al., 2011). Tolerance to HygB was chosen to monitor CHX17 activity, as it is more sensitive than CHX17-dependent tolerance to alkaline pH.

The negatively-charged Asp201 located in the middle of TM5 was changed to Ala (A), Glu (E), or Asn (N). The D201A mutant abolished CHX17 activity, as yeast expressing the D201A mutation was sensitive to 150 µg/ml HygB, similar to yeast carrying an empty vector (Fig III-3A-B). In addition, yeast expressing the D201N mutant was also sensitive to increasing HygB concentrations (Fig. III-3A). However, the D201E mutant, which retains an acidic group on a longer side chain, showed activity similar to WT CHX17 (Fig. III-3A). To confirm and quantitate the results, yeast carrying D201 mutations were tested for growth in liquid culture containing 25-100 µg/ml HygB. Only mutants with the D201E mutation proliferated in culture with HygB similar to WT CHX17. However, yeast expressing the D201A mutation grew poorly (Fig. III-3B). These results show an acidic residue, Asp or Glu, at position 201 is necessary for CHX17 activity.

Fig. III-3. Residues critical for CHX17 activity in yeast.

A-B) An acidic Asp or Glu residue at position 201 is required for CHX17 activity. Panel A shows yeast growth on solid medium. Yeast strain KTA40-2 transformed with a pYES-DEST52-derived vector (EV), vector harboring WT CHX17, or D201 mutations was normalized to $A_{(600nm)}$ of 0.2. Five µl of ten-fold serial dilutions was spotted onto YNB(A) media minus uracil at pH 6.0 with 2% galactose containing 0 or 150 µg/ml HygB, and incubated 3 d at 30°C. Result is representative of 6 independent transformants. Panel B shows growth in liquid medium. Normalized yeast was grown in medium with or without HygB at 0-100 µg/ml at 30 C. Growth was monitored by OD_{600nm} for 50 h. CHX17-dependent growth at 21-30 h is shown. Result from one experiment.

C-D) Lys355 is critical for CHX17 activity and cannot be substituted by Arg. Yeast strain KTA40-2 transformed with an empty vector (EV), vector harboring WT CHX17, or a K355 point mutation was normalized to $A_{(600nm)}$ of 0.2. Yeast growth was assayed on agar plates (C) or liquid medium (D). Results on agar plates are representative of 6 independent transformants. CHX17-dependent growth at 22-32 h on liquid medium is an average of 3 independent experiments with 3 OD readings per experiment.

E-F) Novel residues in the discontinuous region of TM4 and TM11, Thr170 and Lys383, are necessary for CHX17 activity. Assays on agar plate (E) or liquid medium (F) were as described in Fig. III-3A-B. Growth on agar plates is representative of 6 independent transformants. Growth on liquid medium at 22-32 h is average of 3 independent experiments using 3 OD readings per experiment.

G) Residue E111 is not in the core. Yeast carrying an empty vector (EV), or vector with WT or mutated CHX17 was normalized to A(600) of 0.2. Ten-fold serial dilutions of each culture were spotted onto plates containing either 125 µg/ml HygB at pH 6 (left panel); or a plate containing medium at pH 7.5 without HygB (right). Plates were incubation at 30°C for 3 d. Results are representative of 4 independent transformants.

H) Conserved Cys residues in hydrophilic C-tail are not critical for AtCHX17 activity. Growth was assayed on agar plate as described in Fig. III-3A. Results are representative of 6 independent transformants.

D. Czerny performed experiments, assembled the figure, and interpreted data.

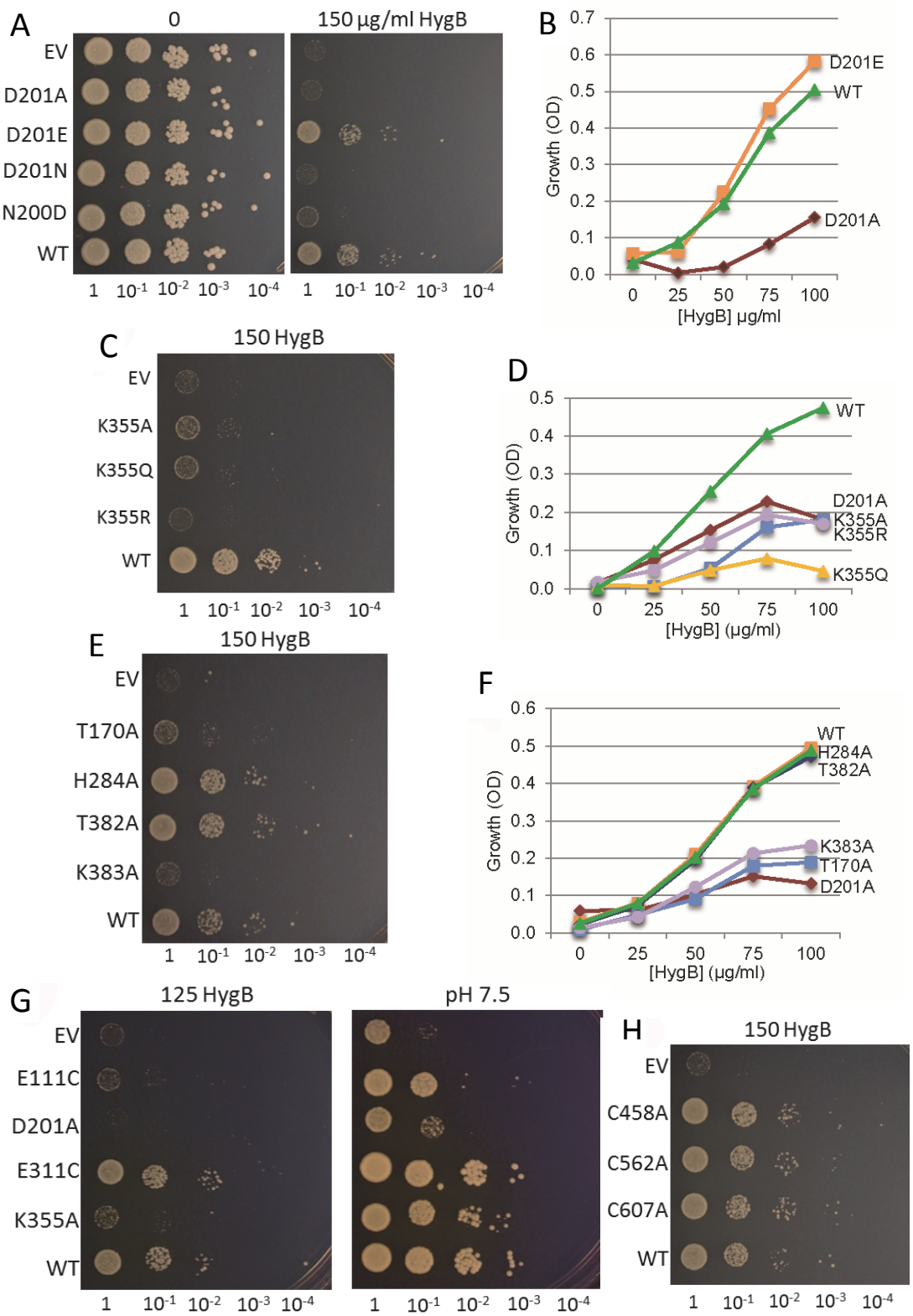
A
0
150 µg/ml HygB
EV
D201A
D201E
D201N
N200D
WT
1 10-1 10-2 10-3 10-4 1 10-1 10-2 10-3 10-4
B
Growth (OD)
[HygB] µg/ml
D201E
WT
D201A
C
150 HygB
EV
K355A
K355Q
K355R
WT
1 10-1 10-2 10-3 10-4
D
Growth (OD)
[HygB] (µg/ml)
WT
D201A
K355A
K355R
K355Q
E
150 HygB
EV
T170A
H284A
T382A
K383A
WT
1 10-1 10-2 10-3 10-4
F
Growth (OD)
[HygB] (µg/ml)
WT
H284A
T382A
K383A
T170A
D201A
G
125 HygB
pH 7.5
EV
E111C
D201A
E311C
K355A
WT
1 10-1 10-2 10-3 10-4 1 10-1 10-2 10-3 10-4
H
150 HygB
EV
C458A
C562A
C607A
WT
1 10-1 10-2 10-3 10-4

We tested if Lys355 in TM10 was critical for CHX17 activity, as a Lys in this location is conserved in EcNhaA as K300 or in TtNapA as K305. Yeast expressing CHX17 carrying K355A was sensitive to HygB. To test if other basic residues were effective, Lys355 was changed to either Gln or Arg. Gln (Q) has a polar uncharged sidechain; Arg (R) has a weak positive charge in its side chain. KTA40-2 yeast expressing either CHX17 with the K355Q or K355R mutations was sensitive to HygB (Fig. III-3C). When tested in liquid media, yeast carrying all K355 point mutations were sensitive to HygB, similar to the D201A mutation (Fig. III-3D). These results show that a strong positive charge, and not just a basic residue, is necessary at position 355 for CHX17 activity. Thus, unlike HsNHA2 or AtNHX1, an Arg residue in TM10 is insufficient for activity in AtCHX17.

D.4b. Residues in the unwound region of TM4 and TM11: Thr170 and Lys383 in CHX17 are necessary for activity.

We tested whether residues within the discontinuous α-helices of TM4 and 11 were important for activity. Thr170 within the extended chain in TM4 was mutated to Ala, and yeast expressing the T170A point mutation was sensitive to HygB (Fig. III-3E-F). In the extended chain of TM11, the T382A mutation did not affect activity, as yeast expressing T382A showed HygB tolerance similar to cells expressing wild-type CHX17. However, yeast expressing the K383A point mutation became sensitive to HygB, indicating Lys383 is critical for CHX17 function (Fig. III-3E-F). These results were confirmed in liquid culture (Fig. III-3E-F). Together, these results show residues T170 and K383 within the discontinuous TM4 and TM11 α-helices are necessary for CHX17 activity.

D.4c. Other residues: E111, H284, E311

In EcNhaA, His225 is thought to specifically function in the pH response of the transporter (Gerchman et al., 1993), and this residues is conserved in CHX17 as His284. Surprisingly, the H284A point mutation did not alter CHX17 activity, although it seemed conserved to *E. coli* His225. Expression of CHX17 carrying the H284A mutation conferred HygB tolerance similar to WT CHX17, both on solid media and in liquid culture (Fig. III-3E-F).

Interestingly, the E111C mutation caused a loss of CHX17 activity, whereas E311C had no effect (Fig. III-3G). E111 in CHX17 is homologous to E78 in EcNhaA or E74 in TtNapA (Table III-1). Mutations in E78 reduced *E. coli* growth and transport activity of In EcNhaA, the E78C mutation caused both an increase in Km for Na^+/Li^+ and an alkaline shift in pH dependence, suggesting roles for this residue in transport activity and pH regulation (Herz et al., 2010). In contrast, mutation of E74A in TtNapA had little to no effect on bacteria growth in the presence of elevated Na^+ (Furrer et al., 2007). Similarly, E252 in TM9 of EcNhaA is thought to have a role in pH regulation (Tzubery et al., 2004). However, the equivalent E311 in AtCHX17 when mutated to Ala showed no change in activity. We compared CHX17 activity monitored either as growth tolerance to HygB or to alkaline medium at pH 7.5. The HygB sensitivity of yeast mutants carrying the D201A or K355A mutations was clearly more severe relative to sensitivity to alkaline pH (Fig. III-3G).

D.4d. Role of Cys residues in the hydrophilic C-tail is unclear.

Amino acid sequence alignments showed that 3 Cys residues of the hydrophilic C-tail are highly-conserved among CHX transporters (Sze et al., 2004). To test if these

cysteines might form disulfide bonds and affect activity, individual Cys residues were mutated to Ala. In the C458A, C562A, and C607A mutations, yeast growth on HygB-containing media was similar to that of WT CHX17 (Fig. III-3H). Thus, these conserved Cys residues do not affect CHX17 activity in yeast.

D.5. CHX17 carrying D201A or K355A mutation was active when expressed in *E. coli*.

We tested the effect of mutated CHX17 in the *E. coli* mutant LB2003 that lacks three K^+ uptake mechanisms (Fig. III-4A). Wild-type CHX17 was shown to rescue LB2003 growth in the presence of minimal (2-4 mM) K^+ at pH 6.2 or higher (Chanroj et al., 2011), suggesting CHX17 facilitated K^+ transport. If so, then an inactive CHX17 should fail to rescue *E. coli* mutant growth. Surprisingly, LB2003 cells harboring CHX17 mutated at D201A, K355A, or E111C grew as well as bacteria carrying wild-type CHX17. Results were similar at pH 6.6 (Fig. III-4B) or pH 6.2 (not shown). LB2003 cells carrying an empty vector (EV) failed to proliferate. Even though WT CHX17 facilitated K^+ uptake into *E. coli*, (Chanroj et al., 2011), it is possible the pathway for K^+ transport via CHX17 at the PM of *E. coli* differs from that taken by K^+ moving in exchange for a H^+.

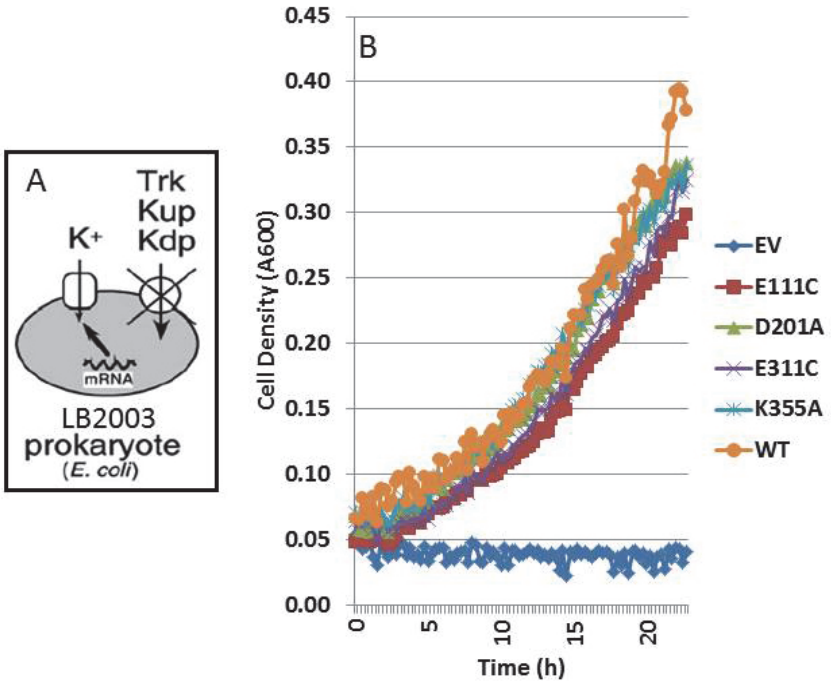

Fig. III-4. Mutations in critical residues failed to inactivate AtCHX17 expressed in *E. coli*.

A) The LB2003 *E. coli* mutant lacks 3 K^+ uptake mechanisms: Trk, Kdp, and Kup.

B) *E. coli* growth at pH 6.6. LB2003 *E. coli* cells were transformed with the pPAB404 plasmid (EV), or pD404 plasmid carrying WT or mutated CHX17. Overnight cultures were washed with K^+-free SGM (minimal) medium buffered to pH 6.6. Cells were added to buffered SGM medium with 2 mM K^+ at pH 6.6. Cultures were incubated for 22 h at 30°C in a Fluostar Optima microplate reader, and OD was taken every 15 min.

D. Czerny performed experiments, assembled the figure, and interpreted data.

D.6. Mutated CHX17 proteins are expressed in yeast. Activity of wild-type or mutated AtCHX17 is unaffected by a GFP tag at the C-tail

To detect mutated CHX17 proteins in yeast, CHX17 constructs were fused to a C-terminal GFP tag. Wild-type CHX17-GFP conferred yeast tolerance to HygB. Similarly, the D201E-GFP mutation conferred HygB tolerance similar to WT CHX17-GFP. However, yeast expressing either the D201A-GFP or D201N-GFP mutation was sensitive to HygB (Fig. III-5A). In addition, yeast expressing either the K355A, K355Q, or K355R point mutations fused to GFP were sensitive to HygB (Fig. III-5B). Yeast expressing the T170A-GFP or K383A-GFP mutations in the discontinuous α-helices was also sensitive to HygB, but yeast expressing H284A-GFP showed HygB tolerance similar to wild-type (Fig. III-5C). Thus, a GFP tag at the C-tail did not alter CHX17 activity in yeast.

D.7. CHX17-GFP proteins are intact and localized to endomembranes.

The level of CHX17-GFP expression in yeast was monitored by immunoblotting with an antibody against GFP. Total protein was extracted from a similar amount of yeast culture and an aliquot with equivalent protein was separated by SDS-PAGE. Immuno-staining with anti-GFP revealed the largest reactive band at 122 to 146 kDa in lanes containing WT CHX17 or mutated CHX17. No immunoreactive band was detected in extract from control yeast carrying the empty vector (Fig. III-5E). An average molecular mass detected by anti-GFP of approximately 130 kDa is consistent with the mass of a full-length CHX17 (89 kD) (Sze et al., 2004) plus the enhanced GFP (33 kD).

Fig. III-5. Mutated and wild-type CHX17 protein tagged with GFP are expressed in yeast. A-C) *A GFP tag had no effect on wild-type or mutated CHX17 activity in yeast.* Yeast strain KTA40-2 carrying an empty vector (EV), wild-type CHX17-GFP, or a mutated CHX17-GFP was normalized to A(600) of 0.2. Ten-fold serial dilutions of yeast were spotted onto YNB(A) media with 0 or 150 µg/ml Hygromycin B, and plates were incubated for 2 d at 30°C. Results are representative of 4 independent transformants. (A) Asp201 mutations. (B) Lys355 mutations. (C) Thr170, His284, or Lys383 mutations. **D-E)** *CHX17-GFP containing single residue changes is expressed in yeast as full-length proteins*. D) GFP fluorescence in KTA40-2 yeast cells carrying either wild-type CHX17-GFP (i), or mutated CHX17-GFP (iii-iv), but not cells harboring empty vector (ii). Cultures were aliquoted onto a multi-well microscope slide and observed by DIC (i) or by fluorescence (ii) using a Nikon E600 microscope at 100x objective lens. Blue excitation and green emission filter set. See Fig. III-S5 for images of yeast cells expressing additional mutations. E) Immunostain with anti-GFP antibody. Proteins extracted from KTA40-2 yeast were separated by SDS-PAGE and transferred. A GFP-tagged protein of approximately 130 kDa is detected from cells transformed with WT CHX17-GFP (lane 1), mutated AtCHX17-GFP (lane 2-15) but not from cell carrying empty vector (EV, lane 16).

D. Czerny prepared yeast cultures and performed experiments in panel A. S. Padmanaban performed experiments in panels B & C.

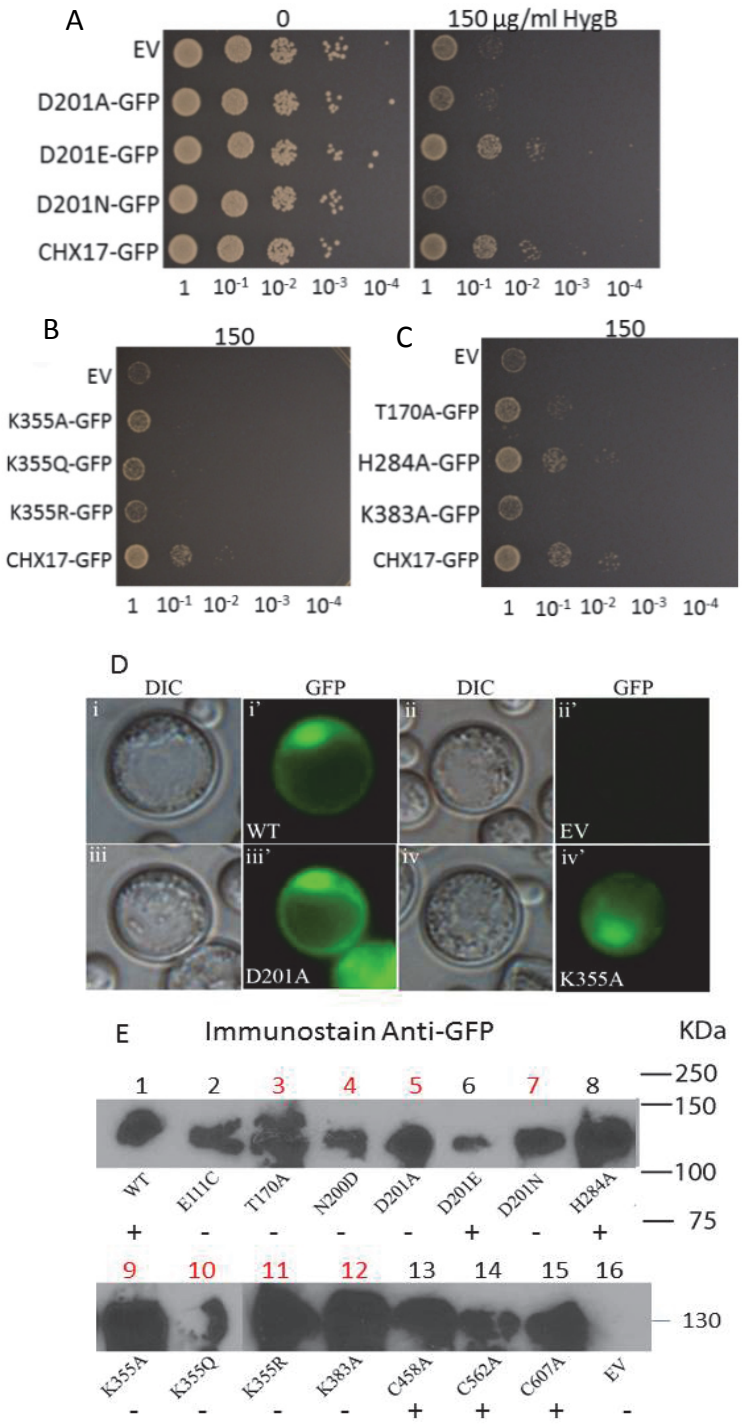
A
0
150 µg/ml HygB
EV
D201A-GFP
D201E-GFP
D201N-GFP
CHX17-GFP
1 10-1 10-2 10-3 10-4 1 10-1 10-2 10-3 10-4
B
150
EV
K355A-GFP
K355Q-GFP
K355R-GFP
CHX17-GFP
1 10-1 10-2 10-3 10-4
C
150
EV
T170A-GFP
H284A-GFP
K383A-GFP
CHX17-GFP
1 10-1 10-2 10-3 10-4
D
DIC
GFP
DIC
GFP
i
i'
WT
ii
ii'
EV
iii
iii'
D201A
iv
iv'
K355A
E
Immunostain Anti-GFP
KDa
1 2 3 4 5 6 7 8
250
150
100
75
WT
E111C
T170A
N200D
D201A
D201E
D201N
H284A
+ - - - - + - +
9 10 11 12 13 14 15 16
130
K355A
K355Q
K355R
K383A
C458A
C562A
C607A
EV
- - - - + + + -

The blot also showed varying levels of smaller mass proteins which are likely degradative products of CHX17 with GFP the tag (Fig. III-S5E). As chemiluminescence is a very sensitive detection method, the immunostain shows that a full-length protein of either WT or mutated CHX17 is expressed in yeast membranes at comparable levels. Therefore, the difference in CHX17 activity detected in yeast is not due to differential expression in protein levels.

Yeast expressing WT CHX17-GFP showed bright intracellular fluorescence and fluorescence at the cell periphery. Similar patterns of fluorescence were observed for yeast expressing CHX17-GFP carrying a point mutation. Control yeast carrying the empty vector showed no fluorescence (Fig. III-5C). Therefore, CHX17 proteins carrying point mutations are expressed in yeast and are localized to membranes similar to that seen for WT CHX17.

D.8. Modeling the hydrophilic C-tail revealed similarity to a universal stress protein (USP)-like domain.

Using Phyre2, we discovered that residues 454-792 of CHX17 shared protein fold homology with prokaryote universal stress proteins (Fig. III-S8). Although the CHX17-C tail (residues 531-820) shared only 15-16% amino acid identity with the *Pseudomonas aerogina* functionally unknown protein PA1789 (PDB 3mt0), the probability that the match between CHX17-C tail and PA1789 was high at 98.8%. Similarly, the probability of a match with an Archaebacteria USP protein (PDB 3loq) was 98.7%, though it has only 12% amino acid identity with the CHX17 C-tail. According to Kelly & Sternberg (2009), when the match has a confidence >90%, one can generally be very confident that the CHX17 C-tail adopts the overall fold shown and that the core of the protein is

modeled at high accuracy (2-4Å rmsd from the native, true structure). One model of the CHX17 C-tail shows a fan-like structure containing two tandem USP-like domains. Each USP-like domain has 5 β-strands alternating with 4 α-helices (Fig. III-6). The β5 and β5' strands associate in antiparallel orientation. This 3D model provides a first glance at the structure of the enigmatic C-tail which is associated with most, if not all, CHX members in plants (Chanroj et al., 2012).

Fig. III-6. Model 3D structure of AtCHX17 C-tail has a universal stress protein-like domain. Hydrophilic sequence from residues 431 to 820 were analyzed by Phyre2 using the normal mode.

A) 3D model of the C-tail. Each USP domain contains β1- to β5-strand alternating with α1 to α4 helices. Second USP-domain is labeled as β1'- to β5'-strand. The two domains are held together probably by H-bonding between anti-parallel β5 and β5' strands. (See Fig. III-S8)

B) Predicted secondary structure (Pred SS) of CHX17 (Query, Q seq) compared with known secondary structure (T SS) of *Pseudomonas aeruginosa* pao1 (template, T seq). Tandem USP domain of pao1 aligns with residues 454 (start of β1) -792 (end of β5') of CHX17. First USP β1- to β5-strands (blue arrow) alternate with α1 to α4 helices (green), and second USP-domain is labeled as β1'- to β5'-strand with α1' to α4' helices. Identical residues are highlighted in grey. S and T refer to bends and turns. Brown and yellow boxes denote gaps inserted for optimum alignment.

A

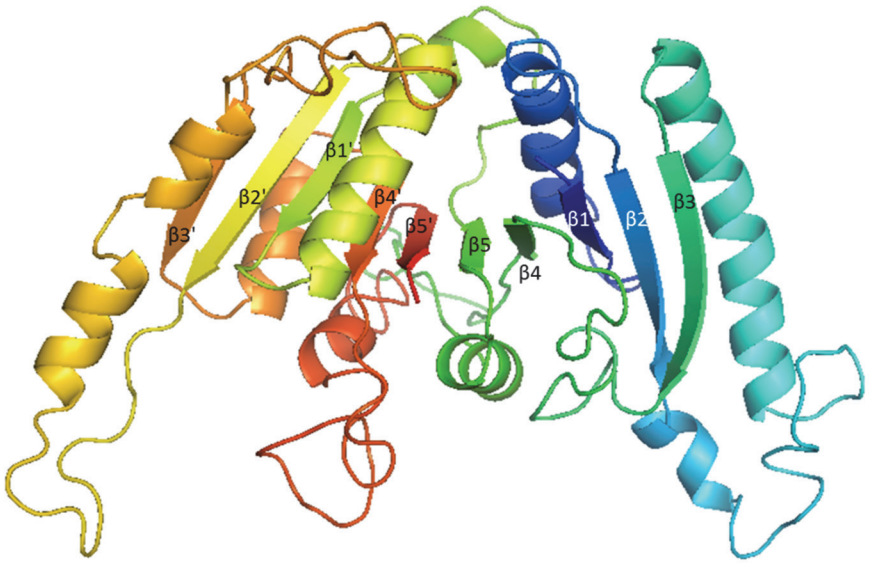
β1'
β2'
β3'
β4'
β5'
β5
β4
β1
β2
β3

B

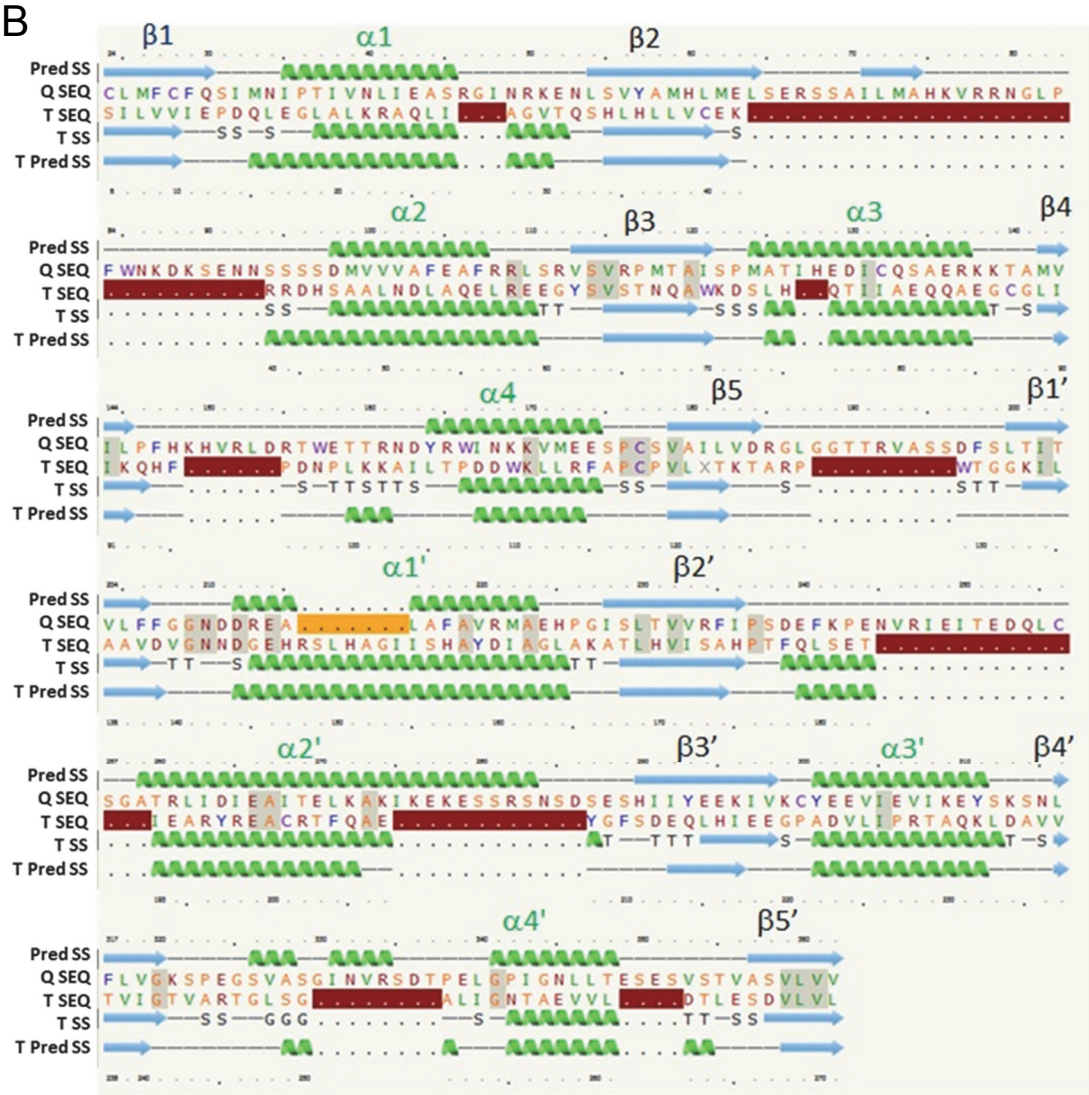
β1
α1
β2
α2
β3
α3
β4
α4
β5
β1'
α1'
β2'
α2'
β3'
α3'
β4'
α4'
β5'
Pred SS
Q SEQ
T SEQ
T SS
T Pred SS

E. DISCUSSION

E.1. Relating secondary transport to protein structure.

It is helpful to briefly review how solutes are moved by secondary active transporters. In antiport or symport, the downhill movement of one species (e.g., H^+ or K^+) provides energy for the uphill movement of another substrate (e.g., K^+ or H^+). The transport protein is hypothesized to have a centrally-located substrate binding site that is alternately accessible to the outside when it is in an outward-facing state and then accessible to the inside when it is in an inward-facing state (Boudker and Verdon, 2010; Forrest et al., 2011). The two states are caused by a rocker-switch conformation change and by the local motion of outside and inside gates. Notably, thermodynamics dictate that transport is driven by only the difference in the electrochemical gradient of the solutes on two sides of the membrane. So that in the case of antiport, the direction of ion or H^+ transport can be in either direction as it depends on the driving force. Regulatory factors, such as ligands, may also affect the gating. The model depends on a few assumptions: i) the transporter is symmetrical, so transport kinetics in the forward and reverse directions are similar; and ii) that there is a common binding site for H^+ and the cation (K^+) (Calinescu et al., 2014). Crystal structures of bacterial secondary active transporters are providing insights into their molecular mechanisms (Forrest et al., 2011). Here we have used the bacterial EcNhaA and TtNapA crystal structures to give insights on the transport mechanism of a related plant CPA2 transporter. AtCHX17 shares 26% identity to TtNapA, thus it is a representative model for studying the function and regulation of eukaryote CPA2 transporters.

E.2. Transport core at TM4-5 and TM11-12

While conserved residues between AtCHX17 and other CPA2 transporters are revealed by multiple protein alignments, the 3D model structures based on the known structures of EcNhaA or TtNapA provided additional insights to critical residues that do not align or are not conserved. In addition, crystal structures of secondary active transporters are demonstrating that the active core of proteins that transport diverse substrates share a similar architecture (Boudker and Verdon, 2010). For instance, both LeuT and EcNhaA have an inverted repeat of 5 TM spans. Transporters with a LeuT fold have a six-helix bundle, at TM1-3 and TM6-8 that form the transport machinery. TM1 and TM6 each contain an unwound region in the middle of the membrane that has roles in ligand binding and transport (Krishnamurthy et al., 2009; Boudker and Verdon, 2010). The 'NhaA' fold is distinct, as it is characterized by an inverted repeat with 5 TM spans, except the crystal structure showed a discontinuous portion in the middle of the membrane at TM4 and TM11 (Hunte et al., 2005). These two TM helices cross each other in anti-parallel fashion in the central part of the protein. TtNapA has a similar protein fold to EcNhaA (Fig. III-2A-B), as both have a four-helix bundle of TM4-5 and TM11-12. Thus, we tested if residues in these four TM helices seen in the 3D model structures of CHX17 affected its activity as assayed in yeast.

In the middle of TM5, both N200 and D201 of AtCHX17 are critical for activity. Although D201 is highly conserved in prokaryote and eukaryote CPA1 or CPA2 transporters (see Table III-1), we show that glutamate (E) can replace aspartate (D), indicating the requirement for an acidic residue with a negative charge in the neutral pH range. This was surprising, as no other CPA transporter we aligned showed glutamate

(E) at TM5, except for a few plant CHX transporters, like AtCHX13/14 and AtCHX1/2 (Sze et al., 2004; Chanroj S., unpublished).

N200 is also required for CHX17 activity, though this residue is not conserved in *E. coli* NhaA, *T. thermophilus* NapA, *Synechocystis* NhaS4, or *H. sapiens* NHA2. All the examples above possess a tandem DD, as in D163-D164 in EcNhaA, or D156-D157 in TtNapA. However, replacing N200 with a D failed to restore CHX17 activity in yeast (Fig. III-3A-B). Yeast KHA1p, and all plant (e.g. *Arabidopsis*) NHX transpoters show an asparagine residue before the conserved D, indicating that ND as in N199-D200 in ScKHA1p is common for most eukaryote CPA1 or CPA2 transporters. An ND, instead of DD, at TM5 is thought to infer an electroneutral exchanger. Mutation of the Asp residue in the middle of TM5 was shown to inactivate plant NHX1/2 as well as AtKEA2 (Aranda-Sicilia et al., 2012). Strangely, the plastid-located AtKEA2 has a Q720-D721 instead of ND in the middle of TM5. These results suggest that N or Q glutamine plays important functions, perhaps in ion translocation if not in substrate coordination.

3D models and superimposition with known templates pinpointed candidate residues in the unwound helices of AtCHX17. We established two previously unrecognized residues, T170 in TM4 and K383 in TM11, as critical for catalysis. The T170A mutation eliminated CHX17 activity in yeast, and we suggest this residue is similar to T132 in EcNhaA or T126 in TtNapA. However, the neighboring I169 and A171 in CHX17 bear no resemblance to the A131 and D133 seen in EcNhaA. Only *Synechocystis* NhaS4 and yeast KHA1 shared the same sequence (TA) as in the unwound region of TM4 in CHX17 (Table III-1, Fig. III-S2). The unwound region of TM11 is less conserved, so we tested two residues, T382 and K383. Only the K383A mutation caused

a loss in CHX17 activity, suggesting Lys is more critical than Thr. We propose a basic residue at this position is important, as it is observed in TtNapA (R331), ScKHA1p (K384), human NHA2 (K460) or AtNHX1 (R390); but not for EcNhaA or AtKEA2. Thus, we experimentally show that the critical residues or core of AtCHX17 reside in a helix bundle within TM4-5 and TM11 (Fig. III-2D).

Our results highlight several residues that contribute to the active site in the central core of AtCHX17. The active site is defined here as the single substrate-binding site which can alternate between access to the inside or the outside face of the membrane (Forrest et al., 2011). We propose that residues N200, D201, T170, and K383, and possibly K355 participate in coordinating a H^+ and/or cation (e.g. K^+), and in translocation. In 3D model structures, the side chains of N200, D201, T170 and K383 are close to one another and in some cases point to one another (Fig. III-7A-B). In particular, residues in the discontinuous helices have been shown to participate in ion recognition, binding and translocation in various cotransporters (Screpanti and Hunte, 2007). This is possible because those residues are more flexible than residues in an α-helix, and thus able to accommodate a charged substrate. The substrate is most likely coordinated by a combination of main chain atoms in the extended peptide, polar and charged side chains, and partial charge of the helix ends. The current concept is that binding of the substrate in the desolvated state ensures high selectivity based on ion charge and size (Screpanti and Hunte, 2007).

The side chain of K355 in TM10 is also close to the center, though whether it participates in substrate binding or charge compensation with the proposed core residues is debatable. A Lys residue at TM10 is strictly conserved in all 28 AtCHX members, and

Fig. III-7. **Residues in the active core of AtCHX17 and mechanism of exchanger**. A-B) Transport core. N200 and D201 in the middle of the membrane at TM5 are in close proximity to T170 and K383 in the discontinuous helices of TM4 and TM11, respectively. They may bind or coordinate the cation substrate, along with K355 at TM10. Model is based on EcNhaA (A) or TtNapA (B).

A

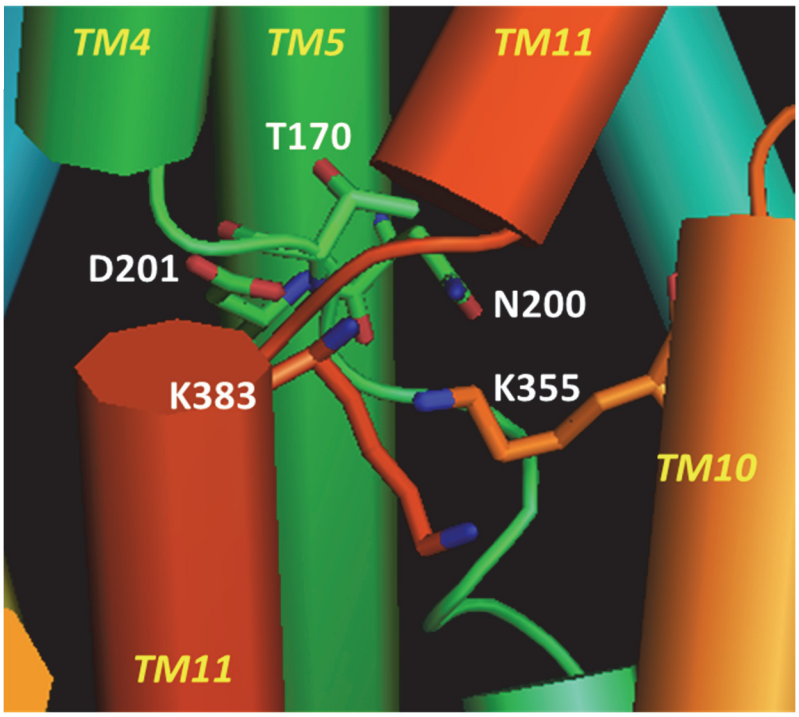
TM4
TM5
TM11
T170
D201
N200
K383
K355
TM10
TM11

B

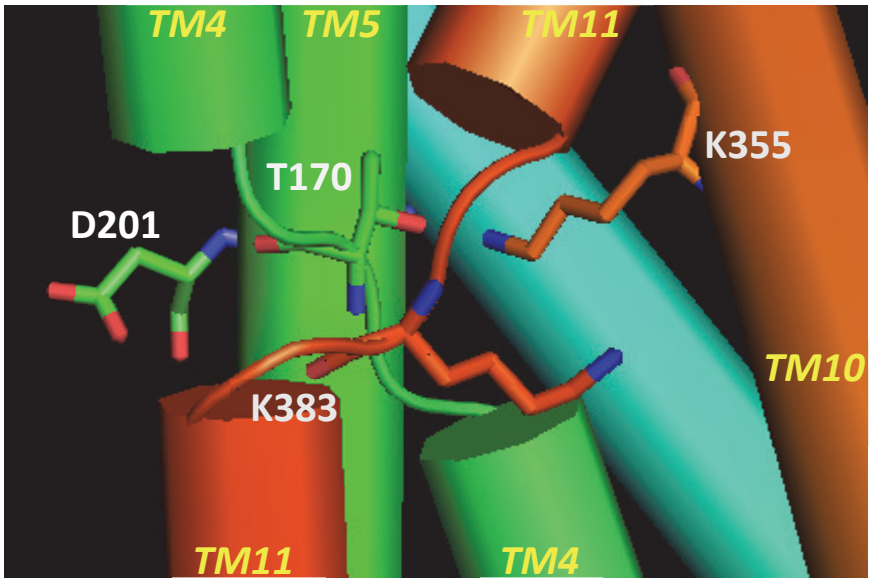
TM4
TM5
TM11
K355
T170
D201
TM10
K383
TM11
TM4

the K355A mutation reduced activity (Fig. III-3C-D). A Lys at this position is also conserved in CPA2 from prokaryote (EcNhaA, TtNapA) or eukaryote (ScKHA1p) sources.

Strangely, replacement of K355 with Arginine or Glutamine did not restore CHX17 activity, suggesting a major difference with CPA1 members, such as AtNHX1 or PeNHX3, which have Arg at R353 or R356, respectively (see Table III-1). Arg432 is found in HsNHA2, though it could be replaced functionally by glutamine and partially by Lysine (Schushan et al., 2010). K300 in TM10 of EcNhaA is thought to form a salt bridge with D163 and is also important in pH regulation. (Lee et al., 2013; Lee et al., 2014; Padan, 2014).

E.3. Distinctions between CPA2 versus CPA1: a pH sensor?

Several residues that are conserved in CHX17, EcNhaA, or TtNapA are not found in AtNHX1 or PeNHX3 (Wang et al., 2014). E311 from CHX17 appeared to be conserved in all CPA2 transporters in Table III-1, such as EcNhaA, TtNapA, ScKHA1p, and HsNHA2, but a homologous glutamate is not found in plant AtNHX1. However the E311C mutation at TM9 of CHX17 had no inhibitory effect on yeast growth, suggesting E308 might be a candidate. Similarly, a mutation of H284A in the loop between TM7/8 had no effect. H284 in CHX17 is conserved in EcNhaA (H225) and ScKHA1p (H285) but not in most other CPA2, thus the function of this residue has clearly evolved. Intriguingly, the E111C mutation nearly eliminated CHX17 activity in yeast (Fig. III-3G). E111 is conserved in all the CPA2 members, but not in HsNHA2 and AtNHX1, which suggests a conserved role of this residue in this family. E111 is located near the cytosolic side of TM2, which forms part of the funnel leading to the active site in the

middle of the membrane (Fig. III-8A). According to the 3D model, TM2 is part of a funnel that provides cytosolic access to the active core (Fig. III-8A) (Hunte et al., 2005). An E78C mutation in EcNhaA reduced its activity by increasing the Km for Na^+ ten-fold and shifting Na^+ transport to a more alkaline pH than in wild-type (Herz et al., 2010). As E78 and E252 in EcNhaA are quite far from the active transport site, the decrease in transport activity is interpreted to infer an allosteric regulatory mechanism involving pH-induced conformational changes (Herz et al., 2010). Thus E78 in EcNhaA is thought to be part of the 'pH sensor'. So far, only the E111C mutation caused a significant decrease in plant CHX17 activity, and this residue in the 3D model superimposes on E78 of EcNhaA (not shown), suggesting E111 could serve as a pH sensor for CHX17. These and other distinctions provide the first structural clues for functional differences, such as cation selectivity and pH regulation, between CPA1 and CPA2 members.

E.4. Two conformational states of CHX.

The crystal structures of TtNapA and EcNhaA provide two snapshot models of the potential CHX17 structure. TtNapA was crystallized at pH 7.8 when the transporter is active; EcNhaA was crystallized at pH4 when the transporter is inactive. We suggest that these two models reflect two conformational states as CHX17 alternates between facing the cytosol (Fig. III-8A) or the outside (Fig. III-8B). In Fig. III-8A, the dotted triangle shows a funnel formed by TM2, 4, 5 and 9 open to the cytosol. In this conformation, a cytosolic ion is accessible to the central core. This model also shows that E111 and E308 line the funnel, so that changes in pH could alter conformation, and thus activity. In contrast, the model in Fig. III-8B shows the cytosolic funnel is nearly closed, and the dashed triangle shows a funnel open to the outside. The helix bundle

Fig. III-8. Two conformational states of CHX17 that allow alternating access of the cation binding site to both sides of the membrane.

A-B) Proposed model of exchanger based on inactive state of EcNhaA (A) and active state of TtNapA (B). In (A), the active core is accessible via the cytoplasmic funnel formed by TM2, 4, 5 and 9 (dotted triangle). In (B), a slight pivot of the TM4-11 assembly makes the active core accessible to the outside via another funnel formed by TM2, 8, and 11 (dashed triangle). E111 at rim of the cytoplasmic funnel is distant from the predicted transport core.

A

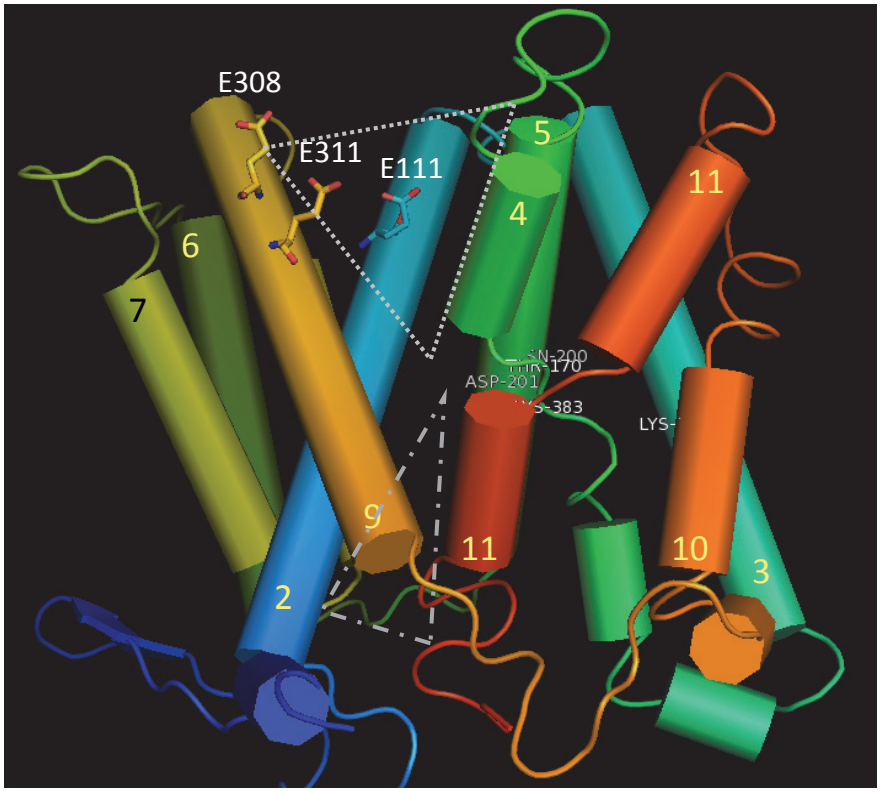
E308
E311
E111
5
4
11
6
7
ASP-201
9
11
10
3
2

B

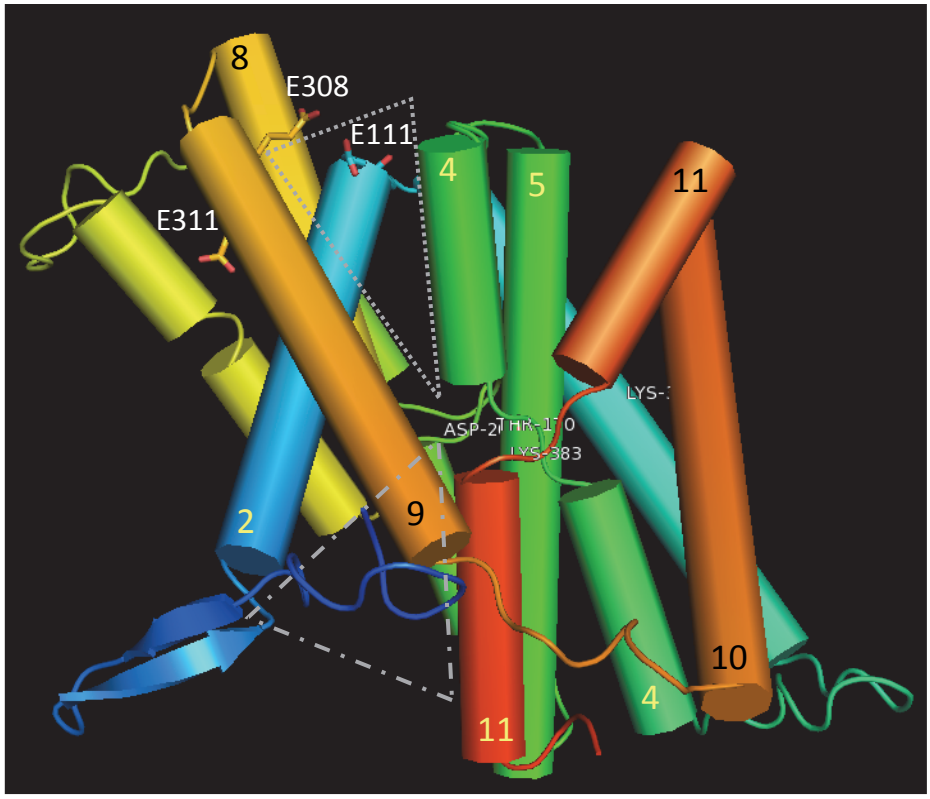
8
E308
E111
4
5
11
E311
LYS-383
2
9
10
4
11

including TM4, 5, 11 has pivoted so that core residues are accessible to the outside. The inverted funnel is lined by TM 2, 8, and 11 (Fig. III-8A). In this conformation, a cation could be released from the core to the outside and the core residues would bind the cotransported cation or H^+ substrate.

A simple model of a transport cycle is illustrated (Fig. III-9). When CHX17 is in an inactive form, salt bridges are likely formed between K355 and an acidic residue such as D201. In the inward-open conformation, the H^+ dissociates and residues, such as D201, bind a K^+. In the outward open confirmation, the core residues D201 or a Lys (383 or 355) is protonated by H^+ from the outside, leading to a conformational change. A switch in conformation will cause release of one K^+ and gain of one H^+. The net effect is loss of cytosolic K^+ and acidification of cytosol. AtCHX17 confers alkaline pH tolerance in yeast, suggesting it has a role in acidifying cytosolic pH under alkaline stress (Chanroj et al., 2011). In contrast, AtNHX1 is active at acidic pH, suggesting its activity helps alkalinize the cytosol when the cell is under acidic pH stress. Alternatively, as these cation/H^+ antiporters are reversible, they can also use pH gradients to mediate cation homeostasis.

E.5. USP-like domain at the C-tail: a regulatory domain?

The C-tail was hypothesized to have a regulatory role (Sze et al., 2004). However, when the C-tail is truncated, CHX17 activity is retained when expressed in yeast (Chanroj et al., 2013). In plant cells, truncated CHX17(1-472) -GFP localized to compartments like ER or large puncta, instead of PVC or PM, suggesting the C-tail has a role in membrane trafficking. The lack of effect on activity from Cys mutations in the C-tail is consistent with the idea that the C-tail has little to no direct effect on

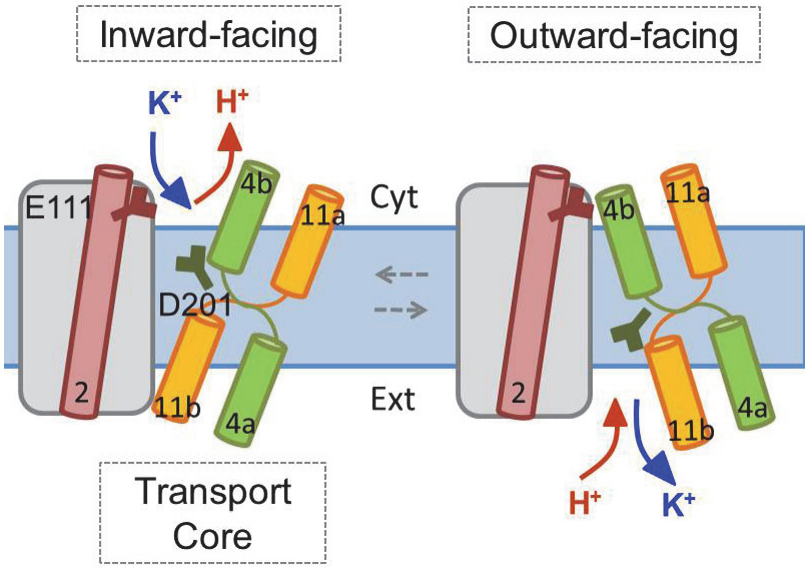

Fig. III-9. The predicted transport cycle of CHX17. In a model of electroneutral K^+/H^+ exchange, D201 within the transport core alternates binding a K^+ and a H^+. When CHX17 is facing the cytosol (Cyt), the H^+ will dissociate from D201, and a K^+ ion will bind in its place. Upon K^+ binding, conformational changes in CHX17 will occlude the cation-binding site from the cytosol. The transporter will go through an intermediate state where the cation binding site is inaccessible from both sides of the membrane before re-opening to the opposite side of the membrane. Upon opening to the external (Ext) face (outside or lumen of a compartment), the K^+ will dissociate from D201 and be replaced by H^+. The transporter will then cycle through another occluded intermediate state before opening to the cytosol. E111 is located on the cytosolic face of CHX17 and could function as a "pH sensor" by regulating transport in response to fluctuations in cytosolic pH.

D. Czerny constructed the figure.

CHX17 activity (Table III-2 summary). Here we provide modeling evidence that the mysterious hydrophilic tail in plant CHX proteins resembles a USP-like domain. Since their initial discovery in *E. coli*, genes encoding USP or USP-like domains have appeared in organisms such as archaebacteria, cyanobacteria, and plants. In *E. coli*, stand-alone USP proteins are induced in response to a wide range of stress cues, though their specific functions are unclear (Kvint et al., 2003). USP-like domains are often fused to another protein, as in some plant protein kinases (Kerk et al., 2003) and in CHX17 as well as related CHX family members of all plants (Chanroj et al., 2012). As one USP protein can interact with another to form dimers or tetramers (Schweikhard et al., 2010), it is tempting to propose that the C-tail of CHX transporters may interact with other USP-containing proteins. If so, such interactions could modulate ion or pH homeostasis and membrane trafficking to possibly enhance the ability of plants to withstand harsh environmental changes, like desiccation, heat, or anoxia.

Table III-2. Summary of residues critical for AtCHX17 activity.

Residues test by point mutations are shown with their transmembrane location. Growth on solid media containing 125-150 µg/ml HygB is expressed as three plus signs (+++) for wild-type CHX17 and half a plus for vector only. Growth is quantitated as the number of serial dilution spots, so partial growth per spot is given 0.5 and full growth is 3. Results were recorded after 3 days at 30°C. For growth on liquid culture containing 100 µg/ml HygB, the average OD of three time points at log and late log phases of growth is given. Protein expression assayed by immunostain with anti-GFP is given as 'yes' or ND (not determined).

D. Czerny constructed the table.

	AA change	Location	Relative Growth	Growth quantity	Cell density (Liquid)	Protein-GFP
Vec			.5	0.5	0	none
CHX17-Wt	none		+ + +	3	0.48	yes
chx17 mut						
TM	E111C	TM2-c end	.5	0.5		yes
	T170A	TM4-dis	+.5	1	0.192	yes
	N200D	TM5-mid	+.5	1		yes
	D201A	TM5-mid	+	0.5	0.164	yes
	D201E	TM5-mid	+ + +	3	0.58	yes
	D201N	TM5-mid	+.5	1		yes
	H284A	TM8	+ + +	3	0.45	yes
	E311C	TM9	+ + +	3		ND
	K355A	TM10-mid	+.5	1	0.18	yes
	K355Q	TM10	+.5	1	0.05	yes
	K355R	TM10	.5	0.5	0.17	yes
	T382A	TM11-dis	+ + +	3	0.47	ND
	K383A	TM11-dis	.5	0.5	0.239	yes
Cytosolic	C458A	C-tail	+ + +	3		yes
	C562A	C-tail	+ + +	3		yes
	C607A	C-tail	+ + +	3		yes

F. CONCLUSION

Using 3D model-guided mutagenesis, we have identified critical residues located in the central core of a representative plant CPA2 transporter. The results support the model that AtCHX17 resembles a cation/H^+ exchanger. Some differences in the core residues could reflect an alkali-cation selectivity for K^+ by CHX17 rather than for Na^+ as seen in AtNHX1. Acidic residues near the edge of a cytoplasmic funnel distant from the central core suggest CHX17 could sense and respond to pH. The C-terminal hydrophilic tail, which has an unknown function, was identified by 3D modeling as a tandem universal stress protein-like domain. This finding highlights the potential role of many plant CPA2 transporters in signaling as plants tolerate and adapt to harsh environmental fluctuations.

Chapter IV: CONCLUSIONS AND FUTURE DIRECTIONS

A. CONCLUSIONS

The significant findings from this research are i) that *A. thaliana* CHX17 behaves as a K^+/H^+ exchanger when expressed in yeast and ii) that *CHX17*, *18*, and *19* have roles in male and female fertility and seed development. How might cation/H^+ exchangers affect reproduction? I suggest that CHX transporters 17, 18, and 19 maintain pH and K^+ homeostasis among subcellular compartments in the male and female gametophytes, which is necessary for successful reproduction in *Arabidopsis*. We have focused especially on male gametophyte function. These results show additional roles for CHX transporters in male gametophyte function and, for the first time, show evidence supporting a transport cycle of CHX17 consistent with a K^+/H^+ exchanger.

A novel finding from this study is CHX17 potentially functions as a K^+/H^+ exchanger when expressed in yeast. Using CHX17-TM model structures built from the crystal structures of the EcNhaA and TtNapA bacterial Na^+/H^+ exchangers, the organization of CHX17-TM was determined using the Phyre2 program. Phyre2 predicted both homology models with 100% confidence, which indicates a 100% probability that CHX17-TM adopts the conformation predicted separately in each model structure (Kelley and Sternberg, 2009). CHX17-TM has 12 predicted TM spans organized into 2 inverted repeat domains of 5 TM spans each. TM spans 4, 5, 11, and 12 form the predicted transport core. TM spans 4 and 11 are discontinuous α-helices containing unwound peptide chains in the center of the membrane. Both discontinuous α-helices and inverted repeat domains are characteristic of ion transporters (Screpanti and Hunte, 2007; Boudker and Verdon, 2010). In CHX17-TM, the two unwound peptide chains

intersect in the middle of the membrane, which is found in the crystal structures of transporters classified as similar to EcNhaA (Boudker and Verdon, 2010).

Using amino acid multiple sequence alignments, amino acids conserved among CHX17 and other cation/H^+ exchangers were identified, and these conserved residues were located within the homology models. Mutation of conserved charged residues within the predicted transport core showed an acidic residue (Asp or Glu) at position 201 and a basic Lys at position 355 were necessary for CHX17 function. These results are in agreement with mutagenesis of EcNhaA and TtNapA (Kozachkov et al., 2007; Lee et al., 2013). Residues in the discontinuous α-helices of CHX17 were also tested by site-directed mutagenesis, since TM spans 4 and 11 are suggested to be essential for transport activity. Thr170 in the unwound region of TM4, which is conserved in EcNhaA and TtNapA, was required for function, as yeast expressing the T170A mutation were sensitive to HygB. In the unwound region of TM11, Lys383 was also necessary for CHX17 function. Intriguingly, Lys383 is not conserved among cation/H^+ transporters, and this result suggests novel aspects of CHX17 transport. The predicted homologous EcNhaA residue for Lys383 is Gly338, which has roles in both pH response and cation transport (Rimon et al., 1998). Combining the structural information from the CHX17 homology models with the mutagenesis results, CHX17 can be postulated to function as a K^+/H^+ exchanger when expressed in yeast.

Previously, expression of *CHX17* in a cation transport-deficient yeast mutant showed CHX17 could confer tolerance to alkaline pH (Chanroj et al., 2011). Consistent with a pH-dependent activity, mutation of Glu111 abolished yeast tolerance to HygB and reduced tolerance to pH 7.5. Glu111 is homologous to Glu78 in EcNhaA and Glu74 in

TtNapA. Mutation of Glu78 in EcNhaA caused an alkaline shift in pH response (Herz et al., 2010). Since Glu78 is located at the cytoplasmic surface of EcNhaA away from the transport core, a possible role for Glu78 is as part of a pH sensor that triggers conformational changes to activate or repress EcNhaA transport activity. However, mutation of Glu74 in TtNapA did not perturb function, as tested by *E. coli* growth in the presence of elevated NaCl or LiCl (Furrer et al., 2007). Taken together, Glu111 in CHX17 could function as a pH sensor by potentially altering CHX17 activity in response to fluctuations in cytosolic pH. However, an unanswered question was "What are the physiological implications of K^+/H^+ exchange mediated by CHX transporters?"

Previously, *chx17/18/19* plants showed a 56-77% reduction in seed set relative to WT, but the biological basis for this phenotype was unknown (Chanroj et al., 2013). From a detailed analysis of *CHX17* using a *pCHX17::YFP* construct, *CHX17* was expressed in developing seeds, stipules, and mature roots (Chanroj et al., 2013). *CHX17* is expressed at a low level in PTs germinated *in vitro* or semi-*in vivo* (see: pollen.umd.edu) (Qin et al., 2009). *CHX18* and *CHX19* are expressed in the male gametophyte (Borges et al., 2008; Qin et al., 2009). *CHX17* and *CHX18* are also highly expressed in both the central cell of the female gametophyte (Schmid et al., 2012) and the developing seed (Le et al., 2010). Thus, the roles for these *CHX* genes were tested in both gametophytes.

Using reciprocal crossing, we observed a severe transmission defect in *chx17/18/19* pollen relative to *chx* double mutant pollen, which indicated *CHX17*, *18*, and *19* share an overlapping role in the male gametophyte. We focused on possible causes for the male defect. Pollen germination *in vitro* showed *chx17/18/19* pollen had reduced

germination percentage and PT length, which suggested possible defects in mutant pollen grains. When *in vivo* PT growth was assayed by Aniline Blue staining, the *in vitro* results were confirmed by observing fewer *chx17/18/19* pollen tubes in a pistil relative to WT. In addition, the *chx17/18/19* PTs appeared to grow slower than WT, which implicates *CHX17*, *18*, and *19* in PT growth.

A transmission defect was also observed in *chx17/18/19* embryo sacs, suggesting additional roles for these genes in the female gametophyte. *CHX17*, *18*, and *19* could function in the endosperm to mediate pH and K^+ homeostasis necessary for vesicle trafficking of nutrients to nourish the developing embryo. Without nourishment from the endosperm, embryo development could arrest or be delayed relative to WT. In self-fertilized *chx17/18/19* seed pods, embryos arrested at the globular stage and embryos showing delayed development relative to WT are both observed. This suggests the maternal contribution from these three *CHX* genes could be in the developing seed.

chx17/18/19 pollen shows reduced germination relative to WT, which could be explained by defects in pollen grain hydration. When a pollen grain lands on a receptive stigma, the grain becomes hydrated before extending a tube (Edlund et al., 2004). The influx of water into the pollen grain is likely mediated by the aquaporins TIP1;3 and TIP5;1 on the pollen grain PM (Soto et al., 2008). Water influx would stimulate cation and anion transport to balance the movement of water. *chx17/18/19* mutants could be defective in K^+ uptake into the pollen grain, which could inhibit tube extension.

Pollen tube extension is a dynamic process requiring communication between the pollen tube and the female tissues (Beale and Johnson, 2013). Vesicle trafficking and exocytosis guide PT growth to the ovule (Qin and Yang, 2011). From heterologous

expression in yeast, *CHX17*, *18*, and *19* were postulated to have roles in K^+ and pH homeostasis in endomembrane compartments (Chanroj et al., 2011). In the pollen tube, these genes likely would have similar roles. Luminal pH and cation homeostasis would be necessary for vesicle trafficking to the PT tip to deliver proteins and cell wall materials necessary for PT extension. Two proteins delivered by vesicle trafficking to the tube tip are the *ANXUR1/2* receptor-like kinases, which have postulated roles in maintaining PT cell wall integrity. *anx1/2* mutant PTs burst randomly upon emergence of the PT tip from the grain (Boisson-Dernier et al., 2009; Boisson-Dernier et al., 2013). If vesicle trafficking is partially or completely disrupted in *chx17/18/19* pollen grains, then PT extension could be slowed or completely blocked.

In pistils pollinated with *chx17/18/19* grains, approximately half of the ovules receiving a mutant PT do not develop into seeds. *chx17/18/19* PTs could have defects in tip burst, which is necessary to release sperm cells for double fertilization. In addition, perturbed gamete fusion could also lead to the observed reduced seed set in *chx17/18/19* plants. *In vitro*, *Arabidopsis* sperm cells redistribute the fusogen HAP2(GCS1) from endomembranes to the PM in response to perceiving small synthetic peptides from the egg cell-secreted EC1 proteins (Sprunck et al., 2012). The membrane protein GEX2 was recently shown to play a role in *Arabidopsis* gamete adhesion, and this protein could be moved to the sperm PM similarly to HAP2(GCS1) (Mori et al., 2014). Since *CHX17*, *18*, and *19* have potential roles in secretion and endocytosis, *chx17/18/19* sperm could be defective in HAP2(GCS1) trafficking, which would inhibit sperm cell fusion with the egg and/or central cells. In conclusion, the *Arabidopsis* transporters *CHX17*, *18*, and *19* have roles in maintaining pH and K^+ homeostasis in the pollen tube and the developing seed,

which are necessary for successful reproduction. These roles could involve vesicle trafficking both in the PT for directional tip growth and in the developing seed for trafficking nutrients from the endosperm.

B. FUTURE DIRECTIONS

This research shows the K^+/H^+ exchanger *CHX17* and the highly-related *CHX18* and *CHX19* function in reproduction and seed development, predominantly in the male gametophyte. Previously, the only known role for CHX transporters in pollen was the role of *CHX21/23* in directing PT growth out of the transmitting tract towards ovules (Lu et al., 2011). Analysis of *chx17/18/19* mutant plants has potentially indicated CHX transporters are required at multiple stages of PT growth. This work also provides preliminary data to support roles for *CHX17*, *18*, and *19* in embryo development. Additionally, model structure-guided mutagenesis of CHX17 produced evidence for the mode of transport. In yeast, six CHX17 residues were shown to be necessary for transporter activity. The mutagenesis results show CHX17 behaves as a K^+/H^+ exchanger when expressed in yeast. A model structure of the CHX17 C-tail identified a tandem USP-like domain, which suggests CHX17 could be regulated by stresses that perturb cellular pH homeostasis.

B.1. Do mutant *chx17/18/19* sperm cells respond to secreted EC1 peptides from the egg cell?

Hypothesis: *chx17/18/19* sperm cells could be defective in sperm cell activation, sperm cell adhesion, or gamete fusion, which could lead to reduced seed set.

CHX18 is highly-expressed in *Arabidopsis* sperm (Borges et al., 2008), and CHX18 localizes to the PM and PVC in transgenic plants (Chanroj et al., 2013). From Aniline Blue staining of *in vivo* PT growth, *chx17/18/19* pollen tubes target and enter ovules that do not develop into seeds, which suggests defects after the pollen tube arrives at the micropyle.

Previously, from *in vitro* experiments, *Arabidopsis* sperm cells move the fusogen HAP2(GCS1) from endomembranes to the PM upon perception of peptides derived from the small secreted egg cell EC1 proteins, which is termed sperm cell activation (Sprunck et al., 2012). Additionally, the gamete attachment protein GEX2 could be trafficked to the sperm cell PM, as with HAP2(GCS1), in order for sperm cells to adhere to the female gametes (Mori et al., 2014). Since CHX transporters are hypothesized to have roles in endomembrane pH and K^+ homeostasis and *CHX18* is highly-expressed in sperm cells, *chx17/18/19* sperm cells could be defective in moving either HAP2(GCS1), GEX2, or both to the plasma membrane.

This hypothesis can be tested by crossing a transgenic plant line expressing a HAP2 or GEX2 fluorescent protein fusion into the *chx17/18/19* mutant. The mutant sperm cells expressing the fluorescent protein fusion can be exposed to synthetic EC1 peptides *in vitro* and any potential redistribution of fluorescent signal can be observed by microscopy as tested by Sprunck and coworkers (Sprunck et al., 2012). If the fluorescent signal cannot be redistributed to the PM as in WT sperm cells, then reduced seed set in *chx17/18/19* plants would be caused by failure of mutant sperm cells to respond to female gametophyte signals to become activated, to adhere to the female gametes, or to undergo membrane fusion.

B.2. What is the 3D structure of CHX17-TM (residues 1-440)? Could additional site-directed mutagenesis of CHX17 provide new information on pH regulation or structural rearrangements during the transport cycle?

Hypotheses: The solved CHX17-TM crystal structure will provide additional information on previously-tested residues as well as identify additional novel or conserved residues necessary for CHX17 activity. Mutagenesis of additional residues adjacent to the discontinuous α-helices or on the cytoplasmic surface of CHX17 will provide further evidence for the transporter functioning as a pH-regulated K^+/H^+ exchanger.

Solving the CHX17-TM crystal structure will provide definitive evidence that CHX17 functions as a K^+/H^+ exchanger. A CHX17-TM fluorescent fusion protein can be expressed in *E. coli* and purified for crystallization using available protocols (Hu et al., 2011; Lee et al., 2013). A CHX17-TM crystal structure is necessary to know the locations and, by extension, potential functions of residues tested by site-directed mutagenesis. Relative to the homology models, any changes in orientation of residues within the TM spans would shift their sidechains to different locations, which would change their potential roles. The CHX17-TM crystal structure can refine the boundaries of both the TM spans and the discontinuous α-helices in TM spans 4 and 11. When the EcNhaA dimer was crystallized, an updated annotation of the monomer crystal structure led to the identification of a salt bridge between Asp163 and Lys300, which was not observed in the 2005 monomeric crystal structure (Lee et al., 2014). Additional residues found within the discontinuous α-helices, adjacent to the transport core, or on the cytoplasmic surface of CHX17 would be candidates to test by site-directed mutagenesis.

In the TM4 discontinuous α-helix in CHX17, Ala171 is not conserved in either EcNhaA (Asp133) or TtNapA (Ser127). The mutations A171D or A171S can be tested to determine if the role of TM4 α-helix in CHX17 transport is similar to EcNhaA, TtNapA, both, or neither. If both CHX17 mutations retain the ability to confer HygB tolerance in yeast, then Ala171 is not crucial for CHX17 activity. The carbonyl oxygen in the main chain from the Ala residue could be involved in coordinating K^+ or H^+. If either A171D or A171S can confer tolerance to HygB, then the CHX17 transport mechanism could be similar to EcNhaA or TtNapA. This result would suggest which homology model more closely resembles the native CHX17 protein structure.

In Chapter 3, Lys355 was shown to be necessary for CHX17 activity. Is a Lys at position 383 also required within the TM11 discontinuous α-helix? The K383R mutation could test the requirement for the strong positive charge on the Lys sidechain in the discontinuous α-helix. In EcNhaA, Lys300 forms a salt bridge with Asp163 (Lee et al., 2014). In CHX17, Asn200 replaces Asp163, which suggests the K383R mutation could retain activity in yeast. A polar Asn residue lacks the strong negative charge of an Asp residue, so a strong positive charge on a potential partner residue would not be required.

Glu387 in TM11 can be changed to Ala to test the role of the negatively-charged sidechain. Theoretical analysis of the CHX17 transport mechanism suggests the Glu387 sidechain could face the discontinuous α-helices, which would implicate Glu387 in cation transport. Glu387 in CHX17 could be homologous to Glu333 in TtNapA, which was shown to have a role in Na^+ transport (Lee et al., 2013). If Glu387 is necessary for CHX17 activity, then CHX17 could function more similarly to TtNapA then EcNhaA.

Previously, the E311C mutation did not perturb CHX17 activity in yeast, so the role of the neighboring Glu308 can be tested. Glu308 could be homologous to Glu252 in EcNhaA, which functions in both in Na^+ transport and pH response (Tzubery et al., 2004). As Glu308 is also on the cytoplasmic surface of the transporter, this experiment could provide additional evidence for a "pH sensor" domain in CHX17.

B.3. What are functions of the CHX17 hydrophilic C-tail? Does the CHX17 C-tail interact with other proteins that have potential roles in stress tolerance?

Hypothesis: Potential roles for the CHX17 C-tail include regulatory, targeting, or ligand/protein interaction functions. One idea is that CHX17 activity is controlled by the hydrophilic C-tail in response to stress conditions.

A model structure of the CHX17 hydrophilic C-tail showed homology to bacterial USPs. This suggests CHX17 could be regulated by abiotic or biotic stresses. A preliminary test for USP activity would be an ATP binding assay. USP proteins are classified into 2 subfamilies by their ability to bind ATP, and USP domains residing within a larger protein nearly always belong to the ATP-binding USP subfamily (Kvint et al., 2003). The modeling results and ATP binding data would provide preliminary evidence for USP-like function in the CHX17 C-tail.

In addition, the functions of *CHX17* and bacterial predicted cation transporters annotated with USP-like domains can be tested by heterologous expression in yeast or *E.coli*. Examples of predicted bacterial genes include a putative K^+ transporter from *Myxococcus xanthus* (NCBI RefSeq: WP_011550405), a cation transporter from

Stigmatella aurantiaca (GenBank: ADO68942.1), and a CPA2 subfamily transporter from *Leptospira yanagawae* (NCBI RefSeq: WP_015676677). The cDNA sequences for these predicted transporters can be cloned into a cation transport-defective yeast mutant. Yeast expressing these transporters can be tested for resistance to alkaline pH and HygB, similar to CHX17. If the bacterial transporters confer tolerance to the restrictive conditions similarly to CHX17, then this provides evidence that bacterial CPA2 transporters have activities similar to *Arabidopsis* CHX17. In the plant, fluorescence intensity from a *pCHX17::YFP* reporter was tested under ionic and osmotic stress conditions, and increased fluorescence signifying upregulation of the promoter was only detected under limiting K^+ (0.5 mM) conditions (Chanroj et al., 2013). In the future, plants carrying the *pCHX17::YFP* reporter can be tested under additional stress conditions such as drought and pathogen attack. An increase in CHX17 promoter activity under a tested stress would show which condition(s) activate CHX17 for stress tolerance.

Another hypothesis for the USP-related function of the CHX17 C-tail is possible involvement in protein-protein interactions with other proteins containing USP domains. Bacterial proteins with USP domains can form oligomers (Heermann et al., 2009; Schweikhard et al., 2010), so predicted *Arabidopsis* USP proteins could interact to mediate how plants respond to stresses. This hypothesis can be tested by a yeast-2-hybrid screen of an *Arabidopsis* cDNA library with the CHX17 C-tail as bait.

Chapter V. APPENDICES

LIST OF APPENDIX TABLES

Supplemental Tables for Chapter II

Table II-S1	Single T-DNA insertion mutants used in this study.	160
Table II-S2	Multiple *chx* T-DNA insertion mutants analyzed for seed set.	160
Table II-S3	Multiple T-DNA insertion mutants used for segregation analysis.	161
Table II-S4	Gene-specific primers and T-DNA border primers used for genotyping plants.	161

Supplemental Tables for Chapter III

Table III-S1	Primers for site-directed mutagenesis of AtCHX17.	172
Table III-S2	Construction of GFP-tagged CHX17.	176
Table III-S3	Primers for truncating the C-tails of CHX17 and CHX20.	177
Table III-S4	Primers for making pD404 *E. coli* expression vector and verifying the presence of recombined DNA sequences in pD404.	178
Table III-S5	Primers for sequencing CHX17 and CHX20 cDNA and testing recombination into Gateway vectors.	178
Table III-S6	YPAD enriched yeast medium containing all amino acids (per L).	178
Table III-S7	YNB(A)- rich yeast medium (per L).	179
Table III-S8	K^+-free YNB(A) wash buffer (per L).	180
Table III-S9	SGM medium for *E. coli* (per L).	181

LIST OF APPENDIX FIGURES

Supplemental Figures for Chapter II

Fig. II-S1	Flower development of *chx17/18/19* mutant and WT is similar.	162
Fig. II-S2	Pod and seed development from 0 to 9 days after pollination.	163
Fig. II-S3	*In vitro* pollen germination and tube growth are reduced by half in triple *chx17/18/19* mutant.	165
Fig. II-S4	Pollen tubes of *chx17/18/19* mutants entered ovules that remain undeveloped	166
Fig. II-S5	Pollen tubes from the *chx16/17/18/19* mutant grow *in vivo* and target ovules, though tube number and lengths are reduced relative to WT plants.	167
Fig. II-S6	Expression of *CHX* genes in sperm cells and in female gametophyte cells.	168
Fig. II-S7	Expression of *CHX17* and *CHX18* in the micropylar and peripheral endosperm of developing embryo.	170
Fig. II-S8	CHX19-RFP is localized to the pollen-tube PM.	171

Supplemental Figures for Chapter III

Fig. III-S1	Phyre results for CHX17-TM domain: Protein fold recognition and predicted secondary structure.	182
Fig. III-S2	Alignment of AtCHX17 with CPA2 and CPA1 members show conserved and nonconserved residues.	186
Fig. III-S3	Effect of HygB concentration on yeast carrying wild-type or mutated CHX17.	187
Fig. III-S4	Effect of HygB concentration on the time-course of yeast growth in liquid medium.	188
Fig. III-S5	CHX17-GFP signal was observed in yeast.	191
Fig. III-S6	Total protein extracted from yeast cultures contained a GFP tag.	192
Fig. III-S7	Testing the role of the CHX17 hydrophilic C-tail on activity.	193
Fig. III-S8	Phyre2 search results for the CHX17-C tail show top hits with several universal stress proteins or USP-like domains.	194

A. SUPPLEMENTAL INFORMATION FOR CHAPTER II

A.1. Tables of materials for Chapter II

Table II-S1: Single T-DNA insertion mutants used in this study. Information in the table is reproduced from Chanroj, et al., 2013, Table S3. All mutant lines were generated in the Columbia-0 ecotype.

Mutant	SALK Line #	Insertion Location (after base)
chx16-10a	SALK_138136	767
chx17-4	SALK_033417	996
chx18-1	SALK_001563	2070
chx19-2	SALK_100047	619

Table II-S2: Multiple *chx* T-DNA insertion mutants analyzed for seed set.

Genotype	Parent	Note
chx17/18	*chx17-4* x *chx18-1*	full seed set
chx17/19	*chx17-4* x *chx19-1*	full seed set
chx16/17/19	*chx* $16^{-/-}$ ***chx17***$^{+/-}$ *chx*$18^{+/+}$ *chx*$19^{-/-}$ selfing	full seed set
chx16/18/19	*chx* $16^{-/-}$ *chx*$17^{+/+}$ ***chx18***$^{+/-}$ *chx*$19^{-/-}$ selfing	full seed set
chx17/18/19_a	*chx*$17^{-/-}$ *chx*$18^{-/-}$ *chx*$19^{+/-}$ selfing	reduced seed set
chx17/18/19_b	*chx*$17^{-/-}$ *chx*$18^{-/-}$ *chx*$19^{+/-}$ selfing	reduced seed set
chx17/18/19_c	*chx*$17^{-/-}$ *chx*$18^{-/-}$ *chx*$19^{+/-}$ selfing	reduced seed set
chx16/17/18/19_a	*chx* $16^{-/-}$ *chx*$17^{-/-}$ ***chx18***$^{+/-}$ *chx*$19^{-/-}$ selfing	reduced seed set
chx16/17/18/19_b	*chx* $16^{-/-}$ *chx*$17^{-/-}$ ***chx18***$^{+/-}$ *chx*$19^{-/-}$ selfing	reduced seed set
chx16/17/18/19_c	*chx* $16^{-/-}$ ***chx17***$^{+/-}$ *chx*$18^{-/-}$ *chx*$19^{-/-}$ selfing	reduced seed set
chx16/17/18/19_d	*chx* $16^{-/-}$ ***chx17***$^{+/-}$ *chx*$18^{-/-}$ *chx*$19^{-/-}$ selfing	reduced seed set

Table II-S3: Multiple T-DNA insertion mutants used for segregation analysis.

Mutant	Parent	Note
chx17$^{-/-}$ ***18***$^{+/-}$ *19*$^{-/-}$_a	*chx17*$^{-/-}$ *chx18*$^{+/-}$ *chx19*$^{+/-}$ selfing	Test role of *CHX18* in the male or female gametophyte.
chx17$^{-/-}$ ***18***$^{+/-}$ *19*$^{-/-}$_b	*chx17*$^{-/-}$ *chx18*$^{+/-}$ *chx19*$^{+/-}$ selfing	Test role of *CHX18* in the male or female gametophyte.
chx17$^{-/-}$ ***18***$^{+/+}$ *19*$^{-/-}$_a	*chx17-4* x *chx19-1*	Used in reciprocal crosses to test role of *CHX18*.
chx17$^{-/-}$ ***18***$^{+/+}$ *19*$^{-/-}$_b	*chx17-4* x *chx19-1*	Used in reciprocal crosses to test role of *CHX18*.
chx17$^{-/-}$ *18*$^{-/-}$ ***19***$^{+/-}$_a	*chx17*$^{-/-}$ *chx18*$^{+/-}$ *chx19*$^{+/-}$ selfing	Test role of *CHX19* in the male or female gametophyte.
chx17$^{-/-}$ *18*$^{-/-}$ ***19***$^{+/-}$_b	*chx17*$^{-/-}$ *chx18*$^{+/-}$ *chx19*$^{+/-}$ selfing	Test role of *CHX19* in the male or female gametophyte.
chx17$^{-/-}$ *18*$^{-/-}$ ***19***$^{+/+}$_a	*chx17-4* x *chx18-1*	Used in reciprocal crosses to test role of *CHX19*.
chx17$^{-/-}$ *18*$^{-/-}$ ***19***$^{+/+}$_b	*chx17-4* x *chx18-1*	Used in reciprocal crosses to test role of *CHX19*.

Table II-S4: Gene-specific primers and T-DNA border primers used for genotyping plants.

Name	Sequence	Product detected
chx17-4TLP	AACTTTGCAGTAAAGGGAAACTAGGACTG	genomic CHX17
chx17-4TRP	TGAGTTTTATATTGTGGTTTTAGGGTGGA	genomic CHX17 *chx17-4* T-DNA
chx18-1TLP	ATTCTACCAACCAAAAACAAATTGCTC	genomic CHX18 *chx18-1* T-DNA
chx18-1TRP	AGAAGAGCGAAGAAAGAAGGAGAATACAA	genomic CHX18
chx19-2LP	TGTAAGTAGATCTCCACTAGGATGGCAAG	genomic CHX19
chx19-2RP_n2	GCGCGTGTATCCCAATAGTGTCTGTC	genomic CHX19 *chx19-2* T-DNA
LB-b1.3	ATTTTGCCGATTTCGGAAC	*chx17-4* T-DNA
LB-b1	GCGTGGACCGCTTGCTGCAAC T	*chx18-1* and *chx19-2* T-DNA

A.2. Supplemental Results for Chapter II

Fig. II-S1. Flower development of *chx17/18/19* mutant and WT is similar. Flowers from stages 9, 11, 12, 13, and 15 were collected from the primary bolts of WT **A)** and *chx17/18/19* **B)** plants. Sepals and petals were removed from each flower to visualize stamens and pistil. Scale bar = 1 mm.

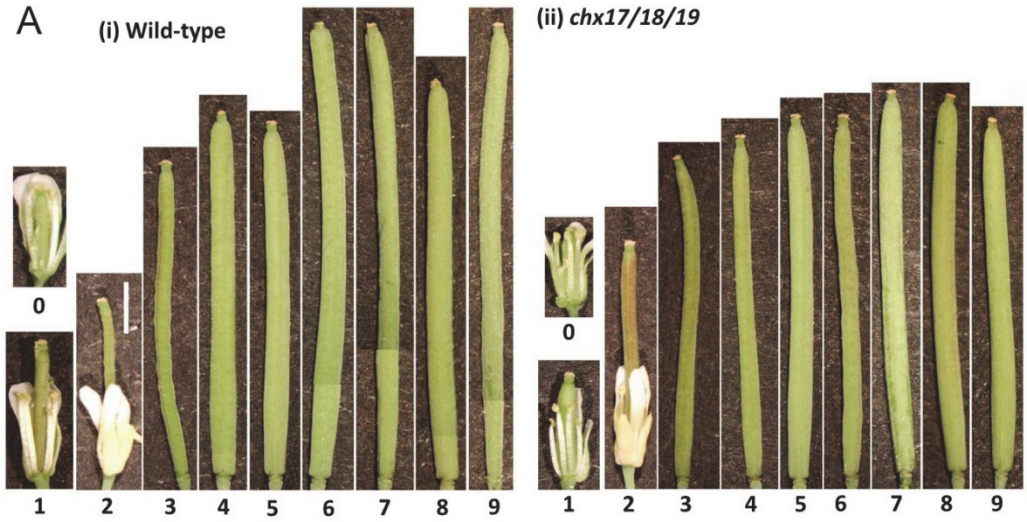

Fig. II-S2. Pod and seed development from 0 to 9 days after pollination. A) Pod elongates rapidly 2-3 days after pollination (DAP)**.** Seed pods were removed from wild-type i) and *chx17/18/19* ii) plants at 0 to 9 DAP. Length of wild-type pods at 5 to 9 DAP is longer than *chx17/18/19* mutant pods. Scale bar = 2 mm**. B)** Pods of *chx17/18/19* mutants show gaps where seeds fail to develop by 3-4 DAP**.** WT and *chx17/18/19* pods were collected and slit open at 0 to 9 DAP. Pods are filled with mature seeds in the WT pod. In *chx17/18/19* mutant pods, some ovules fail to increase in size by 6-7 DAP and shrivel up by 8-9 DAP. Four seed pods were examined per genotype per day. Scale bar = 0.5 mm.

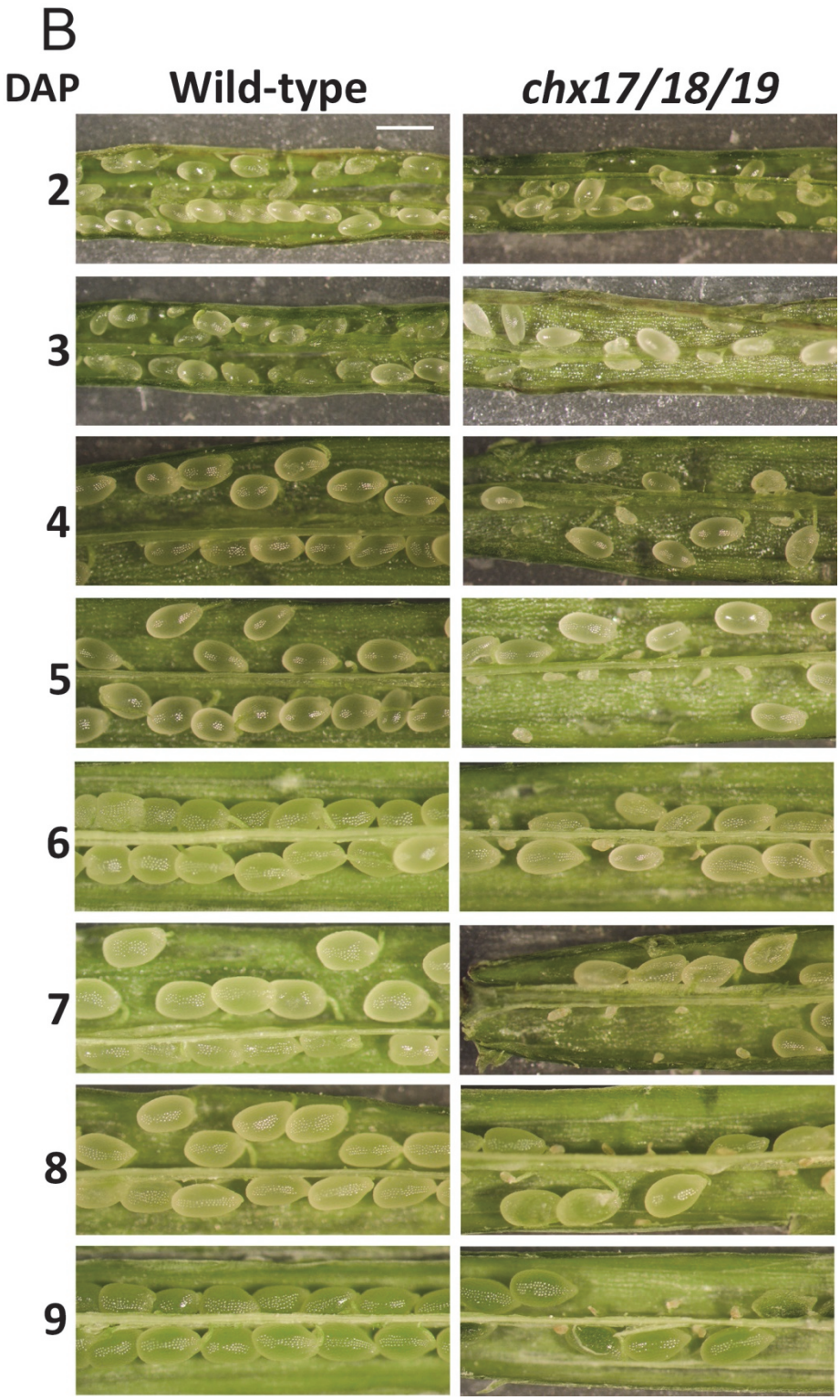
B
DAP
Wild-type
chx17/18/19
2
3
4
5
6
7
8
9

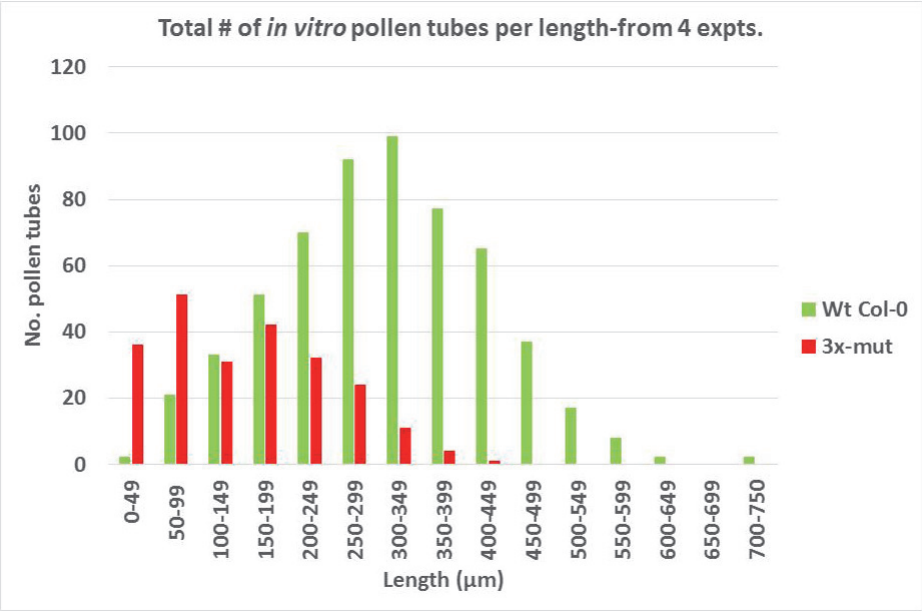

Fig. II-S3. *In vitro* pollen germination and tube growth are reduced by half in triple *chx17/18/19* mutant. Pollen from WT and the *chx17/18/19* mutant were germinated in liquid medium (Li, 2006) using the Pollen RCN protocol. After 6 h at 27°C in a humidity chamber, grains and tubes were photographed using brightfield settings with 10x objective lens on a Nikon E600 microscope. Tube length was measured in ImageJ. In 4 experiments, germination was reduced ~60% in triple mutant, and mean tube length of WT and mutant was 304 and 152 µm, respectively. Total tubes counted were 570 and 230.

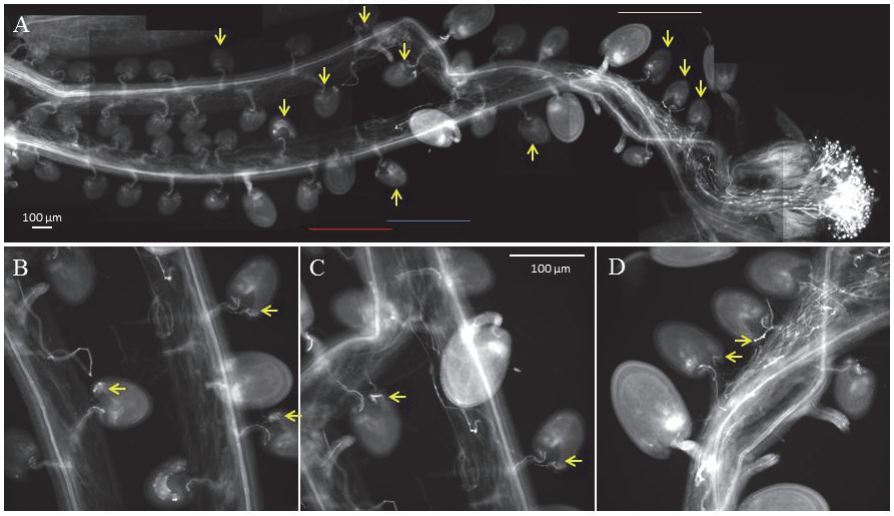

Fig. II-S4. Pollen tubes of *chx17/18/19* mutants entered ovules that remain undeveloped. A WT pistil was manually pollinated with *chx17/18/19* pollen. Pod was examined 2 DAP. **A)** Yellow arrows point to ovules containing a PT. **B-D)** Examples of magnified images show PTs visible inside ovules that remain undeveloped. PTs in large developing seeds are often no longer visible. The red line in panel A represents the magnified image in panel B. The blue line represents the magnified image in panel C, and the white line represents the magnified image in panel in panel D. Scale bars = 100 µm.

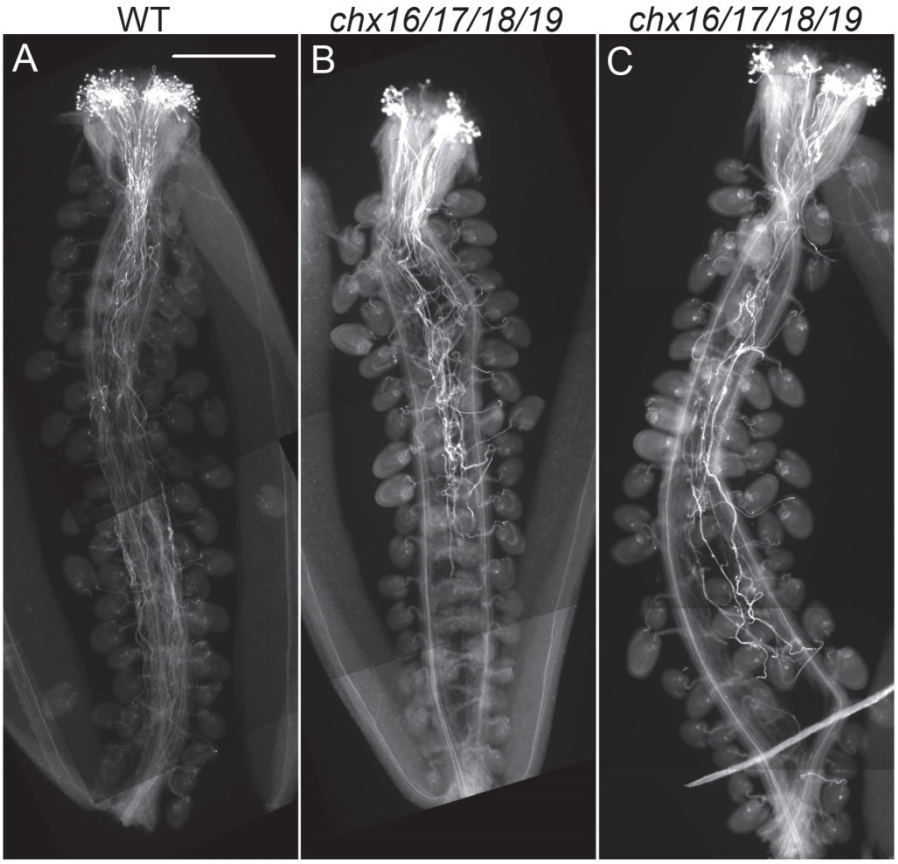

Fig. II-S5. **Pollen tubes from the *chx16/17/18/19* mutant grow *in vivo* and target ovules, though tube number and lengths are reduced relative to WT plants**. Pods from self-pollinated *chx16/17/18/19* mutants were also collected and pistils were fixed and stained with Aniline Blue at 1-4 days after stage 13. **A)** PTs have reached distal end of a WT pod at about 1 DAP. **B-C)** PTs have reached half to three-quarters way down at about 1 DAP. Bar = 300 µm.

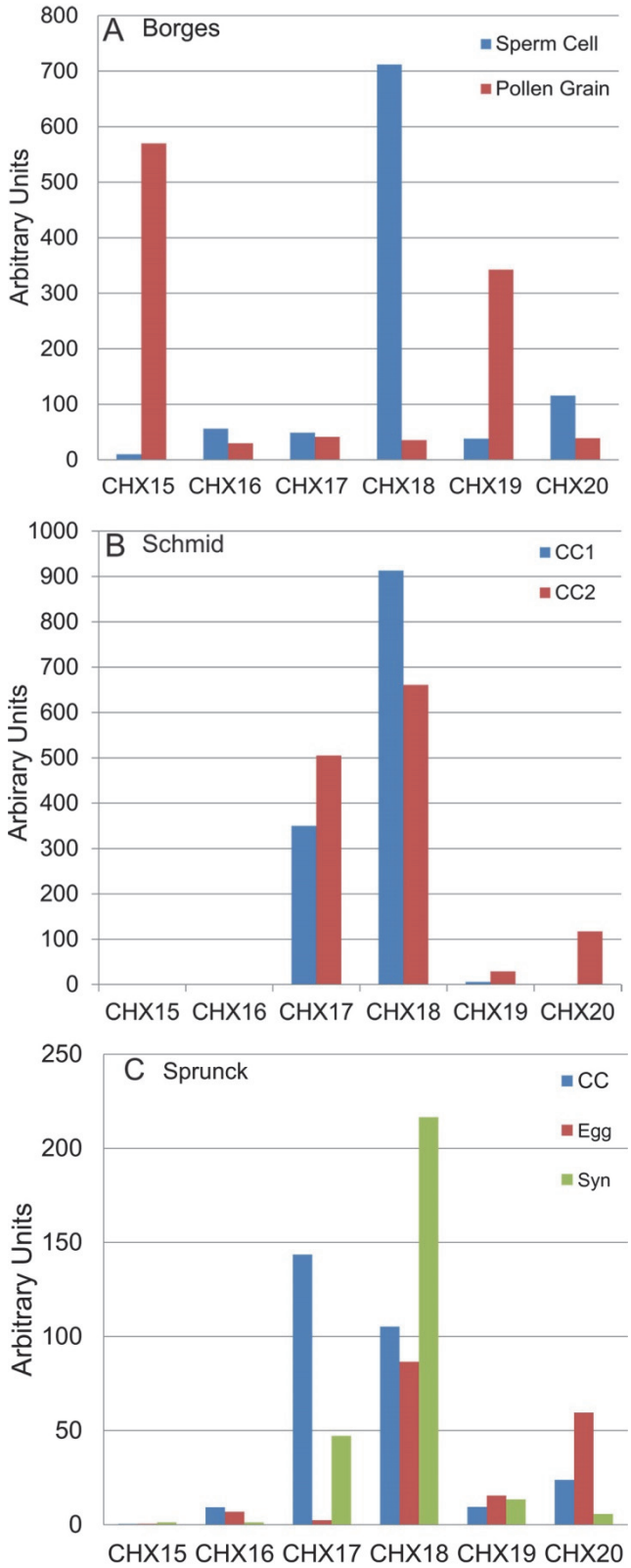

Fig. II-S6. Expression of *CHX* genes in sperm cells and in female gametophyte cells. **A)** *CHX18* is expressed preferentially in sperm cells, whereas *CHX19* is expressed in pollen grains or tubes. Based on ATH1 transcriptome results of Borges et al., 2008; Honys & Twell, 2004; and Qin et al., 2009. **B)** *CHX17* and *CHX18* are expressed in the central cell based RNA-seq results in duplicate experiments published by Schmid et al., 2012. CC = central cell. **C)** Expression of *CHX17* and *CHX18* in the central cell and synergid cell based on ATH1 transcriptome analysis of Stephanie Sprunck, et al. (unpublished). *CHX18* may be expressed in the egg cell. Syn = synergid cell.

Fig. II-S7. Expression of *CHX17* and *CHX18* in the micropylar and peripheral endosperm of the developing embryo. **A)** *CHX17* expression is particularly high in the micropylar endosperm of the preglobular and globular stage embryos. **B)** *CHX18* expression is high in the peripheral endosperm of the preglobular stage embryo in addition to the micropylar endosperm at the preglobular and globular stages. **C)** In the embryo, *CHX18* is expressed highest at the preglobular and mature green stages. *CHX17* is expressed at a low level throughout embryo development. Results summarized from ATH1 transcriptome analysis of laser-dissected tissues from the developing seed published by Le et al., 2010.

Abbreviations are as follows:

A&B) MCE = micropylar endosperm, **PEN** = peripheral endosperm, and **CZE** = chalazal endosperm. **preGlob** = preglobular embryo, **Glob** = globular embryo, **Heart** = heart-stage embryo, **L-cot** = linear cotyledon embryo, and **Mature** = mature green embryo

C) EP = embryo proper, **pg** = preglobular, **g** = globular, **h** = heart, **lc** = linear cotyledon, and **mg** = mature green.

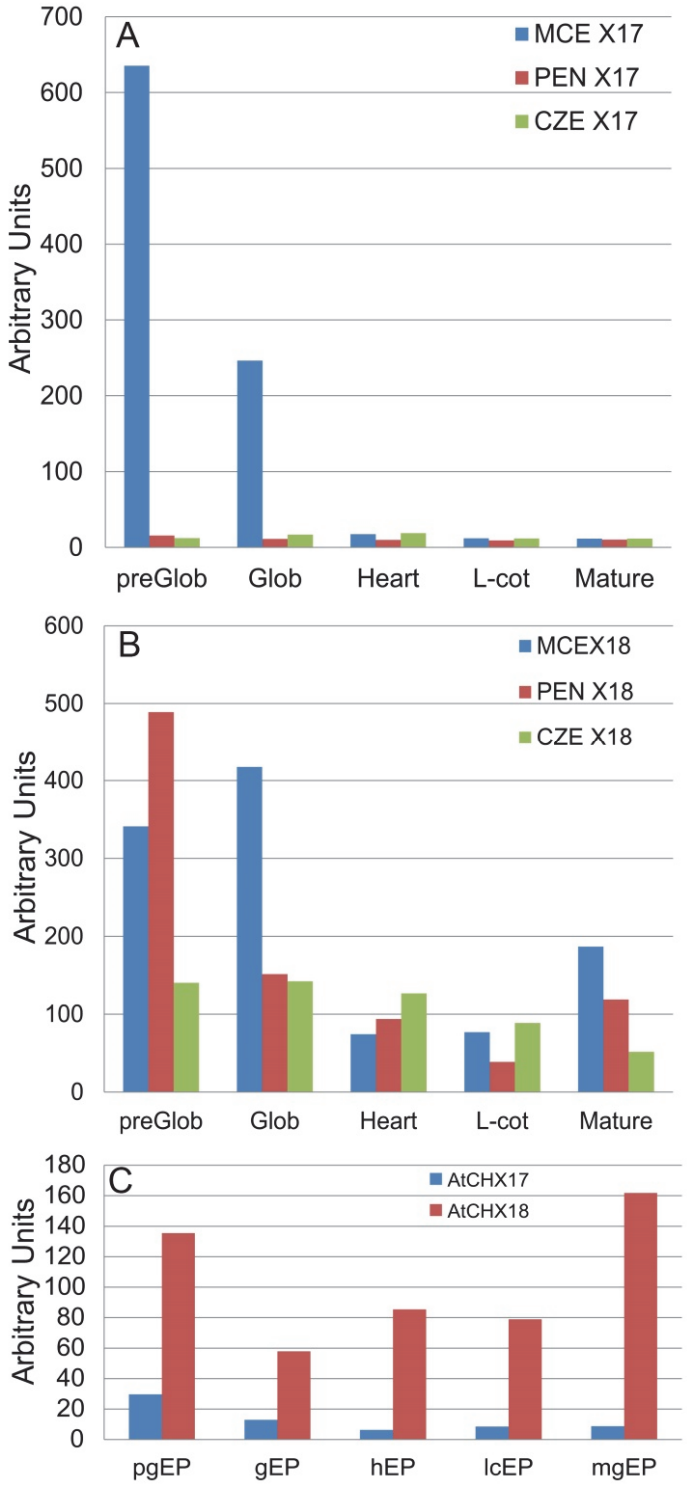
A
MCE X17
PEN X17
CZE X17
Arbitrary Units
700
600
500
400
300
200
100
0
preGlob
Glob
Heart
L-cot
Mature
B
MCEX18
PEN X18
CZE X18
Arbitrary Units
600
500
400
300
200
100
0
preGlob
Glob
Heart
L-cot
Mature
C
AtCHX17
AtCHX18
Arbitrary Units
180
160
140
120
100
80
60
40
20
0
pgEP
gEP
hEP
lcEP
mgEP

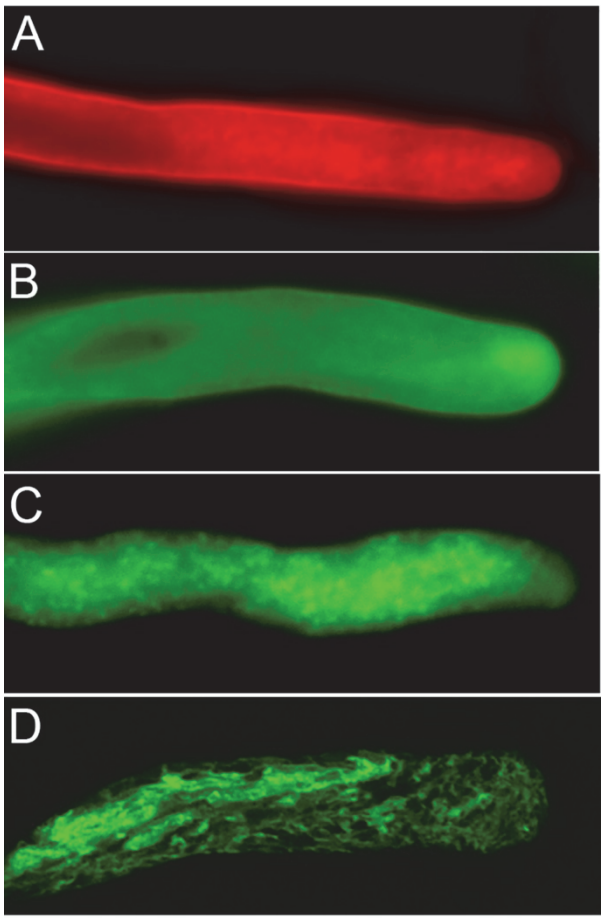

Fig. II-S8. CHX19-RFP is localized to the pollen-tube PM. Fluorescence microscopy images of **A)** CHX19-RFP and **B-D)** membrane markers expressed transiently in tobacco pollen. **A)** CHX19-GFP; **B)** GFP-PRK1, PM marker; **C)** GFP-Rab2, Golgi marker; and **D)** GFP-HDEL, ER marker.

B. SUPPLEMENTAL INFORMATION FOR CHAPTER III

B.1. Tables of materials for Chapter III

Table III-S1. Primers for site-directed mutagenesis of AtCHX17. Blue type indicates wild-type sequence. Red type indicates introduced base change and deduced residue.

CHX17	Primer name	WT Sequence or Primer with base change
Wt Glu111	F (5'->3')	TTC CTC GTT GGT CTC **GAG** CTC GAT CCC AAA TCT
	R (3'->5')	AGA TTT GGG ATC GAG **CTC** GAG ACC AAC GAG GAA
E111C	X17-E111C-F	TTC CTC GTT GGT CTC **TGT** CTC GAT CCC AAA TCT
	X17-E111C-R	AGA TTT GGG ATC GAG **ACA** GAG ACC AAC GAG GAA
		- - - - - **Glu** - - - - - - - - - **Cys** - - - -
Wt Thr170	F (5'->3')	GTT GCT CTC TCC ATC **ACA** GCG TTT CCC GTC TTG
	R (3'->5')	CAA GAC GGG AAA CGC **TGT** GAT GGA GAG AGC AAC
T170A	X17-T170A-F	GTT GCT CTC TCC ATC **GCA** GCG TTT CCC GTC TTG
	X17-T170A-R	CAA GAC GGG AAA CGC **TGC** GAT GGA GAG AGC AAC
		- - - - - **Thr** - - - - - - - - - **Ala** - - - -
Wt Asn200	F (5'->3')	TCC GCT GCT GCG GTC **AAT** GAC GTG GCT GCT TGG
	R (5'->3')	CCA AGC AGC CAC GTC **ATT** GAC CGC AGC AGC GGA
N→D N200D	X17-N200D-F	TCC GCT GCT GCG GTC **GAT** GAC GTG GCT GCT TGG
	X17-N200D-R	CCA AGC AGC CAC GTC **ATC** GAC CGC AGC AGC GGA
		- - - - - **Asn** - - - - - - - - - **Asp** - - - -
W Asp201	F (5'->3')	GCT GCT GCG GTC AAT **GAC** GTG GCT GCT TGG ATT
	R (5'->3')	AAT CCA AGC AGC CAC **GTC** ATT GAC CGC AGC AGC
D→Ala	X17-D201A-F	GCT GCT GCG GTC AAT **GCC** GTG GCT GCT TGG ATT

D201A	X17-D201A-R	AAT CCA AGC AGC CAC **GGC** ATT GAC CGC AGC AGC
		– – – – – **Asp** – – – –
		– – – – – **Ala** – – – –
D201N	X17-D201N-F	GCT GCT GCG GTC AAT **AAC** GTG GCT GCT TGG ATT
	X17-D201N-R	AAT CCA AGC AGC CAC **GTT** ATT GAC CGC AGC AGC
		– – – – – **Asp** – – – –
		– – – – – **Asn** – – – –
D201E	X17-D201E-F	GCT GCT GCG GTC AAT **GAA** GTG GCT GCT TGG ATT
	X17-D201E-R	AAT CCA AGC AGC CAC **TTC** ATT GAC CGC AGC AGC
		– – – – – **Asp** – – – –
		– – – – – **Glu** – – – –
Wt His284	F (5'->3')	GAC TTT ATT GGG ATT **CAT** GCG CTG TTT GGT GCT
	R (5'->3')	AGC ACC AAA CAG CGC **ATG** AAT CCC AAT AAA GTC
H284A	X17-H284A-F	GAC TTT ATT GGG ATT **GCT** GCG CTG TTT GGT GCT
	X17-H284A-R	AGC ACC AAA CAG CGC **AGC** AAT CCC AAT AAA GTC
		– – – – – **His** – – – –
		– – – – – **Ala** – – – –
Wt Glu311	F (5'->3')	TTA GTT GAG AAA GTT **GAG** GAT CTC GTG TCA GGT
	R (3'->5')	ACC TGA CAC GAG ATC **CTC** AAC TTT CTC AAC TAA
E311C	X17-E311C-F	TTA GTT GAG AAA GTT **TGT** GAT CTC GTG TCA GGT
	X17-E311C-R	ACC TGA CAC GAG ATC **ACA** AAC TTT CTC AAC TAA
		– – – – – **Glu** – – – –
		– – – – – **Cys** – – – –
Wt Lys355	F (5'->3')	AAT GCT TGT TTC GGT **AAA** ATC ATC GGT ACA GTC
	R (5'->3')	GAC TGT ACC GAT GAT **TTT** ACC GAA ACA AGC
K355A	X17-K355A-F	AAT GCT TGT TTC GGT **GCA** ATC ATC GGT ACA GTC
	X17-K355A-R	GAC TGT ACC GAT GAT **TGC** ACC GAA ACA AGC
		– – – – – **Lys** – – – –
		– – – – – **Ala** – – – –
K355Q	X17-K355Q-F	AAT GCT TGT TTC GGT **CAA** ATC ATC GGT ACA GTC

	X17-K355Q-R	GAC TGT ACC GAT GAT **TTG** ACC GAA ACA AGC ATT
		- - - - - **Lys** - - - - - - - - - **Gln** - - - -
K355R	X17-K355R-F	AAT GCT TGT TTC GGT **AGA** ATC ATC GGT ACA GTC
	X17-K355R-R	GAC TGT ACC GAT GAT **TCT** ACC GAA ACA AGC ATT
		- - - - - **Lys** - - - - - - - - - **Arg** - - - -
Wt Thr382	F (5'->3')	GGT TTC TTG ATG AAC **ACG** AAA GGT CTT GTT GAG
	R (5'->3')	CTC AAC AAG ACC TTT **CGT** GTT CAT CAA GAA ACC
T382A	X17-T382A-F	GGT TTC TTG ATG AAC **GCG** AAA GGT CTT GTT GAG
	X17-T382A-R	CTC AAC AAG ACC TTT **CGC** GTT CAT CAA GAA ACC
		- - - - - **Thr** - - - - - - - - - **Ala** - - - -
Wt Lys383	F (5'->3')	TTC TTG ATG AAC ACG **AAA** GGT CTT GTT GAG CTC
	R (5'->3')	GAG CTC AAC AAG ACC **TTT** CGT GTT CAT CAA GAA
K383A	X17-K383A-F	TTC TTG ATG AAC ACG **GCA** GGT CTT GTT GAG CTC
	X17-K383A-R	GAG CTC AAC AAG ACC **TGC** CGT GTT CAT CAA GAA
		- - - - - **Lys** - - - - - - - - - **Ala** - - - -
Wt Cys458	F (5'->3')	CTC TGC CTC ATG TTC **TGT** TTC CAG AGC ATA ATG
	R (5'->3')	CAT TAT GCT CTG GAA **ACA** GAA CAT GAG GCA GAG
C458A	X17-C458A-F	CTC TGC CTC ATG TTC **GCT** TTC CAG AGC ATA ATG
	X17-C458A-R	CAT TAT GCT CTG GAA **AGC** GAA CAT GAG GCA GAG
		- - - - - **Cys** - - - - - - - - - **Ala** - - - -
Wt Cys562	F (5'->3')	ATA CAT GAG GAT ATT **TGC** CAA AGC GCG GAA CGC
	R (5'->3')	GCG TTC CGC GCT TTG **GCA** AAT ATC CTC ATG TAT
C562A	X17-C562A-F	ATA CAT GAG GAT ATT **GCC** CAA AGC GCG GAA CGC

	X17-C562A-R	GCG TTC CGC GCT TTG **GGC** AAT ATC CTC ATG TAT
		- - - - - **Cys** - - - - - - - - - **Ala** - - - -
Wt Cys607	F (5'->3')	ATG GAG GAA TCT CCA **TGT** TCT GTT GCG ATT TTG
	R (5'->3')	CAA AAT CGC AAC AGA **ACA** TGG AGA TTC CTC CAT
C607A	X17-C607A-F	ATG GAG GAA TCT CCA **GCT** TCT GTT GCG ATT TTG
	X17-C607A-R	CAA AAT CGC AAC AGA **AGC** TGG AGA TTC CTC CAT
		- - - - **Cys** - - - - - - - - - **Ala** - - - -

Table III-S2. Construction of GFP-tagged CHX17. WT or mutated CHX17 were tagged with GFP at the C-tail using the destination vector pGWFDR196. The binary vector was modified by introduction of the PMA1 yeast constitutive promoter into the Gateway pGWF2 vector.

Residue change	Abbrev	Location	Construct name with GFP tag
CHX17 Wt	none		pDX17-GFP-pGWFDR196
Glu111-> Cyt	E111C	TM2-C end	pDX17-E111C-GFP-pGWFDR196
Thr170→Ala	T170A	TM4-dis	pDX17-T170A-GFP-pGWFDR196
ASN200→ASP	N200D	TM5 mid	pDX17-N200D-GFP-pGWFDR196
ASP201 →Ala	D201A	TM5 mid	pDX17-D201A-GFP-pGWFDR196
ASP201 →ASN	D201N	TM5 mid	pDX17-D201N-GFP-pGWFDR196
ASP201 →GLU	D201E	TM5 mid	pDX17-D201E-GFP-pGWFDR196
His284→Ala	H284A	TM8	pDX17-H284A-GFP-pGWFDR196
GLU311-> CYS	E311C	TM9	pDX17-E311C-GFP-pGWFDR196
LYS355 -> ALA	K355A	TM10 mid	pDX17-K355A-GFP-pGWFDR196
LYS355 -> GLN	K355Q	TM10 mid	pDX17-K355Q-GFP-pGWFDR196
Lys355 -> ARG	K355R	TM10 mid	pDX17-K355R-GFP-pGWFDR196
Thr382→Ala	T382A	TM11 dis	pDX17-T382A-GFP-pGWFDR196
Lys383→Ala	K383A	TM11 dis	pDX17-K383A-GFP-pGWFDR196
Cys458→Ala	C458A	C-Tail	pDX17-C458A-GFP-pGWFDR196
Cys562→Ala	C562A	C-Tail	pDX17-C562A-GFP-pGWFDR196
Cys607→Ala	C607A	C-Tail	pDX17-C607A-GFP-pGWFDR196

Table III-S3: Primers for truncating the C-tails of CHX17 and CHX20. Primers were used for amplifying *CHX* cDNA prior to cloning into Gateway vectors. F and R refer to forward and reverse primers. Lower case sequences denote BP/LR recombination sites. The CHX17-472 (Chanroj, et al., 2013) and CHX20-450 (Padmanaban, unpublished) primers were constructed previously.

Name	Sequence	Template
Chx17_GW_ATG_F	ggggacaagtttgtaccaaaaagcaggctYYATGGGAACAAACGGTACAACAT	CHX17 cDNA in pPAB404 vector
Chx17_GW_582_R	ggggaccacttgtacaagaaagcgggtYCCTAACGTGCTTATGAAACGGA	CHX17 cDNA in pPAB404 vector
Chx17_GW_690_R	ggggaccacttgtacaagaaagcgggtYAGTTGCCCCTGAACAGAGCT	CHX17 cDNA in pPAB404 vector
Chx20_GW_ATG_F	ggggacaagtttgtaccaaaaagcaggctYYATGCCCTTCAACATAACCTCC	CHX20 cDNA in pPAB404 vector
Chx20_GW_483_R	ggggaccacttgtacaagaaagcgggtYGGTGGTTCGGATGGACTC	CHX20 cDNA in pPAB404 vector
Chx20_GW_584_R	ggggaccacttgtacaagaaagcgggtYAGCGTTCCATCGTTTGTGG	CHX20 cDNA in pPAB404 vector
Chx20_GW_710_R	ggggaccacttgtacaagaaagcgggtYGGCATAGTTCTTCTCCTTGCCTT	CHX20 cDNA in pPAB404 vector

Table III-S4: Primers for making pD404 *E. coli* expression vector and verifying the presence of recombined DNA sequences in pD404. F and R refer to forward and reverse primers.

Name	Sequence	Template
pC-DR196cass-FWD	CCCGGTACCACAAGTTTGTACAAAA AAGCTGAAC	pYESDR196
pC-DR196cass-REV	CCCAGATCTTCAATGGTGATGGTGA TGATG	pYESDR196
pD-PAB404-F	TCAAGGCGCACTCCCGTTCT	pPAB404
pD-PAB404-R	CCCATCGCCAATCAGCAA	pPAB404
pD-PAB404-R_DC	GCCGGATAAAACTTGTGCTT	CHX17 cDNA in pPAB404

Table III-S5: Primers for sequencing CHX17 and CHX20 cDNA and testing recombination into Gateway vectors.

Name	Sequence	Template
x17sf1	**GCTTCTAACCACTGATATCGGAA**	CHX17 cDNA
x17sf2	ATGCTTGTTTCGGTAAAATCATC	CHX17 cDNA
x17sf3	AAAGACAAATCTGAGAACAATAGTTCT	CHX17 cDNA
x20sf1	AGCTTTTAACGACTCAGATAGGAGAA	CHX20 cDNA
x20sf2	GGGATGTTGGGTCTTGTTGT	CHX20 cDNA
x20sf3	ACTTCCTTTCGTTCACCGTTAC	CHX20 cDNA

Table III-S6: YPAD enriched yeast medium containing all amino acids (per L). Used for growing yeast cells prior to transformation.

Reagent	MW	[Stock]	Per Litre	[Final]
Yeast extract	N/A	powder	10 g	1 %
Bacto-**p**eptone	N/A	powder	20 g	2 %
Adenine	368.4	powder	0.1 g	27 µM/ 0.01 %
Sterile Glucose (**D**extrose)	180.2	20 %	100 ml	2%
Adjust to pH 6.0 with HCl (initial pH ~6.65)				

Table III-S7: YNB(A)- rich yeast medium (per L). Uracil was omitted for selection media and test media.

Reagent	MW	[Stock]	Per L	[Final]
Yeast nitrogen base	N/A	powder	1.7 g	0.17%
$(NH_4)_2SO_4$	132.1	powder	5.0 g	38 mM
MES	195.2	powder	3.9 g	20 mM
Adenine	368.4	powder	0.1 g	27 µM/0.01 %
Sterile glucose	180.2	20%	100 ml	2%
Adjust pH to 6.0 with Arginine (Fisher Scientific BP2505500)- [Arg] is 12-14 mM				
Added to YNB(A) for selection plates				
KCl	74.6	powder	7.46	100 mM
Histidine	209.6	powder	0.1 g	27 µM/0.01 %
Leucine	131.2	powder	0.1 g	27 µM/0.01 %
Dropout Mix*	N/A	powder	2.0 g	0.2%
Agar	N/A	powder	20 g	2%

*Dropout mix lacks uracil, adenine, histidine, and leucine.

Table III-S8: K^+-free YNB(A) wash buffer (per L). Used for washing yeast cells prior to testing on solid media in the presence of hygromycin B.

Reagent	MW	[Stock]	Per L	[Final]
Vitamins	-------	500x	2.0 ml	1 x
Minerals	-------	200x	5.0 ml	1 x
$MgSO_4 \cdot 7H_2O$	197.9	powder	0.5 g	2.5 mM
$CaCl_2$	111.0	powder	0.1 g	90 µM
NaCl	58.4	powder	0.1 g	1.7 mM
$(NH_4)_2SO_4$	132.1	powder	4.0 g	30 mM
$(NH_4)_2HPO_4$	115.0	powder	1.0 g	8.7 mM
MES	195.2	powder	3.9 g	20 mM
Adenine SO_4	368.4	powder	0.1 g	27 µM/ 0.01 %
Agar	N/A	powder	20 g	2 %
Adjust to pH 6.0 with Arginine, [Arginine] is 3-5 mM.				

Table III-S9: SGM medium for *E. coli* (per L).

Reagent	**MW**	**[Stock]**	**Added**	**[Final]**
Vitamins	N/A	4K x	250 ul	1 x
Minerals	N/A	4K x	250 ul	1 x
H_3PO_4	98.0	14.75 M (85%)	275 ul	4 mM
$MgSO_4 \cdot 7H_2O$	197.9	1 M	400 ul	0.4 mM
$CaCl_2$	111.0	1 M	100 ul	0.1 mM
FeSO4·citrate	488.0	10 mM	1 ml	10 uM
Thiamine HCl	337.3	powder	0.34 g	1 mM
Glycerol	92.1	10.6 M (99%)	6 ml	63 mM
Mannitol	182.2	powder	18.2 g	100 mM
Arginine base	174.2	powder	1.5 g	~8 mM
Add the reagents below for growth media; omit for wash media.				
MES	195.2	powder	3.9 g	20 mM buffer pH 6 +/- 0.5
MOPS	209.3	powder	4.02 g	20 mM buffer pH 7 +/- 0.5
KCl	74.6	powder	2.2 g	30 mM-improve growth
NH_4Cl	53.5	powder	0.3 g	5 mM-improve growth
Adjust pH with Arginine base.				

B.2. Supplemental Results for Chapter III

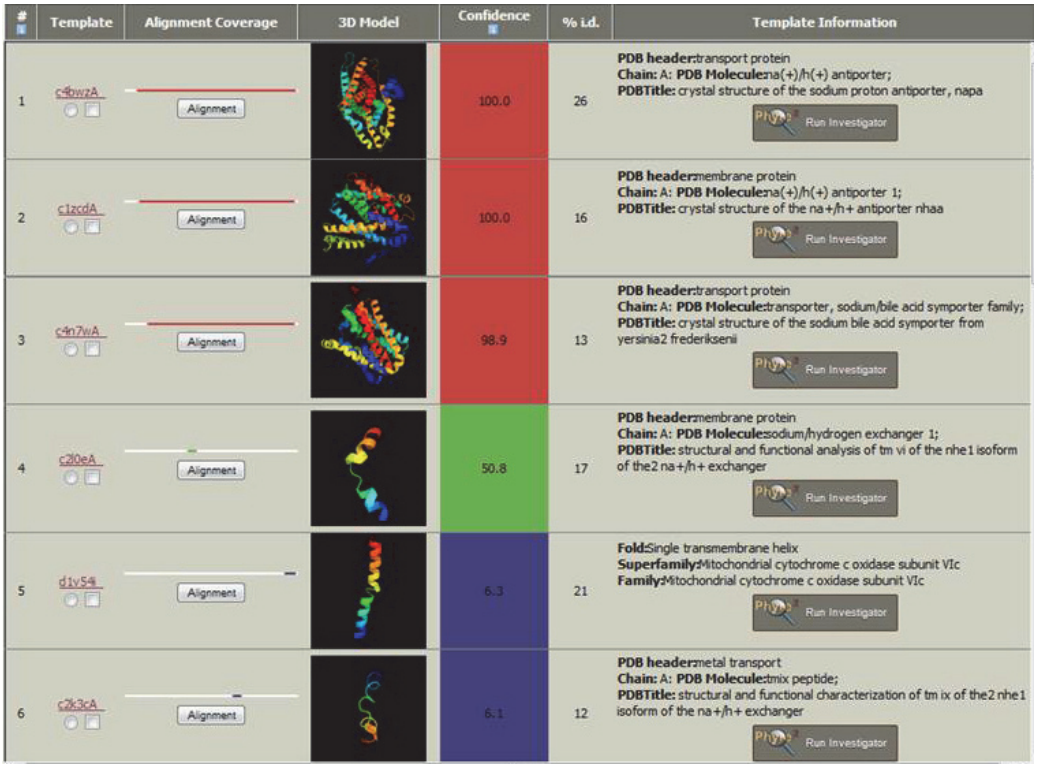

#	Template	Alignment Coverage	3D Model	Confidence	% i.d.	Template Information
1	c4bwzA	Alignment		100.0	26	**PDB header:**transport protein **Chain:** A: **PDB Molecule:**na(+)/h(+) antiporter; **PDBTitle:** crystal structure of the sodium proton antiporter, napa Run Investigator
2	c1zcdA	Alignment		100.0	16	**PDB header:**membrane protein **Chain:** A: **PDB Molecule:**na(+)/h(+) antiporter 1; **PDBTitle:** crystal structure of the na+/h+ antiporter nhaa Run Investigator
3	c4n7wA	Alignment		98.9	13	**PDB header:**transport protein **Chain:** A: **PDB Molecule:**transporter, sodium/bile acid symporter family; **PDBTitle:** crystal structure of the sodium bile acid symporter from yersinia2 frederiksenii Run Investigator
4	c2l0eA	Alignment		50.8	17	**PDB header:**membrane protein **Chain:** A: **PDB Molecule:**sodium/hydrogen exchanger 1; **PDBTitle:** structural and functional analysis of tm vi of the nhe1 isoform of the2 na+/h+ exchanger Run Investigator
5	d1vs4i	Alignment		6.3	21	**Fold:**Single transmembrane helix **Superfamily:**Mitochondrial cytochrome c oxidase subunit VIc **Family:**Mitochondrial cytochrome c oxidase subunit VIc Run Investigator
6	c2k3cA	Alignment		6.1	12	**PDB header:**metal transport **Chain:** A: **PDB Molecule:**tmix peptide; **PDBTitle:** structural and functional characterization of tm ix of the2 nhe1 isoform of the na+/h+ exchanger Run Investigator

Fig. III-S1A. Phyre results for CHX17-TM domain: Protein fold recognition and predicted secondary structure. A) Top domain hits for protein fold recognition are TtNapA and EcNhaA. The template PDB numbers are shown at left. Alignment of CHX17 (residues 1-440, white line) to template (red) is shown. Red color under confidence indicates the probability for a similar fold is over 95%. The protein identity is 26% for TtNapA but only 16% for EcNhaA. Hits #4-6 are too short to be useful.

Fig S1. B-C) Predicted secondary structure of AtCHX17 aligned with known secondary structures of EcNhaA (B) or TtNapA (C).

The predicted secondary structure of CHX17 is aligned with the template sequence (EcNhaA or TtNapA) and the corresponding known secondary structure. The template predicted secondary structure is shown at bottom. Green refers to α-helices, and blue arrows indicate β-strands. Residues highlighted in gray are identical. Brown or yellow bars indicate gaps inserted in the bacteria or plant sequence, respectively. Residue number of AtCHX17 is shown on top, and template residue number is shown below.

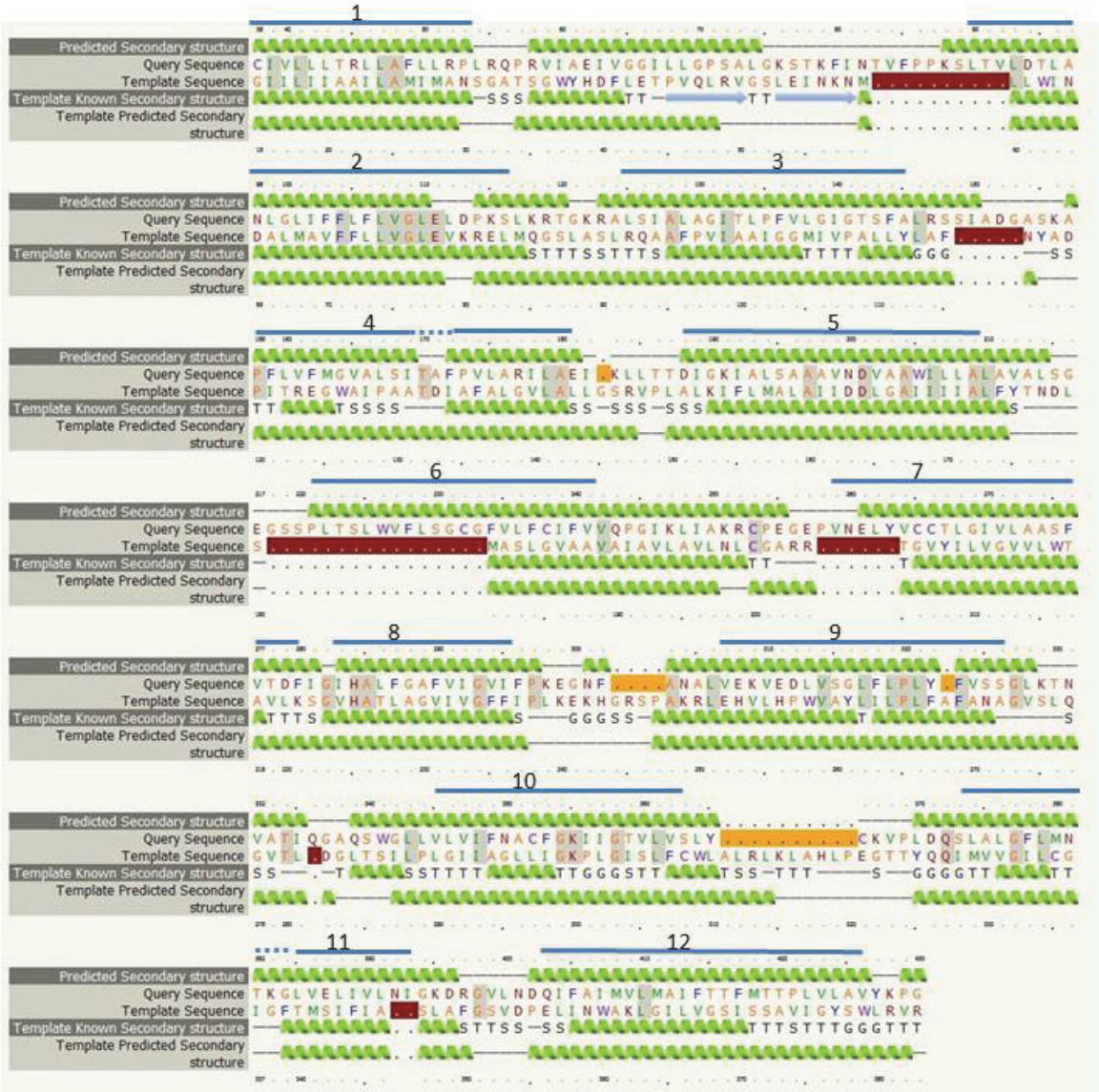
Predicted Secondary structure
Query Sequence
Template Sequence
Template Known Secondary structure
Template Predicted Secondary structure

Fig. III-S2. Alignment of AtCHX17 with CPA2 and CPA1 members show conserved and nonconserved residues. Sequences were aligned using MUSCLE.

A) CHX17 region from end of TM2 to TM5. D201 in AtCHX17 is conserved in all CPA members. E111 is conserved in CPA2 but not in CPA1. T170 is conserved as T or S in most

CPA, but adjacent residues vary.

B) AtCHX17 region from TM9 to TM11. K355 (blue) in TM10 is conserved as a K in most CPA2, but as an R in CPA1. K383 in the discontinuous helix of TM11 is less conserved. E311 or E308 in TM9 appears conserved in CPA2 but not CPA1.

Protein sequences correspond to AtCHX17 (At4g23700; 1-430), EcNhaA (BAB96592, 1-388),SynNhaS4 (NP_440311; 1-420), TtNapA (Q72IM4; 1-386) (Furrer et al., 2007), AtKEA1(At1g01790; 581-1000); AtKEA2 (O65272.2; At4g00630.1; 561-980) (Aranda-Sicilia et al.,2012); HsNha2 (NP_849155.2; 71-490) (Schushan et al., 2010), AtNHX1 (At5g27150; 1-448) PeNHX3 (Wang et al., 2014), and HsNHE1 (91-520; P19634.2). Acidic and basic residues are highlighted in red and blue, respectively. Olive green denotes polar uncharged residues S, T, N, Q, H, W; Light green refers to Y, and grey to C. Nonpolar residues are in yellow.

A

```
                    E111
AtCHX17 106 -FLVGLELDPKSLKRTGKRA------LSIALAGITLP----FVLGIGTSFALRSSIADGAS-- 155
ScKHA1  099 -FFLGLEVDIAFIKKHLKKA------LVIGIVTLAVPFGFGCLLAIPLFHTYANKTEGERHIK 154
AtKEA1  652 -FNIGLELSVERLSSMKKYV------FGLGSAQVLVT---AAVVG-LLAHYVAGQAG------ 697
AtKEA2  632 -FNIGLELSVERLSSMKKYV------FGLGSAQVLVT---AAVIG-LITHYVAGQAG------ 677
SyNhaS4 083 -FLVGLELNPQYLRQKLKVA------ILTSNVSIFFP----FVLGIVLSFFVLYSLNQPNKTS 134
TtNapA  069 -FMVGLETRLKDILAVGKEA------FLVAVLGVALP---------FLGGYLYGLEIGF---- 111
EcNhaA  074 --LVGLEVKREIMQGSLASLRQAAFPVIAAIGGMIVP----ALLYLAFNYADPITREGW---- 126
HsNHA2  186 -VRAGLGLDSKALKKLKGVC------VRLSMGPCIVE---ACTSA-LLAHYLLGLPWQW---- 233
AtNHX1  091 IFNAGFQVKKKQFFRNFVTI------MLFGAVGTIIS---CTIISLGVTQFFKKLDIGTF--- 141
PeNHX3  094 IFNAGFQVKKKQFFRNFMTI------ILFGAVGTLIC---CAIISIGAMQIFEKMDIGPL--- 144
HsNHE1  170 ILDAGYFLPLRQFTENLGTI------LIFAVVGTLWN---AFFLG-GLMYAVCLVGGEQINNI 222
                 *
            TM2                                TM3

                    T170                                D201
AtCHX17 156 KAPFLVFMGVALSITAFPVLARILAEIKLLTTD-IGKIALSAAAVNDVAAWILLALAVAL 214
ScKHA1  155 FSVFMVFIAVSISVTAFPVLCRILNELRLIKDR-AGIVVLAAGIINDIMGWILLALSIIL 213
AtKEA1  698 --PAAIVIGNGLALSSTAVVLQVLQERGESTSR-HGRASFSVLLFQDLAVVVLLILIPLI 754
AtKEA2  678 --PAAIVIGNGLALSSTAVVLQVLQERGESTSR-HGRATFSVLLFQDLAVVVLLILIPLI 734
SyNhaS4 135 FIPFALFIGAAMSITAFPVLARILKDTGLDKTP-LGTLGLTCASVDDISAWCLLAIAIAV 193
TtNapA  112 ETLPALFLGTALVATSVGITARVLQELGVLSRP-YSRIILGAAVIDDVLGLIVLAVVNGV 170
EcNhaA  127 ---------AIPAATDIAFALGVLALLGSRVPLALKIFLMALAIIDDLGAIIIIAL---- 173
HsNHA2  234 GFILGFVLGAVSPAVVVPSMLLLQGGGYGVEKG-VPTLLMAAGSFDDILAITGFNTCLGI 292
AtNHX1  142 DLGDYLAIGAIFAATDSVCTLQVLNQ--DETPL-LYSLVFGEGVVNDATSVVVFNAIQSF 198
PeNHX3  145 DIGDYLAIGAIFAATDSVCTLQVLSQ--DDTPL-LYSLVFGEGVVNDATSVVLFNAIQSF 201
HsNHE1  223 GLLDNLLFGSIISAVDPVAVLAVFEEI-HINEL-LHILVFGESLLNDAVTVVLYHLFEEF 190
                 *                                   *
            TM4a      TM4b                             TM5
```

B

```
                    E311
AtCHX17 299 EGNFANALVEKVE-DLV---SGLFLPLY-FVSSGLKT--NVATIQ-----GAQSWG 342
ScKHA1  300 DDHYVVKLTERME----DIPNIVFIPIY-FAVAGLNV--DLTLLN-----EGRDWG 343
AtKEA1  846 -----TEFSLQVE-SDIAPYRGLLLGLF-FMTVGMSI--DPKLLLS-------NFP 885
AtKEA2  826 -----TEFSLQVE-SDIAPYRGLLLGLF-FMTVGMSI--DPKLLLA-------NFP 865
SyNHaS4 277 NTNLSTELATKTE-DFV---STFLLPIF-FAYSGLST--DLGLLN----KPY-LWA 320
TtNaPA  251 -----VREKYRLE-EPIFAIESFLAPIF-FAMVGVRL--ELSALA----SPV-VLV 292
EcNHaA  240 KEKHGRSPAKRLE--HVLHPWVAYLILPLFAFANAGV--SLQGVT----LDGLTSI 287
HsNHA2  376 MGW--TSEKAEVE-KIIAVAWDIFQPLL-FGLIGAEV--SIASLR-----PE-TVG 419
AtNHX1  286 YTWHNVTESSRITTKHTFATLSFLAETFIFLYVGMDAL-DIDKWRSVSDTPGTSIA 340
PeNHX3  289 YTWHNVTESSRVTTKHAFATLSFVAEIFIFLYVGMDAL-DIEKWRFVSDSPGTSVA 343
HsNHE1  366 YVEANISHKSHTTIKYFLKMWSSVSETLIFIFLGVSTVAGSHHW---------NWT 412
                 *
            TM9

                    K355                                K383
AtCHX17 343 LLVLVIFNACFGKIIGTVLVSLY-CK---------VPLDQSLALGFLMNTKGLVELIVLNIGKDR- 397
ScKHA1  344 YVFATIGIAIFTKIISGTLTAKL-TG---------LFWREATAAGVLMSCKGIVEIVVLTVGLNA- 398
AtKEA1  886 VIVGTLGLLIVGKTMLVVIMGKL-FG---------ISIISAIRVGLLLAPGGEFAFVAFGEAVNQ- 940
AtKEA2  866 LIMGTLGLLLVGKTILVVIIGKL-FG---------ISIISAVRVGLLLAPGGEFAFVAFGEAVNQ- 920
SyNhaS4 321 VCALVVAAAIAGKYCGVYVTTRA-LG---------VEKQEAKALGWLMNTRGLTELIILNVGLKL- 375
TtNapA  293 AGTVVTVIAILGKVLGGFLGALT-QG-----------VRSALTVGVGMAPRGEVGLIVAALGLKA- 345
EcNhaA  288 LPLGIIAGLLIGKPLGISLFCWLALRLKLAHLPEGTTYQQIMVVGILCGIGFTMSIFIASLAF--- 350
HsNHA2  420 LCVATVGIAVLIRILTTFLMVCF-AG---------FNLKEKIFISFAWLPKATVQAAIGSVALDTA 475
AtNHX1  341 VSSILMGLVMVGRAAFVFPLSFL-SNLAKKNQSEKINFNMQVVIWWSGLMRGAVSMALAYNKFTRA 405
PeNHX3  344 VSSILLGLVMVGRAAFVFPLSFV-SNLSKKSPHEKIGFRQQFIIWWAGLMRGAVSMALAYNKFTSA 408
HsNHE1  413 FVISTLLFCLIARVLGVLGLTWF-IN---KFRIVKLTPKDQFIIAYGGL-RGAIAFSLGYLLDKK- 472
            TM10                                TM11a     TM11b
```

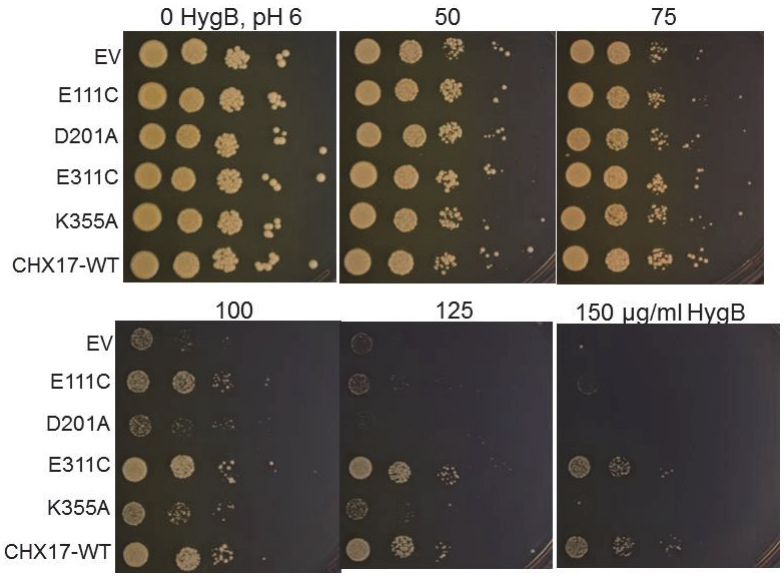

Fig. III-S3. Effect of HygB concentration on yeast carrying wild-type or mutated CHX17. Mutations at CHX17 residues E111, D201, and K355 reduced yeast tolerance to HygB. Yeast strain KTA40-2 carrying the pYES-DEST52 empty vector (EV) or vector with either a mutated or wild-type CHX17 were prepared as described in Methods. Ten-fold serial dilutions were prepared. Five µl of each dilution was spotted onto YNB(A) media, pH 6.0 with indicated concentrations of HygB. After 3 d incubation at 30°C, CHX17-WT and the E311C mutation both conferred yeast tolerance to HygB at 100-150 µg/ml. The E111C mutation conferred yeast tolerance at 100 µg/ml HygB.

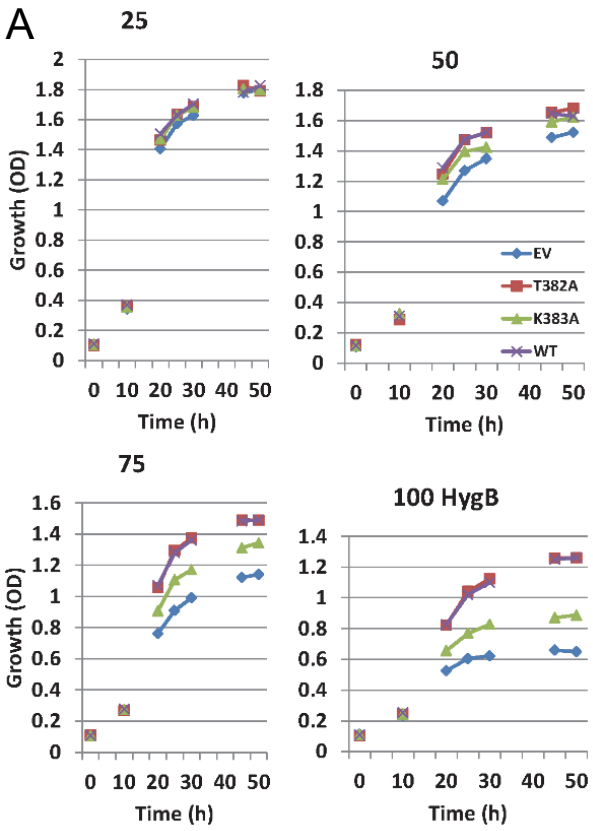

Fig. III-S4. Effect of HygB concentration on the time-course of yeast growth in liquid medium. A) CHX17-K383A inhibited growth, but T382A had no effect.

Yeast strain KTA40-2 was transformed with an empty vector (EV), CHX17-T382A, CHX17-K383A, or CHX17-WT. Normalized yeast cultures were grown in medium with or without HygB at 0-100 µg/ml at 30°C. The OD readings of the liquid cultures were tested at 7 time points over approximately 55 h. CHX-dependent growth was calculated by subtracting OD of yeast harboring vector only. HygB tolerant growth is optimal at 100 µg/ml. The figures show a representative experiment, and the results were highly reproducible in 3 trials with 6 independent transformants.

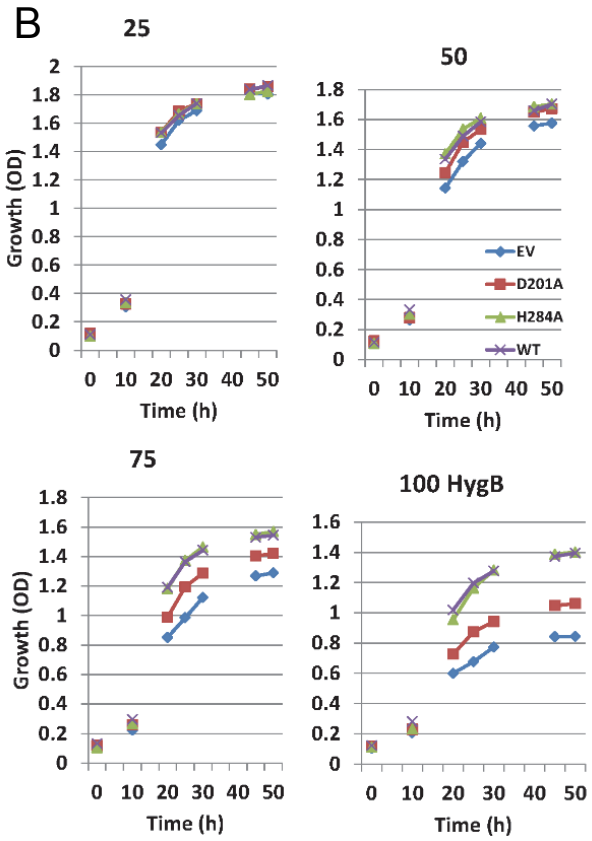

Fig. III-S4. B) CHX17-D201A inhibited HygB tolerant yeast growth, but H284A had no effect. Yeast strain KTA40-2 was transformed with an empty vector (EV), CHX17-D201A, CHX17-H284A, or CHX17-WT. Normalized yeast cultures were grown and assayed as described for Figure S4A. Yeast expressing CHX17-H284A grew similar to yeast expressing CHX17-WT. Yeast expressing CHX17-D201A showed reduced growth. The figures show a representative experiment, and the results were highly reproducible among 3 trials with 6 independent transformants.

Fig. III-S5: CHX17-GFP signal was observed in yeast. KTA40-2 yeast expressing wild-type CHX17-GFP, a mutated CHX17-GFP, or carrying an empty vector was grown in enriched medium minus uracil. An aliquot was observed on a multi-well microscope slide with a Nikon E600 fluorescence microscope using a 100x objective lens with either a white light or a blue light filter set. Results show yeast carrying wild-type (A) or mutated CHX17 (B to O) exhibit green fluorescence at the cell periphery and in the perinuclear region. Yeast carrying the empty vector (P) lack any GFP fluorescence.

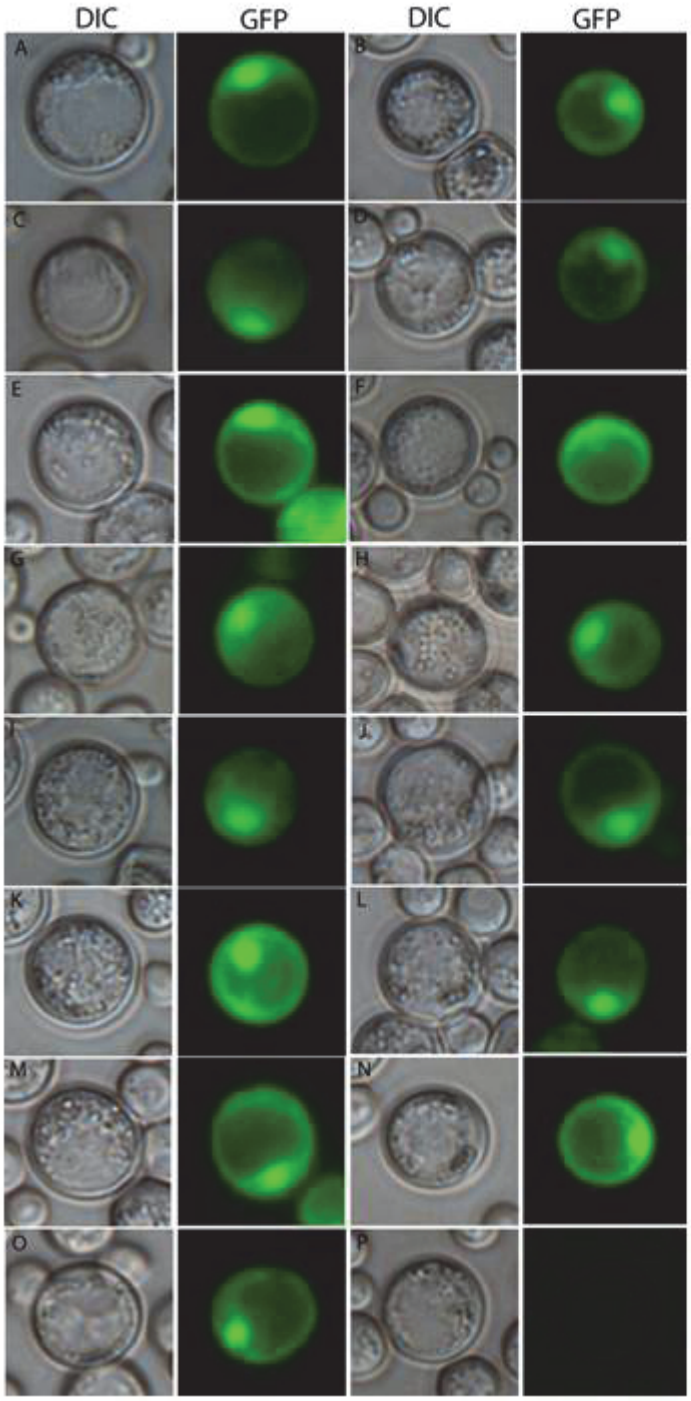

A. WT CHX17-GFP

B. E111C_CHX17-GFP

C. T170A_CHX17-GFP

D. N200D_CHX17-GFP

E. D201A_CHX17-GFP

F. D201E_CHX17-GFP

G. D201N_CHX17-GFP

H. H284A_CHX17-GFP

I. K355A_CHX17-GFP

J. K355Q_CHX17-GFP

K. K355R_CHX17-GFP

L. K383A_CHX17-GFP

M. C458A_CHX17-GFP

N. C562A_CHX17-GFP

O. C607A_CHX17-GFP

P. Empty vector

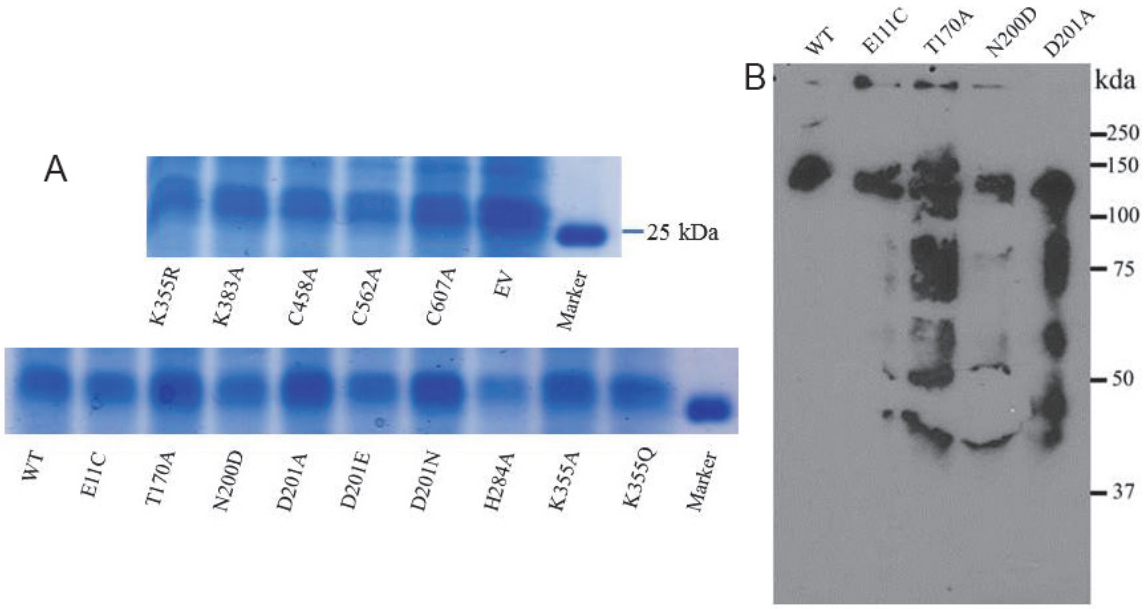

Fig. III-S6. Total protein extracted from yeast cultures contained a GFP tag. A) Protein extracted from yeast carrying WT or mutated CHX17 showed equivalent loading in a Coomassie-stained gel. **B)** An anti-GFP Western blot shows an immunoreactive band at 130 kDa in protein extracted from WT or various mutated CHX17. Smaller mass bands are likely partial degradative products tagged with GFP.

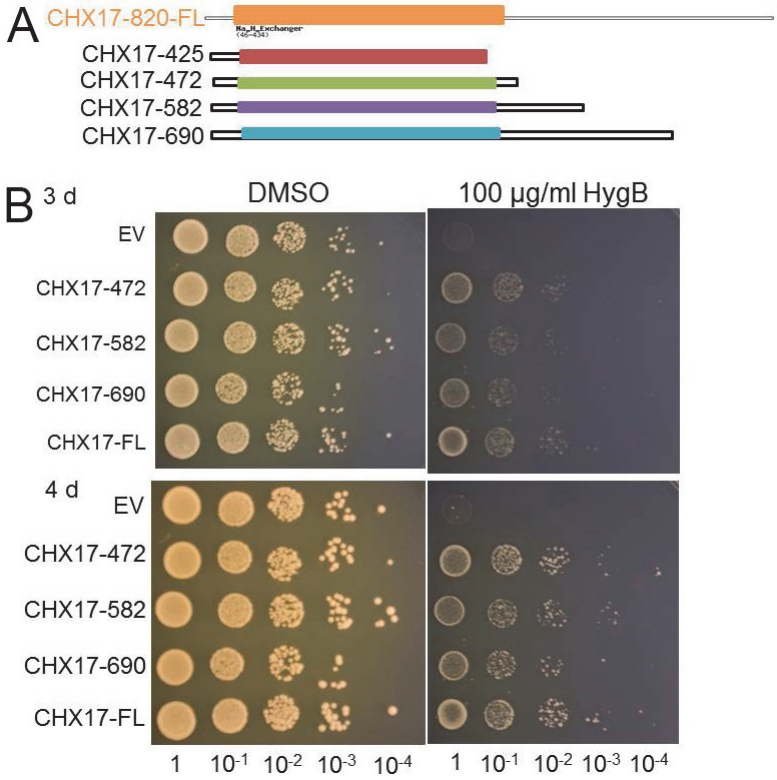

Fig. III-S7: Testing the role of the CHX17 hydrophilic C-tail on activity. A) Diagram of CHX17 C-tail truncations. The TM domain is shown as a colored box and the C-tail as a white box. The numbers listed indicate the last amino acid in each C-tail truncation. Truncations were constructed by PCR-amplifying the respective segments of the CHX17 cDNA and inserting the shortened cDNA into an *E. coli* expression vector using recombination cloning. Successful recombination was verified by PCR using CHX17-specific primers. **B)** CHX17 C-tail truncation has no effect on yeast tolerance to HygB. Yeast strain KTA40-2 carrying the pYES-DEST52 empty vector (EV) or transformed with either CHX17-WT or the indicated CHX17 C-tail truncation were grown in liquid culture, washed, and diluted ten-fold as described for Figure S3. Five µl of each dilution was spotted onto YNB(A) media at pH 6.0 with 100 µg/ml HygB or DMSO as a loading control. The results show full-length WT CHX17 conferred yeast tolerance to HygB. CHX17 with three C-tail truncations after residues 472, 582, or 690 showed similar activity. Results are representative of 5 experiments.

#	Template	Alignment Coverage	3D Model	Confidence	% i.d.	Template Information
1	c3mt0A_	Alignment		98.8	15	**PDB header:**structural genomics, unknown function **Chain:** A: **PDB Molecule:**uncharacterized protein pa1789; **PDBTitle:** the crystal structure of a functionally unknown protein pa1789 from2 pseudomonas aeruginosa pao1
2	c3logA_	Alignment		98.7	12	**PDB header:**structure genomics, unknown function **Chain:** A: **PDB Molecule:**universal stress protein; **PDBTitle:** the crystal structure of a universal stress protein from archaeoglobus2 fulgidus dsm 4304
3	c3ab8B_	Alignment		98.5	12	**PDB header:**unknown function **Chain:** B: **PDB Molecule:**putative uncharacterized protein ttha0350; **PDBTitle:** crystal structure of the hypothetical tandem-type universal stress2 protein ttha0350 complexed with atps.
4	c3olgA_	Alignment		98.0	11	**PDB header:**structural genomics, unknown function **Chain:** A: **PDB Molecule:**universal stress protein e; **PDBTitle:** the crystal structure of a universal stress protein e from proteus2 mirabilis hi4320

Fig. III-S8. Phyre2 search results for the CHX17-C tail show top hits with several universal stress proteins or USP-like domains. The template PDB numbers are shown at left. Alignment of CHX17 (residues 431-820, white line) to template (red) is shown. Red color under 'confidence' indicates the probability for a similar protein fold is over 95%. The protein identity is 16% or less for crystal structures of tandem-type USPs, including *Pseudomonas aeruginosa* pao1 (protein of unknown function), and other archaeal and bacterial USPs.

REFERENCES

Andres, Z., Perez-Hormaeche, J., Leidi, E.O., Schlucking, K., Steinhorst, L., McLachlan, D.H., Schumacher, K., Hetherington, A.M., Kudla, J., Cubero, B., and Pardo, J.M. (2014). Control of vacuolar dynamics and regulation of stomatal aperture by tonoplast potassium uptake. *Proc. Nat. Acad. Sci. USA*. **111,** E1806-E1814.

Arabidopsis Genome Initiative. (2000). Analysis of the genome sequence of the flowering plant Arabidopsis thaliana. *Nature.* **408,** 796-815.

Aranda-Sicilia, M.N., Cagnac, O., Chanroj, S., Sze, H., Rodriguez-Rosales, M.P., and Venema, K. (2012). Arabidopsis KEA2, a homolog of bacterial KefC, encodes a K^+/H^+ antiporter with a chloroplast transit peptide. *BBA-Biomembranes*. **1818,** 2362-2371.

Arkin, I.T., Xu, H.F., Jensen, M.O., Arbely, E., Bennett, E.R., Bowers, K.J., Chow, E., Dror, R.O., Eastwood, M.P., Flitman-Tene, R., Gregersen, B.A., Klepeis, J.L., Kolossvary, I., Shan, Y.B., and Shaw, D.E. (2007). Mechanism of Na^+/H^+ antiporting. *Science*. **317,** 799-803.

Bak, G., Lee, E.J., Lee, Y., Kato, M., Segami, S., Sze, H., Maeshima, M., and Hwang, J.U. (2013). Rapid Structural Changes and Acidification of Guard Cell Vacuoles during Stomatal Closure Require Phosphatidylinositol 3,5-Bisphosphate. *Plant Cell*. **25,** 2202-2216.

Bassil, E., Coku, A., and Blumwald, E. (2012). Cellular ion homeostasis: emerging roles of intracellular NHX Na^+/H^+ antiporters in plant growth and development. *J. Exp. Bot*. **63,** 5727-5740.

Beale, K.M., and Johnson, M.A. (2013). Speed dating, rejection, and finding the perfect mate: advice from flowering plants. *Curr. Opin. Plant Biol*. **16,** 590-597.

Berger, F. (2003). Endosperm: the crossroad of seed development. *Curr. Opin. Plant Biol*. **6,** 42-50.

Berger, F. (2011). Imaging fertilization in flowering plants, not so abominable after all. *J. Exp. Bot*. **62,** 1651-1658.

Berger, F., and Twell, D. (2011). Germline Specification and Function in Plants. *Annu Rev. Plant Biol.* **62,** 461-484.

Berger, F., Grini, P.E., and Schnittger, A. (2006). Endosperm: an integrator of seed growth and development. *Curr. Opin. Plant Biol*. **9,** 664-670.

Berleth, T., and Jurgens, G. (1993). The role of the *MONOPTEROS* gene in organizing the basal body region of the *Arabidopsis* embryo. *Development*. **118,** 575-587.

Boavida, L.C., and McCormick, S. (2007). Temperature as a determinant factor for increased and reproducible in vitro pollen germination in *Arabidopsis thaliana*. *Plant J*. **52,** 570-582.

Bock, K.W., Honys, D., Ward, J.M., Padmanaban, S., Nawrocki, E.P., Hirschi, K.D., Twell, D., and Sze, H. (2006). Integrating membrane transport with male gametophyte development and function through transcriptomics. *Plant Physiol*. **140,** 1151-1168.

Boisson-Dernier, A., Lituiev, D.S., Nestorova, A., Franck, C.M., Thirugnanarajah, S., and Grossniklaus, U. (2013). ANXUR receptor-like kinases coordinate cell

wall integrity with growth at the pollen tube tip via NADPH oxidases. *PLoS Biol*. **11,** e1001719.

Boisson-Dernier, A., Roy, S., Kritsas, K., Grobei, M.A., Jaciubek, M., Schroeder, J.I., and Grossniklaus, U. (2009). Disruption of the pollen-expressed *FERONIA* homologs *ANXUR1* and *ANXUR2* triggers pollen tube discharge. *Development*. **136,** 3279-3288.

Borges, F., Gomes, G., Gardner, R., Moreno, N., McCormick, S., Feijo, J.A., and Becker, J.D. (2008). Comparative transcriptomics of *Arabidopsis* sperm cells. *Plant Physiol*. **148,** 1168-1181.

Boudker, O., and Verdon, G. (2010). Structural perspectives on secondary active transporters. Trends in Pharmacological Sciences **31,** 418-426.

Brett, C.L., Donowitz, M., and Rao, R. (2005). Evolutionary origins of eukaryotic sodium/proton exchangers. *Am. J. Physiol.-Cell Physiol*. **288,** C223-C239.

Brodersen, D.E., Clemons, W.M., Carter, A.P., Morgan-Warren, R.J., Wimberly, B.T., and Ramakrishnan, V. (2000). The structural basis for the action of the antibiotics tetracycline, pactamycin, and hygromycin B on the 30S ribosomal subunit. *Cell*. **103,** 1143-1154.

Calinescu, O., Paulino, C., Kuhlbrandt, W., and Fendler, K. (2014). Keeping It Simple, Transport Mechanism and pH Regulation in Na^+/H^+ Exchangers. *J. Biol. Chem*. **289,** 13168-13176.

Capron, A., Chatfield, S., Provart, N., and Berleth, T. (2009). Embryogenesis: pattern formation from a single cell. *Arabidopsis Book*. **7,** e0126.

Casey, J.R., Grinstein, S., and Orlowski, J. (2010). Sensors and regulators of intracellular pH. *Nat. Rev. Mol. Cell Biol*. **11,** 50-61.

Cellier, F., Conejero, G., Ricaud, L., Luu, D.T., Lepetit, M., Gosti, F., and Casse, F. (2004). Characterization of AtCHX17, a member of the cation/H^+ exchangers, CHX family, from *Arabidopsis thaliana* suggests a role in K^+ homeostasis. *Plant J*. **39,** 834-846.

Chanroj, S. (2011). Plant-specific K^+ transporters with distinct properties and their emerging roles in endomembrane trafficking. College Park, MD: University of Maryland, pp. 254.

Chanroj, S., Padmanaban, S., Czerny, D.D., Jauh, G.Y., and Sze, H. (2013). K^+ transporter AtCHX17 with its hydrophilic C tail localizes to membranes of the secretory/endocytic system: role in reproduction and seed set. *Mol. Plant*. **6,** 1226-1246.

Chanroj, S., Wang, G., Venema, K., Zhang, M.W., Delwiche, C.F., and Sze, H. (2012). Conserved and diversified gene families of monovalent cation/H^+ antiporters from algae to flowering plants. *Front. Plant. Sci*. **3,** 25.

Chanroj, S., Lu, Y., Padmanaban, S., Nanatani, K., Uozumi, N., Rao, R., and Sze, H. (2011). Plant-specific cation/H^+ exchanger 17 and its homologs are endomembrane K^+ transporters with roles in protein sorting. *J. Biol. Chem*. **286,** 33931-33941.

Cheung, A.Y., and Wu, H.M. (2008). Structural and signaling networks for the polar cell growth machinery in pollen tubes. *Annu. Rev. Plant Biol*. **59,** 547-572.

Costa, L.M., Marshall, E., Tesfaye, M., Silverstein, K.A.T., Mori, M., Umetsu, Y., Otterbach, S.L., Papareddy, R., Dickinson, H.G., Boutiller, K.,

VandenBosch, K.A., Ohki, S., and Gutierrez-Marcos, J.F. (2014). Central Cell-Derived Peptides Regulate Early Embryo Patterning in Flowering Plants. *Science*. **344,** 168-172.

Cove, D.J., and Knight, C.D. (1993). The moss *Physcomitrella patens*, a model system with the potential for the study of plant reproduction. *Plant Cell*. **5,** 1483-1488.

Cuming, A.C., Cho, S.H., Kamisugi, Y., Graham, H., and Quatrano, R.S. (2007). Microarray analysis of transcriptional responses to abscisic acid and osmotic, salt, and drought stress in the moss, *Physcomitrella patens*. *New Phytol*. **176,** 275-287.

Dresselhaus, T., and Franklin-Tong, N. (2013). Male-Female Crosstalk during Pollen Germination, Tube Growth and Guidance, and Double Fertilization. *Mol. Plant*. **6,** 1018-1036.

Edgar, R.C. (2004). MUSCLE: multiple sequence alignment with high accuracy and high throughput. *Nuc. Acids Res*. **32,** 1792-1797.

Edlund, A.F., Swanson, R., and Preuss, D. (2004). Pollen and stigma structure and function: The role of diversity in pollination. *Plant Cell*. **16,** S84-S97.

Edwards, K., Johnstone, C., and Thompson, C. (1991). A simple and rapid method for the preparation of plant genomic DNA for PCR analysis. *Nuc. Acids Res*. **19,** 1349-1349.

Escobar-Restrepo, J.M., Huck, N., Kessler, S., Gagliardini, V., Gheyselinck, J., Yang, W.C., and Grossniklaus, U. (2007). The *FERONIA* receptor-like kinase mediates male-female interactions during pollen tube reception. *Science*. **317,** 656-660.

Fernando, D.D., Lazzaro, M.D., and Owens, J.N. (2005). Growth and development of conifer pollen tubes. *Sex. Plant Repro*. **18,** 149-162.

Freeman, S. (2008). Biological Science. New York City: Benjamin Cummings, pp. 416.

Forrest, L.R., Kramer, R., and Ziegler, C. (2011). The structural basis of secondary active transport mechanisms. *BBA-Bioenergetics*. **1807,** 167-188.

Furrer, E.M., Ronchetti, M.F., Verrey, F., and Pos, K.M. (2007). Functional characterization of a NapA Na^+/H^+ antiporter from Thermus thermophilus. *FEBS Lett*. **581,** 572-578.

Gerchman, Y., Olami, Y., Rimon, A., Taglicht, D., Schuldiner, S., and Padan, E. (1993). Histidine-226 is part of the pH-sensor of NhaA, a Na^+/H^+ antiporter in *Escherichia coli*. *Proc. Nat. Acad. Sci. USA*. **90,** 1212-1216.

Gietz, R.D., and Schiestl, R.H. (2007). Frozen competent yeast cells that can be transformed with high efficiency using the LiAc/SS carrier DNA/PEG method. *Nat. Protoc*. **2,** 1-4.

Hamamura, Y., Saito, C., Awai, C., Kurihara, D., Miyawaki, A., Nakagawa, T., Kanaoka, M.M., Sasaki, N., Nakano, A., Berger, F., and Higashiyama, T. (2011). Live-Cell Imaging Reveals the Dynamics of Two Sperm Cells during Double Fertilization in *Arabidopsis thaliana*. *Curr. Biol*. **21,** 497-502.

Higashiyama, T., Yabe, S., Sasaki, N., Nishimura, Y., Miyagishima, S., Kuroiwa, H., and Kuroiwa, T. (2001). Pollen tube attraction by the synergid cell. *Science*. **293,** 1480-1483.

Heermann, R., Weber, A., Mayer, B., Ott, M., Hauser, E., Gabriel, G., Pirch, T., and Jung, K. (2009). The Universal Stress Protein UspC Scaffolds the KdpD/KdpE

Signaling Cascade of *Escherichia coli* under Salt Stress. *J. Mol. Biol*. **386,** 134-148.

Herz, K., Rimon, A., Olkhova, E., Kozachkov, L., and Padan, E. (2010). Transmembrane Segment II of NhaA Na^+/H^+ Antiporter Lines the Cation Passage, and Asp65 Is Critical for pH Activation of the Antiporter. *J. Biol. Chem*. **285,** 2211-2220.

Honys, D., and Twell, D. (2003). Comparative analysis of the *Arabidopsis* pollen transcriptome. *Plant Physiol*. **132,** 640-652.

Honys, D., and Twell, D. (2004). Transcriptome analysis of haploid male gametophyte development in *Arabidopsis*. *Genome Biol*. **5,** 13.

Hu, N.J., Iwata, S., Cameron, A.D., and Drew, D. (2011). Crystal structure of a bacterial homologue of the bile acid sodium symporter ASBT. *Nature*. **478,** 408-411.

Huck, N., Moore, J.M., Federer, M., and Grossniklaus, U. (2003). The *Arabidopsis* mutant *feronia* disrupts the female gametophytic control of pollen tube reception. *Development*. **130,** 2149-2159.

Hunte, C., Screpanti, E., Venturi, M., Rimon, A., Padan, E., and Michel, H. (2005). Structure of a Na^+/H^+ antiporter and insights into mechanism of action and regulation by pH. *Nature*. **435,** 1197-1202.

Inoue, H., Noumi, T., Tsuchiya, T., and Kanazawa, H. (1995). Essential aspartic acid residues Asp-133, Asp-163 and Asp-164, in the transmembrane helices of a Na^+/H^+ antiporter (NhaA) from *Escherichia coli*. Febs Letters **363,** 264-268.

Kelley, L.A., and Sternberg, M.J.E. (2009). Protein structure prediction on the Web: a case study using the Phyre server. *Nat. Protoc*. **4,** 363-371.

Kerk, D., Bulgrien, J., Smith, D.W., and Gribskov, M. (2003). *Arabidopsis* proteins containing similarity to the universal stress protein domain of bacteria. *Plant Physiol*. **131,** 1209-1219.

Kozachkov, L., Herz, K., and Padan, E. (2007). Functional and structural interactions of the transmembrane domain X of NhaA, Na^+/H^+ antiporter of *Escherichia coli*, at physiological pH. *Biochemistry*. **46,** 2419-2430.

Krishnamurthy, H., Piscitelli, C.L., and Gouaux, E. (2009). Unlocking the molecular secrets of sodium-coupled transporters. *Nature*. **459,** 347-355.

Krulwich, T.A., Sachs, G., and Padan, E. (2011). Molecular aspects of bacterial pH sensing and homeostasis. *Nat. Rev. Microbiol*. **9,** 330-343.

Kvint, K., Nachin, L., Diez, A., and Nystrom, T. (2003). The bacterial universal stress protein: function and regulation. *Curr. Opin. Microbiol*. **6,** 140-145.

Lau, S., Slane, D., Herud, O., Kong, J.X., and Jurgens, G. (2012). Early Embryogenesis in Flowering Plants: Setting Up the Basic Body Pattern. *Annu. Rev. Plant Biol*. **63,** 483-506.

Le, B.H., Cheng, C., Bui, A.Q., Wagmaister, J.A., Henry, K.F., Pelletier, J., Kwong, L., Belmonte, M., Kirkbride, R., Horvath, S., Drews, G.N., Fischer, R.L., Okamuro, J.K., Harada, J.J., and Goldberg, R.B. (2010). Global analysis of gene activity during *Arabidopsis* seed development and identification of seed-specific transcription factors. *Proc. Nat. Acad. Sci. USA*. **107,** 8063-8070.

Lee, C., Kang, H.J., von Ballmoos, C., Newstead, S., Uzdavinys, P., Dotson, D.L., Iwata, S., Beckstein, O., Cameron, A.D., and Drew, D. (2013). A two-domain elevator mechanism for sodium/proton antiport. *Nature*. **501,** 573-577.

Lee, C., Yashiro, S., Dotson, D.L., Uzdavinys, P., Iwata, S., Sansom, M.S.P., von Ballmoos, C., Beckstein, O., Drew, D., and Cameron, A.D. (2014). Crystal structure of the sodium-proton antiporter NhaA dimer and new mechanistic insights. *J. Gen. Physiol*. **144,** 529-544.

Lehti-Shiu, M.D., Zou, C., Hanada, K., and Shiu, S.H. (2009). Evolutionary History and Stress Regulation of Plant Receptor-Like Kinase/Pelle Genes. *Plant Physiol*. **150,** 12-26.

Li, X. (2006). The importance of sorting calcium in plant cells: uncovering the roles of a sarcoplasmic/endoplasmic reticulum-like calcium ATPase. College Park, MD: University of Maryland, pp. 219.

Li, X.Y., Chanroj, S., Wu, Z.Y., Romanowsky, S.M., Harper, J.F., and Sze, H. (2008). A distinct endosomal Ca^{2+}/Mn*2*+ pump affects root growth through the secretory process. *Plant Physiol*. **147,** 1675-1689.

Liu, Y.J., Tewari, R., Ning, J., Blagborough, A.M., Garbom, S., Pei, J.M., Grishin, N.V., Steele, R.E., Sinden, R.E., Snell, W.J., and Billker, O. (2008). The conserved plant sterility gene HAP2 functions after attachment of fusogenic membranes in *Chlamydomonas* and *Plasmodium* gametes. *Genes Dev*. **22,** 1051-1068.

Lu, Y.X., Chanroj, S., Zulkifli, L., Johnson, M.A., Uozumi, N., Cheung, A., and Sze, H. (2011). Pollen Tubes Lacking a Pair of K^+ Transporters Fail to Target Ovules in *Arabidopsis*. *Plant Cell*. **23,** 81-93.

Maeder, M.L., Thibodeau-Beganny, S., Sander, J.D., Voytas, D.F., and Joung, J.K. (2009). Oligomerized pool engineering (OPEN): an 'open-source' protocol for making customized zinc-finger arrays. *Nat. Protoc*. **4,** 1471-1501.

Maresova, L., and Sychrova, H. (2005). Physiological characterization of *Saccharomyces cerevisiae kha1* deletion mutants. *Mol. Microbiol*. **55,** 588-600.

Maresova, L., and Sychrova, H. (2006). *Arabidopsis thaliana CHX17* gene complements the *kha1* deletion phenotypes in *Saccharomyces cerevisiae*. *Yeast*. **23,** 1167-1171.

Martiniere, A., Bassil, E., Jublanc, E., Alcon, C., Reguera, M., Sentenac, H., Blumwald, E., and Paris, N. (2013). In Vivo Intracellular pH Measurements in Tobacco and *Arabidopsis* Reveal an Unexpected pH Gradient in the Endomembrane System. *Plant Cell*. **25,** 4028-4043.

Maser, P., Thomine, S., Schroeder, J.I., Ward, J.M., Hirschi, K., Sze, H., Talke, I.N., Amtmann, A., Maathuis, F.J.M., Sanders, D., Harper, J.F., Tchieu, J., Gribskov, M., Persans, M.W., Salt, D.E., Kim, S.A., and Guerinot, M.L. (2001). Phylogenetic relationships within cation transporter families of *Arabidopsis*. *Plant Physiol*. **126,** 1646-1667.

McCormick, S. (2004). Control of male gametophyte development. *Plant Cell*. **16,** S142-S153.

Mori, T., Kuroiwa, H., Higashiyama, T., and Kuroiwa, T. (2006). GENERATIVE CELL SPECIFIC 1 is essential for angiosperm fertilization. *Nat. Cell Biol*. **8,** 64-71.

Mori, T., Igawa, T., Tamiya, G., Miyagishima, S., and Berger, F. (2014). Gamete Attachment Requires GEX2 for Successful Fertilization in *Arabidopsis*. *Curr. Biol*. **24,** 170-175.

Mottaleb, S.A., Rodriguez-Navarro, A., and Haro, R. (2013). Knockouts of *Physcomitrella patens* CHX1 and CHX2 Transporters Reveal High Complexity of Potassium Homeostasis. *Plant Cell Physiol*. **54,** 1455-1468.

Okuda, S., Tsutsui, H., Shiina, K., Sprunck, S., Takeuchi, H., Yui, R., Kasahara, R.D., Hamamura, Y., Mizukami, A., Susaki, D., Kawano, N., Sakakibara, T., Namiki, S., Itoh, K., Otsuka, K., Matsuzaki, M., Nozaki, H., Kuroiwa, T., Nakano, A., Kanaoka, M.M., Dresselhaus, T., Sasaki, N., and Higashiyama, T. (2009). Defensin-like polypeptide LUREs are pollen tube attractants secreted from synergid cells. *Nature.* **458,** 357-361.

Orlowski, J., and Grinstein, S. (2007). Emerging roles of alkali cation/proton exchangers in organellar homeostasis. *Curr. Opin. Cell Biol*. **19,** 483-492.

Padan, E. (2008). The enlightening encounter between structure and function in the NhaA Na^+/H^+ antiporter. *Trends Biochem. Sci*. **33,** 435-443.

Padan, E. (2014). Functional and structural dynamics of NhaA, a prototype for Na^+ and H^+ antiporters, which are responsible for Na^+ and H^+ homeostasis in cells. *BBA-Bioenergetics*. **1837,** 1047-1062.

Padmanaban, S., Chanroj, S., Kwak, J.M., Li, X., Ward, J.M., and Sze, H. (2007). Participation of endomembrane cation/H^+ exchanger AtCHX20 in osmoregulation of guard cells. *Plant Physiol*. **144,** 82-93.

Patel, H., and Barber, D.L. (2005). A developmentally regulated Na-H exchanger in *Dictyostelium discoideum* is necessary for cell polarity during chemotaxis. *J. Cell Biol*. **169,** 321-329.

Peterson, K.M., Rychel, A.L., and Torii, K.U. (2010). Out of the Mouths of Plants: The Molecular Basis of the Evolution and Diversity of Stomatal Development. *Plant Cell*. **22,** 296-306.

Popper, Z.A., Michel, G., Herve, C., Domozych, D.S., Willats, W.G.T., Tuohy, M.G., Kloareg, B., and Stengel, D.B. (2011). Evolution and Diversity of Plant Cell Walls: From Algae to Flowering Plants. *Annu. Rev. Plant Biol*. **62,** 567-588.

Qin, Y., and Yang, Z.B.A. (2011). Rapid tip growth: Insights from pollen tubes. *Sem. Cell Dev. Biol*. **22,** 816-824.

Qin, Y., Leydon, A.R., Manziello, A., Pandey, R., Mount, D., Denic, S., Vasic, B., Johnson, M.A., and Palanivelu, R. (2009). Penetration of the Stigma and Style Elicits a Novel Transcriptome in Pollen Tubes, Pointing to Genes Critical for Growth in a Pistil. *PLoS Genet*. **5,** e1000621.

Quatrano, R.S., McDaniel, S.F., Khandelwal, A., Perroud, P.F., and Cove, D.J. (2007). *Physcomitrella patens*: mosses enter the genomic age. *Curr. Opin. Plant Biol*. **10,** 182-189.

Rimon, A., Gerchman, Y., Kariv, Z., and Padan, E. (1998). A point mutation (G338S) and its suppressor mutations affect both the pH response of the NhaA Na^+/H^+ antiporter as well as the growth phenotype of *Escherichia coli*. *J. Biol. Chem*. **273,** 26470-26476.

Robinson, D.G., Jiang, L.W., and Schumacher, K. (2008). The endosomal system of plants: Charting new and familiar territories. *Plant Physiol*. **147,** 1482-1492.

Sanders, P.M., Lee, P.Y., Biesgen, C., Boone, J.D., Beals, T.P., Weiler, E.W., and Goldberg, R.B. (2000). The *Arabidopsis* DELAYED DEHISCENCE1 gene encodes an enzyme in the jasmonic acid synthesis pathway. *Plant Cell*. **12,** 1041-1061.

Schmid, M.W., Schmidt, A., Klostermeier, U.C., Barann, M., Rosenstiel, P., and Grossniklaus, U. (2012). A Powerful Method for Transcriptional Profiling of Specific Cell Types in Eukaryotes: Laser-Assisted Microdissection and RNA Sequencing. *PLoS One*. **7**, e29685.

Schushan, M., Xiang, M.H., Bogomiakov, P., Padan, E., Rao, R., and Ben-Tal, N. (2010). Model-Guided Mutagenesis Drives Functional Studies of Human NHA2, Implicated in Hypertension. *J. Mol. Biol*. **396,** 1181-1196.

Schwacke, R., Schneider, A., van der Graaff, E., Fischer, K., Catoni, E., Desimone, M., Frommer, W.B., Flugge, U.I., and Kunze, R. (2003). ARAMEMNON, a novel database for *Arabidopsis* integral membrane proteins. *Plant Physiol*. **131,** 16-26.

Schweikhard, E.S., Kuhlmann, S.I., Kunte, H.J., Grammann, K., and Ziegler, C.M. (2010). Structure and Function of the Universal Stress Protein TeaD and Its Role in Regulating the Ectoine Transporter TeaABC of *Halomonas elongata* DSM 2581(T). *Biochemistry*. **49,** 2194-2204.

Screpanti, E., and Hunte, C. (2007). Discontinuous membrane helices in transport proteins and their correlation with function. *J. Struc. Biol*. **159,** 261-267.

Shen, J.B., Zeng, Y.L., Zhuang, X.H., Sun, L., Yao, X.Q., Pimpl, P., and Jiang, L.W. (2013). Organelle pH in the *Arabidopsis* Endomembrane System. *Mol. Plant*. **6,** 1419-1437.

Shi, H.Z., Quintero, F.J., Pardo, J.M., and Zhu, J.K. (2002). The putative plasma membrane $Na^{+/}H^{+}$ antiporter SOS1 controls long-distance Na^{+} transport in plants. *Plant Cell*. **14,** 465-477.

Sieburth, L.E., and Deyholos, M.K. (2006). Vascular development: the long and winding road. *Curr. Opin. Plant Biol*. **9,** 48-54.

Smyth, D.R., Bowman, J.L., and Meyerowitz, E.M. (1990). Early flower development in *Arabidopsis*. *Plant Cell*. **2,** 755-767.

Soto, G., Alleva, K., Mazzella, M.A., Amodeo, G., and Muschietti, J.P. (2008). AtTIP1;3 and AtTIP5;1, the only highly expressed *Arabidopsis* pollen-specific aquaporins, transport water and urea. *FEBS Lett*. **582,** 4077-4082.

Sprunck, S., Rademacher, S., Vogler, F., Gheyselick, J., Grossniklaus, U., and Dresselhaus, T. (2012). Egg Cell-Secreted EC1 Triggers Sperm Cell Activation During Double Fertilization. *Science*. **338,** 1093-1097.

Sundaresan, V., and Alandete-Saez, M. (2010). Pattern formation in miniature: the female gametophyte of flowering plants. *Development*. **137,** 179-189.

Sze, H. (1985). H^{+}-translocating ATPases – advances using membrane vesicles. *Annu. Rev. Plant Physiol. Plant Mol. Biol*. **36,** 175-208.

Sze, H., Padmanaban, S., Cellier, F., Honys, D., Cheng, N.H., Bock, K.W., Conéjéro, G., Li, X., Twell, D., Ward, J.M., and Hirschi, K.D. (2004). Expression patterns of a novel *AtCHX* gene family highlight potential roles in osmotic adjustment and K^{+} homeostasis in pollen development. *Plant Physiol*. **136,** 2532-2547.

Taglicht, D., Padan, E., and Schuldiner, S. (1991a). Overproduction and purification of a functional Na^+/H^+ antiporter coded by *nhaA* (*ant*) from *Escherichia coli*. *J. Biol. Chem*. **266,** 11289-11294.

Taglicht, D., Padan, E., and Schuldiner, S. (1991b). Overproduction and purification of a functional Na^+/H^+ antiporter coded by *nhaA* (*ant*) from *Escherichia coli*. *J. Biol. Chem*. **266,** 11289-11294.

Takeuchi, H., and Higashiyama, T. (2011). Attraction of tip-growing pollen tubes by the female gametophyte. *Curr. Opin. Plant Biol*. **14,** 614-621.

Tamura, K., Peterson, D., Peterson, N., Stecher, G., Nei, M., and Kumar, S. (2011). MEGA5: Molecular Evolutionary Genetics Analysis Using Maximum Likelihood, Evolutionary Distance, and Maximum Parsimony Methods. *Mol. Biol. Evol*. **28,** 2731-2739.

Timme, R.E., and Delwiche, C.F. (2010). Uncovering the evolutionary origin of plant molecular processes: comparison of *Coleochaete* (Coleochaetales) and *Spirogyra* (Zygnematales) transcriptomes. *BMC Plant Biol*. **10,** 12.

Tzubery, T., Rimon, A., and Padan, E. (2004). Mutation E252C increases drastically the Km value for Na^+ and causes an alkaline shift of the pH dependence of NhaA Na^+/H^+ antiporter of *Escherichia coli*. *J. Biol. Chem*. **279,** 3265-3272.

Uozumi, N. (2001). *Escherichia coli* as an expression system for K^+ transport systems from plants. *Am. J. Physiol.-Cell Physiol*. **281,** C733-C739.

von Besser, K., Frank, A.C., Johnson, M.A., and Preuss, D. (2006). *Arabidopsis* HAP2 (GCS1) is a sperm-specific gene required for pollen tube guidance and fertilization. *Development*. **133,** 4761-4769.

Wang, L.G., Feng, X.Y., Zhao, H., Wang, L.D., An, L.Z., and Qiu, Q.S. (2014). Functional Analysis of the $Na^+,K^+/H^+$ Antiporter PeNHX3 from the Tree Halophyte *Populus euphratica* in Yeast by Model-Guided Mutagenesis. *PLoS One*. **9,** e104147.

Williams, J.H. (2008). Novelties of the flowering plant pollen tube underlie diversification of a key life history stage. *Proc. Nat. Acad. Sci. USA*. **105,** 11259-11263.

Yadegari, R., and Drews, G.N. (2004). Female gametophyte development. *Plant Cell*. **16,** S133-S141.

Zhao, J., Cheng, N.H., Motes, C.M., Blancaflor, E.B., Moore, M., Gonzales, N., Padmanaban, S., Sze, H., Ward, J.M., and Hirschi, K.D. (2008). AtCHX13 is a plasma membrane K^+ transporter. Plant Physiol. **148,** 796-807.